THERMOPHORETIC FABRICATION OF GRADIENT HYDROGELS FOR MECHANOBIOLOGY APPLICATIONS

Shin Wei Chong

A thesis submitted in fulfilment of
the requirements for the degree of
Doctor of Philosophy

School of Biomedical Engineering
Faculty of Engineering
The University of Sydney

October 2025

Statement of originality

This is to certify that to the best of my knowledge, the content of this thesis is my own work. This thesis has not been submitted for any degree or other purposes.

I certify that the intellectual content of this thesis is the product of my own work and that all the assistance received in preparing this thesis and sources have been acknowledged.

The experimental work presented in this thesis was primarily performed in the facilities within the School of Biomedical Engineering, J03 Engineering and Technology Precinct, The University of Sydney. Some of the experimental work was performed in the facilities within the School of Chemistry, The University of Sydney; Katharina Gaus Light Microscope Facility (KGLMF), University of New South Wales; Science and Engineering Building, University of New South Wales.

Signed: Date:

Shin Wei Chong

Authorship attribution statement

This thesis is based on material contained in the following published work or manuscript in preparation:

i. Alexandros Kosmidis Papadimitriou, Shin Wei Chong, Yi Shen, Oisin Stefan Lee, Tuomas P J Knowles, Liam M Grover, Daniele Vigolo, "*Fabrication of gradient hydrogels using a thermophoretic approach in microfluidics*", Biofabrication, 16 (2), 025023, 2024.

This publication forms part of "Chapter 5: Foundational development of the thermophoretic fabrication platform". I performed the thermophoresis experiments using fluorescent polystyrene nanoparticles, including data analysis. I performed the computational simulation experiments together with O.S.L, including data analysis and visualization. I interpreted the material characterization and biological data collected and analyzed by A.K.P.. I wrote, formatted and prepared the final manuscript together with A.K.P..

ii. Shin Wei Chong, Jameel Sardharwalla, Gweneth Sofia P Masonsong, Joshua Cosgrove, Anthony Katselas, Isaac J Gresham, Marcela M M Bilek, Yi Shen, Chiara Neto, Daniele Vigolo, "*A modular microfluidic system to generate gradient hydrogels with simple-to-complex stiffness profiles for mechanobiology*", Advanced Materials Technologies, e01457, 2025.

This publication forms "Chapter 6: A modular platform to create simple-to-complex stiffness gradient profiles" and part of "Chapter 4: Thermophoretic migration of biopolymers in solution". I designed and performed all the experiments, including data analysis, with assistance from J.S., G.M., J.C., A.K., and I.J.G, as detailed in the "Author Contributions" section of the manuscript. I wrote, formatted and prepared the final manuscript.

iii. Shin Wei Chong, Li Liu, Daryan Kempe, Yingqi Zhang, Kourosh Kalantar-Zadeh, Marcela M M Bilek, Lining Arnold Ju, Maté Biro, Daniele Vigolo, *"Fluorescently labeled gradient hydrogels reveal matrix-dependent cell responses to substrate stiffness*". (Submitted. Available as preprint on bioRxiv: https://doi.org/10.1101/2025.09.23.677581).

This publication forms "Chapter 7: Fluorescently labelled stiffness gradient hydrogels to probe cell-matrix interplay" and part of "Chapter 4: Thermophoretic migration of biopolymers in solution". I designed and performed all the experiments, including data analysis, with assistance from L.L., D.K., and Y.Z, as detailed in the "Author Contributions" section of the manuscript. I wrote, formatted and prepared the original manuscript.

iv. Shin Wei Chong, Daniele Vigolo, "*Microengineered gradient hydrogels for mechanobiology*". (In preparation).

This publication forms "Chapter 2: Microengineered gradient hydrogels for mechanobiology" and part of "Chapter 8: Conclusion and outlook". I conceptualize the review paper, performed literature searches, and wrote the original manuscript.

In addition to the statements above, in cases where I am not the corresponding author of a published item, permission to include the published material has been granted by the corresponding author.

Signed: Date:

Shin Wei Chong

As supervisor for the candidature upon which this thesis is based, I can confirm that the authorship attribution statements above are correct. In cases where I am the corresponding author of a published item, permission to include the published material has been granted to Ms. Shin Wei Chong for her thesis.

Signed: Date:

Daniele Vigolo

Use of generative artificial intelligence

During the preparation of the thesis the author used Chat-GPT for the purposes of text enhancement. The use of this generative AI tool includes sentence structuring and paraphrasing. The author confirms that where text was modified by generative AI, the content was reviewed for possible errors, inaccuracies, and bias. The author takes full responsibility for the submitted thesis and ensures the work is their own and has used generative AI within the parameters of use.

Acknowledgement of research support

This research was supported by the Faculty of Engineering Research Scholarship, and the Postgraduate Research Supplementary Scholarship in Sydney Nano Institute Frontier.

Abstract

Microengineered stiffness gradient hydrogels offer exciting opportunities as *in vitro* experimentation platform to probe how cells sense and respond to biophysical cues in various biological contexts, particularly towards the identification of new mechanistic understanding and therapeutic strategies. However, the need to spatially manipulate the properties of soft hydrogels at the micron scale poses challenges in developing fabrication platforms that can reliably modulate the gradient gel characteristics according to user needs.

This thesis describes the development, optimization, and application of a novel gradient hydrogel fabrication approach based on thermophoresis – the directed migration of solutes along temperature gradients. The thermophoretic technique overcomes several limitations of conventional approaches through its unique features: 1) active process enabling highly precise and reproducible patterning, 2) compatibility with a wide range of hydrogel chemistries and crosslinking mechanisms, 3) tunable stiffness range and gradient strengths across the broad biological mechanical landscape, and 4) the ability to create complex stiffness patterns.

The thermophoretic technique utilizes microfluidics strategy to pattern microscale temperature landscapes and leverages thermophoresis effect to precisely guide the redistribution of hydrogel precursor molecules into the desired gradient pattern, which directly translates into stiffness gradients upon hydrogel crosslinking. Fabrication of linear stiffness gradient Gellan gum hydrogels was first demonstrated to elicit stiffness-dependent maturation of pre-osteoblast cells, confirming the effectiveness of the technique in modulating the mechanical microenvironment of cells.

To increase technology accessibility, a modular platform was designed for simplified and streamlined operation. The versatility of the platform was demonstrated through fabrication of a series of linear, periodic, and anisotropic stiffness gradients using thermosensitive Gellan gum and photopolymerized gelatin methacryloyl (GelMA) hydrogels. Extensive stiffness characterization using atomic force microscopy (AFM)

firmly established the precision and reproducibility of the thermophoretic technique. Furthermore, quantitative analysis of fibroblast behavior on these gradient gels demonstrated that the modular thermophoretic platform is suitable in the context of mechanobiology for studying how cellular stiffness responses can be modulated beyond classically investigated linear gradients.

The universality of the thermophoretic technique allowed for systematic investigations into the role of absolute stiffness, gradient slope, and hydrogel matrix composition on cell mechanosensitivity. Using 3T3-L1 fibroblasts as model system, the findings suggested that both the hydrogel type and ECM protein coating can jointly influence cell responses to stiffness gradients. Notably, the Gellan gum and GelMA gradient hydrogels were fabricated using fluorescently labelled polymers. The resulting fluorescence signal positively correlated with the hydrogel stiffness, enabling 1) rapid visual validation of the stiffness gradient and 2) direct correlation of the local substrate stiffness and the biological readout. This fluorescence-based characterization method should be generalizable to other hydrogel systems and presents a potential solution to improve the reliability of stiffness gradient hydrogels for cell studies.

Overall, the thesis contributes new additions to the toolbox of engineered biomaterials crucial in enabling advanced *in vitro* platforms for mechanobiology research.

Acknowledgements

Completing this thesis has been a marathon of grit and resilience, one made possible by the many people who helped me along the way.

I want to thank Daniele Vigolo, my primary supervisor, for the opportunity to share the startup journey of his new research group here in Sydney. I am most grateful for his trust in me to take ownership and full accountability for my own research and progress. I also want to thank Chiara Neto, who kindly opened her laboratory to me and enabled me to delve into the depths of AFM. And to Yi Shen, for her guidance during the early stages of my PhD and continuing support in co-authored publications. I would like to acknowledge my PhD progression panel, Marcela Bilek and Clara (Thao) Tran, for valuable advice and encouragements through each stage of my candidature.

A big thank you to my friends and colleagues from USYD: Bonny Tsoi, Dominic Francis, and Antonio Tricoli for bringing the best out of me; Anthony Katselas and Isaac Gresham for their technical support on AFM; Chris Vega-Sanchez for useful discussions on microfabrication; Bingyan Liu and Jiayan Shao for helpful advice on polymer synthesis; Kaitlyn Zhang and Jameel Sardhawalla for introducing me to cell culture; Li Liu for help with SEM imaging; Ann-Na Cho for critical discussions on my project; Joseph Yang, Alex Yin, and Aaron Zhang for opening the door to exciting collaborations; my undergraduate thesis students and interns, particularly Oisin Lee, Gwen Masonsong and Joshua Cosgrove for their outstanding contributions.

I owe a great intellectual debt to the Australian Society for Mechanobiology (AusMB), particularly Maté Biro, Sara Baratchi, Daryan Kempe, Arnold Ju, and Charles Cox, whose introduction into mechanobiology, support, encouragements, and insightful discussions had a profound impact on the trajectory of my PhD research.

Finally, I extend my deepest thanks to my family who are my greatest counsel and my strongest foundation.

To my parents, for their wisdom and their tireless love and support.

Contents

Chapter 1

Introduction

The first chapter introduces readers to the growing field of mechanobiology, highlighting the role of engineered hydrogels as essential tools for studying how biophysical forces influence cellular signaling and behavior. The thesis is framed within the context of advancing stiffness gradient hydrogel technology, and particularly, using a thermophoresis-based technique. The chapter then outlines the specific aims of the project, followed by a brief overview of the subsequent chapters in the thesis.

1.1 Biomaterials for mechanobiology

The idea that biophysical forces influence tissue structure and function has a long history dating back more than a century ago. The classical work by D'Arcy Thompson introduced a physics-based view of tissue development beyond the dogma of molecular genetics in biology[1]. In recent decades, many experimental studies and computational models have expanded our understanding of the regulatory role that biophysical cues play in many biological phenomena[2,3]. Throughout the human body, cells respond to biomechanical forces such as fluid shear in blood vessels, compressive stresses during muscle contraction, and cyclic stretching during breathing. Conversely, cells also generate forces on the extracellular matrix (ECM) and neighboring cells to probe the mechanics of their local surroundings. As a result, mechanobiology has emerged as a rapidly growing field to study how these forces translate into cellular signaling and responses, which have important implications in health and disease[4,5].

Central to the rise of modern mechanobiology is the utilization of biomaterials as highly controlled mimics of the native ECM[6]. These materials provide an *in vitro* alternative to animal models for studying cell mechanosensing and mechanotransduction – the processes by which cells "feel" and integrate biophysical cues to direct biological function from the molecular to the tissue scale. In particular, hydrogels with tunable mechanical properties have become indispensable tools for uncovering the complex cell-material interactions underpinning adaptive and integrated cellular behaviors. Beyond fundamental research, biomaterials-based approaches have also inspired new therapeutic opportunities through targeted interventions of cell interactions with their mechanical microenvironment[7]. In other areas, engineered hydrogels have been harnessed as a handle to control cell fate and function with diverse applications in disease modeling, tissue engineering, and regenerative medicine[8].

Conventionally, hydrogels are fabricated as homogenous substrates, and most studies have been focused on examining cell responses to the substrate bulk properties[9,10]. However, native tissues often exhibit a high degree of spatial variation in the form of structural and mechanical gradients, such as at ligament-bone and muscle-tendon interfaces[11]. In the case of disease or injury, changes in the microscale tissue stiffness can be drastic, leading to aberrant cell signaling and compromised tissue function.

Modeling such micrometer-scale spatial heterogeneity using traditional methods of fabricating bulk hydrogels poses difficult and often insurmountable challenges. This limitation provided the impetus for ongoing efforts to develop technologies that enable studies to measure and probe cell responses to these spatially dynamic microenvironmental cues.

Over the past two decades, researchers have leveraged advances in microfabrication strategies to create stiffness gradient hydrogels that mimic the stiffness range and gradient profile characteristic of the target tissue type or biological process (**Figure 1.1**)[12]. To date, the majority of the fabrication techniques are dedicated to creating linear stiffness gradient hydrogels[13–15]. A key aspect of these gradient materials is the continuous and tunable variation in mechanical stiffness across a defined spatial range, from hundreds of micrometers to a few centimeters in size. Their development was initially intended as a reductionist approach to screen cell-material interplay on a continuum of conditions[16,17]. As the field continues to grow, increasing biological and technical complexity of stiffness gradient hydrogel systems will be achieved[18–21]. These developments reflect many exciting opportunities in the future, both to pursue fundamental research on cell mechanobiology and to work on its applications in the life sciences.

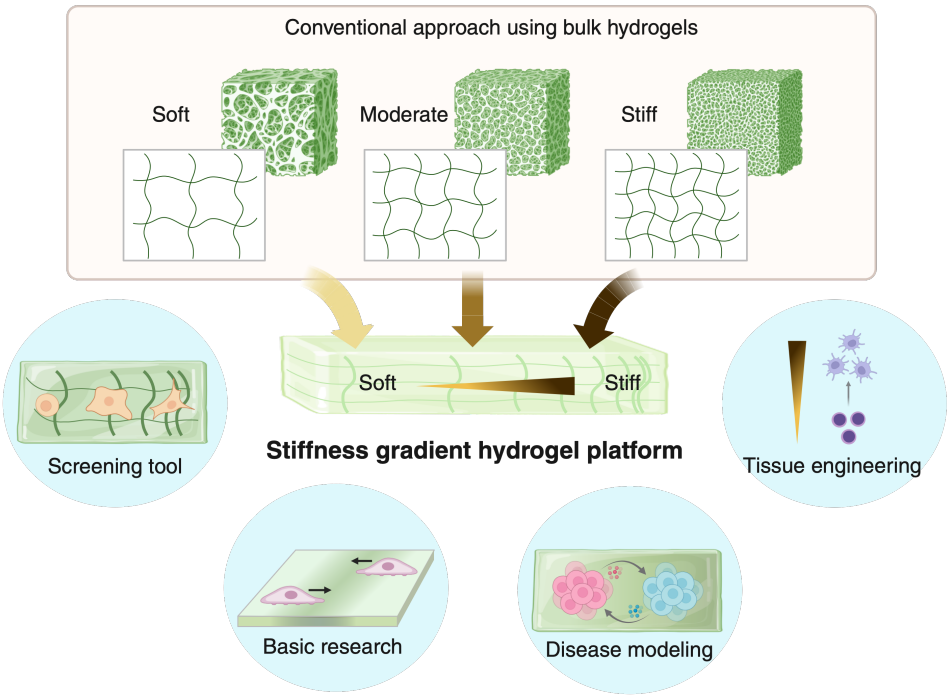

Figure 1.1: Concept of stiffness gradient hydrogels and the promising areas for fundamental mechanobiology research and its applications.

1.2 Thermophoresis to fabricate stiffness gradient hydrogels

The modulation of hydrogel stiffness is generally accomplished through manipulation of polymer concentration or crosslinking density. This means that the generation of well-defined stiffness gradients necessitates intricate control over these parameters with sufficiently high spatial resolutions.

This thesis project was motivated by the vision of a versatile gradient hydrogel fabrication toolkit that can be streamlined for diverse hydrogel systems and *in vitro* applications, particularly for studying cell-material interactions at the single-cell level.

The fabrication platform developed in this work builds on a thermophoresis-based technique pioneered in the Vigolo Lab[22]. Thermophoresis is the directional motion of particles or molecules in fluids induced by temperature gradients[23]. In essence, the technique leverages microfluidic heating control strategies to drive the redistribution of hydrogel components into user-defined gradient profiles. Unlike current mainstay techniques where gradient formation occurs passively, thermophoresis is an active process, which offers the potential of superior precision and flexibility in controlling the gradient properties. Another important attribute of this approach is its inherent ability to decouple gradient formation from the hydrogel crosslinking process. As such, thermophoresis would be universally compatible with a wide range of hydrogel types, regardless of their origin (e.g. natural or synthetic), biochemical composition (e.g., carbohydrate or protein-based), or crosslinking mechanism (e.g., photocrosslinking or temperature-induced). This unique combination of features makes thermophoresis a compelling alternative to conventional techniques, with the aim to address longstanding challenges in stiffness gradient hydrogel fabrication – namely precision, reproducibility, and flexibility, to facilitate widespread adoption and broad utility in mechanobiology research.

The application of thermophoresis for gradient hydrogel fabrication has been largely enabled by advances in PDMS microfluidics and our experimental understanding of thermophoresis at the micron scale. The first major milestone was the development of an integrated on-chip heating system (**Figure 1.2**)[24]. Briefly, temperature control was achieved by using embedded micro-Joule heater (or “heating element”) for localized heat generation and water flow in adjacent microchannels for cooling, enabling the

generation of microscale temperature gradients. This offered new approaches to how miniaturized systems could be designed to manipulate molecules and colloids, as well as to characterize their thermophoretic behavior. There was no longer a need for expensive external heaters that are cumbersome to implement. PDMS microfluidics methods allow for rapid design-to-prototype iteration, reduced costs, and simplified experimental setup and operation – all of which are essential for broad and scalable deployment. Crucially, the optically transparent microdevices enables direct observation of the thermophoresis process using various microscopy techniques, providing a new lens into the complex physics phenomena in microscale geometries[23].

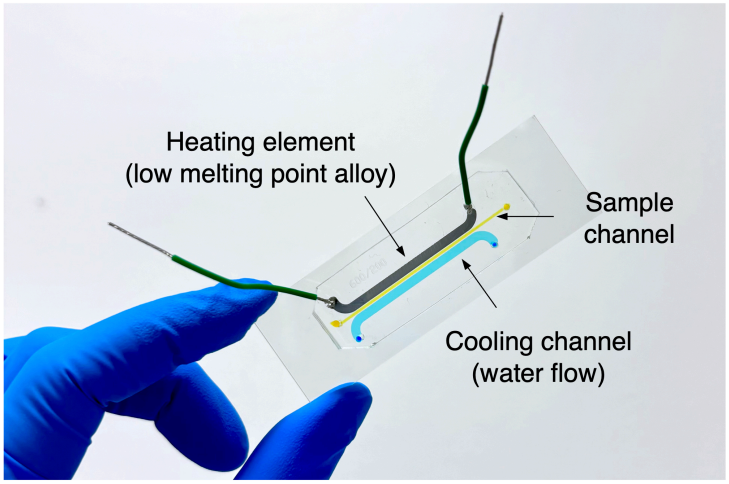

Figure 1.2: Photograph of a thermophoresis microdevice with on-chip heating functionality. Sample channel (yellow) and cooling channel (blue) are filled with color dye for visualization. For technical details, see [refs. 22, 25].

Thermophoresis was first demonstrated to fabricate stiffness gradient hydrogels using ionically crosslinked alginate[22]. By leveraging a two-layer microchannel construct separated by a permeable PDMS membrane, it was possible to achieve a pH-dependent delay in hydrogel crosslinking while allowing sufficient time for thermophoresis to create a local concentration gradient. Here, it is important to emphasize that the thermophoretic gradient generation process occurs when the hydrogel solution remains in its liquid, uncrosslinked state. After the specified duration, rapid crosslinking “locks in” the concentration gradient, yielding a stable stiffness gradient hydrogel. From this point onward, thermophoresis or heating is no longer required to maintain the stiffness gradient.

More recently, the thermophoretic gradient generation technique was demonstrated using thermosensitive Gellan gum hydrogel[25]. This work showcased the versatility of the technique with different crosslinking mechanisms, and importantly, provided the first biological demonstration in the context of pre-osteoblast cell migration, proliferation, and maturation (detailed discussion in **Chapter 5**).

Although still a relatively nascent technology, the thermophoresis approach already allows users to take advantage of the flexibility to pattern different hydrogels, which would otherwise be practically difficult to achieve using a single technique. Pairing this with the possibility of highly configurable microfluidic network designs, the proposed thermophoretic fabrication technique offers the promise to expand the catalogue of biological gradient hydrogels available for mechanobiology research.

1.3 Rationale and scope of the thesis

The fact that new tools and approaches are needed to drive a better understanding of cell mechanobiology is indisputable[26–28]. However, as I progressed through my PhD research, one main observation for me is that despite technical advances in stiffness gradient hydrogels as *in vitro* experimental platform, the adoption of novel fabrication techniques in mainstream mechanobiology research has not lived up to the initial enthusiasm surrounding the field[14].

In my thesis, I argue that the technology is still in search of a practical and enabling solution that strikes the “right” balance between ease of fabrication, reproducibility, and biological relevance. The emphasis would be to make stiffness gradient hydrogels sufficiently easy to fabricate, customize, and integrate into existing workflows, so that labs naturally switch to them over standard bulk hydrogel methods.

This led me to a string of big picture questions that shaped the trajectory of my research: How could we develop a universally accessible method for fabricating stiffness gradient hydrogels to democratize their use in mechanobiology research? If we could apply the same technique to independently modulate stiffness gradient and other hydrogel properties, what useful systematic comparisons could we make, and what level of differences would we expect in terms of their effect on cellular responses?

Specifically, I was interested in basic cellular phenomena such as spreading, proliferation, and migration, as they underpin much of mechanobiology. Another big question for me was, how could we simplify the validation of fabricated gradient gels and reduce reliance on sophisticated equipment like atomic force microscopy. This is considered to be crucial in enabling high-throughput biological studies.

These questions naturally led me to a very broad and interdisciplinary body of work in pursuing the frontier of stiffness gradient hydrogel technology. The specific aims of this thesis can be summarized as:

- To characterize the thermophoretic behavior of biopolymers in microconfined environments.
- To develop a streamlined thermophoresis platform for creating simple (linear) and complex stiffness gradients.
- To develop a fluorescence microscopy framework for non-invasive mechanical characterization of gradient hydrogels.
- To study the interplay of stiffness gradient and matrix composition on stiffness-mediated cell responses.

Altogether, this work represents a holistic exercise in method development that serves to advance the thermophoretic gradient hydrogel platform from a proof-of-concept into a robust and versatile research tool.

1.4 Outline of thesis

To first provide the scientific and technological background for this thesis, **Chapter 2** examines the different fabrication techniques to create microscale stiffness gradients in hydrogels. Also included is a discussion on the progress made by gradient hydrogel technology across different research areas over the past two decades, as well as emerging trends in the field that will influence the future development of this technology.

Chapter 3 details the methodological framework of this thesis. The chapter starts by introducing the principles of thermophoresis, followed by the microfabrication process and experimental setup. The chapter then details the hydrogel characterization

techniques, along with cell culture protocols and biological assays commonly used in subsequent chapters of the thesis.

As the foundational work of this thesis, **Chapter 4** describes the development of a fluorescence-based temperature measurement technique by integrating established microscopy and image processing methods. The technique enables precise mapping of temperature distribution within the thermophoresis microdevice, providing valuable information for users to optimize their desired gradient profile. This chapter also details an experimental investigation of the key process variables that influence thermophoresis-driven gradient formation. These experiments were crucial for identifying a reliable set of process parameters for gradient gel fabrication, which vary depending on the hydrogel system.

Next, **Chapter 5** presents the first iteration of the thermophoresis microdevice and its application to study pre-osteoblast cell behavior on linear stiffness gradient Gellan gum hydrogels. Furthermore, the achievements and limitations of this initial design are critically analyzed, inferring important lessons that guide the next steps of the thermophoretic platform development.

The following chapters are dedicated to the development and application of a new, modular platform for streamlined thermophoretic fabrication of stiffness gradient hydrogels.

Chapter 6 details the design, optimization, and characterization of the platform. Its versatility is demonstrated through fabrication of Gellan gum and GelMA hydrogels with a range of linear, periodic, and anisotropic stiffness gradients. Biological validation was performed in the context of fibroblast proliferation and migration on GelMA gradient hydrogels of varying stiffness patterns.

Using the developed platform, **Chapter 7** focuses on applying linear stiffness gradient hydrogels to study how different design parameters, including absolute stiffness, gradient strength, and matrix composition, will jointly influence cell behavior. By leveraging fluorescent labelling strategies, this chapter also introduces a generalizable approach for non-invasive structural and mechanical characterization of the thermophoretically fabricated stiffness gradient hydrogels.

Finally, **Chapter 8** consolidates the outcomes from this thesis, and provides an outlook for future development of biophysical gradient hydrogel technology and its applications.

Overall, this thesis contributes to a new gradient hydrogel fabrication system that features increased, but controlled, complexity. The developed platform could help enable new mechanistic insights into cell-substrate interplay, with potential far-reaching impacts toward realizing designer approaches to control cell function.

References

1. Thompson, D. W. On growth and form. *Cambridge University* (1942).

2. Vining, K. H. & Mooney, D. J. Mechanical forces direct stem cell behaviour in development and regeneration. *Nat Rev Mol Cell Biol* **18**, 728–742 (2017).

3. Li, L., Eyckmans, J. & Chen, C. S. Designer biomaterials for mechanobiology. *Nat Mater* **16**, 1164–1168 (2017).

4. Wozniak, M. A. & Chen, C. S. Mechanotransduction in development: a growing role for contractility. *Nat Rev Mol Cell Biol* **10**, 34–43 (2009).

5. Iskratsch, T., Wolfenson, H. & Sheetz, M. P. Appreciating force and shape — the rise of mechanotransduction in cell biology. *Nat Rev Mol Cell Biol* **15**, 825–833 (2014).

6. Blache, U. *et al.* Engineered hydrogels for mechanobiology. *Nat Rev Methods Primers* **2**, 98 (2022).

7. Holle, A. W. *et al.* Cell-Extracellular Matrix Mechanobiology: Forceful Tools and Emerging Needs for Basic and Translational Research. *Nano Lett* **18**, 1–8 (2018).

8. Qazi, T. H. *et al.* Programming hydrogels to probe spatiotemporal cell biology. *Cell Stem Cell* **29**, 678–691 (2022).

9. Engler, A. J., Sen, S., Sweeney, H. L. & Discher, D. E. Matrix elasticity directs stem cell lineage specification. *Cell* **126**, 677–689 (2006).

10. Przybyla, L., Lakins, J. N. & Weaver, V. M. Tissue mechanics orchestrate Wnt-dependent human embryonic stem cell differentiation. *Cell Stem Cell* **19**, 462–475 (2016).

11. Guimarães, C. F., Gasperini, L., Marques, A. P. & Reis, R. L. The stiffness of living tissues and its implications for tissue engineering. *Nat Rev Mater* **5**, 351–370 (2020).

12. Sunyer, R. & Trepat, X. Durotaxis. *Curr Biol* **30**, R383–R387 (2020).

13. Hadden, W. J. *et al.* Stem cell migration and mechanotransduction on linear stiffness gradient hydrogels. *Proc Natl Acad Sci* **114**, 5647–5652 (2017).

14. Zaari, N., Rajagopalan, P., Kim, S. K., Engler, A. J. & Wong, J. Y. Photopolymerization in microfluidic gradient generators: Microscale control of substrate compliance to manipulate cell response. *Adv Mater* **16**, 2133–2137 (2004).

15. Sunyer, R., Jin, A. J., Nossal, R. & Sackett, D. L. Fabrication of Hydrogels with Steep Stiffness Gradients for Studying Cell Mechanical Response. *PLoS One* **7**, e46107 (2012).

16. Wang, P. Y., Tsai, W. B. & Voelcker, N. H. Screening of rat mesenchymal stem cell behaviour on polydimethylsiloxane stiffness gradients. *Acta Biomater* **8**, 519–530 (2012).

17. Kim, C. *et al.* Stem Cell Mechanosensation on Gelatin Methacryloyl (GelMA) Stiffness Gradient Hydrogels. *Ann Biomed Eng* **48**, 893–902 (2020).

18. Chin, I. L. *et al.* Volume adaptation of neonatal cardiomyocyte spheroids in 3D stiffness gradient GelMA. *J Biomed Mater Res A* **111**, 801–813 (2023).

19. Cao, Z., Clark, A. T., Vite, A. & Corbin, E. A. A Dynamic Gradient Stiffness Material Platform to Manipulate Cardiac Fibroblasts' Spatio-Temporal Behavior. *Adv Funct Mater* **34**, 2402808 (2024).

20. García, S. *et al.* Generation of stable orthogonal gradients of chemical concentration and substrate stiffness in a microfluidic device. *Lab Chip* **15**, 2606–2614 (2015).

21. Kuo, C. H. R., Xian, J., Brenton, J. D., Franze, K. & Sivaniah, E. Complex stiffness gradient substrates for studying mechanotactic cell migration. *Adv Mater* **24**, 6059–6064 (2012).

22. Vigolo, D., Ramakrishna, S. N. & DeMello, A. J. Facile tuning of the mechanical properties of a biocompatible soft material. *Sci Rep* **9**, 7125 (2019).

23. Vigolo, D., Rusconi, R., Stone, H. A. & Piazza, R. Thermophoresis: microfluidics characterization and separation. *Soft Matter* **6**, 3489–3493 (2010).

24. Vigolo, D., Rusconi, R., Piazzaa, R. & Stone, H. A. A portable device for temperature control along microchannels. *Lab Chip* **10**, 795–798 (2010).

25. Kosmidis Papadimitriou, A. *et al.* Fabrication of gradient hydrogels using a thermophoretic approach in microfluidics. *Biofabrication* **16**, 025023 (2024).

26. Burdick, J. A. & García, A. J. Special Issue: Biomaterials in Mechanobiology. *Adv Healthc Mater* **9**, 10–12 (2020).

27. Chen, W., Kim, D. H. & Lim, C. T. Special Issue: Biomaterials for Cell Mechanobiology. *ACS Biomater Sci Eng* **5**, 3685–3687 (2019).

28. Baratchi, S., Khoshmanesh, K., Cox, C. D. & Gomez, G. A. Editorial: Mechanobiology: Emerging Tools and Methods. *Front Bioeng Biotechnol* **8**, 30–44 (2020).

Chapter 2

Microengineered gradient hydrogels for mechanobiology

This chapter provides an overview of the concept of mechanobiology and the different fabrication techniques to produce microscale stiffness gradients in hydrogels. Particular attention is given to the application these gradient materials for fundamental research, disease modeling, and tissue engineering. The chapter also discusses the near-term challenges and outlook of gradient hydrogel technology to facilitate a better understanding of the complex cell-microenvironment interplay.

2.1 Overview of the cell microenvironment

The behavior of cells during development, disease, and wound healing is influenced by a variety of signals found within their cellular microenvironment, and in particular, the extracellular matrix (ECM). ECM is a non-cellular component of our tissues, composed of families of polysaccharides, proteins, and glycoproteins[1]. They are deposited by cells, and while similar ECM components are found throughout the body, each tissue has a unique ECM composition and structure that dictates the specialized functions on a local tissue level.

Within tissues, the ECM provides structural support to resident cells as well as facilitates signaling through the presentation of chemical and physical cues to regulate cellular activity. For example, secretion of a laminin-rich form of ECM is necessary to direct the development of mammary tissue during adolescence[2]. However, dysfunctional regulation of this matrix eventually leads to tumor progression and cancer. In another example, wound healing occurs in stages immediately following an injury, starting with the formation of a provisional matrix that is rich in fibrin and fibronectin, followed by matrix remodeling to either restore tissue function or cause fibrosis resulting from excessive collagen buildup[3].

The ECM is also known to be implicated in stem cell fate decisions. Specifically, there is a dynamic interplay at the cell-ECM interface whereby cells actively remodel their surrounding matrix. At the same time, the inherent properties of the ECM can interact with cells to influence their behavior. Indeed, extensive studies have demonstrated that the differentiation of both mesenchymal stem cells (MSCs) and pluripotent stem cells (PSCs) can be strongly influenced by various physicochemical properties of the ECM, including mechanics (i.e., stiffness, viscoelasticity), degradation, architecture, and signaling ligands[4–7]. In a recent example, substrate stiffness (400 Pa vs. 60 kPa) was shown to differentially modulate embryonic stem cell specification into mesodermal lineages in response to cell-secreted Wnt factors[4].

Besides the ECM properties, cells also interact with soluble cues (e.g., growth factors, cytokines), neighboring cells, and external forces present in their milieu[8]. Cell-extrinsic shear, tensile and compressive forces may be imposed by external loads, for example, due to blood flow through blood vessels and cyclic breathing in the lungs[9,10].

Furthermore, local environmental factors such as pH, oxygen tension, and osmolality also play a role in coordinating the biophysical and biochemical regulation of cells[8,11].

Collectively, these features contribute to the complex environment which cells can "sense" and respond to via cell-matrix and cell-cell interactions (**Figure 2.1**)[12]. In turn, these interactions define the molecular, structural, and functional phenotypes of matured tissue cells as well as stem cells that reside in specialized microenvironments known as niches[13,14].

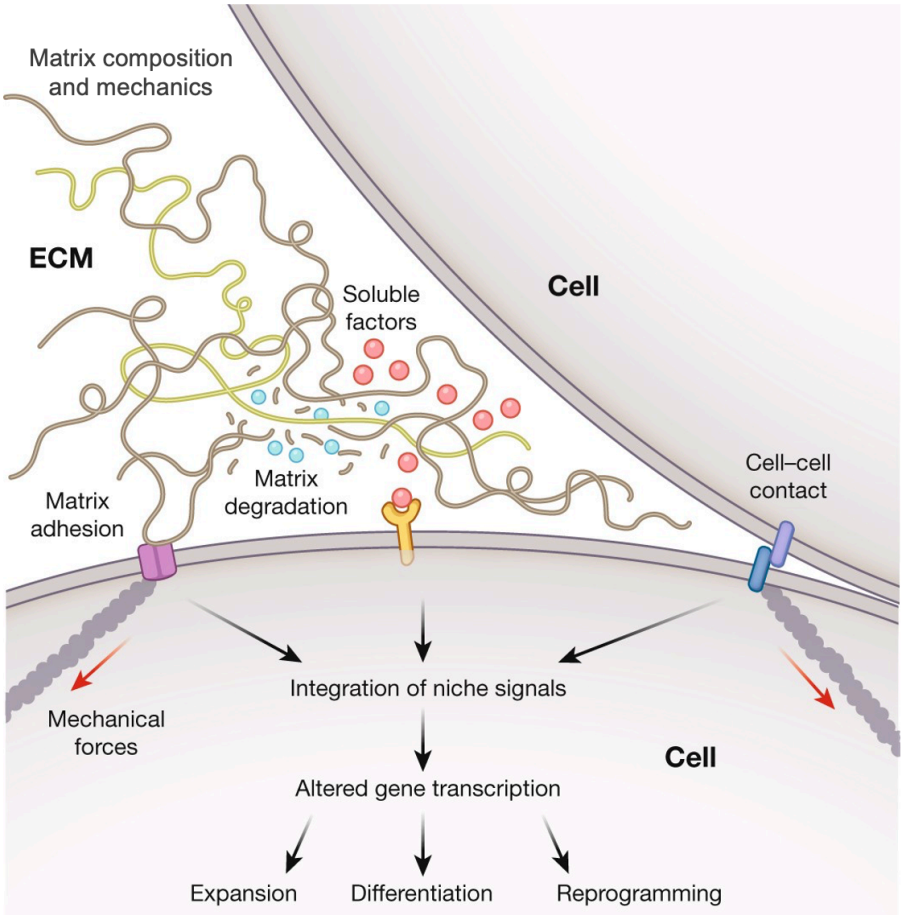

Figure 2.1: Cells can integrate various biophysical and biochemical signals within the native ECM to modulate their cell behaviour. Image adapted from [ref.12].

2.2 Cell mechanosensing and mechanotransduction

Cell-matrix interactions are key in enabling biological systems to contextualize stimuli, because the response of cells to the same stimulus will depend on the combined biophysical and biochemical states of their microenvironment.

The range of mechanosensing structures offer multiple ways for cells to sense mechanical cues (**Figure 2.2**). Integrins in focal adhesion complexes[15] and cadherins in adherens junctions[16] are key mechanosensors that mediate cell-ECM and cell-cell interactions, respectively. Both of these structures are connected to the actin cytoskeleton, providing a direct linkage to transmit mechanical signals between the cell exterior and interior. Furthermore, ion channels such as Piezo1 can be activated in response to a host of mechanical stimuli, including substrate stiffness and shear stress[17]. More recently, a growing number of studies also point toward the nucleus[18,19], cytoskeleton[20], and cortical membrane[21] as being putative sites for mechanosensing.

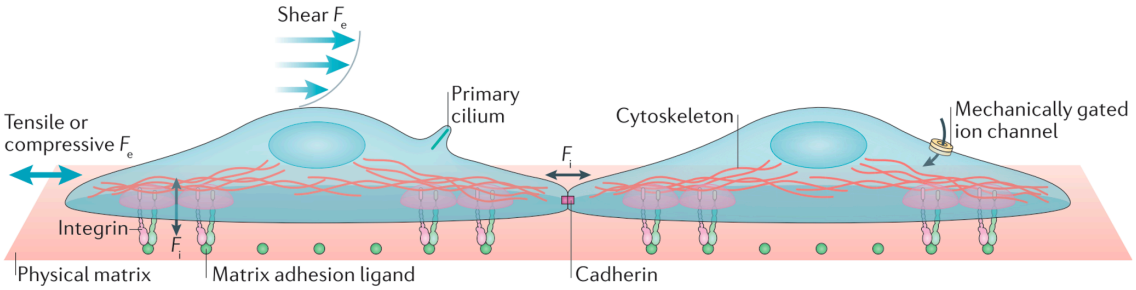

Figure 2.2: Cells can generate intrinsic forces (F_i) to probe its surroundings and are able to sense externally applied forces (F_e) through mechanosensitive receptors, which regulate cell activity by influencing their downstream signaling pathways. Image adapted from [ref. 27].

ECM mechanics influence cell processes and communication at several levels through a process called mechanotransduction[22,23]. At the cell surface, cells directly interact with the ECM via transmembrane protein complexes or proteins capable of sensing changes in the plasma membrane mechanics. These mechanical signals activate intracellular effectors that transduce the signals internally to subcellular structures such as the nucleus via a cascade of molecular signaling pathways. Finally, the effectors induce changes in gene expression at the transcriptomic and/ or epigenetic level, which drive specific cellular responses. For example, mechanosensing of stiffness leads to downstream upregulation of specific transcriptional factors such as

Ras homolog gene family member A (RhoA), yes-associated protein (YAP), and transcriptional coactivator with PDZ-binding motif (TAZ)[24,25]. In turn, upregulation of these proteins in MSCs promotes lineage commitment to more osteogenic fate[26].

Cells probe the mechanics of their surrounding matrix through an active process. As cells engage with the ECM, they exert a traction force on the matrix to “feel” how much it deforms. These forces are generated intracellularly, for example, due to actomyosin contractility or cytoskeletal assembly. On the other hand, since the ECM has varying composition and structural features, it provides external resistance or compliance that may store or dissipate these cell-mediated forces[27,28]. This implies that the physical properties of the ECM such as stiffness govern how mechanical cues are transduced, and the level of resistance that cells are able to experience may alter their behavior. Recent studies have also shown that cell-ECM interactions play a role in modulating the sensitivity of cells to matrix-bound biochemical factors and soluble cues[29,30], highlighting the importance of ECM mechanics in biological processes. In mechanobiology studies, cellular responses to ECM biophysical cues are assessed by both the subcellular abundance and distribution of mechanosensitive proteins (e.g., YAP, TAZ, lamin A), as well as cell morphological markers (e.g., cell area, aspect ratio, nuclear size).

2.3 Matrix stiffness from a tissue and materials perspective

Over the last two decades, ECM stiffness has emerged as a major regulator of cell behavior, such as adhesion[31], migration[32], proliferation[33], and stem cell fate[34]. Altogether, these cellular responses on the microscale are thought to mediate a myriad of biological processes on a broader level, such as early development, tissue homeostasis, and disease progression[35,36].

“Stiffness” is a general term often used to describe the mechanical property of substrates and matrices for cell culture. The basic definition of stiffness from a materials science point of view is based on the force required to achieve a certain deformation of a structure[37]:

$$\text{Stiffness} = \text{Load} / \text{Deformation}$$

Although the stiffness of a tissue or substrate can be quantitatively analyzed, there are many possible configurations of “load” (e.g., compressive force, tensile force) and measurable points of deformation (e.g., deformation, strain). For this reason, the reported stiffness values in literature should be interpreted in the context of the measurement technique. Moreover, the concept of moduli and stiffness are intimately related, thus, are often used interchangeably. However, when comparing studies in the literature, it is important to note the distinction that stiffness is a property of a structure that depends on its shape, whereas modulus is solely dependent on the intrinsic properties of the materials composing that construct[36]. In order to study cell-substrate interactions in a biologically relevant manner, it is also important to characterize the substrate mechanics in a similar manner to how cells would probe their surrounding matrix in tissues. Since cells typically experience forces on the order of pico- to nano-Newtons and in micrometer length scales (i.e., the size of a single cell), highly sensitive measurement techniques have been developed, including microsphere indentation, micro-indenters, and atomic force microscopy (AFM).

In the context of mechanobiology, it is the most common practice to define stiffness as the material’s Young’s modulus (kilopascals, kPa), which is a measure of its ability to undergo non-permanent deformation. The Young’s modulus of native tissues is thought to be largely governed by the density of fibrillar type 1 collagen, being the most abundant ECM protein. In general, adult tissues exhibit a characteristic Young’s modulus that increases from soft brain and liver (several hundreds of pascals to several kPa), to slightly stiffer striated muscle (around 10 kPa), and to much stiffer cartilage and bone matrices (over hundreds of kPa) (**Figure 2.3**)[36,38].

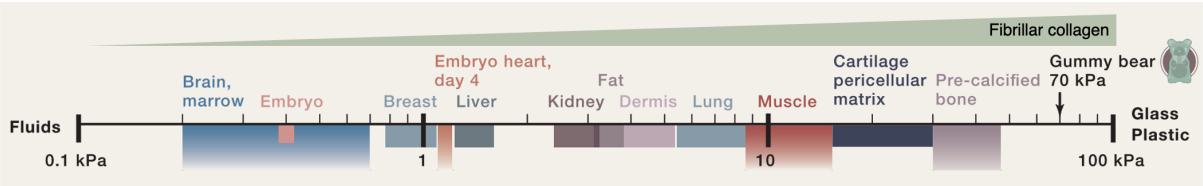

Figure 2.3: Typical Young’s modulus of different tissues in the body. An increase in tissue stiffness is generally correlated with increased density of fibrillar collagen in the local ECM. Image adapted from [ref. 38].

Beyond basic variation in the range of mechanical stiffness across different tissue types, heterogeneities in the spatial matrix organization also result in variation on the local tissue level, typically in the form of gradients. For instance, tissue stiffening following injury creates a stiffness gradient away from the wound site which promotes fibroblast cell recruitment to aid wound healing[39]. In another example, breast tissues during tumorigenesis have been reported to be ~10-fold stiffer than healthy mammary tissues, and the increased tissue stiffness has been linked to increased propensity of aggressive cancer cell invasion[40]. These cellular migratory responses to spatial stiffness gradients, collectively known as durotaxis, are thought to play a key role in diverse biological phenomena, making it a subject of intense research interest in mechanobiology[41,42]. On the other hand, stiffness gradients can also occur through natural gradation within tissues, for example, in the tissue interfacing tendons and bones known as enthesis[43,44]. Furthermore, the mechanics of many tissues may naturally change with time. For example, blood vessels become progressively stiffer during aging (20-30 kPa in young adults vs. ~200 kPa in adults over 80 years), contributing to the onset and progression of many age-related cardiovascular diseases[45].

Similar to tissues, hydrogels are a versatile class of biomaterials that can be designed to mimic specific features of the *in vivo* microenvironment. To that end, hydrogels comprise three-dimensional polymeric networks that display unique biophysical and biochemical properties, offering the possibility of a highly controlled platform for studying cell-ECM and cell-cell interactions in health and disease conditions[46]. Hydrogels used for cell culture can be formed from a wide selection of natural (e.g., collagen, hyaluronic acid, alginate), synthetic (e.g., polyacrylamide, polyethylene glycol), and semi-synthetic (e.g., gelatin methacryloyl, methacrylated Gellan gum) sources. Each hydrogel system has its own set of advantages and disadvantages, thus, the choice of hydrogel system will primarily be dependent on the specific application and objectives. Natural hydrogels (with a typical Young's modulus on the order of ~Pa to kPa) have a long history for cell culture applications due to their superior cytocompatibility, but their batch-to-batch variability can pose challenges in experimental reproducibility. Nevertheless, natural hydrogels can be chemically

modified to provide better control over their mechanical properties. Conversely, fully synthetic hydrogels provide a chemically defined system with mechanical properties that can be modulated over a much wider range (~Pa to MPa), making them a popular choice for mechanobiology studies. However, these systems typically involve synthetic chemistry methods for hydrogel crosslinking and biofunctionalization, which can be inaccessible and daunting to many laboratories.

With recent advances in hydrogel design and fabrication techniques, there is increasing interest in designing hydrogels to probe cell responses to spatiotemporal changes in the cellular microenvironment[47,48]. Of note, hydrogels presenting stiffness gradients have been explored to mimic the heterogenous *in vivo* tissue mechanics[49–51], or used as a screening tool to probe cell mechanobiology on a continuum of conditions[52,53]. While a range of hydrogel systems have been engineered to replicate the native ECM *in vitro*, stiffness gradient hydrogel platforms are intentionally simple to decouple the complexity of the cellular microenvironment. These platforms can be a powerful tool in driving our mechanistic understanding of how cells sense the physical cues in their surrounding matrix, with implications in cell signaling and how to modulate cell behavior by programming the ECM.

2.4 Fabrication of stiffness gradient hydrogels

The basic premise for biomimicry of stiffness gradient hydrogels is that they represent the stiffness range and gradient strength characteristic of the target tissue type or biological process. To that end, empirical stiffness measurements of *ex vivo* tissues are commonly performed to provide a physiological reference to guide the development of stiffness gradient hydrogels for *in vitro* cell studies[52,54]. In general, the stiffness gradient strengths can range from ~1 kPa mm^{-1} in physiological tissues to ~10 kPa mm^{-1} in pathological tissues, and >100 kPa mm^{-1} at tissue interfaces[55]. Of note, the drastically steeper stiffness gradients across regions of healthy and diseased tissues often arise from aberrant ECM remodeling, where imbalanced matrix turnover leads to excessive deposition of connective-tissue-like ECM, disorganized fibrous network, and even altered cell mechanics – which altogether drive pathological changes in tissue stiffness.

A number of approaches to engineer gradient biomaterials aimed at recreating the gradient properties of native tissues and induce desired cell mechanotransduction responses have been described in literature[56–58]. Here, special attention is given to microscale stiffness gradients for *in vitro* cell culture, which can be classified into four overarching strategies (**Table 2.1**): diffusion-based, controlled polymerization, component redistribution, and micro-molding.

Table 2.1: Representative examples of different methods for fabricating hydrogel substrates with stiffness gradients. Unless stated otherwise, the stiffness range (*E*) is reported in terms of Young's modulus measured by AFM, whereas 'slope' denotes the achievable slopes of stiffness gradient.

Technique	Polymer/ Component	Culture system	Gradient properties	Cell type	Major results	Ref.
Diffusion-based						
Sandwiching	PA	2D cell seeding	Continuous linear gradient at mixed interface of two drops *E: ~0.5-60 kPa* *Slope: ~5-15 kPa mm^{-1}*	human telomerase-immortalized fibroblasts	Incorporation of fluorescent microbeads in polymer solution allows stiffness readout from bead density; growth of cell fibrillar adhesions is mechanosensitive in a tensin-dependent manner	60
Microfluidic gradient generator	PA	2D cell seeding	Continuous linear gradient across planar substrate *E: ~1-12 kPa* *Slope: ~10 kPa mm^{-1}*	hMSCs	MSCs migrated from soft-to-stiff region (positive durotaxis); migration velocity is dependent on stiffness gradient slope	55
Sequential layering	GelMA	3D cell encapsulation	Discrete stiffness layers blended at interface *E (compressive): ~5-80 kPa* *Slope: ~15 kPa mm^{-1}*	NIH-3T3 fibroblasts	Fibroblasts displayed differential morphology and migrated along gradient axis	63
Two-step polymerization	PA	2D cell seeding	Continuous linear gradient across planar substrate (24x20x1 mm) *E: ~0.1-159.2 kPa* *Slope: ~0.5-8.2 kPa mm^{-1}*	hADSCs; C2C12 mouse myofibroblasts	Stiffness gradient can be tuned to impose durotactic or non-durotactic effect on cells; shallower gradients enable observation of dose-dependent (instead of ON-OFF response) of YAP nuclear translocation	64
Controlled polymerization						
Gradient photomask	GelMA	3D cell encapsulation	Continuous linear gradient across planar substrate (12x12x1 mm) *E: ~5-38 kPa* *Slope: ~3.4 kPa mm^{-1}*	hADSCs	hADSCs encapsulated in soft regions exhibited increased cellular and nuclear volume, with increased expression of osteogenic markers; study suggests that volume is sufficient to direct 3D stem cell differentiation	66
Sliding photomask	PA	2D cell seeding	Continuous linear gradient across planar substrate *E:* ~1-240 kPa *Slope: ~7.5-115 kPa mm^{-1}*	NIH-3T3 fibroblasts; SY5Y neuroblastoma cells	Wide-range stiffness gradient slopes achievable; less steep gradients with narrower stiffness ranges also possible with this method	68

(cont.)

Sliding photomask	PA	2D cell seeding	Continuous linear gradient embedded within a microfluidic device *E: ~1-40 kPa* *Slope: ~5 kPa mm^{-1}*	U87-MG glioma cells	Substrate stiffness promotes cell chemotaxis, while epidermal growth factor gradient can accelerate cell migration	69
Repeated gradual freezing-thawing	PVA/HA	2D cell seeding on cut sections of gel cylinder	Continuous gradient along height of gel column (25 mm diameter, 80 mm height) *E (compressive): ~20-200 kPa* *Slope: ~2.2 kPa mm^{-1}*	hMSCs (bone marrow)	Favorable stiffness range for hMSC differentiation: ~20 kPa for nerve cell, ~40 kPa for muscle cell, ~80 kPa for chondrocyte, and ~190 kPa for osteoblast	71
Temperature gradient during curing	PDMS	2D cell seeding	Continuous gradient across 12 mm distance on PMDS sheet *Indentation modulus: ~0.19-3.1 MPa* *Slope: ~242.5 kPa mm^{-1}*	rMSCs (bone marrow)	Osteogenic differentiation is influenced by stiffness, but also depends on the availability of appropriate adhesion molecules	70
Component redistribution						
Temperature gradient-driven	Alginate	-	Linear gradient across 600μm-wide hydrogel strip *E: ~10-80 kPa* *Slope: ~10-100 kPa mm^{-1}*	-	First proof-of-concept of exploiting thermophoresis phenomenon to pattern microscale stiffness gradients in soft hydrogels	73
Electric field-driven	β-sheet rich silk nanofibers (BSNF)	2D cell seeding on cut sections of gel cylinder	Continuous gradient along gel column (2 mm diameter, 10 mm height) *E (compressive): 20-130 kPa* *Slope: ~11 kPa mm^{-1}*	rMSCs (bone)	BSNF can be incorporated into different hydrogel systems. Tunable gradients of multiple bioactive cargos can also be achieved simultaneously	76
Micro-molding						
Hydrogel on topographically defined stiff supports	PA	2D cell seeding	Linear and nonlinear gradient pattern depending on topography of underlying support structure (e.g., step, beads, grooves)	CCL-92 mouse embryonic fibroblasts	15 μm is the critical depth below which cells will respond to the underlying substrate; this critical thickness is independent of gel's bulk shear modulus	78

Cell types: hADSC (human adipose-derived stem cells); hMSC (human mesenchymal stem cell); rMSC (rat mesenchymal stem cells)
Hydrogel types: GelMA (gelatin methacryloyl); PA (polyacrylamide); PAH/PAA (poly(allylamine hydrochloride)/poly(acylic acid)); PDMS (poly(dimethylsiloxane)); PVA/HA (polyvinyl alcohol/ hyaluronic acid)

2.4.1 Diffusion-based

Diffusion is among the most common strategy to create microscale mechanical gradients in soft hydrogels. This approach covers a broad family of techniques that, at some stage of the fabrication process, harness the passive movement of hydrogel precursor molecules from regions of high to low concentration to generate spatially varying compositions.

The most rudimentary implementation involves polymerizing two adjacent drops of polyacrylamide solution with different concentrations of acrylamide and its crosslinker, whereby diffusive mixing at the boundaries results in a continuous linear gradient (**Figure 2.4a**). Originally presented by Lo et al. in 2000[ref. 59], this coverslip "sandwiching" technique is still widely employed today given its simplicity and cost-effectiveness, but the resulting stiffness gradients can be extremely variable[60,80].

To enable more precise patterning, researchers subsequently explored microfluidic gradient generators with photopolymerization process (**Figure 2.4b**)[61,62]. Using this technique, a microfluidic network is designed to split and mix the precursor solutions in a controlled manner, generating stable streams of varying composition that combine at a single broad channel. By carefully tuning the system flow rates, the initial step profile observed at the inlet of the broad channel blurs into a smooth gradient by diffusion as the streams flow down the channel, which is then polymerized into stiffness gradient hydrogels via UV exposure. Although this method allows for fabrication of well-defined and relatively steep (~10 kPa mm^{-1}) gradients, they are more restricted in the achievable stiffness range and are cumbersome to operate, limiting widespread adoption[55].

A more straightforward approach to create microscale stiffness gradients is by sequential layering of partially polymerized hydrogels in a predefined mold. In this method, each gel layer has a distinct stiffness (controlled by varying the polymer and/ or crosslinker concentration), and a new layer is deposited before the previous layer has fully polymerized, allowing for diffusive mixing at the layer interface. For example, Ko et al. demonstrated this layer-by-layer stacking technique using photopolymerized hydrogels such as gelatin methacryloyl (GelMA) and poly(ethylene glycol) (PEG), showcasing their potential for 3D cell encapsulation applications[63]. Since the gradient

gel construct is still essentially composed of discrete layers, the final gradient can be a stepwise profile, or the UV intensity can be tuned to adjust the degree of diffusion at the interface, thereby resulting in continuous gradients. In another example, Hadden et al. employed a ramp-shaped mold and a two-step polymerization technique[64]. A first gel layer of varying thickness is first polymerized, on top of which a second gel layer is polymerized to form a 2D planar substrate (**Figure 2.4c**). In this case, a stiffness gradient is created due to the differential diffusion of unreacted acrylamide and its crosslinker across the varying thickness of the first gel layer. An inherent limitation of this technique is that the resulting gradient slope is relatively shallow (~0.5 to 8 kPa mm^{-1}), while the overall gel thickness (~1 mm) may pose challenges for high-magnification imaging. Nevertheless, these layering techniques are easy to implement without the need for clean-room facilities, making it an attractive option for biological laboratories.

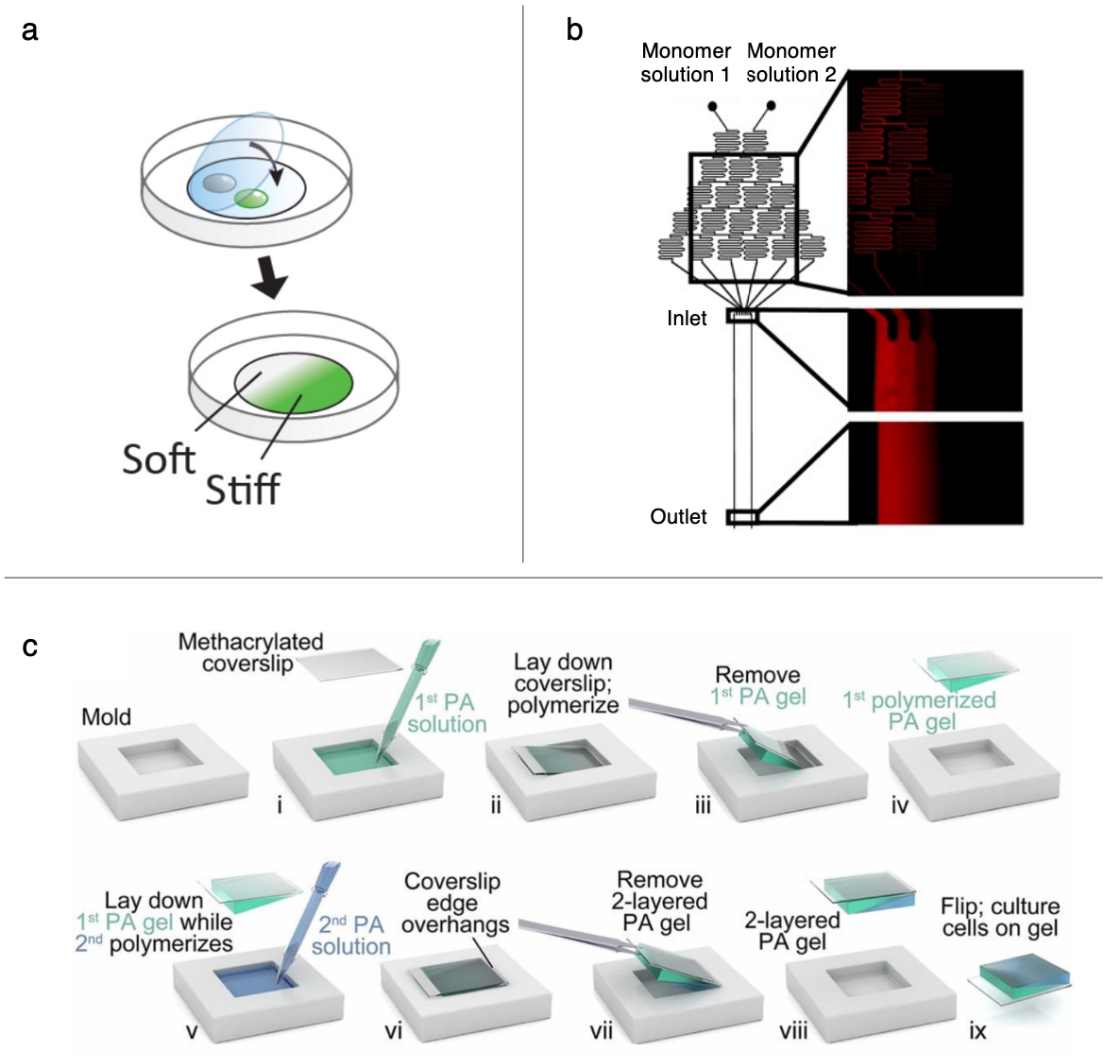

Figure 2.4: Representative examples of diffusion-based strategies to create gradient hydrogels. (a) The simplest approach involves polymerizing two adjacent drops of different hydrogel precursor solution between two flat surfaces[80]. (b) Microfluidic mixing of different hydrogel precursor solutions can be used to create narrow, steep gradients[61]. (c) Two-step polymerization of polyacrylamide hydrogels; the compositions of both layers could be either be the same or varied to tune the final stiffness gradient properties[64].

2.4.2 Controlled polymerization

Besides spatial modulation of the hydrogel precursor concentration, another main route to creating substrates with mechanical or architectural gradients relies on spatially controlling the degree of crosslinking during the crosslinking process.

Graded light exposure in combination with photopolymerizable hydrogels (e.g. polyacrylamide, GelMA) has been widely explored to generate microscale stiffness gradients in mechanobiology studies. This is achieved either by using photomasks patterned with varying degrees of transparency[65–67] or sliding an opaque photomask across the polymer solution at a controlled speed[68]. The sliding mask technique is one of the most flexible methods, allowing the creation of shallow (1-10 kPa mm^{-1}) to very steep (>200 kPa mm^{-1}) stiffness gradients, though its widespread adoption remains limited by the need for specialized equipment (e.g., stepper motor). In an interesting example, Dou et al. recently used the sliding mask technique to create polyacrylamide hydrogels with combined stiffness gradient and growth factor gradient in the lateral direction to probe glioma cell migration (**Figure 2.5a**)[69]. Compared to sliding photomasks, masks with patterned gray-intensity allow for a simpler fabrication process and a more well-defined stiffness profile (**Figure 2.5b**)[65]. However, the resolution of conventional photomask printing techniques limits these gels to a softer substrate range of ~1-20 kPa and shallow gradient strength of ~1 kPa mm^{-1} in practice[68].

Alternatively, temperature control-based techniques have also been proposed, including the application of a gradient temperature during the curing process of poly(dimethylsiloxane) (PDMS) and the repeated gradual freeze-thawing method[70,71]. Of note, the freeze-thawing method works by creating ice fronts that travel through the polymer solution to induce the formation of localized polymer crystallites that, in turn, facilitate network crosslinking among the PVA chains upon thawing (**Figure 2.5c**). This is possible due to the unique hydrogelation mechanism of polyvinyl alcohol (PVA). Oh et al. demonstrated this technique using a PVA/ hyaluronic acid (HA) composite to generate a wide stiffness gradient range of 20-200 kPa[ref. 71]. Gradual freezing of the PVA/HA solution within a cylindrical mold was accomplished via direct contact with liquid nitrogen at the bottom, allowing the freeze front to progress upward. The stiffness gradient properties can be tuned by controlling the freezing temperature,

freezing time, and the number of freeze-thawing cycles, thus offering a useful hydrogel patterning approach that does not require any specific laboratory equipment.

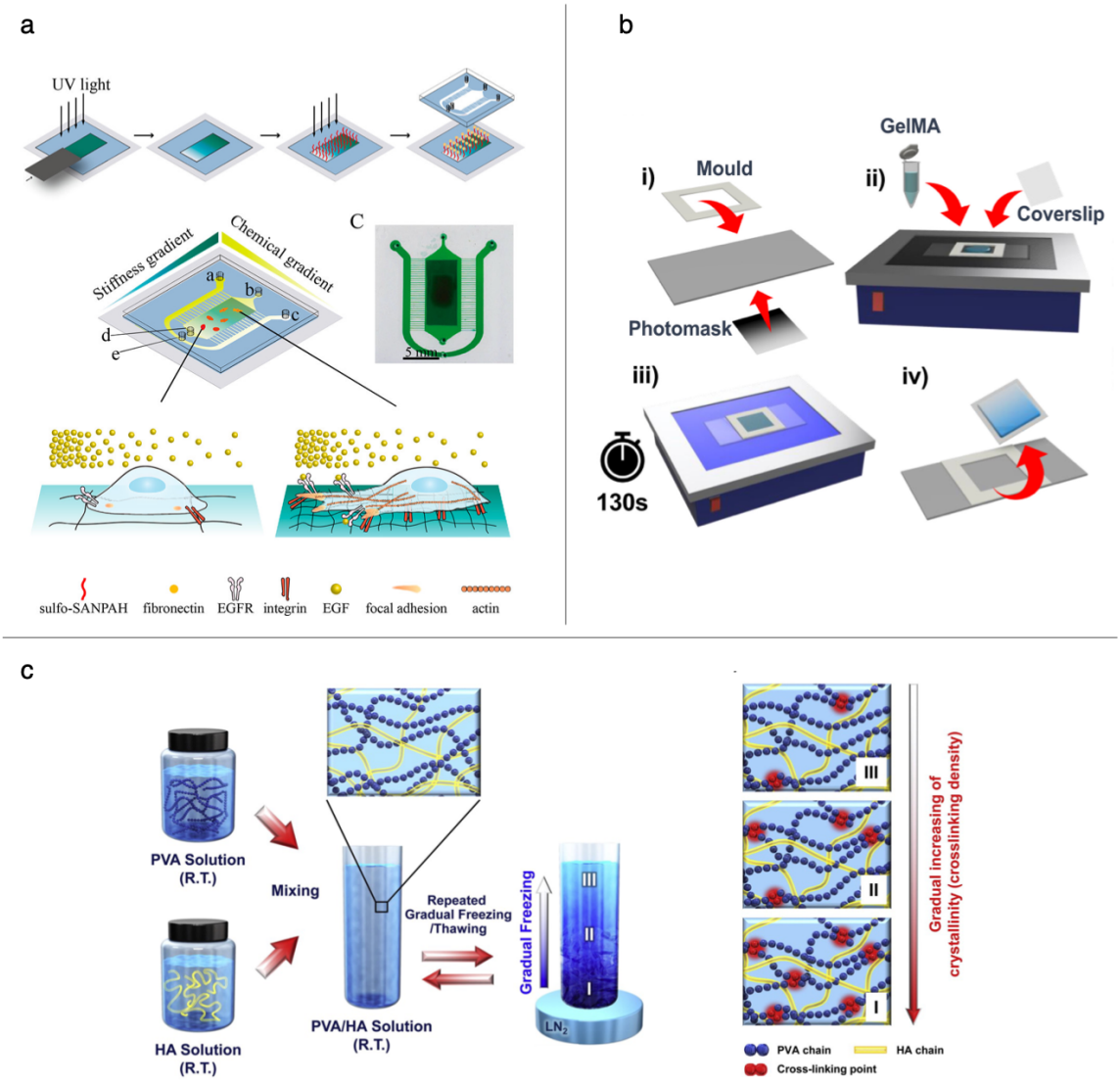

Figure 2.5: Representative examples of creating gradient hydrogels through controlled crosslinking. (a) Acrylamide/bis-acrylamide substrates with combined stiffness and chemical (epidermal growth factor) gradients; the stiffness gradient was formed using a sliding photomask technique whereas the chemical gradient was generated via microfluidics[69]. (b) Gradient hydrogel fabricated using a patterned gray-intensity photomask for photopolymerization of gelatin methacryloyl (GelMA)[65]. (c) Repeated freeze-thawing method to introduce transitions in crystallinity of polyvinyl alcohol/ hyaluronic acid (PVA/HA) hydrogels[71].

2.4.3 Component redistribution

Recently, there has also been a growing number of reports to create stiffness gradients by leveraging an external force to guide the redistribution of solutes within an initially homogenous precursor solution. By decoupling the gradient generation mechanism from the hydrogel crosslinking process, this family of techniques offer the promise of greater control and reproducibility compared to the previous methods.

One of the earliest concepts exploited shear flow in microfluidics to develop a compositional gradient, which can be preserved through subsequent photopolymerization[72]. The study employed fully passive means of driving flow within the microfluidic channel, which although greatly lowered the barrier of entry to microfluidic-based techniques, are subject to a high degree of inconsistency.

Driven by the unmet need to access platforms that allow a flexible yet reliable control over the gradient pattern and type of hydrogel, Vigolo et al. developed a fundamentally new technique that exploits the physical phenomenon of thermophoresis to fabricate gradient hydrogels with micron-scale geometries[74]. Unlike the gradual freeze-thawing method which relies on gradient temperatures to induce spatial variations in crosslinking density, the thermophoresis technique uses a controlled temperature gradient to actively direct the movement of precursor components in solution before gelation. As demonstration, stiffness gradient alginate hydrogels were fabricated in a 2-layered microfluidic device designed for on-chip temperature control (concentration gradient generation step) and slow release of calcium ions to facilitate hydrogel crosslinking (**Figure 2.6a**). In this method, the stiffness range and gradient slope can be tuned by controlling the polymer concentration and the strength of applied temperature gradient, respectively. Although thermophoresis is not currently a standardized method to fabricate stiffness gradients in mechanobiology studies, it is believed that the potential versatility with different hydrogel chemistries would be very useful in upcoming applications for investigating cell responses to more complex substrate mechanics (e.g., non-linear elastic materials[74]). To that end, there are critical improvements that must first be made, including simplifying the device operation and accelerating the process to identify optimal process conditions; both of these issues will go on to become the basis of this thesis.

On the other hand, emerging methods have sought to functionalize the biomaterial components, which can then be actively manipulated using externally applied forces via magnetic or electric fields, for example[75,76]. An interesting example from David Kaplan's group reported the simultaneous formation of compositional and mechanical gradients through electric field migration (**Figure 2.6b**)[76]. This method relies on the progressive movement of negatively charged β-sheet rich silk nanofibers (BSNF) that serve to fine-tune the mechanical gradients in a variety of base polymers (e.g. GelMA, N-isopropylacrylamide, amorphous silk nanofiber solution (ASNF)). Interestingly, the possibility to incorporate bioactive cargos (e.g., growth factors, gold nanoparticles) into the BSNF blocks can open new avenues to simultaneously define the biophysical and biochemical cues at micron-scale resolution, enhancing our capabilities to study cell mechanobiology behavior in a more physiologically relevant and dynamic context.

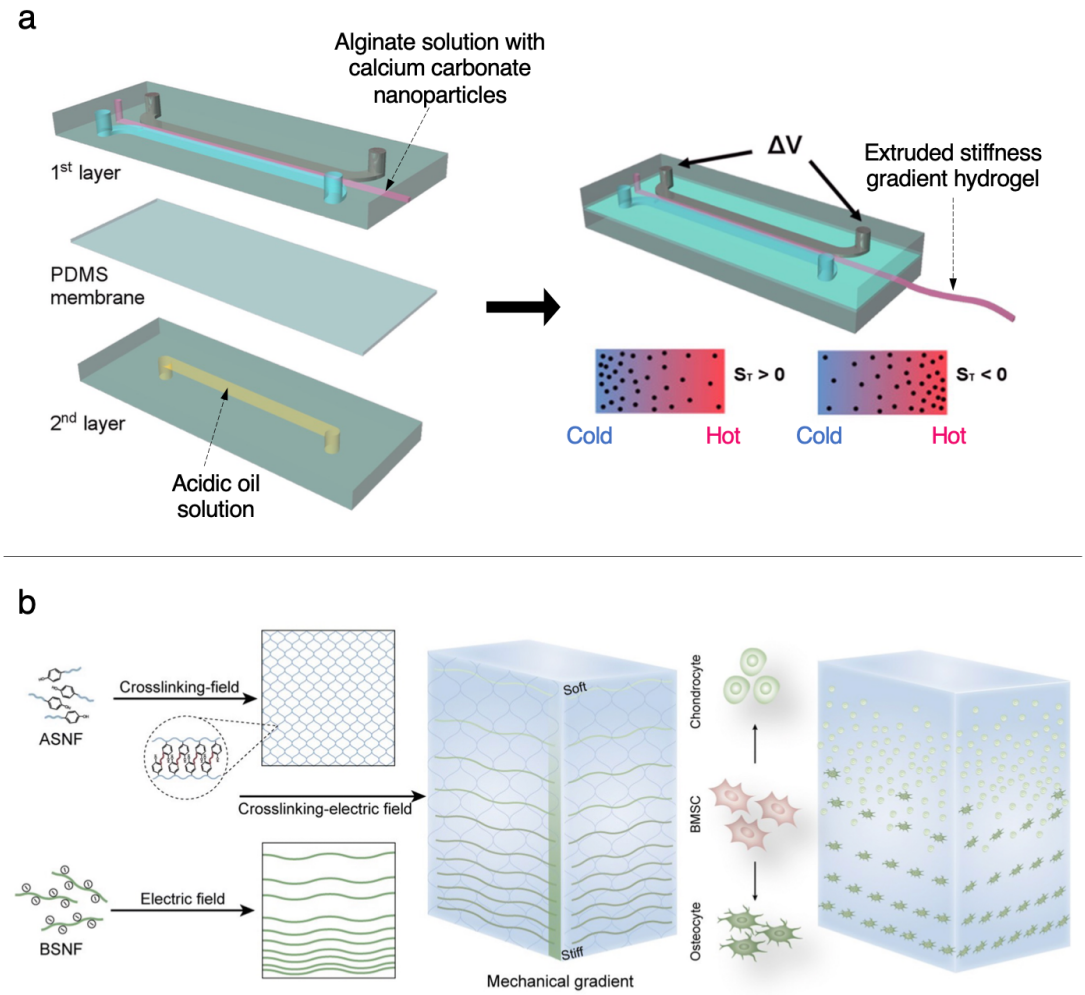

Figure 2.6: Representative examples of external force-driven component redistribution approach for gradient hydrogel fabrication. (a) Thermophoretic migration of solutes along temperature gradient, implemented in a PDMS microfluidic device with cooling (blue) and heating (grey) channels. The precursor molecules in solution can either accumulate toward the cold or hot side of the device, depending on the system's Soret coefficient (S_T)[74]. (b) Electrical-driven migration of negatively charge β-sheet rich silk nanofibers (BSNF) in amorphous silk nanofiber hydrogel solution under the influence of an electric field[76]. The BSNF blocks can be functionalized to create bioactive mechanical gradients for tissue engineering applications.

2.4.4 Micro-molding

Micro-molding is an alternative variation to the previously described hydrogel layering methods. This approach is based on creating abrupt changes in the gel thickness using microfabricated molds. It works on the principle that the extent to which an underlying (stiff) substrate is felt through a second layer of (compliant) material will vary as a function of the depth of the superficial compliant layer[77,78]. This method is particularly useful to generate step stiffness gradients of up to 300 kPa mm^{-1}. For example, Choi et al. demonstrated the use of micro-patterned SU-8 photoresist molds to generate alternating soft and stiff stripes in polyacrylamide hydrogels, which can be used to simulate the striations in muscle tissues[79]. Furthermore, the base substrate could also be patterned with different topographies to generate more complex gradient patterns, first proposed by Kuo et al. using a dispersed array of polystyrene microbeads which resulted in radial stiffness gradients (**Figure 2.7**)[78]. A main advantage of this approach is that gels with spatially varying stiffness but uniform pore size can be created. However, the differential hydrogel swelling may cause a considerable variation in the overall substrate thickness along the gradient, raising the question of whether cells are responding to stiffness or topographical cues. Moreover, it is important to note that when the gel thickness is <20 μm, cells can sense the underlying substrate[78]. This makes it difficult to evaluate the effective matrix stiffness that cells are sensing, which can explain why ultra-thin hydrogels are generally avoided in stiffness gradient studies.

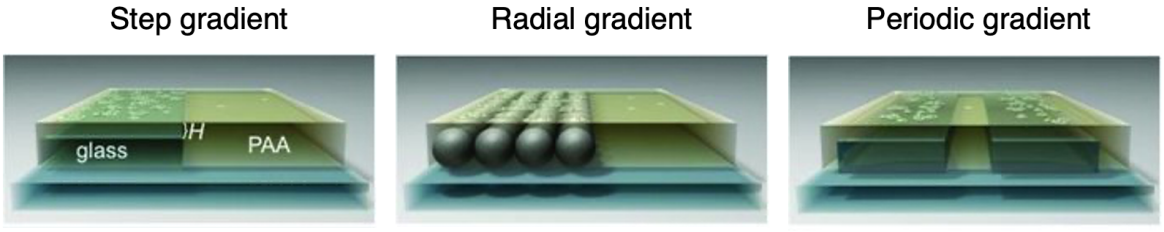

Figure 2.7: Representative examples of micro-molding methods to create mechanically patterned polyacrylamide (PAA) hydrogels. The apparent hydrogel stiffness varies as a function of the gel thickness (H)[79].

2.5 The present and future role of biophysical gradient hydrogels in mechanobiology research and applications

The mechanical environment of living tissues exhibits a high degree of spatial heterogeneity, and as such, mimicking these variations is fundamental to developing *in vitro* models with improved biological relevance. Over the last two decades, there have been numerous developments in hydrogel technology and fabrication strategies to recreate the microscale gradient properties in specific tissue contexts. Although the focus of this thesis is on mechanobiology applications, this chapter also draws on technologies in the adjacent field of tissue engineering that can be harnessed for spatial control and patterning of hydrogels. However, it should be noted that while the primary goal of tissue engineering is to build in physiological complexities to guide functional tissue formation, gradient hydrogels used in mechanobiology research are generally simpler with the aim of understanding how cells respond to isolated mechanical cues in a dose-dependent manner. Nonetheless, this highlights the growing synergy between mechanobiology and tissue engineering, emphasizing the need for continued progress in mechanobiology research toward realizing designer biomaterials in biology and medicine[48].

In the context of mechanobiology, the development of stiffness gradient hydrogels has taken off in three main directions: 1) fundamental studies of cell durotaxis, 2) high throughput screening of cell mechanoresponses, and 3) disease modeling.

2.5.1 Durotaxis studies

In vitro stiffness gradient hydrogels have become indispensable tools for probing the diverse cell migratory behavior, especially given the technical difficulties associated with *in vivo* durotaxis studies[41,42]. Yet, durotaxis is prevalent in complex biological processes, from embryonic development to immune response and cancer metastasis. The study of cell durotaxis requires analysis on a wide range of stiffness gradients slopes (from <1 kPa mm^{-1} to ~400 kPa mm^{-1}), which are most commonly achieved using photopolymerization methods and leveraging the highly tunable stiffness (~1-200 kPa) of polyacrylamide hydrogels. In a notable example, Odde et al. used

fibronectin-coated polyacrylamide stiffness gradients to demonstrate the negative durotactic behavior of glioma cells from stiff-to-soft environments[80]. The findings revealed that cells tend to migrate toward an optimal stiffness on the substrate and their specific durotactic responses can vary depending on the cellular contractile and adhesive machinery. This likely explains the diverse durotactic behaviors (i.e., positive durotaxis, negative durotaxis, adurotaxis) observed in different cell types[81]. In another example, step-gradient hydrogels with alternating soft and stiff regions were used to elucidate how weakly adherent cancer cells can migrate against stiffness gradients, leading to enhanced metastatic potential[82]. Furthermore, other studies have shown how the slope of stiffness gradients[55,83,84] can influence the propensity of cell durotaxis, and further unveiled the distinct behaviors of cell clusters compared to single cells[39,85,86].

2.5.2 Reductionist screening platform

Stiffness gradient hydrogels are also a powerful platform for screening cell-substrate interactions along a continuum of mechanical cues[61,70]. They present the opportunity to uncover unique insights that might be missed from testing discrete values. Importantly, by removing the need to compare multiple discrete conditions across separate samples, gradient hydrogels allow for greatly reduced experimental variability, making them an attractive solution for scaling complex biological experiments. For such applications, the slope of stiffness gradient should be designed below the cell durotactic threshold to avoid the confounding effect of cell migration in the biological outcomes. For example, Tan et al. used a 2D linear stiffness gradient hydrogel (~2-30 kPa; 4 kPa mm^{-1}) fabricated using the two-step polymerization method to study the interplay between stiffness and ECM protein type on the mechanosensitivity of human airway smooth muscle cells, with direct links to airway remodeling in obstructive air diseases[52].

Considering that cells in native tissues reside in a 3D matrix, recent studies have also explored strategies to enable live cell encapsulation within stiffness gradient hydrogels to better mimic the complex matrix environments *in vivo*. Particularly, the information gained from such 3D culture studies can complement those found in 2D cultures, with

potential far reaching impacts to design hydrogels for advanced disease models and regenerative therapies[87]. However, despite the widespread use of polyacrylamide and PDMS substrates for 2D mechanobiology studies, they are unsuitable for cell encapsulation due to inherent cytotoxicity and restricted capacity for cell-mediated matrix remodeling[61,70]. To overcome this challenge, researchers have turned to alternative hydrogel types (e.g. GelMA, decellularized ECM), which in turn also drove the emergence of new gradient patterning strategies[50,65,88]. For instance, Vahala et al. demonstrated the culture of non-metastatic breast cancer (MCF-7) spheroids within homogenous allylated gelatin (GelAGE) hydrogels for 5 days before exposing them through a graded UV photomask to induce a linear stiffness gradient, simulating both dynamic spatial and temporal changes encountered in tumor microenvironments[88]. In an interesting approach, Daniel Alge's group combined microfluidic mixing and droplet generation modules to create spatial gradients in microporous annealed particle (MAP) hydrogels that maintained gradient stability after implantation into a mouse femoral defect, highlighting the potential of gradient hydrogels for cell-based therapy[89].

2.5.3 Disease modeling

A major upcoming application of stiffness gradient hydrogels is in developing complex tissue models. While conventional disease modeling approaches largely focused on recreating a single tissue region, microfabricated gradient gels can better recapitulate the cellular-scale variation across complex tissue interfaces. The work by Zhang et al. is a good example that leverages stiffness gradients of different slopes (50 kPa mm^{-1} vs. 250 kPa mm^{-1}) to model the weakened gradient across the periodontal ligament (PDL)-alveolar bone (AB) enthesis in periodontitis compared to the healthy state[51]. These systems enabled new insights into the molecular mechanisms underpinning mesenchymal stem cell (MSC) immunoregulation in response to stiffness changes at the PDL-AB enthesis, which were practically impossible to achieve using conventional bulk hydrogels. Beyond static gradient hydrogel studies, researchers have also devised more sophisticated platforms that allow for greater spatiotemporal control in the gradient properties. For example, Cao et al. recently proposed a gradient platform based on magnetorheological elastomers for dynamic and reversible tuning of stiffness gradients[90]. The platform was applied to study the combined effects of

antifibrotic drug dosing and stiffness changes on cardiac fibroblasts under post-myocardial infarction conditions, demonstrating its clinical relevance for drug screening. To further enable modeling of the structure-to-function relationships in native tissues, Soliman et al. exploited droplet microfluidics to create radial stiffness gradients in shape-controlled microgels[91]. A breast cancer model in which MCF-7 cancer cells were encapsulated within the microgels revealed a stiffness gradient-induced phenotypic plasticity in cell aggregation, implying a contributing role of mechanical heterogeneity in cancer metastasis. Together, these examples underscore the significant value of incorporating microscale physical gradients to enable more physiologically relevant *in vitro* tissue models.

2.5.4 Probing beyond stiffness

Although ECM stiffness is established as a major regulator of cell behavior, recent studies have highlighted viscoelasticity[94,74] and fibrous microstructure[95] as key emerging matrix cues influencing cell function and behavior. Thus, it is expected that future development of gradient hydrogel systems will transition away from the purely elastic planar substrates (e.g., polyacrylamide, PDMS) toward more complex hydrogel chemistries and biofunctionalization approaches that can emulate these intrinsic features of native ECM.

Indeed, living tissues exhibit a range of stress-relaxation properties (i.e., reduced resistance to mechanical deformation over time)[36]. Studies have postulated that the viscous dissipation is critical in permitting cells to apply cellular traction forces and to remodel their surrounding matrix[96,97]. These phenomena might partially explain why more degrading, physically crosslinked hydrogels (e.g., collagen, supramolecular assemblies) have been amongst the more successful biomaterials in regenerative medicine to date[98]. Moreover, the viscoelastic behavior of native ECM is also related to its fibrous architecture. The forces exerted by cells on the surrounding fiber structures can lead to transient nonlinear strain stiffening of the matrix, which have been implicated in self-generated stiffness gradients[99] and long-range cell communication[100]. Therefore, deliberate efforts to introduce these attributes into

engineered gradient hydrogel systems will be key in enabling a more accurate interpretation of the dynamic cell-matrix interactions.

2.5.5 Technical challenges

Despite significant promise, precise and reliable fabrication of stiffness gradients remains a major challenge that hampers their widespread adoption in mechanobiology research. Diffusion-based methods appear to be the simplest among the suite of fabrication techniques but exhibit a high degree of variability and lack controllability. Some researchers have tried to address this issue through highly sophisticated, digitalized photolithography systems[92]; however, progress has been slow, and adoption has been restricted by technical complications and cost issues. Clearly, each fabrication technique has its own set of tradeoffs between achievable stiffness ranges, generated gradient shape fidelity, and ease of operation. In fact, the common practice now is to combine multiple different techniques, each of which covers a specific range of the broad biological mechanical landscape[55]. Improvements could be made in the development of gradient hydrogel platforms to make them more generalizable and accessible for biological research.

Development of fabrication strategies should also be paired with advances in analytical characterization techniques. The ability to probe a continuum of material cues on gradient hydrogels is a double-edged sword, because it hinders the use of many molecular assays such as PCR and Western blot. Instead, most gradient hydrogel studies rely on live-cell imaging and immunostaining techniques to inform cell state and responses. However, it can be difficult to precisely correlate the local substrate stiffness with the cellular responses due to the lack of a direct stiffness indicator along the gradient hydrogel. The current gold standard technique for measuring the elastic modulus of soft hydrogels is by atomic force microscopy (AFM)[93]; however, this requires physical nanoindentation on the hydrogel surface and is very time-consuming, making it practically intractable to characterize every sample replicate for large-scale cell studies. In this respect, new experimental workflows that can link the spatially resolved analyses of both material properties and cellular biological outcomes will be highly valuable in enhancing the applicability of gradient

hydrogel platforms. As a potential solution, this thesis will explore the use of fluorescently labelled polymers in combination of the thermophoresis process; the fluorescence signal could provide a material-intrinsic indicator which not only allows real-time visualization of the gradient formation process, but also enables visual assessment of the resulting stiffness gradient by standard fluorescence microscopy.

Finally, in order to increase the *in vivo* relevance of gradient hydrogel systems, better ways of associating the biological readouts obtained from 2D/ 3D hydrogel culture studies with the mechanics of biological tissues should be developed. Ideally, stiffness characterization of the (*ex-vivo*) tissue samples and hydrogel substrates should be performed using the same technique (e.g. AFM), though this can be technically very challenging with uneven tissue surfaces[52]. On the other hand, other analytical modalities could be used on the tissue samples to extract additional relevant biological signals. For example, in the previously described study by Zhang et al.[51], they used Raman microprobe spectroscopy (RMS) to show that the lower stiffness gradient of PDL-AB enthesis in periodontitis is associated with lower mineral content gradient across the tissue interface. Progress in this direction could further enhance confidence in the causal relationships deduced from *in vitro* studies and will be critical in enabling deeper mechanistic insights into cell mechanobiology.

2.6 Summary

This chapter provides a snapshot of how advances in mechanobiology research is fueled by the continued progress and refinement of biomaterials-based experimentation platforms. Precise and reproducible fabrication of stiffness gradients remains a critical challenge to successful applications of microengineered gradient hydrogel technology. As the field strives toward a better understanding of the complex cell-microenvironment interactions involved in diverse physiological and pathological processes, the function of gradient hydrogel systems will also expand beyond linear stiffness gradients and purely elastic substrates.

To that end, a flexible yet reliable fabrication technique that can adapt to different hydrogel chemistries and wide-range gradient profiles would enable gradient hydrogel culture models to be developed more efficiently. The fundamental issue of precisely matching the spatial material cues and biological responses should also be first addressed to improve practical utility. These themes will be central to the development of this thesis.

References

1. Frantz, C., Stewart, K. M. & Weaver, V. M. The extracellular matrix at a glance. *J Cell Sci* **123**, 4195–4200 (2010).

2. Alcaraz, J. *et al.* Laminin and biomimetic extracellular elasticity enhance functional differentiation in mammary epithelia. *EMBO J* **27**, 2829–2838 (2008).

3. Midwood, K. S., Williams, L. V. & Schwarzbauer, J. E. Tissue repair and the dynamics of the extracellular matrix. *Int J Biochem Cell Biol* **36**, 1031–1037 (2004).

4. Przybyla, L., Lakins, J. N. & Weaver, V. M. Tissue Mechanics Orchestrate Wnt-Dependent Human Embryonic Stem Cell Differentiation. *Cell Stem Cell* **19**, 462–475 (2016).

5. Zhao, W., Li, X., Liu, X., Zhang, N. & Wen, X. Effects of substrate stiffness on adipogenic and osteogenic differentiation of human mesenchymal stem cells. *Mater Sci Eng C* **40**, 316–323 (2014).

6. Khetan, S. *et al.* Degradation-mediated cellular traction directs stem cell fate in covalently crosslinked three-dimensional hydrogels. *Nat Mater* **12**, 458–465 (2013).

7. Han, P. *et al.* Five piconewtons: The difference between osteogenic and adipogenic fate choice in human mesenchymal stem cells. *ACS Nano* **13**, 11129–11143 (2019).

8. Van Den Berg, A., Craighead, H., Yang, P., Young, E. W. K. & Beebe, D. J. Fundamentals of microfluidic cell culture in controlled microenvironments. *Chem Soc Rev* **39**, 1036–1048 (2010).

9. Yang, J., Pan, X., Wang, L. & Yu, G. Alveolar cells under mechanical stressed niche: critical contributors to pulmonary fibrosis. *Mol Med* **26**, 95 (2020).

10. Kutys, M. L. & Chen, C. S. Forces and mechanotransduction in 3D vascular biology. *Curr Opin Cell Biol* **42**, 73–79 (2016).

11. Yin, Q. *et al.* Application of microfluidic technologies in veterinary science with a view toward development of animal-on-a-chip models. *VIEW* **6**, 20240073 (2025).

12. Madl, C. M., Heilshorn, S. C. & Blau, H. M. Bioengineering strategies to accelerate stem cell therapeutics. *Nature* **557**, 335–342 (2018).

13. Scadden, D. T. The stem-cell niche as an entity of action. *Nature* **441**, 1075–1079 (2006).

14. Morrison, S. J. & Spradling, A. C. Stem cells and niches: Mechanisms that promote stem cell maintenance throughout life. *Cell* **132**, 598–611 (2008).

15. Kechagia, J. Z., Ivaska, J. & Roca-Cusachs, P. Integrins as biomechanical sensors of the microenvironment. *Nat Rev Mol Cell Biol* **20**, 457–473 (2019).

16. Angulo-Urarte, A., van der Wal, T. & Huveneers, S. Cell-cell junctions as sensors and transducers of mechanical forces. *BBA - Biomembranes* **1862**, 183316 (2020).

17. Atcha, H. *et al.* Ion channel mediated mechanotransduction in immune cells. *Curr Opin Solid State Mater Sci* **25**, 100951 (2021).

18. Killaars, A. R., Walker, C. J. & Anseth, K. S. Nuclear mechanosensing controls MSC osteogenic potential through HDAC epigenetic remodeling. *Proc Natl Acad Sci* **117**, 21258–21266 (2020).

19. Werner, M. *et al.* Surface curvature differentially regulates stem cell migration and differentiation via altered attachment morphology and nuclear deformation. *Adv Sci* **4**, 1600347 (2017).

20. Gupta, M. *et al.* Adaptive rheology and ordering of cell cytoskeleton govern matrix rigidity sensing. *Nat Commun* **6**, 7525 (2015).

21. Pittman, M. *et al.* Membrane ruffling is a mechanosensor of extracellular fluid viscosity. *Nat Phys* **18**, 1112–1121 (2022).

22. De Belly, H., Paluch, E. K. & Chalut, K. J. Interplay between mechanics and signalling in regulating cell fate. *Nat Rev Mol Cell Biol* **23**, 465–480 (2022).

23. Hayward, M. K., Muncie, J. M. & Weaver, V. M. Tissue mechanics in stem cell fate, development, and cancer. *Dev Cell* **56**, 1833–1847 (2021).

24. Sun, Y., Chen, C. S. & Fu, J. Forcing stem cells to behave: A biophysical perspective of the cellular microenvironment. *Annu Rev Biophys* **41**, 519–542 (2012).

25. Dupont, S. *et al.* Role of YAP/TAZ in mechanotransduction. *Nature* **474**, 179–184 (2011).

26. McBeath, R., Pirone, D. M., Nelson, C. M., Bhadriraju, K. & Chen, C. S. Cell Shape, Cytoskeletal Tension, and RhoA Regulate Stem Cell Lineage Commitment. *Dev Cell* **6**, 483–495 (2004).

27. Vining, K. H. & Mooney, D. J. Mechanical forces direct stem cell behaviour in development and regeneration. *Nat Rev Mol Cell Biol* **18**, 728–742 (2017).

28. Chaudhuri, O., Cooper-White, J., Janmey, P. A., Mooney, D. J. & Shenoy, V. B. Effects of extracellular matrix viscoelasticity on cellular behaviour. *Nature* **584**, 535–546 (2020).

29. Shin, J. W. & Mooney, D. J. Extracellular matrix stiffness causes systematic variations in proliferation and chemosensitivity in myeloid leukemias. *Proc Natl Acad Sci* **113**, 12126–12131 (2016).

30. Buscemi, L. *et al.* The single-molecule mechanics of the latent TGF-β1 complex. *Curr Biol* **21**, 2046–2054 (2011).

31. Pelham, R. J. & Wang, Y. L. Cell locomotion and focal adhesions are regulated by substrate flexibility. *Proc Natl Acad Sci* **94**, 13661–13665 (1997).

32. Lo, C. M., Wang, H. B., Dembo, M. & Wang, Y. L. Cell movement is guided by the rigidity of the substrate. *Biophys J* **79**, 144–152 (2000).

33. Schrader, J. *et al.* Matrix stiffness modulates proliferation, chemotherapeutic response, and dormancy in hepatocellular carcinoma cells. *Hepatology* **53**, 1192–1205 (2011).

34. Engler, A. J., Sen, S., Sweeney, H. L. & Discher, D. E. Matrix elasticity directs stem cell lineage specification. *Cell* **126**, 677–689 (2006).

35. Lenne, P. F. & Trivedi, V. Sculpting tissues by phase transitions. *Nat Commun* **13**, 664 (2022).

36. Guimarães, C. F., Gasperini, L., Marques, A. P. & Reis, R. L. The stiffness of living tissues and its implications for tissue engineering. *Nat Rev Mater* **5**, 351–370 (2020).

37. Baumgart, F. Stiffness - An unknown world of mechanical science? *Injury* **31**, 14–84 (2000).

38. Irianto, J., Pfeifer, C. R., Xia, Y. & Discher, D. E. SnapShot: Mechanosensing Matrix. *Cell* **165**, 1820-1820.e1 (2016).

39. Sunyer, R. *et al.* Collective cell durotaxis emerges from long-range intercellular force transmission. *Science* **353**, 1157–1161 (2016).

40. Levental, K. R. *et al.* Matrix Crosslinking Forces Tumor Progression by Enhancing Integrin Signaling. *Cell* **139**, 891–906 (2009).

41. Sunyer, R. & Trepat, X. Durotaxis. *Curr Biol* **30**, R383–R387 (2020).

42. Shellard, A. & Mayor, R. Durotaxis: The Hard Path from In Vitro to In Vivo. *Dev Cell* **56**, 227–239 (2021).

43. Genin, G. M. *et al.* Functional grading of mineral and collagen in the attachment of tendon to bone. *Biophys J* **97**, 976–985 (2009).

44. Thomopoulos, S., Williams, G. R., Gimbel, J. A., Favata, M. & Soslowsky, L. J. Variation of biomechanical, structural, and compositional properties along the tendon to bone insertion site. *J Orthop Res* **21**, 413–419 (2003).

45. Lai, A. *et al.* Endothelial Response to the Combined Biomechanics of Vessel Stiffness and Shear Stress Is Regulated via Piezo1. *ACS Appl Mater Interfaces* **15**, 59103–59116 (2023).

46. Blache, U. *et al.* Engineered hydrogels for mechanobiology. *Nat Rev Methods Primers* **2**, 98 (2022).

47. Qazi, T. H. *et al.* Programming hydrogels to probe spatiotemporal cell biology. *Cell Stem Cell* **29**, 678–691 (2022).

48. Li, L., Eyckmans, J. & Chen, C. S. Designer biomaterials for mechanobiology. *Nat Mater* **16**, 1164–1168 (2017).

49. Zhang, H., Lin, F., Huang, J. & Xiong, C. Anisotropic stiffness gradient-regulated mechanical guidance drives directional migration of cancer cells. *Acta Biomater* **106**, 181–192 (2020).

50. Zhao, F. *et al.* Fibroblast alignment and matrix remodeling induced by a stiffness gradient in a skin-derived extracellular matrix hydrogel. *Acta Biomater* **182**, 67–80 (2024).

51. Zhang, H. *et al.* Cellular-Scale Matrix Stiffness Gradient at Soft-Hard Tissue Interfaces Regulates Immunophenotype of Mesenchymal Stem Cells. *Adv Funct Mater* **34**, 2309676 (2024).

52. Tan, Y. H. *et al.* Stiffness Mediated-Mechanosensation of Airway Smooth Muscle Cells on Linear Stiffness Gradient Hydrogels. *Adv Healthc Mater* **13**, 2304254 (2024).

53. García, S. *et al.* Generation of stable orthogonal gradients of chemical concentration and substrate stiffness in a microfluidic device. *Lab Chip* **15**, 2606–2614 (2015).

54. Berry, M. F. *et al.* Mesenchymal stem cell injection after myocardial infarction improves myocardial compliance. *Am J Physiol Heart Circ Physiol* **290**, H2196-203 (2006).

55. Vincent, L. G., Choi, Y. S., Alonso-Latorre, B., Del Álamo, J. C. & Engler, A. J. Mesenchymal stem cell durotaxis depends on substrate stiffness gradient strength. *Biotechnol J* **8**, 472–484 (2013).

56. Li, C., Ouyang, L., Armstrong, J. P. K. & Stevens, M. M. Advances in the fabrication of biomaterials for gradient tissue engineering. *Trends Biotechnol* **39**, 150–164 (2021).

57. Kühn, S. *et al.* Cell-instructive multiphasic gel-in-gel materials. *Adv Funct Mater* **30**, 1908857 (2020).

58. Xia, T., Liu, W. & Yang, L. A review of gradient stiffness hydrogels used in tissue engineering and regenerative medicine. *J Biomed Mater Res A* **105**, 1799–1812 (2017).

59. Lo, C. M., Wang, H. B., Dembo, M. & Wang, Y. L. Cell movement is guided by the rigidity of the substrate. *Biophys J* **79**, 144–152 (2000).

60. Barber-Pérez, N. *et al.* Mechano-responsiveness of fibrillar adhesions on stiffness-gradient gels. *J Cell Sci* **133**, jcs242909 (2020).

61. Burdick, J. A., Khademhosseini, A. & Langer, R. Fabrication of gradient hydrogels using a microfluidics/photopolymerization process. *Langmuir* **20**, 5153–5156 (2004).

62. Zaari, N., Rajagopalan, P., Kim, S. K., Engler, A. J. & Wong, J. Y. Photopolymerization in microfluidic gradient generators: Microscale control of substrate compliance to manipulate cell response. *Adv Mater* **16**, 2133–2137 (2004).

63. Ko, H. *et al.* A simple layer-stacking technique to generate biomolecular and mechanical gradients in photocrosslinkable hydrogels. *Biofabrication* **11**, 025014 (2019).

64. Hadden, W. J. *et al.* Stem cell migration and mechanotransduction on linear stiffness gradient hydrogels. *Proc Natl Acad Sci* **114**, 5647–5652 (2017).

65. Chin, I. L. *et al.* Volume adaptation of neonatal cardiomyocyte spheroids in 3D stiffness gradient GelMA. *J Biomed Mater Res A* **111**, 801–813 (2023).

66. Major, L. G. *et al.* Volume adaptation controls stem cell mechanotransduction. *ACS Appl Mater Interfaces* **11**, 45520–45530 (2019).

67. Marklein, R. A. & Burdick, J. A. Spatially controlled hydrogel mechanics to modulate stem cell interactions. *Soft Matter* **6**, 136–143 (2009).

68. Sunyer, R., Jin, A. J., Nossal, R. & Sackett, D. L. Fabrication of Hydrogels with Steep Stiffness Gradients for Studying Cell Mechanical Response. *PLoS One* **7**, e46107 (2012).

69. Dou, J., Mao, S., Li, H. & Lin, J. M. Combination stiffness gradient with chemical stimulation directs glioma cell migration on a microfluidic chip. *Anal Chem* **92**, 892–898 (2020).

70. Wang, P. Y., Tsai, W. B. & Voelcker, N. H. Screening of rat mesenchymal stem cell behaviour on polydimethylsiloxane stiffness gradients. *Acta Biomater* **8**, 519–530 (2012).

71. Oh, S. H., An, D. B., Kim, T. H. & Lee, J. H. Wide-range stiffness gradient PVA/HA hydrogel to investigate stem cell differentiation behavior. *Acta Biomater* **35**, 23–31 (2016).

72. He, J. *et al.* Rapid generation of biologically relevant hydrogels containing long-range chemical gradients. *Adv Funct Mater* **20**, 131–137 (2010).

73. Vigolo, D., Ramakrishna, S. N. & DeMello, A. J. Facile tuning of the mechanical properties of a biocompatible soft material. *Sci Rep* **9**, 7125 (2019).

74. Chaudhuri, O. *et al.* Hydrogels with tunable stress relaxation regulate stem cell fate and activity. *Nat Mater* **15**, 326–334 (2016).

75. Li, C. *et al.* Glycosylated superparamagnetic nanoparticle gradients for osteochondral tissue engineering. *Biomaterials* **176**, 24–33 (2018).

76. Xu, G. *et al.* Electric field-driven building blocks for introducing multiple gradients to hydrogels. *Protein Cell* **11**, 267–285 (2020).

77. Janarthanan, G. *et al.* How deeply cells feel: methods for thin gels. *J Phys Condens Matter* **22**, 194116 (2010).

78. Kuo, C. H. R., Xian, J., Brenton, J. D., Franze, K. & Sivaniah, E. Complex stiffness gradient substrates for studying mechanotactic cell migration. *Adv Mater* **24**, 6059–6064 (2012).

79. Choi, Y. S. et al. The alignment and fusion assembly of adipose-derived stem cells on mechanically patterned matrices. Biomaterials **33**, 6943–6951 (2012).

80. Isomursu, A. *et al.* Directed cell migration towards softer environments. *Nat Mater* **21**, 1081–1090 (2022).

81. Mathieu, M., Isomursu, A. & Ivaska, J. Positive and negative durotaxis – mechanisms and emerging concepts. *J Cell Sci* **137**, jcs261919 (2024).

82. Yeoman, B. *et al.* Adhesion strength and contractility enable metastatic cells to become adurotactic. *Cell Rep* **34**, 108816 (2021).

83. Hakeem, R. M. *et al.* A Photopolymerized Hydrogel System with Dual Stiffness Gradients Reveals Distinct Actomyosin-Based Mechano-Responses in Fibroblast Durotaxis. *ACS Nano* **17**, 197–211 (2023).

84. Moriyama, K. & Kidoaki, S. Cellular Durotaxis Revisited: Initial-Position-Dependent Determination of the Threshold Stiffness Gradient to Induce Durotaxis. *Langmuir* **35**, 7478–7486 (2019).

85. Pallarès, M. E. *et al.* Stiffness-dependent active wetting enables optimal collective cell durotaxis. *Nat Phys* **19**, 279–289 (2022).

86. Balcioglu, H. E. *et al.* A subtle relationship between substrate stiffness and collective migration of cell clusters. *Soft Matter* **16**, 1825–1839 (2020).

87. Huebsch, N. Translational mechanobiology: Designing synthetic hydrogel matrices for improved in vitro models and cell-based therapies. *Acta Biomater* **94**, 97–111 (2019).

88. Vahala, D. *et al.* 3D Volumetric Mechanosensation of MCF7 Breast Cancer Spheroids in a Linear Stiffness Gradient GelAGE. *Adv Healthc Mater* **12**, 2301506 (2023).

89. Xin, S., Dai, J., Gregory, C. A., Han, A. & Alge, D. L. Creating Physicochemical Gradients in Modular Microporous Annealed Particle Hydrogels via a Microfluidic Method. *Adv Funct Mater* **30**, 1907102 (2020).

90. Cao, Z., Clark, A. T., Vite, A. & Corbin, E. A. A Dynamic Gradient Stiffness Material Platform to Manipulate Cardiac Fibroblasts' Spatio-Temporal Behavior. *Adv Funct Mater* **34,** 2402808 (2024).

91. Soliman, B. G. *et al.* Droplet-based microfluidics for engineering shape-controlled hydrogels with stiffness gradient. *Biofabrication* **16**, 045026 (2024).

92. Norris, S. C. P., Tseng, P. & Kasko, A. M. Direct Gradient Photolithography of Photodegradable Hydrogels with Patterned Stiffness Control with Submicrometer Resolution. *ACS Biomater Sci Eng* **2**, 1309–1318 (2016).

93. Norman, M. D. A., Ferreira, S. A., Jowett, G. M., Bozec, L. & Gentleman, E. Measuring the elastic modulus of soft culture surfaces and three-dimensional hydrogels using atomic force microscopy. *Nat Protoc* **16**, 2418–2449 (2021).

94. Charrier, E. E., Pogoda, K., Wells, R. G. & Janmey, P. A. Control of cell morphology and differentiation by substrates with independently tunable elasticity and viscous dissipation. *Nat Commun* **9**, 449 (2018).

95. Davidson, M. D. *et al.* Programmable and contractile materials through cell encapsulation in fibrous hydrogel assemblies. *Sci Adv* **7**, eabi8157 (2021).

96. Huebsch, N. *et al.* Harnessing traction-mediated manipulation of the cell/matrix interface to control stem-cell fate. *Nat Mater* **9**, 518–526 (2010).

97. Loebel, C., Mauck, R. L. & Burdick, J. A. Local nascent protein deposition and remodelling guide mesenchymal stromal cell mechanosensing and fate in three-dimensional hydrogels. *Nat Mater* **18**, 883–891 (2019).

98. Boekhoven, J., Stupp, S. I., Stupp, S. I. & Boekhoven, J. 25th Anniversary Article: Supramolecular Materials for Regenerative Medicine. *Adv Mater* **26**, 1642–1659 (2014).

99. Clark, A. G. *et al.* Self-generated gradients steer collective migration on viscoelastic collagen networks. *Nat Mater* **21**, 1200–1210 (2022).

100. Pakshir, P. *et al.* Dynamic fibroblast contractions attract remote macrophages in fibrillar collagen matrix. *Nat Commun* **10**, 1850 (2019).

Chapter 3

Experimental Methods and Procedures

This chapter presents the general experimental techniques and procedures used throughout the thesis. The chapter begins with a comprehensive list of materials used for all experiments, followed by a brief overview of the principles of thermophoresis. Then, the microfluidic platform design and fabrication are described, along with the suite of common methods used across multiple studies.

More specialized methods or specific modifications, including details on the sample preparation and process conditions for each study, are provided in the corresponding results chapters.

3.1 Materials

Table 3.1 lists the chemical reagents and substrates used for all the experiments in this thesis. The materials were sourced from Australia, unless stated otherwise.

Table 3.1: Summary of the details of materials used in this thesis.

Material	Supplier	Product code
Bovine serum albumin (BSA)	Sigma-Aldrich	A3858-10G
Calcein AM	Invitrogen (UK)	C1430
Calcium chloride	Sigma-Aldrich	C4901-100G
Dibutyltin dilaurate (DBTDL)	Sigma-Aldrich	291234-25G
Dimethyl sulfoxide (DMSO)	AJAX FineChem	2225-500ML
Dulbecco's Modified Eagle Medium (DMEM, high glucose, pyruvate)	Gibco	11995065-500ML
Dulbecco's phosphate buffered saline (DPBS)	Sigma-Aldrich	D8537-500ML
1-ethyl-3-(-3-dimethylaminopropyl) carbodiimide (EDC)	Thermo Scientific	22980
Epoxy glue (Araldite)	RS Components	756-0111
Fetal bovine serum (FBS, New Zealand origin)	Thermo Fisher	A3160901-50ML
Fibronectin (human plasma)	Gibco	33016015
Formaldehyde solution (PFA, 4%)	Sigma-Aldrich	1.00496-700ML
Fluorescein isothiocyanate isomer I (FITC)	Sigma-Aldrich	F7250-100MG
Gelatin from procine skin (Type A, ~175 Bloom)	Sigma-Aldrich	G2625-100G
Gellan gum (Gelzan™)	Sigma-Aldrich	G1910-1KG
Glass microcapillary	ProSciTech	G346-0101-50
β-Glycerophosphate disodium salt hydrate	Sigma-Aldrich (UK)	G9422-10G
Goat anti-rabbit IgG antibody (Alexa Fluor 568)	Invitrogen	A11036
Hoechst 33342	Sigma-Aldrich	14533

2-Hydroxy-4'-(2-hydroxyethoxy)-2-methylpropiophenone (Irgacure 2959)	Sigma-Aldrich	410896-10G
Low melting point alloy (LMPA, Rose's A, composed of 54% Bi, 28% Pb, 18% Sn)	5N Plus (Germany)	N/A (obtained as a gift)
Methacrylic anhydride	Sigma-Aldrich	276685-100ML
Minimum essential medium (MEM)	Sigma-Aldrich (UK)	M4526
2-(N-morpholino)ethanesulfonic acid (MES)	Sigma-Aldrich	M3671-50G
N-hydroxysuccinimide (NHS)	Thermo Scientific	24500
Penicillin-Streptomycin (10,000 U/mL)	Gibco	15140122
Rhodamine phalloidin	Sigma-Aldrich	94072
Poly(dimethylsiloxane) (PDMS, Sylgard 184)	Element14	101697
Poly(ethyleneimine) (PEI)	Sigma-Aldrich	03880-100ML
Polystyrene beads (0.5 μm, carboxylate-modified, fluorescent orange)	Sigma-Aldrich	L5530-1ML
Propidium iodide	Invitrogen (UK)	P1304MP
Propylene glycol monomethyl ether acetate (PGMEA)	Sigma-Aldrich	484431-1L
Rabbit monoclonal anti-fibronectin antibody	Abcam	ab26820
Rhodamine B	Sigma-Aldrich	R6626-25G
Silicon wafer	ProSciTech	EMS71893-07
SU-8 photoresist (Kayaku 2075)	Micro Materials	Y111074-500ML
Thermal paste (Chemtronics)	RS Components	277-8200
3-(Trimethoxysilyl) propyl methacrylate (3-TMSPM)	Sigma-Aldrich	440159-100ML
Triton X-100	Merck	9400-100ML
TrypLE Express (1×)	Gibco	12604021
Trypsin-EDTA (1×)	Sigma-Aldrich (UK)	T3924-100ML

3.2 The principles of thermophoresis

Thermophoresis is a transport phenomenon by which solutes, broadly encompassing ions, molecules, and particles, dispersed in a solution migrate towards the cold side or the hot side along a temperature gradient (**Figure 3.1**)[1,2]. This directed motion of solutes was first described by Ludwig in 1856[ref. 3] and later by Soret in 1879[ref. 4]. Since then, this phenomenon has been a subject of ongoing research, leading to the development of a wealth of theories and experimental methods to understand the physics at play[5–7].

Although the physical mechanisms of thermophoresis are complex and still not fully understood, the possibility to generate a significant concentration gradient with relatively small temperature differences (e.g., typically 2-6 ºC using MicroScale Thermophoresis in bioanalytics[8,9]) has attracted increasing interest in its development for practical applications. Notable examples in the context of biomedical engineering include biophysical characterization of proteins[10], drug delivery[11,12], and biomarker enrichment and detection for *in vitro* diagnostics[13–17].

A diverse range of soft biocolloidal systems has also been explored to date, such as proteins, DNA, extracellular vesicles, microgels, and polymers[18–21]. Among these, our group is the first to utilize thermophoresis for microengineering stiffness gradient hydrogels[22].

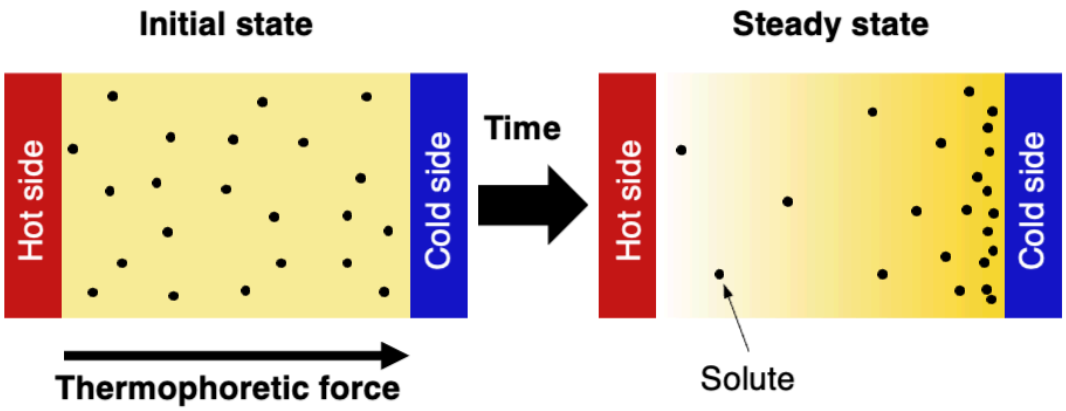

Figure 3.1: Schematic illustration of thermophoresis demonstrating directional motion of solutes driven by a temperature gradient.

From a theoretical standpoint, the mass flux, J_m, of solutes driven by temperature gradients is described by considering Brownian mass diffusion in combination with thermophoretic motion (**Equation 3.1**):

$$J_m = -\rho \left[D \frac{dc}{dx} + c(1-c) D_T \frac{dT}{dx} \right] \tag{3.1}$$

where D is the Brownian diffusion coefficient, D_T is the thermophoretic mobility, ρ is the solute density, c is the concentration, and T is the temperature. The direction of the induced concentration gradient would be along the same spatial axis as the imposed temperature gradient, defined here as the x-position.

Thermophoresis effect causes the build-up of a concentration gradient in a progressive manner. When the force of the concentration gradient is balanced by that of the imposed temperature gradient, the system is said to have reached steady state. At this point, there is no net movement of solutes ($J_m = 0$), and the mass balance reduces to **Equation 3.2**:

$$\frac{dc}{dx} = -c(1-c) S_T \frac{dT}{dx} \tag{3.2}$$

where $S_T = D_T/D$ is defined as the Soret coefficient. Importantly, S_T is the key parameter used to characterize the thermophoretic behavior of a specific system, and depends on multiple factors, including solute-solvent interactions[1], solute size[23,24], average temperature of the system[25], and the type of electrolytes dispersed in solution[26]. In most cases, solutes tend to accumulate toward the cold side, as characterized by a positive Soret coefficient ($S_T > 0$). However, some systems may exhibit accumulation toward the hot side ($S_T < 0$). Additionally, the magnitude of S_T dictates the ratio of concentration between the hot and cold regions at steady state.

Given a linear temperature gradient ($dT/dx = \alpha$, a constant) and a dilute system ($c(1-c) \approx c$), the resulting concentration profile, $c(x)$, is exponential (**Equation 3.3**):

$$c(x) = C_0 \exp\left(-S_T \alpha \cdot x\right) \tag{3.3}$$

where C_0 is a constant set by the initial conditions. In practice, it is still possible to observe a reasonably linear profile by employing smaller temperature gradients, which

will later prove to be a valuable feature for developing stiffness gradient hydrogel platforms.

Additionally, it is important to note in **Equation 3.4** that the characteristic time for thermophoresis, τ, is consistent with the characteristic time for mass diffusion, τ_D, via the Stokes-Einstein relation (**Equation 3.5**):

$$\tau = \tau_D = \frac{d^2}{\pi^2 D} \tag{3.4}$$

$$D = \frac{kT}{6\pi\mu R} \tag{3.5}$$

where D is the diffusion coefficient, k is the Boltzmann constant, T is the system temperature, μ is the fluid viscosity, R is the characteristic size of solute, and d is the diffusion length. This relationship will be useful to experimentally determine the diffusion coefficient for a particular system, and the time required to achieve a steady state concentration gradient.

Overall, thermophoresis appeals as a promising alternative approach to fabricate stiffness gradient hydrogels due the following advantages:

- Directed motion of solutes enables highly controllable and predictable patterning via selective heating.
- Progressive gradient generation process allows the creation of smooth, continuous gradients.
- Universality of the effect permits broad applicability with a variety of hydrogels, independent of their crosslinking mechanism.
- Thermophoresis effect becomes more efficient on downscaling, enabling high-fidelity patterning at microscale resolution.

These features make thermophoresis uniquely suited as a modular approach to create stiffness gradient hydrogels. By streamlining the design, optimization and fabrication process, thermophoresis would enable rapid prototyping of customizable gradient materials, promising to expand their accessibility and versatility for cell culture studies.

3.3 Design and construction of the thermophoresis platform

3.3.1 Design rationale

The foremost requisite for utilizing thermophoresis as an engineering tool is the controllable generation of temperature gradients. To this end, the gradient hydrogel platform developed in this thesis draws on microfluidic heating control techniques previously developed in our research group[27,28], generally referred to here as thermal microfluidics. In this respect, thermal microfluidics offers the significant advantage of precise temperature control at the micron-scale, which is important to create stiffness gradient hydrogels with high-resolution and tunable stiffness profiles.

Another critical design requirement is the containment of the hydrogel sample solution within microconfined geometries, achieved in this work using microfluidic channels or microchambers. In the context of thermophoresis-driven process, such microconfinement is essential to suppress free convective flow[29], which may otherwise distort the temperature and concentration fields.

For practical utility, additional aspects of the platform construction, operation, and functional requirements must be considered. These are summarized in **Figure 3.2**, which serves as a guide for design and operational decisions throughout this thesis.

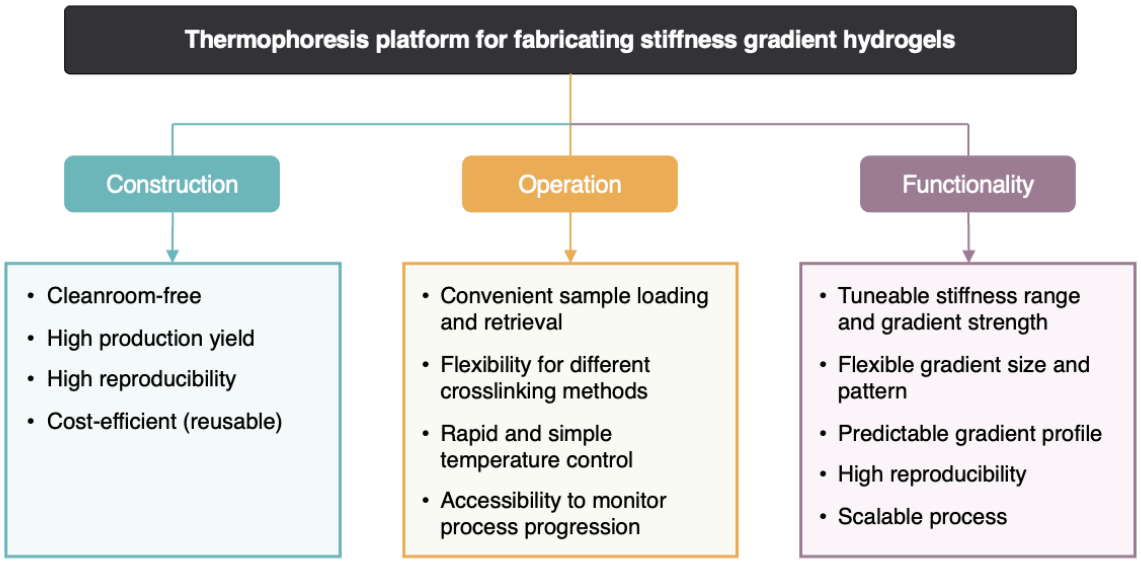

Figure 3.2: Key requirements for developing a thermophoresis microfluidic platform to fabricate stiffness gradient hydrogels.

3.3.2 Microfluidic design

The thermophoresis platform was inspired by a microfluidic device concept introduced by Vigolo et al.[22] (**Figure 1.2**). In this design, microchannels are employed to establish smooth, continuous temperature gradients by providing localized sources of cooling and heating. Particularly, cooling is achieved by driving water through the microchannel using a syringe pump, while heating is provided by a micro-Joule heater embedded in the corresponding channel and powered by a DC current.

All microfluidic devices were designed using AutoCAD software (Autodesk, USA) to produce a high-resolution film photomask (Micro Lithography Services, UK). The devices were fabricated using PDMS by replica molding from SU-8 masters following established soft lithography protocols[30].

3.3.3 Microfabrication process

The construction of a complete thermophoresis microdevice consists of two main steps: (1) preparation of PDMS chip, and (2) creation of Joule heaters. The full fabrication workflow is summarized in **Figure 3.3**. Note that the same procedures may be similarly applied to different designs of the thermophoresis platform that will be explored in this thesis.

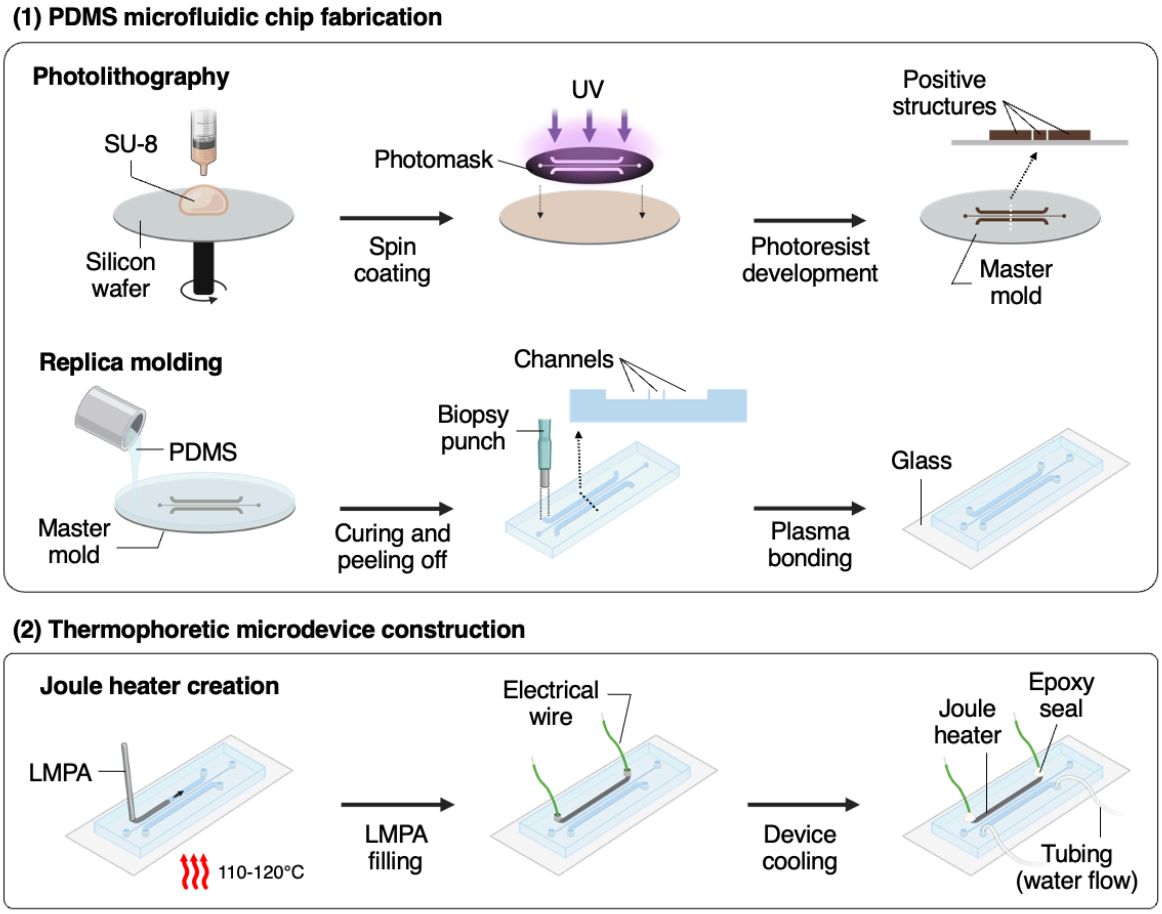

Figure 3.3: Schematic illustration of the generic workflow for fabricating a thermophoresis microdevice based on PDMS microfluidics.

First, master molds were fabricated on silicon wafers by photolithography. This process involves spin coating SU-8 photoresist onto a silicon wafer to achieve the desired microchannel height. The specific spin coating process and subsequent baking steps were carried out according to the manufacturer's guidelines[31]. Then, the photoresist was exposed through the film photomask for 30-40 s using a custom-built UV exposure system[32], and developed by washing in PGMEA for approximately 15 min until the unpolymerized SU-8 were completely removed. Finally, the wafer was rinsed with isopropanol and carefully dried using compressed air. This process resulted in a master mold with positive structures of the microfluidic device, and the critical structure dimensions were confirmed using optical microscopy. As a common practice, multiple copies of the microfluidic design would be patterned onto a single wafer to facilitate efficient PDMS device fabrication through batch processing. Moreover, the custom-built UV system offers a simplified, cleanroom-free approach for

wafer scale lithography patterning, which should increase accessibility to more laboratories.

To fabricate PDMS microfluidic devices, PDMS prepared at 10:1 mass ratio of base elastomer to curing agent was casted on top of the SU-8 master mold to achieve a thickness of 4-5 mm, degassed, and baked at 65 ºC for 80 min. Once fully cured, the PDMS device was carefully cut out of the mold, yielding a PDMS replica of the microfluidic design. Next, a 1.5 mm biopsy punch (KAI Medical) was used to create openings in selected channels according to the desired thermal patterning configuration. Finally, the PDMS replicas were treated with air plasma, then bonded to standard glass slides or glass coverslips.

Embedded micro-Joule heaters were created by filling the preheated microchannels with LMPA. Specifically, the PDMS devices were preheated on a hot plate to 110-120 ºC, then a thin LMPA rod was inserted into one of the channel openings. Within 1 min, the LMPA would be heated above its melting point (~98 ºC) and start flowing into the microchannel by capillary action. During this step, it is critical to maintain a slight pressure on the rod until liquid LMPA overflows out of the other channel opening, taking care not to induce abrupt motions which may cause undesired air plugs within the microchannel. After that, the LMPA rod was gently removed from the device, then a short length of electrical wire was placed into each channel opening. It is also recommended to prewarm the electrical wires on the hot plate, which prevents sudden cooling and partial solidification of the LMPA at the channel opening upon contact. Otherwise, this could result in the wire not properly inserted into the device or discontinuities in the LMPA segment, leading to faulty electrical connection. The devices were allowed to cool at room temperature, and once the LMPA solidified, it effectively formed an electrically conductive path along the microchannel. Before use, epoxy glue was used to secure the electrical connection at the channel openings to ensure its structural stability and prevent damage during handling.

3.4 General experimental setup

A typical setup of the thermophoresis platform is illustrated in **Figure 3.4**. For cooling, room temperature water was delivered using standard syringe pumps (DK Infusetek) connected via Tygon tubing, with a flowrate of 50-200 µL min^{-1} per channel. It is recommended to degas the water in a vacuum desiccator before the start of each experiment session, which helps minimize air bubble formation in the microchannels and thus ensure a consistent temperature profile. For heating, multiple Joule heaters can be operated in a parallel circuit based on the desired gradient configuration, and the power supply unit (Multicomp Pro) was adjusted to provide a current flow of 0.6-1.1 A through each Joule heater. The combined control of water flow and Joule heating determines the local temperature gradient profile. Additionally, a Peltier module (15 mm × 30 mm, RS Components) was attached to the PDMS side of the microdevice, used to fine tune the temperature range of the system and to maintain a constant average system temperature. The specific conditions used for each study are detailed in the dedicated results chapters.

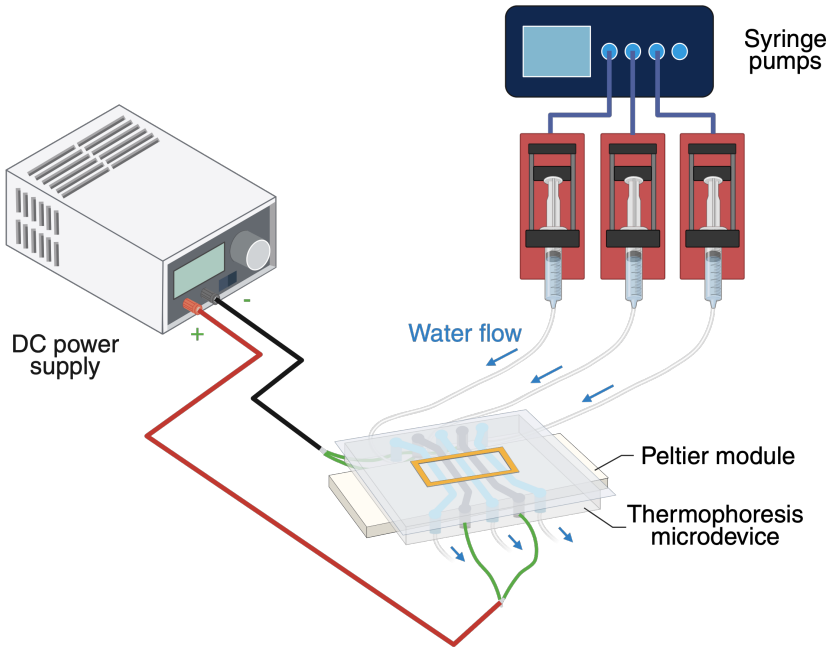

Figure 3.4: Schematic illustration of a typical experimental setup demonstrated using the modular thermophoresis platform configured with alternating cold (blue) and hot (grey) channels to generate periodic gradients (detailed description in Chapter 6).

3.5 General experimental methods

3.5.1 Polymer synthesis

To demonstrate the versatility of the thermophoretic technique, this thesis explored two distinctly different hydrogels in terms of their crosslinking mechanism, biochemical composition, and network architecture: Gellan gum and gelatin methacryloyl (GelMA). In **Chapter 5** and **Chapter 6**, Gellan gum was sourced commercially and used as received. GelMA was synthesized in-house using standard methacrylation procedures. Furthermore, in **Chapter 4** and **Chapter 7**, Gellan gum and GelMA were covalently conjugated with FITC to allow direct visualization and quantification of the polymers.

3.5.1.1 GelMA

GelMA was synthesized by reacting gelatin with methacrylic anhydride (MA), as previously described[33,34]. The reaction scheme is shown in **Figure 3.5**.

For a single batch production (yield ~5 g), 7 g gelatin powder was dissolved in 70 mL PBS at 50 °C in a water bath. Then, 5.6 mL MA was added at a rate of 0.5 mL min^{-1} under vigorous stirring. The mixture was left to react for 2 h and the resulting solution was dialyzed against Milli-Q water for 7 days at 40 °C and finally freeze-dried to obtain a white solid product. Lyophilized GelMA was stored protected from light at -80 °C until use. All experiments reported in this thesis were performed using the same batch of GelMA. The degree of functionalization was 85% (mean of n=3 independent samples), as determined by ^{1}H-NMR analysis. The NMR experiments and data analysis were performed by Dr. Paige Hawkins at Sydney Analytical, The University of Sydney.

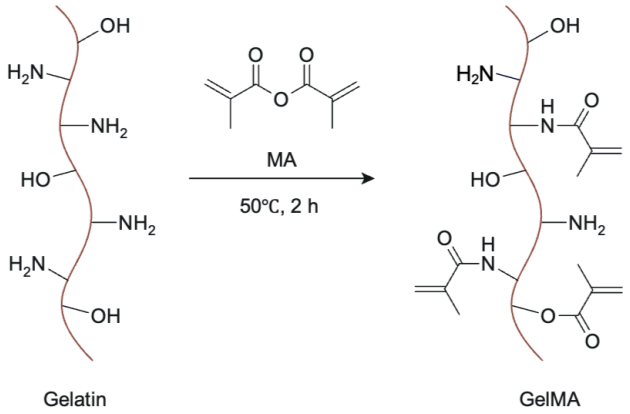

Figure 3.5: Reaction scheme of GelMA synthesis.

3.5.1.2 FITC-GelMA (F-GM)

F-GM was synthesized following a previously described procedure by Onofrillo et al.[35] with slight modifications (**Figure 3.6**).

0.4 g of freeze-dried GelMA was dissolved in 10 mL PBS under magnetic stirring at 50 °C. Then, 0.4 mg of FITC dissolved in 400 µL DMSO was added to the GelMA solution. The reaction mixture was allowed to mix for 2 h at 50 °C, protected from light. The product was dialyzed against Milli-Q water at 40 °C for 6 days, lyophilized, and stored at -80 °C until use.

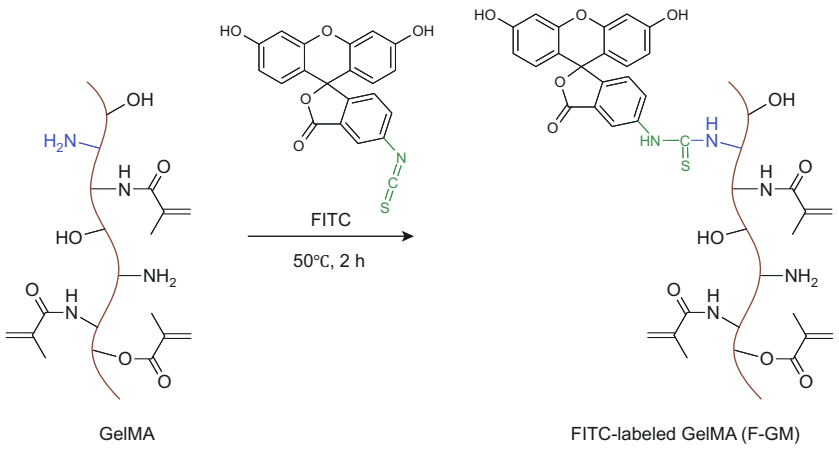

Figure 3.6: Reaction scheme for FITC labelling of GelMA.

3.5.1.3 FITC-Gellan gum (F-GG)

F-GG was synthesized by adapting previously published protocols on fluorescent labeling of polysaccharides (**Figure 3.7**)[36–38].

1 g of Gellan gum was dissolved in 100 mL DMSO by stirring at 90 °C for 30 min. Once fully dissolved, 10 mg of FITC was added to the solution and allowed to mix for 10 min, after which 80 µL DBTDL was added as a catalyst. The reaction was carried out for a further 4 h under continuous stirring and heating at 90 °C, protected from light. The product was washed by three cycles of precipitation in a 5x reaction volume of acetone, followed by centrifugation (Eppendorf 5810; 11000 rpm for 5 min) to remove impurities in the supernatant. Finally, the F-GG precipitate was redissolved in Milli-Q water, dialyzed against Milli-Q water at 40 °C for 6 days, lyophilized, and stored at -80 °C until use.

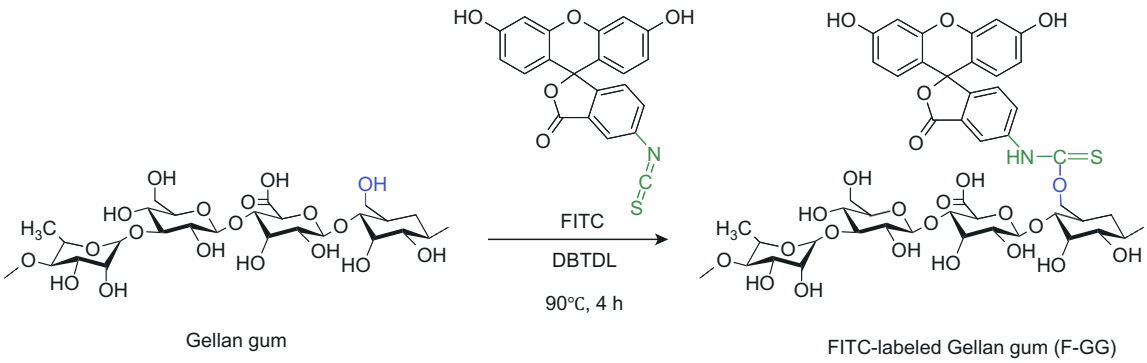

Figure 3.7: Reaction scheme for FITC labelling of Gellan gum.

3.5.2 Hydrogel solution preparation

This section describes the preparation of precursor solutions for hydrogel fabrication. The same procedures were followed for both unlabelled and FITC-labelled polymers. It should also be noted that while a range of polymer concentrations was used to prepare the stock solutions for both Gellan gum (0.5-1.5 wt%) and GelMA (5-20 wt%), the crosslinker/photoinitiator concentration was kept constant throughout the thesis.

3.5.2.1 Gellan gum

Gellan gum precursor solution was prepared by dissolving the specified weight percentage (wt%) of Gellan gum powder in Milli-Q water at 72 °C and under continuous stirring. Once Gellan gum had completely dissolved, 5 mM calcium chloride solution (prepared in Milli-Q water) was added dropwise as crosslinker. The Gellan gum solution was kept warm at 72 °C throughout each experiment session to prevent premature hydrogel crosslinking. Note that once prepared, the Gellan gum solution was used within 3 h to minimize experimental variability due to inevitable evaporation which might alter the concentration of the stock solution.

3.5.2.2 GelMA

GelMA solution was prepared 24 h prior to use. First, a fresh photoinitiator stock solution was prepared by dissolving Irgacure 2959 powder in PBS at 40 °C to a concentration of 0.5 wt%. The specified weight percentage (wt%) of lyophilized GelMA was dissolved in PBS and combined with the photoinitiator solution to a final concentration of 0.1 wt% Irgacure 2959. The mixture was then placed in a water bath at 50 °C for 1 h to allow the GelMA polymer to rehydrate. Finally, the prepared solution was wrapped in aluminium foil, stored at 4 °C overnight, and used within 1 week.

3.5.3 Coverslip functionalization

Attachment of hydrogels to a glass coverslip is essential to facilitate sample handling during material characterization and cell experiments. For Gellan gum, this was achieved either by transferring a prefabricated hydrogel onto a PEI-coated coverslip (**Chapter 5**) or by fabricating the hydrogel directly onto the coverslip (**Chapter 6**, **Chapter 7**). For GelMA, this was achieved by photopolymerization of GelMA directly on 3-TMSPM functionalized coverslip (**Chapter 6**, **Chapter 7**).

3.5.3.1 Poly(ethyleneimine) (PEI)

PEI-coated coverslips enable attachment of Gellan gum hydrogels via electrostatic interaction. Glass coverslips (No.1, 12 mm × 12 mm, Marienfield) were cleaned of organics and surface-activated by plasma treatment for 90 s. The coverslips were immediately immersed in 1 wt% aqueous PEI solution and allowed to coat overnight at room temperature. After that, the coverslips were rinsed under a stream of Milli-Q water and air dried. The PEI-coated coverslips were stored at room temperature in a dry environment, used within 1 month.

3.5.3.2 3-(Trimethoxysilyl) propyl methacrylate (3-TMSPM)

Methacrylated coverslips enable attachment of GelMA hydrogels via covalent bonding when exposed to UV. Glass coverslips (12x12 mm, No.1, Marienfield) were plasma treated for 90 s and then immersed in a 200:6:1 solution of absolute ethanol, acetic acid, and 3-TMSPM for 5 min. Then, the coverslips were washed in absolute ethanol for 3 min and air dried. The 3-TMSPM functionalized coverslips were stored at room temperature in the dark, used within 2 weeks.

3.5.4 Material characterization

3.5.4.1 Atomic force microscopy (AFM)

Throughout this thesis, AFM nanoindentation was employed as the primary technique for hydrogel stiffness characterization. The technique works by using a nano-sized or micro-sized probe to investigate a small area of material and measure its resistance to indentation[39]. Crucially, this method captures the stiffness variation on a similar length scale at which a cell "sense" its matrix in the context of mechanobiology. All stiffness data reported were acquired using an MFP-3D atomic force microscope (Asylum Research), following previously described protocols with some adaptations[39,40]. Note that throughout this thesis, the term "stiffness" is discussed in terms of Young's modulus.

Hydrogel samples were indented in liquid conditions using a 10 μm diameter borosilicate glass colloidal probe, with 30 kHz resonance frequency and 0.1 N m^{-1} nominal spring constant (CP-qp-CONT-BSG-B-5, NanoAndMore). The cantilever was recalibrated at the start of each experiment session to determine the cantilever's spring constant and the deflection sensitivity. Both of these parameters are critical to allow the AFM to convert the cantilever deflection (nm) to force (N). Specifically, the cantilever was stabilized in PBS at room temperature, calibrated using thermal noise method, and indented on a clean glass slide to measure deflection sensitivity. To ensure accuracy, the thermal calibration and deflection sensitivity measurement were repeated 3-5 times until the values remained relatively constant.

To prepare samples for measurement, the hydrogel-laden coverslip was mounted onto a standard glass slide using double-sided adhesive tabs, then the whole glass slide was mounted onto the AFM stage. Samples were immersed in a drop of PBS and allowed to equilibrate for 5-10 min before starting measurements.

For force curve generation, hydrogels were indented with an approach velocity of 2 μm s^{-1}, until a 15 nN trigger force was registered, then retracted at 10 μm s^{-1} (**Figure 3.8a**). The indentation parameters were optimized and validated by comparing the AFM measurements on a set of reference polyacrylamide gels (0.2 kPa, 8 kPa, 50 kPa; Softslip 12, Matrigen) (**Figure 3.8b**). For stiffness gradient hydrogels, measurements were taken at 200-500 μm intervals in the known direction of the

gradient. At each point, the local stiffness was calculated by taking the average of a nanomechanical map generated in a 4×4 grid over an area of 20 μm × 20 μm (16 force curves in total).

The force-displacement curves were analyzed directly in the Asylum MFP-3D software, using the Hertz model. The commonly applied Hertz model assumes that the probe is spherical, and the material being indented is significantly thicker than the indentation depth. These considerations were accounted for in the selection of suitable indentation parameters. Although more complicated analysis methods would typically be employed for complex (e.g., viscoelastic, multilayered) materials[40], the current protocol was deemed sufficient to obtain information on the elastic properties for 2D hydrogels in this thesis.

Nonetheless, it is recognized that stiffness measurements using AFM may vary considerably depending on the indentation parameters and analysis model applied. Therefore, instead of relying on the absolute stiffness values, data interpretation and discussions in this work are based on comparing relative values along a gradient and between samples, which were measured using the same indentation parameters.

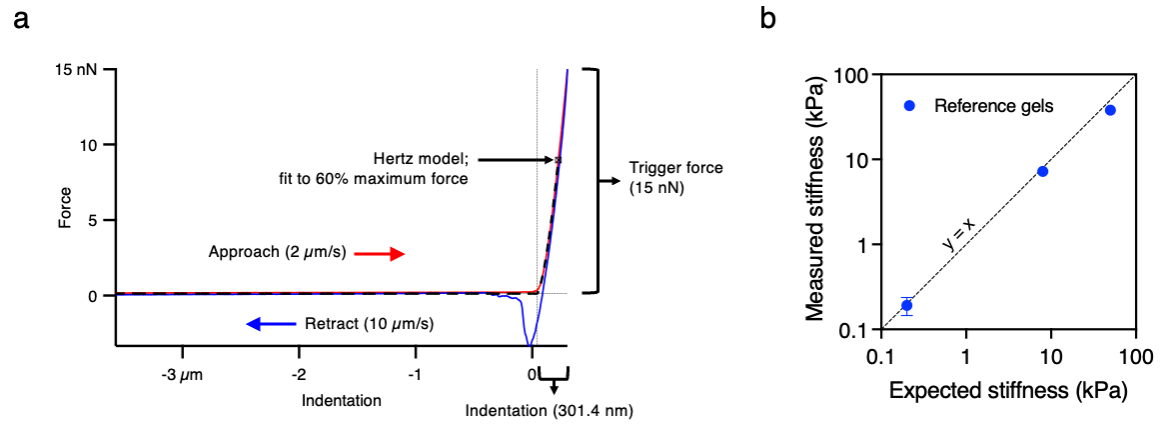

Figure 3.8: (a) Example of a typical nanoindentation force curve generated using AFM. The value of Young's modulus is calculated using the Hertz model, by fitting the approach curve to 60% of the maximum trigger force. (b) Validation of the accuracy of stiffness measurements using commercial reference samples of known Young's modulus (data shown as mean ± standard deviation, n=3 independent samples). Results show that the measurements are in good agreement with the expected stiffness values over the range of 0.2-50 kPa.

3.5.4.2 Scanning electron microscopy (SEM)

In **Chapter 5** and **Chapter 7**, SEM was used for visualization and quantification of the hydrogel pore structures.

Fabricated hydrogel samples were flash frozen using liquid nitrogen and freeze-dried for 1 day. After that, all samples were coated with 10 nm platinum using a Leica ACE600 sputter coater and imaged using a JEOL JSM-IT500HR scanning electron microscope at 5-10 kV. For the uniform stiffness samples, images were taken at multiple random locations across the hydrogel surface. For the gradient samples, images were taken at regular intervals along the known direction of the stiffness gradient, using the recorded x and y coordinates to locate the soft side ("soft"), center region ("mid"), and stiff side ("stiff") on a sample.

SEM images were processed and analyzed using the open-source FIJI software[41] (https://imagej.net/software/fiji/). The images were first converted into an 8-bit image format, then the pores were segmented by performing pixel intensity thresholding. Each image was inspected and manually corrected for erroneous segmentation (e.g., due to uneven illumination or shadowing effects). Finally, the "Analyze Particle" tool was used to count the number of pores and quantify the pore size.

3.5.5 Cell culture

3.5.5.1 Cell maintenance

The main cell type used in this work (**Chapter 6** and **Chapter 7**) is mouse fibroblasts (3T3-L1), kindly provided by the group of Prof. Marcela Bilek (School of Biomedical Engineering, The University of Sydney). Note that a second cell line, MC3T3 osteoprogenitor cells, was also used in a collaborative study described in **Chapter 5**; the cell work was performed by Dr Alexandros Kosmidis Papadimitriou (The University of Birmingham, UK), and while the key associated methods can be found here in **Chapter 5**, this should be supplemented with Dr Papadimitriou's doctoral thesis for further information[42].

3T3-L1 cells were maintained in DMEM containing high glucose and pyruvate supplemented with 10% FBS, 100 U mL^{-1} penicillin and 100 µg mL^{-1} streptomycin, in a humified environment at 37 °C and 5% CO_2. Cells were split using TrypLE Express when they reached 70-80% confluence, and were used up to passage 20 for experiments.

For passaging, cells were first washed with warm DPBS before adding TrypLE solution at room temperature. Then, the culture flask was immediately transferred into the incubator at 37 °C for 3-4 mins to induce enzyme mediated cell detachment. After inspecting the flask under a microscope to ensure that most (>80%) of the cells have been lifted from the surface, the TrypLE enzyme was neutralized by adding warm culture media into the flask. The cell suspension was centrifuged at 200 g for 5 min to form a pellet. Finally, the supernatant was discarded, the cells were resuspended in fresh culture media, and subcultured in a 1:5 split ratio. Media changes were performed every 2-3 days.

3.5.5.2 Cell cryopreservation

The cell freezing medium was prepared by mixing FBS and DMSO at a 9:1 volume ratio. Cells were harvested using TrypLE in the log growth phase (70-80% confluent), following the same procedure for cell passaging. The harvested cells were counted using a hemocytometer with trypan blue stain, resuspended in freezing medium at a concentration of 1 million cells per mL, and aliquoted into 1 mL cell suspension per cryopreservation vial. The vials were then placed into a Mr. Frosty™ container filled with fresh isopropanol, stored in a -80 °C overnight to allow gradual freezing (approximately -1 °C per min), then transferred to liquid nitrogen cryobank for long term storage.

3.5.5.3 Cell thawing

To thaw cells, the cryovial was retrieved from the liquid nitrogen cryobank and immediately thawed in a water bath at 37 °C until only 1/3 of the volume remains frozen.

Then, the 1 mL cell suspension was quickly transferred into 4 mL of cold culture media in a 15 mL centrifuge tube to minimize heat shock and to dilute the DMSO. Cells were centrifuged at 200 g for 5 min to form a pellet. Finally, the supernatant was discarded, the cells were resuspended in warm media, and transferred into a T25 flask. The first media change was performed after 24 h, and cells were only used for experiments after at least one passage after thawing.

3.5.5.4 Cell seeding

All cell culture experiments were performed using 12 well plates. Prior to cell seeding, hydrogel samples were transferred to a new well plate (one gel per well) and UV sterilized in the biosafety cabinet for 30 min. For this step, the well plate cover was removed to allow direct UV exposure, and a drop of sterile PBS was added to fully cover each hydrogel, which was important to prevent sample dehydration.

For all experiments, cells were seeded on the gels at 3000 cells cm^{-2} in a total volume of 50 µL per sample. An even distribution of cells across the entire hydrogel surface was visually confirmed via brightfield microscopy. Then, the cells were allowed to settle in the incubator for 45 min before topping up with fresh media to prevent the samples from drying out.

3.5.5.5 Immunostaining

At the required observation time point, samples were fixed using 4% paraformaldehyde for 20 min at room temperature. Then, the samples were washed (2 x 5 min) with PBS followed by soaking in PBS-T (PBS with 0.5% Triton X-100) for 15 min to permeabilize the cells. Cells were subsequently stained with rhodamine phalloidin for actin visualization and Hoechst for nuclei quantification.

Specifically, a new vial of rhodamine phalloidin lyophilizate (10 nmol, as received from supplier) was dissolved in 1 mL methanol to make a 10 µM stock solution, and used at a dilution of 1:500. Stock Hoechst solution was prepared at 10 mg/mL in Milli-Q water, and used at a dilution of 1:2000. The working stain solution was prepared in PBS. To stain the cells, each gel sample was incubated in the stain solution for 20-

30 min at room temperature, protected from light. Then, the samples were washed (3 x 5 min) in PBS, gently rinsed in Milli-Q water, and mounted on a glass slide using Fluoromount-G™ (Invitrogen) for subsequent imaging.

3.5.5.6 Cell imaging and analysis

Stained hydrogel samples were imaged using an Olympus IX73 inverted microscope with a Prime BSI Express sCMOS camera (Teledyne Photometrics), acquired at 10x or 40x magnification. For each gradient hydrogel, an image mosaic was generated by stitching multiple images acquired along the length of the gradient, using DAPI as the reference channel. Resulting stitched images were then cropped into multiple segments representing regions of different stiffness along the hydrogel, then analyzed using FIJI software. For each segment, cell nuclei were detected as objects through manual thresholding and counted using the "Analyze Particle" tool. In some instances, watershed separation was applied to segment connecting objects. The cell density was then calculated by dividing the total number of cells by the hydrogel segment area. Additionally, cell area and aspect ratio were quantified in a similar manner using the phalloidin channel.

3.5.6 Statistical analysis

Unless stated otherwise, data are presented as mean ± standard error of the mean (SEM) for a minimum of three independent experiments. Where appropriate, statistical tests were performed on GraphPad Prism (v10) using one-way ANOVA with Tukey post-hoc test. Statistical significance between experimental groups of interest was denoted as * ($p < 0.05$), ** ($p < 0.01$), *** ($p < 0.005$), or ns (non-significant).

3.5.7 Code availability

All custom image analysis and processing code developed as part of this thesis is available at: https://github.com/shinwei-chong/gradient-gels

References

1. Piazza, R. & Parola, A. Thermophoresis in colloidal suspensions. *J Phys Condens Matter* **20**, 153102 (2008).

2. Piazza, R. Thermophoresis: Moving particles with thermal gradients. *Soft Matter* **4**, 1740–1744 (2008).

3. Ludwig, C. Diffusion zwischen ungleich erwärmten Orten gleich zusammengesetzter Lösungen. *Sitz Math Naturwiss Classe Kaiserichen Akad Wiss* **20**, 539 (1856).

4. Soret, C. Sur l'etat d'équilibre que prend au point de vue de sa concentration une dissolution saline primitivement homogène dont deux parties sont portées a des températures différentes. *Arch Sci Phys Nat* **2**, 48 (1879).

5. Vigolo, D., Rusconi, R., Stone, H. A. & Piazza, R. Thermophoresis: microfluidics characterization and separation. *Soft Matter* **6**, 3489–3493 (2010).

6. Köhler, W. & Morozov, K. I. The Soret Effect in Liquid Mixtures - A Review. *J Non-Equilib Thermodyn* **41**, 151–197 (2016).

7. Rahman, M. A. & Saghir, M. Z. Thermodiffusion or Soret effect: Historical review. *Int J Heat Mass Transf* **73**, 693–705 (2014).

8. Wienken, C. J., Baaske, P., Rothbauer, U., Braun, D. & Duhr, S. Protein-binding assays in biological liquids using microscale thermophoresis. *Nat Commun* **1**, 100 (2010).

9. Jerabek-Willemsen, M. *et al.* MicroScale Thermophoresis: Interaction analysis and beyond. *J Mol Struct* **1077**, 101–113 (2014).

10. Seidel, S. A. I. *et al.* Microscale thermophoresis quantifies biomolecular interactions under previously challenging conditions. *Methods* **59**, 301–315 (2013).

11. Wang, Z. H. *et al.* Biological chemotaxis-guided self-thermophoretic nanoplatform augments colorectal cancer therapy through autonomous mucus penetration. *Sci Adv* **8**, eabn3917 (2022).

12. Maier, C. M. *et al.* Optical and Thermophoretic Control of Janus Nanopen Injection into Living Cells. *Nano Lett* **18**, 7935–7941 (2018).

13. Zhang, M. *et al.* Thermophoresis-Controlled Size-Dependent DNA Translocation through an Array of Nanopores. *ACS Nano* **12**, 4574–4582 (2018).

14. He, Y. *et al.* Thermophoretic manipulation of DNA translocation through nanopores. *ACS Nano* **7**, 538–546 (2013).

15. Tian, F., Han, Z., Deng, J., Liu, C. & Sun, J. Thermomicrofluidics for biosensing applications. *View* **2**, 20200148 (2021).

16. Ling, H. *et al.* Thermophoretic Assay for Biosensing. *Adv Mater Technol* **9**, 2301746 (2024).

17. Liu, C. *et al.* Low-cost thermophoretic profiling of extracellular-vesicle surface proteins for the early detection and classification of cancers. *Nat Biomed Eng* **3**, 183–193 (2019).

18. Wongsuwarn, S. *et al.* Giant thermophoresis of poly(N-isopropylacrylamide) microgel particles. *Soft Matter* **8**, 5857–5863 (2012).

19. Vigolo, D. *et al.* Continuous Isotropic-Nematic Transition in Amyloid Fibril Suspensions Driven by Thermophoresis. *Sci Rep* **7**, 1211 (2017).

20. Talbot, E. L., Kotar, J., Parolini, L., Di Michele, L. & Cicuta, P. Thermophoretic migration of vesicles depends on mean temperature and head group chemistry. *Nat Commun* **8**, 15351 (2017).

21. Reineck, P., Wienken, C. J. & Braun, D. Thermophoresis of single stranded DNA. *Electrophoresis* **31**, 279–286 (2010).

22. Vigolo, D., Ramakrishna, S. N. & DeMello, A. J. Facile tuning of the mechanical properties of a biocompatible soft material. *Sci Rep* **9**, 7125 (2019).

23. Braibanti, M., Vigolo, D. & Piazza, R. Does thermophoretic mobility depend on particle size? *Phys Rev Lett* **100**, 108303 (2008).

24. Vigolo, D., Brambilla, G. & Piazza, R. Thermophoresis of microemulsion droplets: Size dependence of the Soret effect. *Phys Rev E* **75**, 040401 (2007).

25. Iacopini, S., Rusconi, R. & Piazza, R. The 'macromolecular tourist': Universal temperature dependence of thermal diffusion in aqueous colloidal suspensions. *Eur Phys J E* **19**, 59–67 (2006).

26. Vigolo, D., Buzzaccaro, S. & Piazza, R. Thermophoresis and thermoelectricity in surfactant solutions. *Langmuir* **26**, 7792–7801 (2010).

27. Miralles, V., Huerre, A., Malloggi, F. & Jullien, M.-C. A Review of Heating and Temperature Control in Microfluidic Systems: Techniques and Applications. *Diagnostics* **3**, 33–67 (2013).

28. Dos-Reis-Delgado, A. A. *et al.* Recent advances and challenges in temperature monitoring and control in microfluidic devices. *Electrophoresis* **44**, 268–297 (2023).

29. Lee, N. & Wiegand, S. Thermophoretic micron-scale devices: Practical approach and review. *Entropy* **22**, 950 (2020).

30. Mcdonald, J. C. *et al.* Fabrication of microfluidic systems in poly(dimethylsiloxane). *Electrophoresis* **21**, 27–40 (2000).

31. Kayaku Advanced Materials. https://kayakuam.com/.

32. Challa, P. K., Kartanas, T., Charmet, J. & Knowles, T. P. J. Microfluidic devices fabricated using fast wafer-scale LED-lithography patterning. *Biomicrofluidics* **11**, 014113 (2017).

33. Loessner, D. *et al.* Functionalization, preparation and use of cell-laden gelatin methacryloyl-based hydrogels as modular tissue culture platforms. *Nat Protoc* **11**, 727–746 (2016).

34. Yue, K. *et al.* Synthesis, properties, and biomedical applications of gelatin methacryloyl (GelMA) hydrogels. *Biomaterials* **73**, 254–271 (2015).

35. Onofrillo, C. *et al.* FLASH: Fluorescently LAbelled Sensitive Hydrogel to monitor bioscaffolds degradation during neocartilage generation. *Biomaterials* **264**, 120383 (2021).

36. Cho, H. H. *et al.* Development of fluorescein isothiocyanate conjugated gellan gum for application of bioimaging for biomedical application. *Int J Biol Macromol* **164**, 2804–2812 (2020).

37. Horinaka, J. I., Kani, K., Honda, H., Uesaka, Y. & Kawamura, T. Local chain mobility of gellan in aqueous systems studied by fluorescence depolarization. *Macromol Biosci* **4**, 714–720 (2004).

38. Liu, Y. *et al.* Fluorescent labeling affected the structural/conformational properties of arabinoxylans. *Carbohydr Polym* **265**, 118064 (2021).

39. Norman, M. D. A., Ferreira, S. A., Jowett, G. M., Bozec, L. & Gentleman, E. Measuring the elastic modulus of soft culture surfaces and three-dimensional hydrogels using atomic force microscopy. *Nat Protoc* **16**, 2418–2449 (2021).

40. Whitehead, A. J., Kirkland, N. J. & Engler, A. J. Atomic Force Microscopy for Live-Cell and Hydrogel Measurement. *Methods Mol Biol* **2299**, 217 (2021).

41. Schindelin, J. *et al*. Fiji: an open-source platform for biological-image analysis. *Nat Methods*, **9**, 676–682 (2012).

42. Kosmidis-Papadimitriou, A. Thermophoretic manipulation of the mechanical properties of biomaterials in microfluidics. *PhD thesis, The University of Birmingham* (2020).

Chapter 4

Thermophoretic migration of biopolymers in solution

This chapter presents the foundational methodologies underpinning subsequent development of this thesis. The first part of the chapter details a protocol for in situ, high-resolution mapping of temperature distribution within microscale systems, based on standard fluorescence microscopy and image processing techniques. In the second part, a strategy employing fluorescently labelled polymers was established, allowing for direct, real-time visualization of the gradient formation process. Thermophoresis of Gellan gum and GelMA polymers in solution are characterized and discussed, offering high level insights on the design and optimization of the thermophoretic gradient hydrogel fabrication process. Altogether, this chapter provides two new technical innovations enabling significant practical advances of the thermophoresis fabrication technique.

While the ability to generate and control intricate thermal landscapes in microfluidic systems is well established (Chapter 3), there is surprisingly far less development of simple and economical methods that allow precise temperature measurement within such small geometries. In our group, initial efforts relied on thermocouples and although this was tractable for the earlier platform iterations, these point-based measurements proved to be inadequate as we moved toward more complex and spatially varied gradient patterns. In the context of building a thermophoretic biofabrication platform, another related and recurring question is its universality across different hydrogel systems, and how the thermophoretic behavior may vary with different polymer physicochemical properties. However, this has been difficult to study due to the optical transparency of polymer solutions. In this chapter I address these technical challenges through the development of new experimental protocols. Specifically, I present a noninvasive fluorescence-based thermometry method (Section 4.2) and leverage fluorescent labelling of polymers to enable direct visualization of their thermophoretic behavior (Section 4.3). As experimental techniques, these protocols potentially pave the way for novel investigations into thermophoretic hydrogel fabrication and thermophoresis in micro-confinements itself.

4.1 Overview of the microfluidic platform

The new protocols presented in this chapter were originally developed using a thermophoresis microdevice design as shown in **Figure 4.1**. This design is a single layer microfluidic device, comprising a straight sample channel flanked by two parallel side channels to impose a linear temperature gradient across the sample channel (**Figure 4.1a**). The sample channel is 600 µm (width) x 100 µm (height) x 4 cm (length), with a 100 µm PDMS wall between each side channel. The side channels have a larger width of 2 mm to ensure efficient cooling and heating.

Both temperature measurement (Section 4.1) and thermophoresis characterization (Section 4.2) experiments were performed using an Olympus IX73 inverted microscope. Fluorescent images were acquired using a highly sensitive fluorescent camera (Prime BSI Express, Teledyne Photometrics) interfaced with the open-source Micro-Manager software (https://micro-manager.org/). For these experiments, the thermophoretic microdevice was mounted on the standard microscope stage and secured at its edges using Blu Tack adhesive (**Figure 4.1b**). This was vital to ensure that the device was kept at a fixed position throughout the imaging session.

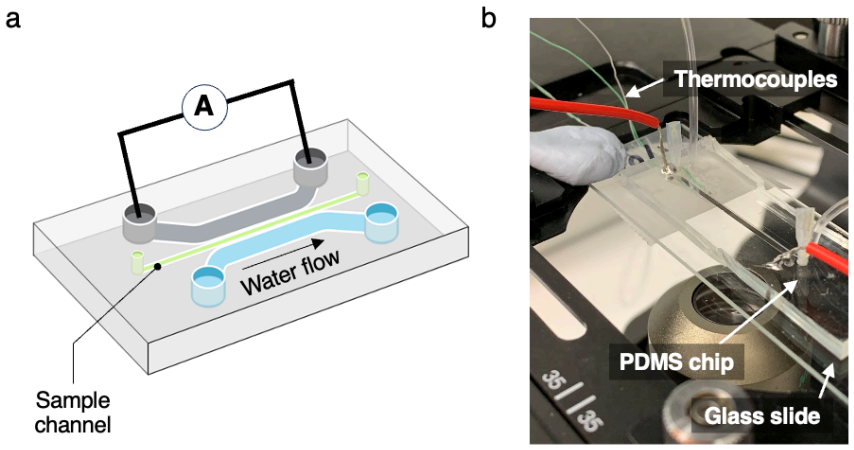

Figure 4.1: (a) Schematic of thermophoresis microdevice comprising a main sample channel (green) and two parallel channels. Heating (grey channel) is achieved using an embedded Joule heater operated by DC current, whereas cooling (blue channel) is achieved through water flow controlled by syringe pumps. (b) Photograph of the device setup for microscopy experiments. Note that thermocouples are attached to the underside of the glass slide for continuous temperature monitoring.

4.2 Fluorescence-based temperature mapping in microsystems

4.2.1 Introduction to fluorescence thermometry

A number of non-contact methods based on optical detection have been proposed to obtain spatially resolved information on the temperature distribution within microsystems, including fluorescence thermometry, infrared thermometry, and laser interferometry[1,2]. Among these, fluorescence thermometry appeals as the most practical and accessible option, primarily because it can be implemented just by using standard fluorescence microscopes, which are widely available in most research laboratories today, and thus can be easily integrated into existing experimental workflows. As noted in this chapter, the calibration standards for temperature measurement can also be precisely transferred across different setups, enabling a plug-and-play solution for routine temperature in microsystems.

Fluorescence thermometry works by exploiting the temperature-dependent changes in fluorescence intensity of a low-concentration fluorophore solution[3]. In essence, it relies on comparing the fluorescence intensity recorded under a known, uniform temperature condition to that measured under an unknown, potentially nonuniform temperature field. Specifically, the recorded intensities are converted to temperature values based on a pre-established correlation between temperature and fluorescent intensities. Other studies have also demonstrated the utilization of fluorescence lifetime imaging for temperature measurements which offer higher accuracy and stability against fluctuations in external environment, but require more sophisticated optical setups (e.g. confocal microscope)[4–6].

A wide range of fluorescent probes have been explored for fluorescence-based temperature measurement, for example, Rhodamine B[ref. 7], ruthenium complex[8], and SYBR Green dye[9]. Of all, Rhodamine B dye remains a popular choice given its strong temperature-dependent fluorescence in the range of 0-120 ºC and reversible responses[2]. A good example was demonstrated by Ross et al. using standard fluorescence microscope and a CCD camera to measure temperature variation of fluids within acrylic microfluidic devices[3]. In this setup, the spatial and temporal resolutions are primarily limited by the specifications of the imaging system, with micrometer-scales and millisecond-levels being typical for commercially available

microscope cameras today. However, existing protocols require Rhodamine B to be dissolved in the working fluid[3,7], which introduces two major problems: (1) Rhodamine B readily absorbs into PDMS microdevices leading to measurement artifacts[10], and (2) the fluid is unable to reach areas with solid-state heating elements, thus preventing temperature measurement in those regions. The latter was particularly crucial in our application given the use of embedded Joule heaters within the microfluidic system.

The rest of this section proposes a new protocol for implementing the fluorescence thermometry technique, which decouples the fluorescent dye from the fluidic system, enabling noninvasive and spatially resolved temperature mapping across the entire device.

4.2.2 The temperature measurement method

General setup

In search of a method that would preserve the advantages of fluorescence thermometry while extending its applicability for measurements beyond the confines of the fluidic domain, we quickly decided on a capillary-based strategy whereby a glass microcapillary filled with Rhodamine B solution serves as an independent temperature probe. More specifically, the probe was prepared by drawing 0.1 mM Rhodamine B solution into a glass micro-capillary (G346-0101-50, ProSciTech), then both ends of the capillary were sealed using epoxy glue to prevent evaporation. To attach a probe on the microdevice, a thin layer of thermal paste was first applied on the glass side surface, then the capillary probe was gently pressed onto the device, taking care to avoid any air pockets (**Figure 4.2a**). The probe could be further secured in place by taping down at both sides of the device.

The general idea of this method is that the microcapillary probe can be flexibly positioned on the microfluidic device at the channel-interfacing surface, enabling precise temperature mapping at the contact plane, including normally inaccessible areas such as heaters, air-filled microchannels, and the PDMS substrate (**Figure 4.2b**).

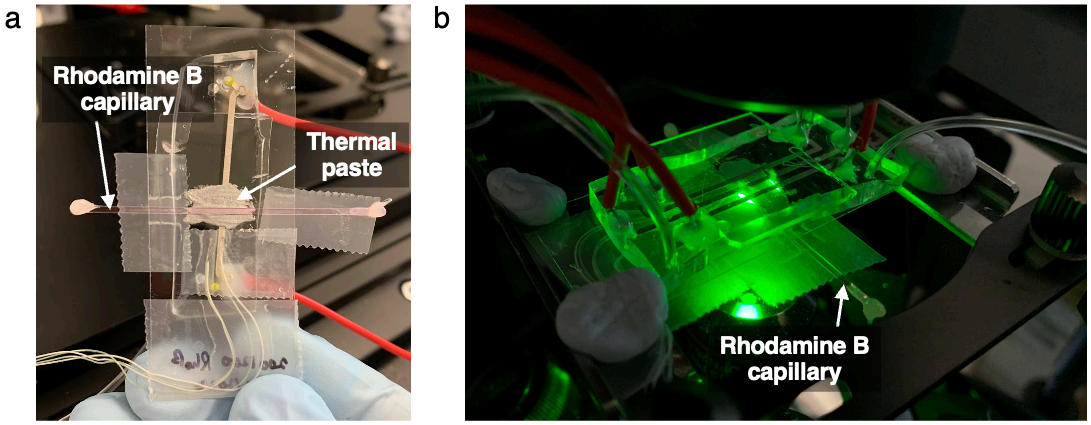

Figure 4.2: Representative photographs of (a) Rhodamine B temperature probe attachment to the microdevice, and (b) the mounted setup on a fluorescence microscope for temperature characterization.

A typical experiment setup is shown in **Figure 4.3a**, while **Figure 4.3b** shows a uniform fluorescence intensity within the microcapillary at room temperature. **Figure 4.3c** shows local intensity changes of the Rhodamine B dye in response to application of a linear temperature gradient, highlighting the effectiveness of this method in resolving temperature differences across diverse regions of the microfluidic device – which includes zones with solid-state heating elements (H), stationary fluid (S), and flowing liquid (C).

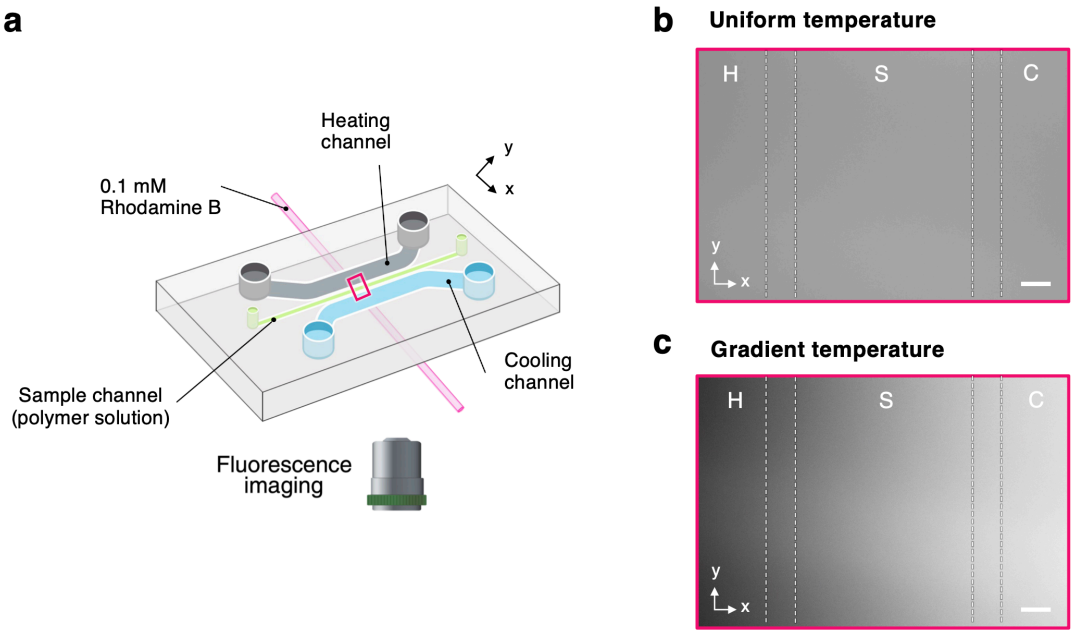

Figure 4.3: (a) Schematic illustration of the general fluorescence thermometry setup, utilizing a glass microcapillary filled with Rhodamine B solution as temperature probe. Example fluorescence images

within the capillary (b) before and (c) after a linear temperature gradient is applied to the interfacing microfluidic device. Dotted lines indicate the positions of the underlying microchannels for reference (H: heating channel; S: sample channel; C: cooling channel). Scale bars = 100 μm.

The surface-level temperature measurements are particularly relevant to the subsequent development of a modular thermophoresis platform (**Chapter 6**), where heat transfer across the microfluidic-substrate interface dictates the local temperature gradient experienced by the polymer solution confined within an external microchamber. However, it is worth noting that this approach should still provide a reliable approximation of the temperatures inside the microchannels, given the effective thermal coupling between the microfluidic circuit and the microcapillary. Particularly, the small thermal masses involved allow for rapid heat transfer, while the relatively good conductivity of the glass substrates helps minimize heat loss.

Calibration

The first step of the fluorescence-based temperature measurement technique was the generation of a calibration curve to quantify the relationship between fluorescence intensity and temperature. This was achieved by taking fluorescence images at various uniform temperatures ranging from 15-74 ºC (controlled by a Peltier module attached to the PDMS side of the microdevice), encompassing the typical thermal conditions used for hydrogel fabrication in this thesis.

For each measurement, fluorescence images of the Rhodamine B dye solution were acquired for 1 s at 30 frames per second, then averaged across the 30 sequential frames to obtain a single image representative of that thermal condition. The camera gain settings were kept constant throughout all experiments to ensure consistency in fluorescence quantification. LED intensity and exposure time were optimized during initial setup to avoid saturation and minimize photobleaching, then kept constant for all comparative sets of measurements. The Image processing and analysis were performed using a customized MATLAB script. This image acquisition procedure was also followed in the subsequent temperature measurement steps.

The measured fluorescence intensity at each temperature point was normalized against the intensity at 22 ºC (typical room temperature), and the resulting calibration

curve is shown in **Figure 4.4**. In order to assess the reproducibility of the microcapillary probe technique, independent calibration curves were generated using two different Rhodamine B-filled capillaries (Probe 1 & 2). A third-order polynomial fit to the average of both curves yields **Equation 4.1**:

$$T\,[°\mathrm{C}] = 118 - 198I + 155I^2 - 53I^3 \tag{4.1}$$

where T is the temperature and I is the normalized fluorescence intensity. Importantly, the calibration data generated within our laboratory demonstrated good agreement with the data originally reported by Ross et al.[3], and further revealed measurement consistency across different Rhodamine B probe preparations. These findings validate the accuracy of the measurement protocol and establish the reliability of the proposed microcapillary setup for fluorescence thermometry.

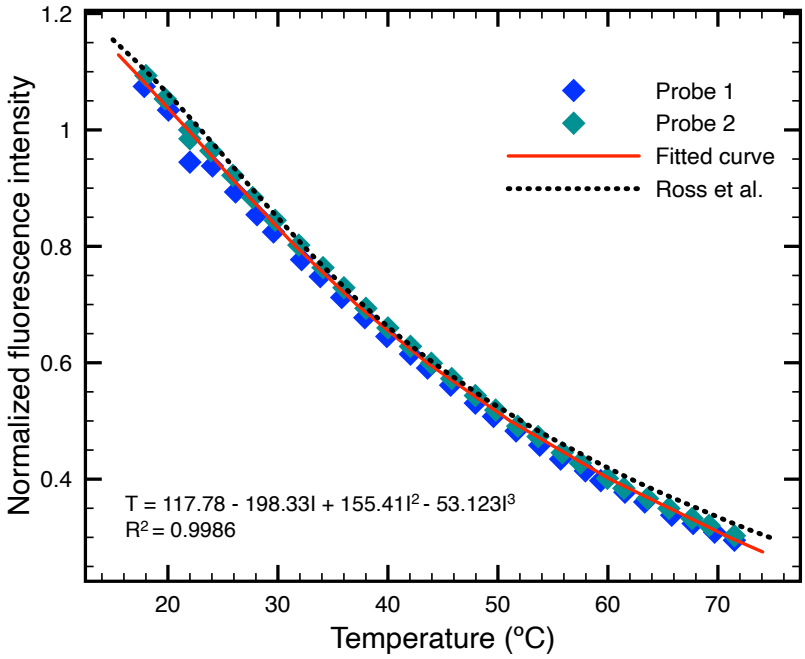

Figure 4.4: Correlation between temperature (T) and fluorescence intensity (I) of Rhodamine B solution, normalized to the intensity value at room temperature. Each data point represents a single measurement. Solid line is a third-order polynomial fit.

Temperature measurement

The workflow for subsequent temperature measurement is summarized in **Figure 4.5**, based on an example of thermal microfluidic module for patterning periodic gradients (**Chapter 6.5**). This was chosen to further demonstrate the versatility of the technique with more complex temperature landscapes.

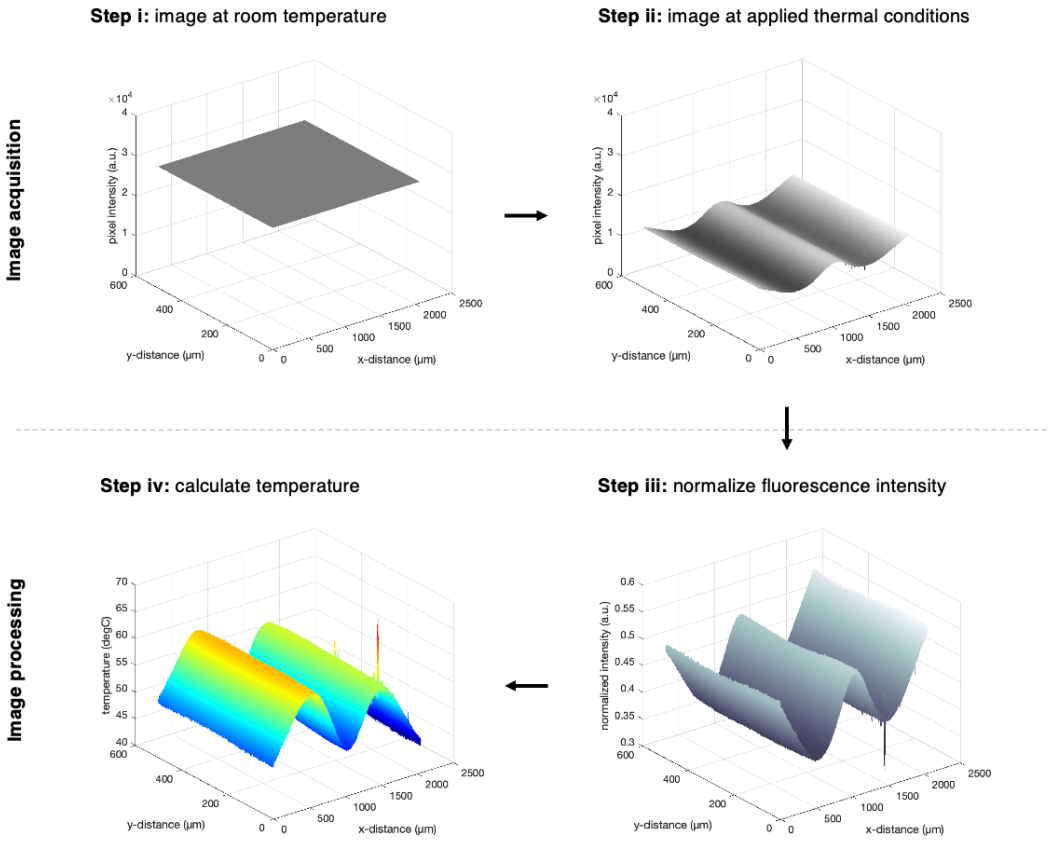

Figure 4.5: Summary of workflow for fluorescence-based temperature measurement. Reference fluorescence images were first acquired at room temperature (step i). Then, fluorescence images were taken at the same position under an applied thermal condition (step ii). The images from step ii were normalized against the reference image (step iii), and finally converted to temperature measurements using the previously established calibration curve (step iv).

A critical step of this protocol was the application of a thin layer of thermal paste which served to hold the microcapillary in place on the microdevice surface, and to maximize heat transfer between the microfluidic layer and the Rhodamine B probe (**Figure 4.2a**). Just as importantly, the thermal paste layer provided a uniform, non-reflective background to eliminate optical artifacts from the underlying microchannels (e.g., light

reflection from the metallic Joule heater interfering signal from fluorescent sample solution). Notably, despite the application of an opaque thermal paste layer, increasing the intensity of transmitted (brightfield) illumination should allow sufficient contrast to visualize the underlying microfluidic structure, facilitating optical alignment during experiment setup.

Once the device is fixed on the microscope stage (**Figure 4.2b**), a set of reference images was first taken at room temperature without any application of microfluidic cooling or heating (**Figure 4.5**, step i). Following that, another set of images was taken under an applied temperature gradient (**Figure 4.5**, step ii). Throughout the experiment, it is essential to maintain precise optical alignment of the device, otherwise the calibration may be lost.

Another critical step of the protocol prior to image analysis was an image correction process to account for inhomogeneous illumination of the microscope (**Figure 4.6**). The image correction process involved calibrating the reference image to the average pixel intensity of the whole frame, under the assumption that the entire region was at a uniform temperature and so would exhibit uniform fluorescence intensity (**Figure 4.6a**). Specifically, a correction factor was calculated for each frame pixel following **Equation 4.2**:

$$Correction\ factor = \frac{Global\ average\ pixel\ intensity\ of\ reference\ image}{Pixel\ intensity\ of\ reference\ image} \quad (4.2)$$

Then, **Equation 4.3** was applied to correct image pixels:

$$Corrected\ pixel\ intensity = Original\ pixel\ intensity \times\ Correction\ factor \quad (4.3)$$

The same correction factor matrix determined from the reference frame was subsequently applied to correct all fluorescence images acquired under unknown temperature conditions (**Figure 4.6b**). This ensured that any spatial variations in fluorescence intensity could be accurately attributed to local temperature differences.

After correction, the pixel intensities of the images captured at unknown temperatures were normalized by **Equation 4.4** (**Figure 4.5**, step iii):

$$Normalized\ intensity = \frac{Pixel\ intensity\ of\ reference\ image}{Intensity\ of\ corresponding\ pixel\ in\ reference\ frame} \quad (4.4)$$

Finally, the calibration curve was applied to calculate the temperature pixel-by-pixel (**Figure 4.5**, step iv). Thus, the spatial resolution of this measurement technique is dictated by the pixel size, which is 0.62 μm in this study.

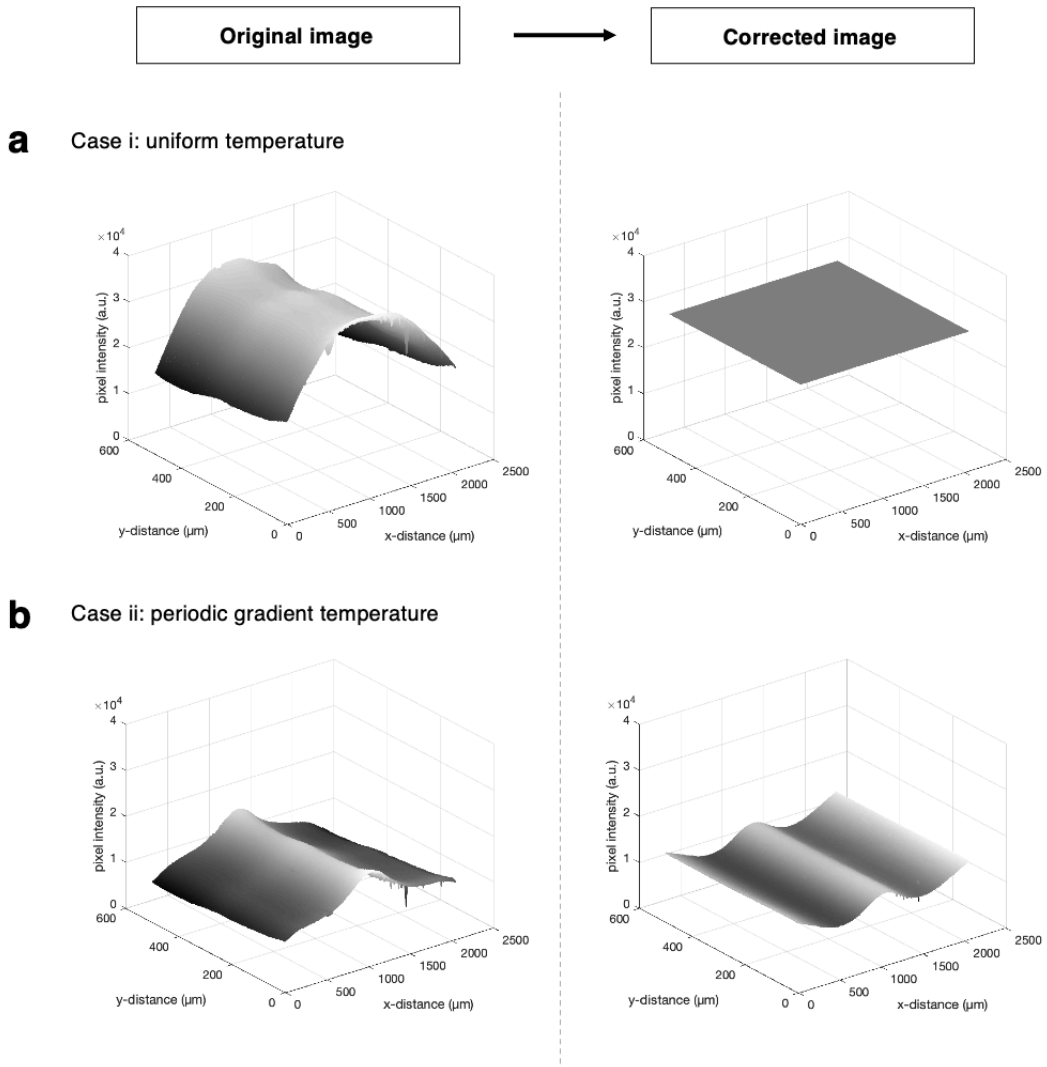

Figure 4.6: Example fluorescence images demonstrating the image correction process. (a) Original and corrected images acquired under uniform (room temperature) conditions, used to generate the correction factor matrix. (b) Original and corrected images acquired under non-uniform temperature conditions. Image correction compensates for uneven illumination. Note that the corrected images are the same images displayed in Figure 4.5.

4.2.3 Practical significance and considerations

The proposed microcapillary-based fluorescence thermometry protocol was intended as a simple and accessible method, utilizing readily available materials (i.e., Rhodamine B dye, glass microcapillaries) and basic laboratory instruments (i.e., fluorescence microscope). A key advantage of this approach is that the microcapillary probe can be reused many times. As a test, the same Rhodamine B probe used repeatedly over 3 months from preparation was found to retain consistent temperature-dependent fluorescence, demonstrating excellent long-term stability. Provided that the Rhodamine B solution composition (0.1 mM, prepared in Milli-Q water) is kept constant, the calibration curve in **Figure 4.4** can be directly applied across multiple experiments, thus streamlining the temperature measurement workflow.

A potential source of error using this measurement technique is photobleaching. Ross et al. reported that no evident photobleaching in 0.1 mM Rhodamine B solution after 30 min of constant illumination with the excitation light[3]. In our case, the longest experiment, performed to assess thermal stability of the microfluidic device (**Figure 6.5e**), involved a total exposure time of <1 min. Such short exposure duration in general significantly reduces the risk of photobleaching. As good practice, fluorescence intensity at the end of each imaging session was also re-evaluated at room temperature and compared with the initial reference image to confirm that the signal remained stable and within acceptable deviation.

In practice, thermocouples remain useful for quick, coarse-grained checks to assess the microdevice temperature during the thermophoretic gradient hydrogel fabrication process. However, the use of fluorescence-based temperature mapping can provide significantly higher spatial resolution and thus offers a more informative approach for characterization of the thermophoresis platform. Throughout the thesis, the fluorescence-based temperature measurement technique is integrated into various stages of the work from supporting process understanding to informing platform design, and contributing to process optimization.

4.3 Fluorescence characterization of thermophoretic behavior

Note: Chapter 4.3 describes the use of fluorescently labelled polymers developed as part of a broader study presented in Chapter 7, which covers the fabrication, characterization, and cell culture studies of the resulting hydrogels. The focus of this section is to elucidate the thermophoretic behavior of the (uncrosslinked) polymers in solution, providing generalizable insights into the process design and analysis.

4.3.1 The need for experimental characterization of thermophoresis

Up to this point, the thesis has explored microfluidic systems to control temperature gradients and a method for high spatial resolution mapping of the temperature distribution within the sample microchamber. These developments set the stage for further implementation of thermophoresis to manipulate biopolymer molecules in micron-scale geometries. Given the application focus on fabricating stiffness gradient hydrogels, it would also be crucial to first characterize the thermophoretic behavior of the desired hydrogel systems. Since the thermophoretic behavior is highly specific to each material, this step is useful to guide the reliable estimation of the required conditions for robust material design and optimization.

In particular, this section aims to address two key practical questions: 1) what magnitude of temperature gradient is required to induce a dominant thermophoresis effect, and 2) how long the applied temperature gradient must be maintained to attain a discernable gradient concentration profile. In line with the scope of this thesis, the thermophoresis characterization experiments presented in this section were performed using GelMA and Gellan gum systems, demonstrating how thermophoretic migration of hydrogel-forming polymers depends on their physicochemical properties. However, the experimental and analysis framework should be generalizable for the development of any material system using the established thermophoresis platform.

It is important to clarify that the goal here is not to quantify the thermophoretic properties (i.e. Soret coefficient, S_T; see definition in **Chapter 3.2**) of each material system through systematic investigations of their dependence on an exhaustive list of variables. In the field of thermophoresis, these investigations are classically performed

using highly diluted solutions, narrow confinements, and ideally, very weak temperature gradients (e.g., <1 K mm^{-1})[11]. In principle, since S_T dictates the strength and direction of the "concentrating effect", a comprehensive knowledge will be useful to develop theories and models that accelerate the search for optimal fabrication parameters and improve material predictability[12,13]. Indeed, early on, attempts were made to perform such systematic investigations on both GelMA and Gellan gum, using the microfluidic design described in section 4.1, with varying sample channel widths from 50 μm to 600 μm. However, the results were inconsistent from experiment to experiment, mainly due to a high propensity of polymer aggregation and clogging in narrow channels <100 μm. This was an especially difficult problem with Gellan gum due to its large polymer chains. On the other hand, empirical determination of S_T requires the system to reach steady state (i.e., the thermophoresis-induced concentration gradient reaches a plateau), which may take hours if not days in wider microchannels. In contrast, the process objective for gradient hydrogel fabrication is more practical: to generate a sufficiently defined and stable concentration gradient within a limited time frame, which can typically be accomplished well before the point of thermophoretic equilibrium. Therefore, given the application-driven focus of this thesis, it was decided that a more targeted experimental strategy that prioritizes understanding of the thermophoretic behavior under fabrication-relevant conditions would be more beneficial at this stage.

4.3.2 The experiment design and workflow

Specifically, a relatively high polymer concentration of 1 wt% Gellan gum and 10 wt% GelMA were used in subsequent thermophoresis experiments, representative of the typical precursor formulations employed for gradient hydrogel fabrication required to achieve biologically relevant stiffness ranges. Additionally, given that the concentration (and stiffness) gradient induced by thermophoresis is directly proportional to the imposed temperature gradients (i.e., $\nabla c \propto \nabla T$; see **Equation 3.2**), experiments were focused on investigating relatively large temperature gradients, ensuring that the observed thermophoretic behaviors are directly translatable to produce stiffness gradients of sufficient and useful magnitude in the final hydrogels.

A key enabling step in this study was the fluorescent labelling of Gellan gum and GelMA polymers with fluorescein isothiocyanate (FITC). The synthesis of FITC-labelled Gellan gum (F-GG) and FITC-tagged GelMA (F-GM) are described in **Chapter 3.5.1**, and the detailed material characterization of the resulting hydrogels are presented in **Chapter 7**. The ability to directly visualize the polymers allowed for material-specific insight into the thermophoretic migration process and obviated the need for model proxies (e.g., fluorescent polystyrene nanoparticles used to generate Figure 5.2 and Figure 6.6). For thermophoresis experiments, sample solutions were prepared by mixing the FITC-labelled polymer with unlabelled polymer in Milli-Q water at a mass ratio of 1:9. This provided a sufficiently strong fluorescence signal for imaging, while ensuring that the overall physicochemical properties of the system still closely reflect those of the native, unmodified polymers.

As shown in **Figure 4.7a**, the experiments were conducted using a microfluidic device designed with a straight sample microchannel (600 μm in width) flanked by a heating and cooling channel to generate linear temperature gradients across the sample volume. This approach of studying thermophoresis by monitoring changes in the concentration profile under a microscope has been used extensively within our laboratory group[14–18], offering a much simpler and accessible alternative to traditional setups that involve highly specialized instrumentation.

To set up a thermophoresis experiment, the polymer solution was injected into the sample microchannel, then the channel openings were plugged (using a short piece of Tygon tubing with the ends sealed using epoxy) to contain the solution and prevent sample evaporation. After that, the microdevice was left to stabilize on the microscope stage for at least 5 min without applying a temperature gradient. This step ensured that no flow was present at the start of the experiment, allowing for accurate measurement of thermophoretic behavior.

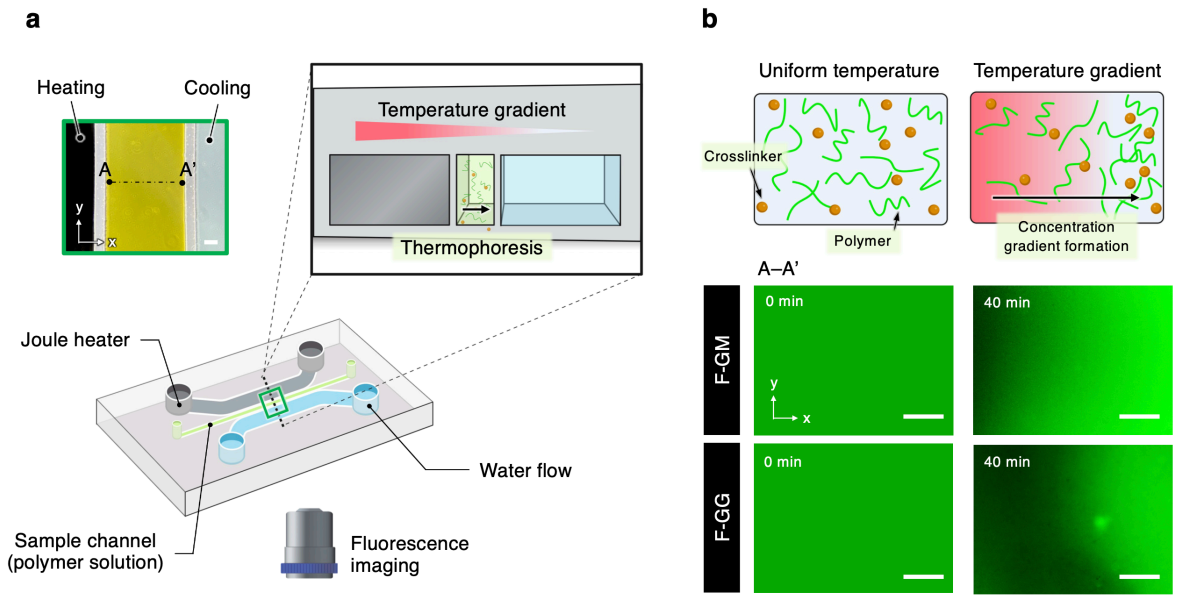

Figure 4.7: (a) Schematic of the thermophoresis experimental setup. The green bounding box shows a zoom-in optical image from the top view of the microfluidic device. The black bounding box depicts the cross-section of the device. (b) Schematic of the mechanism of gradient formation by thermophoretic migration in the presence of a temperature gradient (top), with representative fluorescent images demonstrating the accumulation of F-GM and F-GG polymer chains from hot to cold regions (bottom). Note that the images for F-GM and F-GG correspond to the data in Figure 4.8b and Figure 4.9b, respectively.

As has already been introduced extensively in this thesis, thermophoresis is induced in the presence of a temperature gradient, which in turn causes directed spatial redistribution of polymers in solution (**Figure 4.7b**). The result is a progressive formation of a concentration gradient which can be measured by assessing the fluorescence intensity across the microchannel over time. To that end, a fluorescence image was captured every 30 s for up to 1 h, then the images were processed using a custom MATLAB workflow to analyze the intensity profile. Specifically, the set of images was normalized to the first frame taken at t = 0 min (immediately before starting application of temperature gradient), which assumed a uniform temperature within the sample channel. This approach was used to compensate for uneven baseline fluorescence that may be caused by static sample defects, and allowed the intensity to be quantified as relative intensity shifts corresponding to local concentration changes. Additionally, to account for potential photobleaching, the intensity of each frame was calibrated to match the average intensity value of the first frame. Importantly, this image processing step reflects mass conservation in the material system, meaning

that the observed changes in fluorescence intensity should only be due to polymer redistribution rather than a loss or gain in total polymer content, which remained constant throughout the experiment. An example set of output images for F-GM and F-GG are shown in **Figure 4.7b**. In all cases, the left boundary was maintained at a higher temperature than the right boundary. Evidently, the polymers moved from the hot region to the cold region, exhibiting a thermophobic behavior ($S_T > 0$) which is consistent with the results from AFM measurements throughout this thesis.

In the next step of analysis, a single intensity line profile at each measured time point was obtained by averaging in the direction perpendicular to the imposed temperature gradient (i.e., y-axis with reference to Figure 4.7). As shown in **Figure 4.8b** and **Figure 4.9b**, the concentration gradient developed inside the microchannel was linear around the middle of the channel. Therefore, in order to calculate the concentration gradient, a linear interpolation was fitted to the central 65% segment of the intensity profile and the slope was extracted. As a first approximation, the correlation between fluorescence intensity and concentration of the polymers is generally linear (**Figure 4.8a, Figure 4.9a**). Therefore, based on the known initial polymer concentration, the fluorescence intensity values from each image data were converted into concentration, finally yielding a corresponding concentration gradient (**Figure 4.8c, Figure 4.9c**).

The rest of this section discusses the effect of varying applied temperature gradient strength; in each scenario, the average system temperature was maintained around 61-65 ºC. The temperature across the sample channel was pre-characterized using the fluorescence thermometry technique (previously described in Section 4.2), confirming a linearly varying profile.

4.3.3 GelMA

Figure 4.8b shows a representative example of the concentration gradient generated in 10 wt% GelMA solution over 40 min.

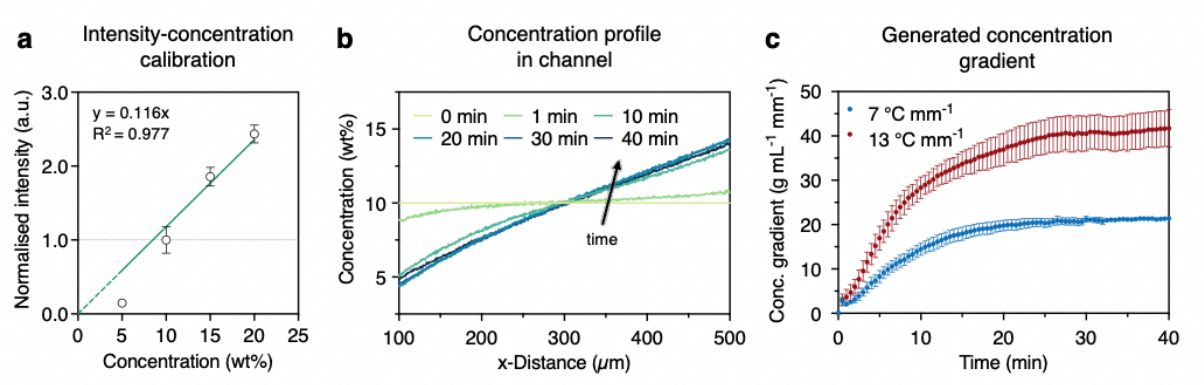

Figure 4.8: (a) Correlation curve connecting fluorescently labelled GelMA (F-GM) polymer concentration to fluorescence intensity (n=3 independent samples; mean ± SEM). (b) An example data set showing thermophoretic migration of F-GM under an applied temperature gradient of 7 °C mm^{-1}, with progressive accumulation of polymers to the cold side. (c) The resulting concentration gradient as a function of time, evaluated under different applied temperature conditions (n=3 independent experiments; mean ± SEM).

Overall, the results demonstrated a highly linear concentration profile across the channel, with the gradient approaching steady state after about 30 min. This trend was also consistently observed across both "low" (7 °C mm^{-1}) and "high" (13 °C mm^{-1}) temperature gradients. As shown in **Figure 4.8c**, when the imposed temperature gradient was approximately doubled, the (quasi-)steady state concentration gradient was also nearly doubled, confirming the proportional relationship between temperature and concentration gradients. The ability to achieve strong concentration gradients (>20 g mL^{-1} mm^{-1}) signifies the potential of the thermophoresis approach to create GelMA hydrogels with orders of magnitude steep stiffness gradients, noting that shallower stiffness gradients should equally be attainable by applying a weaker temperature gradient input.

Interestingly, however, the observed linear concentration distribution contrasts with classical thermophoresis theory, which anticipates an exponential profile at steady state (see **Equation 3.3**). A key assumption of **Equation 3.3** is that S_T remains constant throughout the system. Thus, it is reasonable to hypothesize that in this case,

S_T varied spatially within the microchannel, which meant that the thermophoretic-driven redistribution of polymers would deviate from an exponential profile. One possible explanation to this behavior is that the temperature differences experienced inside the microchannel were significant enough to cause a noticeable variation in S_T. In other words, the polymers were migrating at different rates in different regions. Although there is currently no publication reporting the temperature dependence of S_T for GelMA (or any other common hydrogel-forming) polymers, this effect has been well established in the field[11–13]. Another possible explanation could be attributed to polymer-polymer interactions at higher sample concentrations. In a related study using polystyrene beads, Zhao et al. described the presence of such "collective effects" in thermophoresis[19], where higher concentrations not only altered the magnitude of S_T but could potentially also change its sign (i.e., particles could switch between thermophilic and thermophobic behaviors). Although the influence of solute concentration on thermophoretic behavior is less well understood in comparison, it is perhaps reasonable to expect that such polymer-polymer interactions, which are likely present at the typical working concentrations used in most hydrogel formulations, may lead to deviations from the simplistic theoretical model (**Equation 3.3**) for dilute, non-interacting colloidal systems. Nevertheless, this deviation should not undermine the utility of thermophoresis, but rather, it highlights the complex yet predictable and controllable nature of the process.

From a gradient hydrogel fabrication standpoint, the consistent linear concentration profile in response to a linear temperature gradient is highly beneficial. Such linearity should enable precise control over the stiffness gradients without requiring complex temperature inputs or additional calibration steps, simplifying the fabrication process design.

4.3.4 Gellan gum

Figure 4.9b shows a representative example of the concentration gradient generated in 1 wt% Gellan gum solution over 40 min.

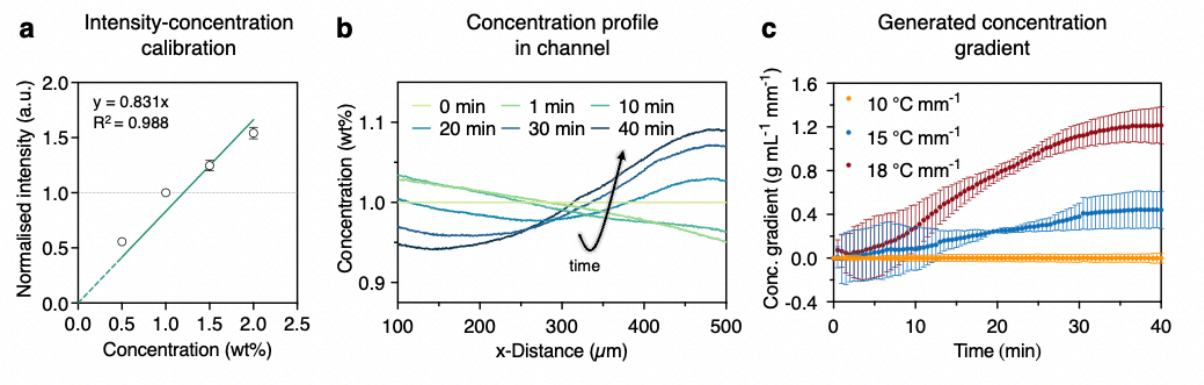

Figure 4.9: (a) Correlation curve connecting fluorescently labelled Gellan gum (F-GG) polymer concentration to fluorescence intensity (n=3 independent samples; mean ± SEM). (b) An example data set showing thermophoretic migration of F-GG under an applied temperature gradient of 15 °C mm^{-1}, with progressive accumulation of polymers to the cold side. (c) The resulting concentration gradient as a function of time, evaluated under different applied temperature conditions (n=3 independent experiments; mean ± SEM).

When subjected to a temperature gradient, Gellan gum demonstrated the gradual formation of a concentration gradient that was characteristic of thermophoretic migration. However, notable differences in thermophoretic behavior were observed compared to GelMA, highlighting the material-specific nature of this process.

First, the minimum temperature gradient required to induce a discernible concentration gradient in Gellan gum was higher than that for GelMA. Of note, there was no apparent concentration gradient in Gellan gum below 10 °C mm^{-1} (**Figure 4.9c**), whereas GelMA exhibited a clear concentration gradient formation even at 7 °C mm^{-1} (**Figure 4.8c**). These findings were interpreted in terms of weaker thermophoretic mobility of Gellan gum compared to GelMA, meaning that under similar thermal conditions, Gellan gum would respond more slowly to the temperature gradient. In this respect, stronger applied temperature gradients were required to amplify the thermophoretic force and make it sufficiently dominant to overcome diffusion and other competing transport forces, at which point a clear measurable concentration gradient can be attained.

Second, the time to reach steady state in the Gellan gum system was noticeably longer even at higher applied temperature gradient conditions. This observation can be explained by the significantly larger molecular size of Gellan gum (~1000 kDa)[20] compared to GelMA (~100 kDa)[21]. Larger polymers will have smaller diffusion coefficients, resulting in a longer time to reach thermophoretic equilibrium (see **Table 4.1** and further discussion in Section 4.3.5). Furthermore, the long polymer chain lengths were expected to increase the effect of polymer-polymer interactions, which may contribute to greater fluctuations in polymer distribution, especially during the initial stages of the experiment, as indicated by the large error bars in **Figure 4.9c**.

In a similar manner to GelMA, Gellan gum did not exactly follow an exponential spatial distribution. In this case, the resulting concentration profiles were generally linear for the most part, except near the channel walls (**Figure 4.9b**).

4.3.5 Implications for thermophoretic fabrication of gradient hydrogels

The concentration gradient plots generated from the thermophoresis experiments are also useful to extract the characteristic time, τ, which describes how quickly the system reaches a steady state. To do this, the concentration gradient, ∇c, vs. time, t, plots were fitted to an exponential curve of the form (**Equation 4.1**):

$$\nabla c = A - B\exp(-t/\tau) \tag{4.1}$$

where A and B are constants. An example of the curve fitting is shown in **Figure 4.10**. As good practice in the field, the fit was started at approximately 1/3 of τ (estimated from the trajectory of the full plot), which was done to discount potential noise or instability in the initial stages of the process.

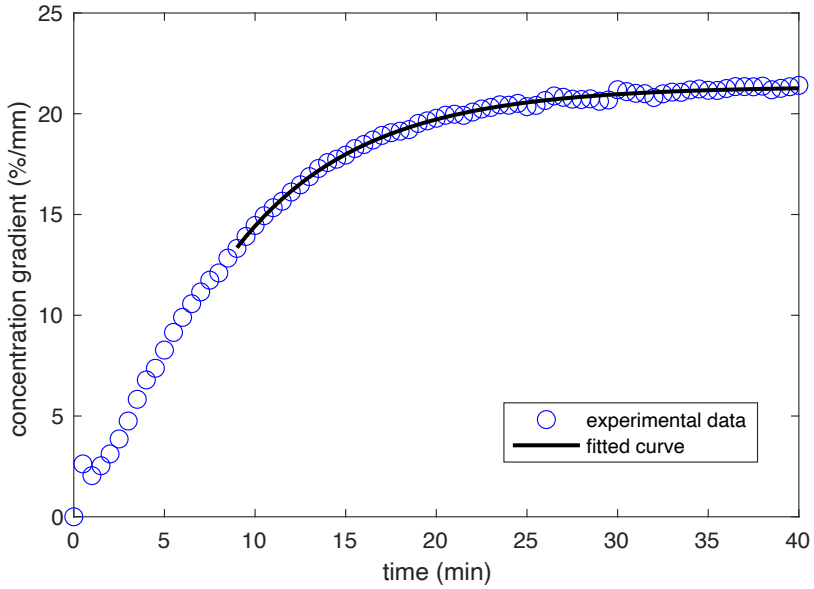

Figure 4.10: Example demonstrating exponential fit to the curves in Figure 4.8c and Figure 4.9c for evaluating thermophoresis characteristic time, τ.

Finally, the diffusion coefficient, D, for each system can be calculated from $\tau = d^2/\pi^2 D$ (**Equation 3.4**). The resulting values of τ and D are summarized in **Table 4.1**.

Table 4.1: Summary of thermophoresis characteristic time, τ and diffusion coefficient values, D, extracted from the data in Figure 4.8c and Figure 4.9c. R^2 values are reported as a measure of goodness of curve fit.

Polymer type	Temperature gradient [°C mm^{-1}]	τ [min]	R^2 value	D [cm^2 s^{-1}]
GelMA	~7	~7	0.9975	~8.7×10^{-7}
GelMA	~13	~9	0.9940	~6.8×10^{-7}
Gellan gum	~15	~45	0.9825	~1.4×10^{-7}
Gellan gum	~18	~16	0.9946	~3.8×10^{-7}

The results revealed that the thermophoresis characteristic time of GelMA is nearly invariant across the range of temperature gradients tested. On the contrary, Gellan gum showed a stark reduction in the characteristic time with just a slight increase in temperature gradient strength. This likely reflects the strong dependence of Gellan gum viscosity on temperature (**Equation 3.5**), which in turn affects the diffusion coefficient and thereby the kinetics of thermophoretic migration.

Based on the findings from this set of experiments, I propose several practical guidelines for implementing thermophoresis to fabricate stiffness gradient hydrogels.

Exploratory process analysis

While thermophoresis is broadly applicable to different (polymer) systems, careful considerations must be given to the material-specific nuances of thermophoretic migration. There are a number of parameters that may influence the final properties in the gradient gels, including polymer concentration, applied temperature gradient strength, average system temperature, and process duration. When working with a new material, initial thermophoretic characterization experiments, as demonstrated in this section, can be a strategic way to accelerate the identification of suitable process parameters. As a rule of thumb, it is recommended to only vary the applied temperature gradient strength, keeping other parameters constant. Often, the polymer concentration is guided by the target average substrate stiffness, while the average system temperature is governed by material (e.g. critical gelation temperature) or application (e.g., the need for cell encapsulation) requirements. Under such fabrication-relevant conditions, the goal of these experiments should be to establish the directionality of thermophoretic migration as well as linearity of the resulting concentration distribution, assess the threshold temperature gradient required to generate well-defined concentration gradients, and learn how changes in the magnitude of temperature gradient input would influence the resulting concentration gradient output. The latter is particularly useful for fine-tuning the process to achieve desired stiffness gradient slopes without relying solely on trial-and-error gradient gel fabrication.

It is fully acknowledged that the need for fluorescently labelled polymers might be perceived as an additional experimental burden. However, it should be emphasized that the process insights gained from these experiments are generally transferable across different thermophoresis microdevice designs and sample dimensions. Provided that the degree of fluorescence labelling is sufficiently low to not cause significant alterations in the polymer's physicochemical properties, the findings can also be directly applied to the unmodified polymers for gradient gel fabrication. In this context, one could perhaps envision how the exploratory thermophoresis experiments

serve as a one-time calibration exercise that supports technology accessibility and repeatability in the long run. It is worth noting that a similar extent of trials for process optimization is also expected using previously established methods, see for example, the excellent protocol written up by Tse and Engler on the gradient photomask technique[22]. Indeed, the approach proposed within the scope of my thesis was inspired by the different process design and optimization strategies reported in the gradient hydrogel literature over the years[22,23], but seeks to introduce a physics-informed framework that aims to move beyond empirical tuning toward more rational and predictable gradient material designs.

In **Chapter 7**, I further explore how the fabrication of gradient gels using the fluorescently labelled polymers could prove useful for the characterization and application of stiffness gradients for cell studies.

Adapting to varying polymer concentrations

The concentration of each polymer used for the thermophoresis experiments represents the higher end of the typical working range used for gradient hydrogel fabrication in practice. This was a deliberate choice that serves as a conservative benchmark. At higher concentrations, the expected increase in polymer-polymer interactions might lead to dampened thermophoresis effects at a given thermal condition. In this respect, anchoring the characterization of thermophoretic behavior at these more complex and demanding conditions provides a stringent test of the robustness of the protocol. If functional concentration (and thus stiffness) gradients can be consistently achieved under such conditions, it strongly supports the feasibility of applying the thermophoresis method for equally, if not more, effective control of polymer distribution in lower concentration systems. For example, in Chapters 6 and 7 in this thesis, the same fabrication process conditions were found to be effective in producing stiffness gradients in both 10 wt% and 5 wt% GelMA hydrogels.

Scaling the thermophoresis process time for different geometries

Furthermore, for gradient gel fabrication, it is recommended to carry out the thermophoresis process for a duration of at least the measured characteristic time,

noting that this may differ with varying thermal conditions. In general, this duration has proven sufficient to achieve consistent stiffness gradient quality in the final hydrogels. Importantly, the required process time should also be scaled according to the desired gradient span, which would be defined by the distance between the hottest and coldest regions within the microdevice. To illustrate an example, we take the case of GelMA in which the characteristic time was approximately 10 min in a 600 μm channel (**Table 4.1**). Since the characteristic time scales linearly with the distance squared ($\tau \propto d^2$; see **Equation 3.4**), it would require approximately 30 min to establish a similar magnitude of concentration gradient in a 1000 μm channel.

Overall, these material and process knowledge for gradient hydrogel fabrication were also found to be directly transferable between implementation in a fully enclosed microchannel system or a tape-based microchamber, the latter of which is newly introduced in this thesis. This suggests that the thermophoretic fabrication technique can be reliably adapted to any micro-confinement setups based on the user's expertise or resource availability, but careful attention must be paid to avoid non-thermophoretic effects such as thermal convection.

4.4 Conclusion

The early stages of my PhD research were dedicated to understanding the operation of thermophoresis microdevices and the various parameters that influence thermophoretic migration. During this process, limitations of thermocouple-based temperature measurements in capturing the fine spatial details within the devices prompted the development of a meticulously optimized fluorescence thermometry protocol that enables noninvasive mapping of temperature fields with micron-scale resolution. On the other hand, in recognizing the material-specific nuances of thermophoresis, I pursued fluorescent labelling strategies that allowed direct visualization and characterization the target polymers under conditions representative of the gradient gel fabrication process in practice.

The establishment of these refined experimental methodologies in turn opened up new avenues to explore thermophoretic fabrication of spatially complex stiffness patterns (**Chapter 6**) as well as the potential utility of fluorescently labelled stiffness gradient hydrogels (**Chapter 7**). These would form the central themes that continue throughout the thesis.

References

1. Kim, M. M. *et al.* Microscale thermometry: A review. *Microelectron Eng* **148**, 129–142 (2015).

2. Yang, F., Yang, N., Huo, X. & Xu, S. Thermal sensing in fluid at the micro-nano-scales. *Biomicrofluidics* **12**, 041501 (2018).

3. Ross, D., Gaitan, M. & Locascio, L. E. Temperature measurement in microfluidic systems using a temperature-dependent fluorescent dye. *Anal Chem* **73**, 4117–4123 (2001).

4. Liu, W., Zhao, D., Zhang, R. J., Yao, Q. X. & Zhu, S. Y. Fluorescence Lifetime-Based Luminescent Thermometry Material with Lifetime Varying over a Factor of 50. *Inorg Chem* **61**, 16468–16476 (2022).

5. Mendels, D. A., Graham, E. M., Magennis, S. W., Jones, A. C. & Mendels, F. Quantitative comparison of thermal and solutal transport in a T-mixer by FLIM and CFD. *Microfluid Nanofluidics* **5**, 603–617 (2008).

6. Lee, N., Afanasenkau, D., Rinklin, P., Wolfrum, B. & Wiegand, S. Temperature profile characterization with fluorescence lifetime imaging microscopy in a thermophoretic chip. *Eur Phys J E* **44**, 130 (2021).

7. Liu, C. *et al.* Low-cost thermophoretic profiling of extracellular-vesicle surface proteins for the early detection and classification of cancers. *Nat Biomed Eng* **3**, 183–193 (2019).

8. Thamdrup, L. H., Larsen, N. B. & Kristensen, A. Light-induced local heating for thermophoretic manipulation of DNA in polymer micro- And nanochannels. *Nano Lett* **10**, 826–832 (2010).

9. Mao, H., Holden, M. A., You, M. & Cremer, P. S. Reusable platforms for high-throughput on-chip temperature gradient assays. *Anal Chem* **74**, 5071–5075 (2002).

10. Glawdel, T., Almutairi, Z., Wang, S. & Ren, C. Photobleaching absorbed Rhodamine B to improve temperature measurements in PDMS microchannels. *Lab Chip* **9**, 171–174 (2009).

11. Talbot, E. L., Kotar, J., Parolini, L., Di Michele, L. & Cicuta, P. Thermophoretic migration of vesicles depends on mean temperature and head group chemistry. *Nat Commun* **8**, 15351 (2017).

12. Iacopini, S., Rusconi, R. & Piazza, R. The 'macromolecular tourist': Universal temperature dependence of thermal diffusion in aqueous colloidal suspensions. *Eur Phys J E* **19**, 59–67 (2006).

13. Wolff, M. *et al.* Quantitative thermophoretic study of disease-related protein aggregates. *Sci Rep* **6**, 22829 (2016).

14. Vigolo, D., Rusconi, R., Stone, H. A. & Piazza, R. Thermophoresis: microfluidics characterization and separation. *Soft Matter* **6**, 3489–3493 (2010).

15. Vigolo, D., Rusconi, R., Piazzaa, R. & Stone, H. A. A portable device for temperature control along microchannels. *Lab Chip* **10**, 795–798 (2010).

16. Vigolo, D. *et al.* Continuous Isotropic-Nematic Transition in Amyloid Fibril Suspensions Driven by Thermophoresis. *Sci Rep* **7**, 1211 (2017).

17. Vigolo, D., Ramakrishna, S. N. & DeMello, A. J. Facile tuning of the mechanical properties of a biocompatible soft material. *Sci Rep* **9**, 7125 (2019).

18. Kosmidis Papadimitriou, A. *et al.* Fabrication of gradient hydrogels using a thermophoretic approach in microfluidics. *Biofabrication* **16**, 025023 (2024).

19. Zhao, Y., Zhao, C., He, J., Zhou, Y. & Yang, C. Collective effects on thermophoresis of colloids: A microfluidic study within the framework of DLVO theory. *Soft Matter* **9**, 7726–7734 (2013).

20. Vieira, S. *et al.* Gellan gum-coated gold nanorods: An intracellular nanosystem for bone tissue engineering. *RSC Adv* **5**, 77996–78005 (2015).

21. Shin, H., Olsen, B. D. & Khademhosseini, A. The mechanical properties and cytotoxicity of cell-laden double-network hydrogels based on photocrosslinkable gelatin and gellan gum biomacromolecules. *Biomaterials* **33**, 3143–3152 (2012).

22. Tse, J. R. & Engler, A. J. Preparation of Hydrogel Substrates with Tunable Mechanical Properties. *Curr Protoc Cell Biol* **47**, 10161 (2010).

23. Dertinger, S. K. W., Chiu, D. T., Noo Li Jeon & Whitesides, G. M. Generation of gradients having complex shapes using microfluidic networks. *Anal Chem* **73**, 1240–1246 (2001).

Chapter 5

Foundational development of the thermophoretic fabrication platform

This chapter reports the first biological demonstration of thermophoretically fabricated stiffness gradient hydrogels for interrogating stiffness-dependent cellular behavior. Using the foundational platform design, Gellan gum hydrogels with stiffness gradients ranging from 20-90 kPa over 600 μm were created, covering the elastic moduli typical of moderately-hard to hard tissues. MC3T3 osteoblast cells were then cultured on these gradient gels, which exhibited preferential migration and enhanced osteogenic potential toward the stiffest region on the gradient. At the end, this chapter provides an account of the early challenges and lessons learned from implementing thermophoresis as a new fabrication method. These were used to guide the subsequent development of the platform technology.

A large part of the excitement behind starting from first principles of thermophoresis is the potential for building practical technological applications. Toward that goal, the study presented in this chapter was the proof of its application to fabricate stiffness gradient hydrogels for *in vitro* cell studies. This work was conducted in close collaboration with Dr Alexandros Kosmidis Papadimitriou, which initiated during his PhD research with Vigolo LAB back at the University of Birmingham (UK). In addition to my contributions to this foundational work, another one of my key achievements was transferring the platform's capabilities to our new laboratory at The University of Sydney. Importantly, this process allowed me to critically evaluate the platform's limitations and opportunities. Thus, in this chapter, I first present the complete study which is now published (Section 5.3)[1], then I further provide my perspectives on how the platform could be advanced for broader mechanobiology applications (Section 5.4).

5.1 Introduction

The role of stiffness gradient hydrogels for studying how spatial variations in tissue stiffness impact cell activity has already been introduced extensively in this thesis. In this context, the thermophoresis technique was developed as a potential alternative that offers a non-toxic, versatile route for fabricating stiffness gradients hydrogels independently of their crosslinking mechanism. A key advantage of this approach is to provide users active control of the material properties down to micron-scale resolution, promising precise and reproducible stiffness gradients for probing cell-substrate interactions.

To demonstrate this, we fabricated 600 µm-wide Gellan gum hydrogel strips and showed that these substrates presented continuous gradients of physical properties which in turn endowed them with spatially distinct osteogenic capacity. Gellan gum was chosen given its demonstrated performance as scaffolds for tissue engineering applications, especially for cartilage or osteochondral tissues[2–4]. In particular, the steep stiffness gradients enabled recapitulation of the biophysical characteristics of the tissue interfacing tendons and bones known as enthesis (~500 µm width)[5–7]. For biological assessment, MC3T3 preosteoblast cells were seeded on the fabricated gradient Gellan gum hydrogels and their stiffness responses were observed for up to 30 days.

5.2 Experimental methods

This section contains additional methods that are specific to the experiments in this chapter, and should be read in conjunction with the general materials and methods presented in **Chapter 3**.

5.2.1 Microfluidic device design

This study was performed using the microfluidic platform previously described in **Chapter 4** with slight modifications (**Figure 5.1a**). Specifically, the middle sample channel had cross-sectional dimensions of 600 μm (width) × 140 μm (height), whereas the side channels for cooling and heating were 2000 μm (width) × 140 μm (height). The middle channel was separated from the side channels by a 200 μm-thick PDMS wall, and the length of all the microchannels were 4 cm. Furthermore, a small reservoir was cut out at one end of the sample microchannel to allow extrusion of the hydrogel post-fabrication for material characterization and cell culture (**Figure 5.1b**).

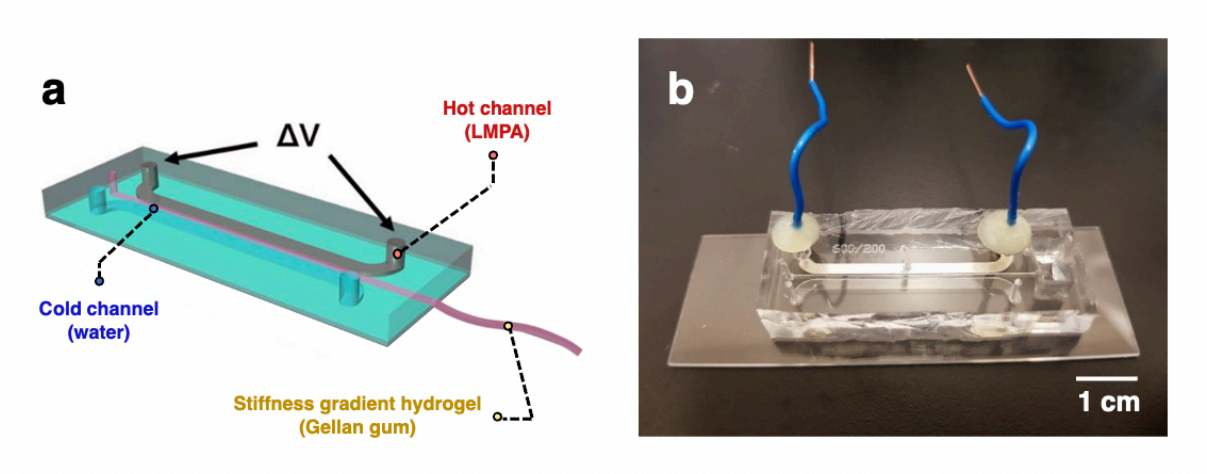

Figure 5.1: (a) Schematic illustration of microfluidic device which consists of a main sample channel and two side channels used to generate a temperature gradient across the main channel. (b) Image of the assembled microfluidic device.

5.2.2 Gradient hydrogel fabrication

Stiffness gradient hydrogels were fabricated using Gellan gum solution with an initial polymer concentration of 0.8 wt%, 1 wt%, or 1.5 wt%. First, hot Gellan gum solution (~70 °C) was quickly injected into the sample microchannel until it overfilled at both ends, whereby the excess solution would crosslink rapidly upon exposure to ambient conditions, forming hydrogel plugs to seal the channel. Meanwhile, the rest of the microfluidic chip was kept warm at 72 °C by placing it on a thermoelectric Peltier module (40 mm × 40 mm, RS components), which maintained the polymer solution in its uncrosslinked state.

A linear temperature gradient ranging from 3.6 °C mm^{-1} to 7.5 °C mm^{-1} was applied across the sample channel for 20-30 min by setting the water flowrate constant at 300 µl min^{-1} using a syringe pump, and varying the power supply unit settings. After the concentration gradient was formed, the temperature gradient was removed and by switching the Peltier module to cooling mode, we were able to decrease the device temperature down to 0.5 °C within 1-2 min. This enabled rapid crosslinking and prevented disruption to the concentration gradient. After 20 min, the Gellan gum gradient hydrogel was extruded from the microchannel, attached to a PEI-coated glass slide, and stored in deionized water at 4 °C.

5.2.3 Temperature evaluation

At the time of this study, the fluorescence thermometry method was still under development. As such, measurements of the applied temperature gradient for the main study were obtained using thermocouples (1×0.076 mm, K-type, ZO-PFA-K-1 X 5, element14) inserted into each of the side channels. For the cold channel, this was achieved by threading a thermocouple through the channel outlet before connecting to Tygon tubing. For the hot channel, an additional opening was created from the top of the PDMS layer using a biopsy punch, then a thermocouple was placed in direct contact with the exposed LMPA and sealed with an appropriate amount of thermal paste to ensure good heat conduction.

Subsequently, the actual temperature gradient across the sample microchannel can be estimated from these measurements and known thermal conductivities of the device substrates, assuming a linear gradient profile and using an electrical resistance analogy model[8].

5.2.4 Computational simulation

3D steady state numerical simulations were performed in ANSYS Fluent 2022 on a finite element photolithography masking process. To model heat transfer through the polymer and the glass slide, we expanded the default Fluent materials library to include the thermal properties of PDMS and solid glass. Convective cooling was applied to all faces except the base of the glass substrate, which contacted the Peltier. The Peltier and LMPA were modeled as interfaces of constant temperature, using values that had previously been experimentally measured[8]. The <1.5 wt% Gellan gum sample was treated as having the thermal properties of liquid water. We simulated the experimental conditions for 3.6 °C mm^{-1}, 4.5 °C mm^{-1}, and 5.4 °C mm^{-1} applied temperature gradients. The temperature gradient profile across the width of the sample was evaluated by inspecting the temperatures at the middle cross-sectional plane of the simulated microfluidic device. Temperature distributions along the length of the sample channel were extracted by taking vertex averages at 100 equidistant points.

5.2.5 Cell culture

All cell culture experiments were performed using gradient Gellan gum hydrogels prepared using 1 wt% initial polymer concentration, with a temperature gradient of 7.5 °C mm^{-1} and 30 min application time. Samples were sterilized under a custom UV lamp (11 W, 254 nm) for 10 min and transferred to a 6-well plate for cell seeding. MC3T3 osteoprogenitor cells were seeded on top of the substrate at a seeding density of 5000 cells mm^{-2} (for live/dead assay) or 20 000 cells mm^{-2} (for XRF study), followed by incubation at 37 °C at 5% CO_2 for 3 h to allow cell attachment. Then, each well was filled with 3 mL of α-MEM cell culture medium, refreshed every 3 days and

kept in the incubator. As a control experiment, MC3T3 cells were cultured onto uniform stiffness Gellan gum hydrogels, prepared using 1 wt% polymer concentration.

5.2.6 Cell viability, attachment, proliferation, and migration studies

Live/dead assays were carried out by staining the cells with calcein-AM and propidium iodide at a concentration of 2.5 μl ml^{-1} and 5 μl ml^{-1}, respectively. Fluorescent images were captured at days 1, 3 and 7 of culture using a confocal laser scanning microscope (OLYMPUS FV1000 Fluoview) coupled to a 10x fluorescent objective. In addition, cells were also labeled with PKH67 green fluorescent cell linker (Sigma Aldrich), a cell membrane dye, which enabled observation of cell migration across the substrates over 7 days. The cell viability experiments were performed in triplicate. Cell morphological assessments were performed on three uniform stiffness samples and one stiffness gradient sample. To compare the cell behavior between the softer and stiffer regions of the gradient sample, confocal image of the full length of hydrogel (obtained by stitching multiple images that were acquired side-by-side) was first segmented along the width axis into three strips, each 200 μm thick. Note that the middle segment was excluded from subsequent analysis, to allow a clearer distinction between “low” and “high” substrate stiffness and their impact on cell behavior. Cell spreading was evaluated using n=39 and n=99 cells that were successfully segmented from the soft and stiff regions on the substrate, respectively. Additionally, cell density was evaluated by counting the number of cells in three randomly sampled areas for each analyzed condition.

5.2.7 X-ray fluorescence (XRF) imaging

XRF analysis was performed to detect calcium and phosphate deposition. Osteoprogenitor cells were seeded on the surface of the substrates and cultured for up to 30 days, using normal (α-MEM) or osteogenic (α-MEM supplemented with ascorbic acid and glycerol-2-phosphate) media. At day 15 or 30, samples were washed with PBS and deionized water, then dried at room temperature for 20 min.

Later, they were placed on the Bruker M4 Tornado XRF for x-ray imaging which was conducted at 50 keV under vacuum. All experiments were performed in triplicate.

5.3 Proof-of-concept: Stiffness gradient Gellan gum hydrogels

5.3.1 Overview of the platform

By carefully imposing and controlling temperature gradients across a sample microchannel filled with an initially homogenous Gellan gum solution containing calcium ions as crosslinkers, we exploited thermophoresis to form a concentration gradient of Gellan gum polymer coils inside the microchannel, which directly translates into stiffness and porosity gradients upon hydrogel crosslinking.

Initially, the effectiveness of this platform in providing a suitable environment for thermophoresis process was verified by visualizing the directional migration of fluorescent polystyrene nanoparticles in solution (**Figure 5.2**). Notably, when subjected to a temperature gradient imposed by the microdevice, time-lapse imaging demonstrated that the fluorescent nanoparticles readily accumulate toward the cold side of the microchannel within 45 min, in the direction of the thermophoretic force. By extension, it was reasoned that the thermophoretic behavior in these microdevices would be similar for biopolymer molecules such as Gellan gum. Indeed, this is established to be true in this thesis by repeating the thermophoresis characterization experiments directly using fluorescently labelled Gellan gum (**Chapter 4**).

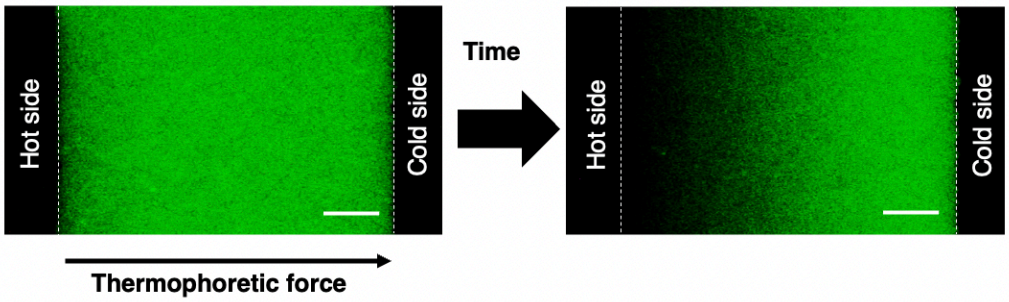

Figure 5.2: This establishment of suitable conditions for thermophoresis within the sample microchannel was experimentally validated using 500 nm fluorescent polystyrene nanoparticles suspension (1% in water), scale bars: 100 μm.

Using this microfluidic system design, it is important to note that the temperature will always assume a linear variation across the width of the sample microchannel. To verify the experimental measurements (as described in Section 5.2.3), we evaluated the temperature distribution across the whole system by performing computational simulations over the virtual microfluidic model (**Figure 5.3a**). The results confirmed that the temperature across the sample channel decreased linearly from the hot side to the cold side (**Figure 5.3b**). Additionally, by simulating the experimental process parameters (i.e., water flowrate through the cold channel and set temperature of the Joule heating channel), it was found that the strength of the temperature gradient was directly proportional to that of the stiffness gradients yielded experimentally (**Figure 5.4d**). Furthermore, the simulations revealed that the temperature gradient was highest near the front end of the device and gradually decayed down the length of the device (**Figure 5.3c**). This variation can be attributed to the progressive heating of water as it flowed through the channel (**Figure 5.3a**). However, by utilizing only a small (1-2 cm) segment from the mid-region of the fabricated Gellan gum gradient hydrogels in subsequent cell culture studies, we ensured reasonably uniform stiffness gradient throughout the sample, as verified by AFM measurements.

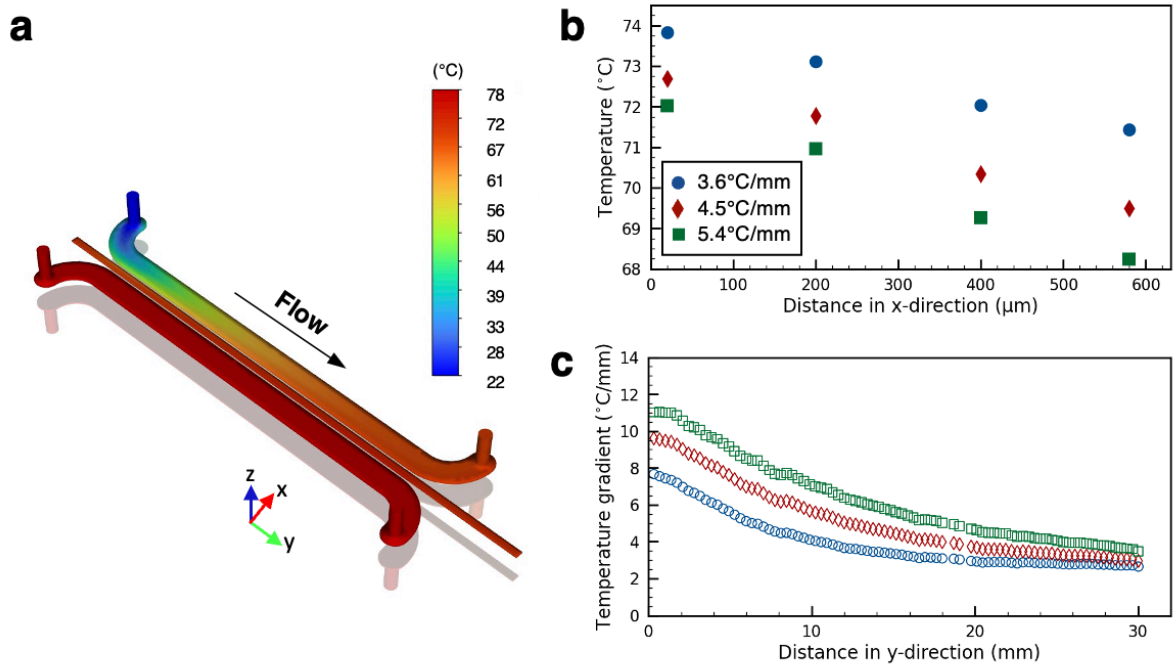

Figure 5.3: (a) Example computational simulation of temperature profile across the microfluidic system, based on experimental conditions for 4.5 ºC mm^{-1} applied temperature gradient. (b) Temperature distribution across the channel width for 3.6 ºC mm^{-1} (blue circles), 4.5 ºC mm^{-1} (red diamonds), and

5.4 ºC mm^{-1} (green squares), measured at the middle section of the device. (c) Corresponding variation in the strength of temperature gradient along the channel length.

5.3.2 Mechanical and structural characterization

In this thermophoresis technique, Gellan gum solution was maintained in its uncrosslinked state by keeping the whole microfluidic system above the sol-gel transition temperature of Gellan gum (approximately 40 °C)[9], enabling gradual redistribution of the polymer chains within the microchannel. After the specified duration, rapid hydrogel crosslinking was induced by promptly decreasing the temperature below the critical gelation temperature, thereby preserving the established concentration (and thus, stiffness) gradient profile.

Following crosslinking, the gradient Gellan gum hydrogel was manually extruded from the microfluidic channel into an adjacent PDMS reservoir filled with Milli-Q water (**Figure 5.8**). To do this, a 1 mL syringe was used to gently inject water through the inlet while using a fine-point tweezer to guide the hydrogel strip as it exited the channel. In this way we obtained a 600 μm wide, 4 cm long, and 140 μm thick substrate which exhibited a stiffness gradient across its width (**Figure 5.4b**). Moreover, by maintaining the orientation of the hydrogel after extrusion, we were able to confirm that the stiffest region was along the edge of the sample nearest to the cold channel. An accompanying transition in average pore size from the largest (~350 nm^2) at the soft ends to the smallest (~150 nm^2) at the stiff ends further supported the presence of locally varying polymer distribution generated by thermophoresis effects (**Figure 5.4a, 5.5b**). Importantly, these findings indicate a positive Soret coefficient and Gellan gum polymers experience a driving force toward the lower temperature region of the device, which also corroborates the results across multiple studies presented in this thesis (**Chapters 4,6,7**).

Next, we demonstrated the capability of the thermophoresis platform to create stiffness gradients of varying absolute ranges and gradient strengths. Notably, an increase in the concentration of initial Gellan gum concentration resulted in a higher hydrogel stiffness overall (**Figure 5.4c**). On the other hand, steeper gradients were achieved by increasing the temperature difference across the microfluidic system (**Figure 5.4d**).

Overall, the stiffness gradients produced in this study have a range spanning several native tissues, such as muscle (~20 kPa) and pre-mineralized bone (>30 kPa). While these represent a relatively stiff regime within the physiological mechanical landscape, this can be ascribed to the inherently stiffer nature of Gellan gum hydrogels even when used at low concentrations.

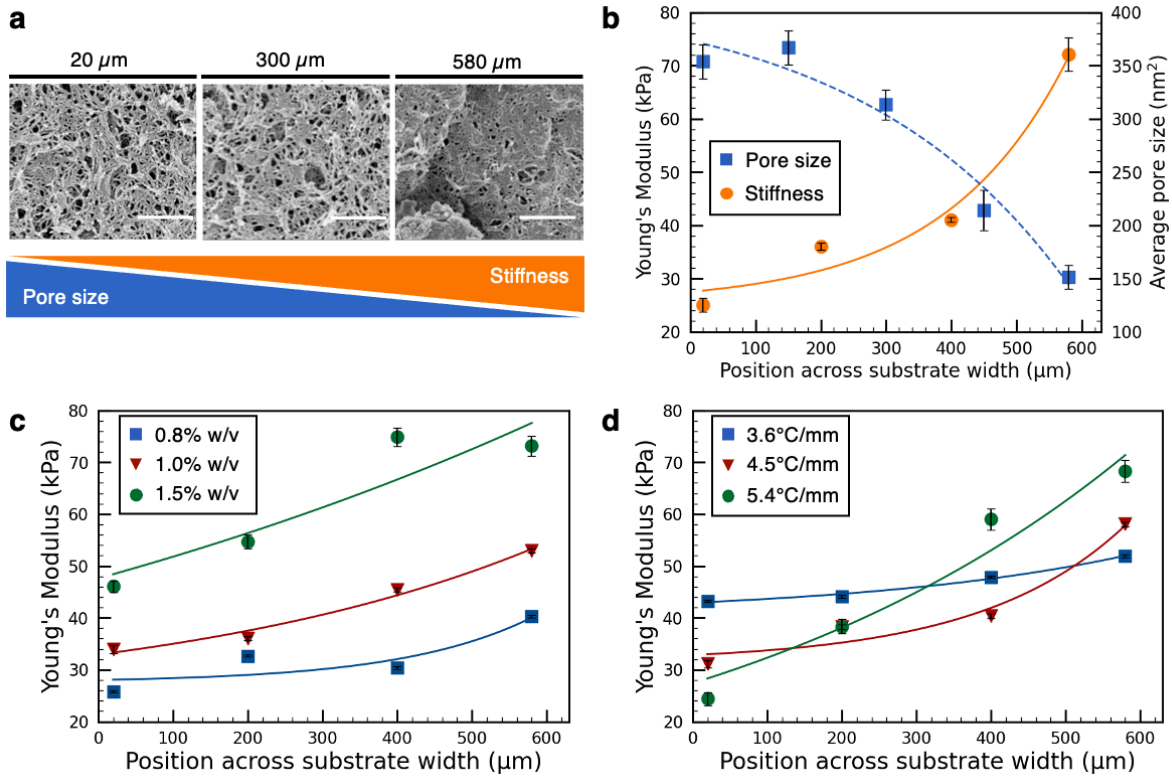

Figure 5.4: (a) Representative scanning electron microscopy (SEM) images taken at multiple locations across the substrate width, scale bars: 500 nm. (b) The pore size of fabricated Gellan gum hydrogels decreased proportionally with increasing stiffness along the gradient. (c) Young's moduli of hydrogels prepared with 0.8 wt%, 1.0 wt%, and 1.5 wt% Gellan gum concentration at a fixed temperature gradient of 4.5 ºC mm^{-1}. (d) Young's moduli of hydrogels prepared with 3.6 ºC mm^{-1}, 4.5 ºC mm^{-1}, and 5.4 ºC mm^{-1} applied temperature gradient with a fixed initial Gellan gum concentration of 1 wt%. All lines are an exponential fit, error bars represent standard error.

5.3.3 Stiffer regions promoted osteoprogenitor cell migration and maturation

As a first demonstration of the utility of this platform for interrogating stiffness-dependent behavior, it was postulated that MC3T3 preosteoblast cells cultured on the Gellan gum gradient hydrogels spanning the osteoid tissue ranges (>30 kPa) will show enhanced osteogenic activity toward the stiffer region of the substrate in a mechanical dose-dependent manner (**Figure 5.5a**).

We first measured cell viability through the relative volumes of calcein-AM and propidium iodide positive cells, indicating live and dead cells, respectively. Observation after 7 days of culture showed a high cell viability of ~85% on Gellan gum hydrogels without additional ECM protein coating (**Figure 5.5c**), confirming the nontoxic fabrication process as well as the biocompatibility of pure Gellan gum hydrogels for MC3T3 cell growth. We also performed 2D confocal imaging at days 1, 3, and 7 to investigate cell spreading and migration in response to a stiffness gradient (**Figure 5.5b**, **Figure 5.6**). We calculated cell spreading as the cell area and further evaluated cell migration by calculating the distribution of cell densities across the substrate surface over 7 days. The results showed more spreading (**Figure 5.5d**) and migration (**Figure 5.5e**) toward stiffer (~40-70 kPa) regions of the substrate. Furthermore, the cell area and cell density were found to be lower on the softer (~20-30 kPa) region of the gradient gel compared to the control sample (~50 kPa). Presumably, the hydrogel density affected these cellular responses since stiffer matrices generally cause cells to spread more due to higher formation of focal adhesion complexes[10,11], and cells can exhibit directional migration along stiffness gradients through a biological process known as durotaxis[12,13]. In this study, variation in mechanical stiffness is directly related to the hydrogel concentration level and consequently the degree of crosslinking. While cell behavior is influenced by the substrate mechanical stiffness, it is also important to consider potential confounding effects due to variation in pore architecture. However, in the context of probing stiffness-dependent cellular behavior on planar (2D) substrates, matrix porosity was found to have no interacting effects on these behaviors[14].

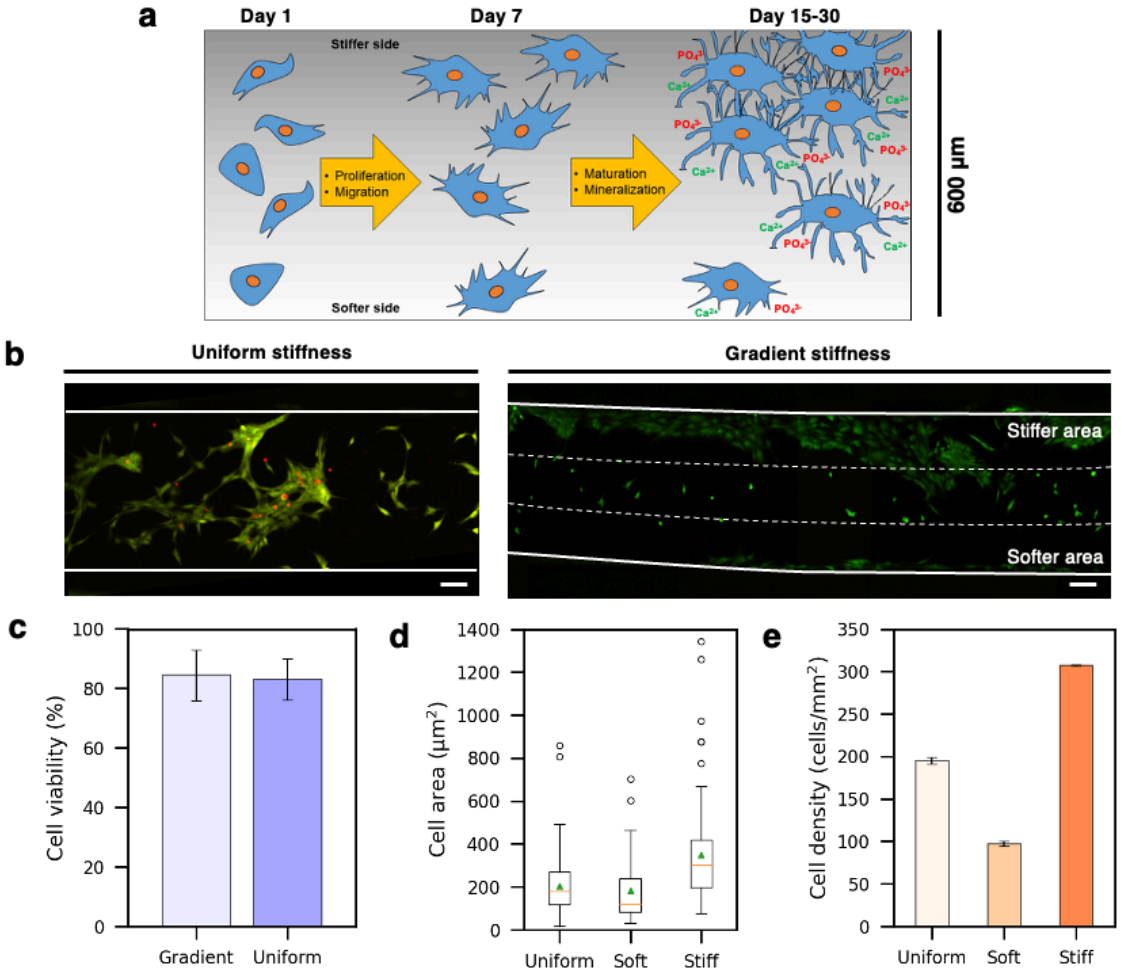

Figure 5.5: (a) Schematic representation of MC3T3 osteoblast cell activity in response to stiffness gradient. (b) Representative confocal images showing the live (green) and dead (red) cells distribution after 7 days of culture on Gellan gum hydrogels with uniform stiffness (left; control sample) and gradient stiffness (right), scale bar: 100 µm. (c) Cell viability, (d) cell spreading, and (e) cell density after 7 days of culture. Error bars represent standard error. For the box and whisker plots in (d), individual green triangles represent the average value for the indicated condition, and the orange lines represent the median value.

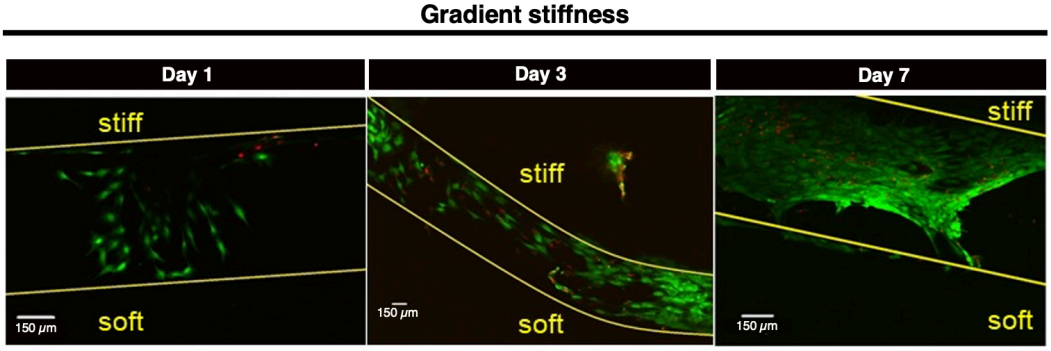

Figure 5.6: Representative confocal images showing the live (green) and dead (red) cells distribution at day 1, 3, and 7 of culture on stiffness gradient Gellan gum hydrogels. Edges of the substrates are marked using yellow lines.

In another set of experiments, we investigated the effects of stiffness in modulating the extent of substrate mineralization, which is an indicator of cell differentiation into mature osteoblast phenotype[12]. To investigate the degree of mineralization, we performed XRF analysis to quantify the amount of calcium and phosphorus (phosphate) deposition on the Gellan gum substrates after culturing for 15 days (**Figure 5.7**) and 30 days (**Figure 5.8**). The distribution of calcium and phosphorus content consistently showed a gradient pattern which increases from the soft to stiff side of the gradient, meaning stiffer substrates promoted maturation of preosteoblast cells. It is interesting to note that despite the stiffness of the control sample (~50 kPa) being within the range of the stiffer region of the gradient substrate (40-70 kPa), overall, the cells exhibited lower amount of mineral deposition on the uniform gels compared to the gradient gels. One possible explanation to this is due to the stiffness-induced migration and increased proliferation rate of cells along the stiffness gradient. Additionally, to probe the interplay between chemical and mechanical factors, we compared the mineralization activity of cells cultured in normal and osteogenic media. The latter resulted in an upregulated calcium and phosphorus deposition on both uniform and gradient stiffness Gellan gum hydrogels, and the mineral deposits were similarly distributed in a stiffness-dependent fashion. Altogether, our results add to the wealth of existing literature which suggest that matrix mechanics play an equally, if not more significant role in controlling osteoblast cell function and behavior[15,16].

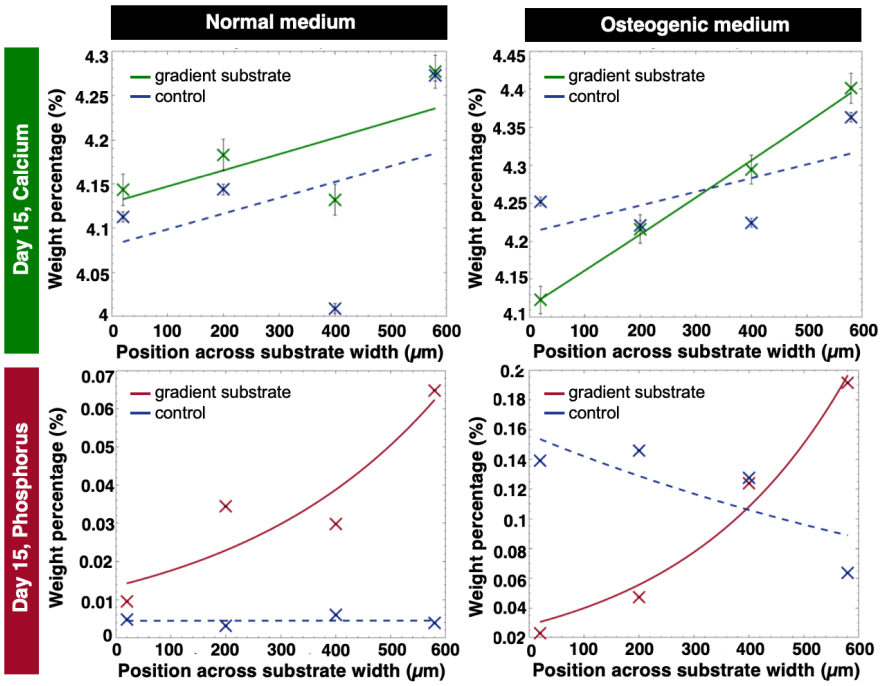

Figure 5.7: Calcium (top) and phosphorus (bottom) deposition measured after 15 days of culture using normal or osteogenic medium. Error bars represent standard error.

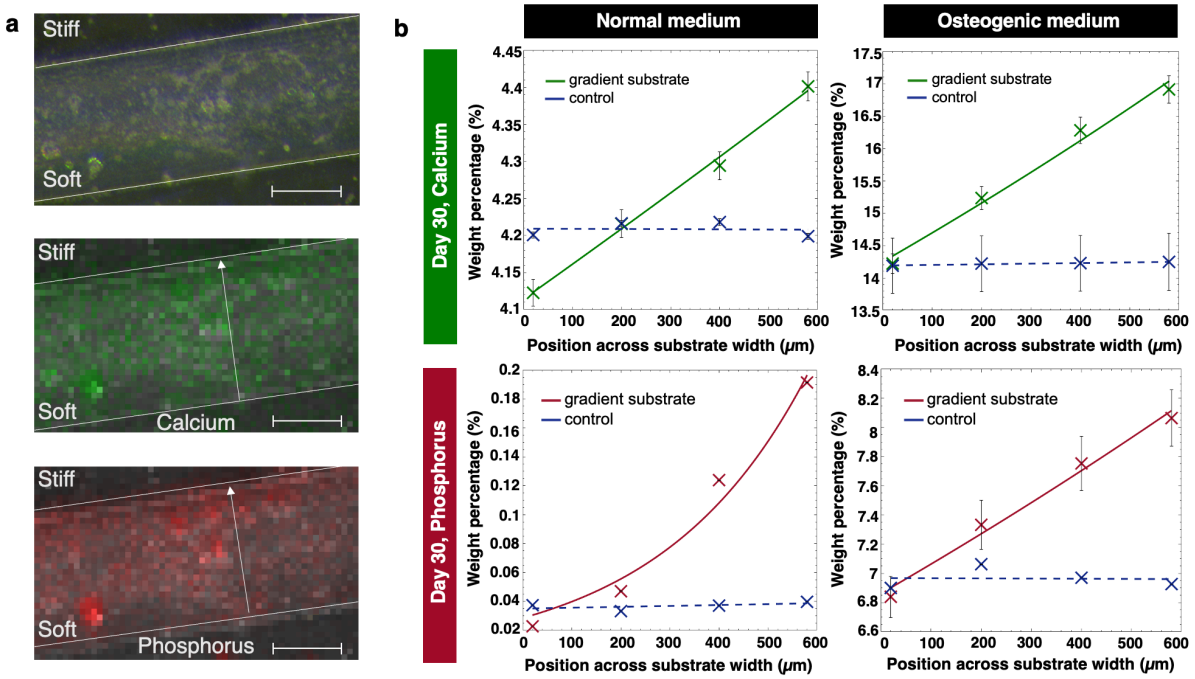

Figure 5.8: (a) Representative brightfield (top) as well as calcium (middle) and phosphorus (bottom) XRF images for cells grown on stiffness gradient Gellan gum hydrogels, scale bars: 300 μm. (b) Calcium (top) and phosphorus (bottom) content measured after 30 days of culture using normal or osteogenic medium. Error bars represent standard error.

5.4 A perspective on the early challenges

This foundational study presented in Section 5.3 demonstrated the successful fabrication of Gellan gum hydrogel strips with steep stiffness gradients and their compatibility for *in vitro* cell culture. As proof-of-concept, the biological findings importantly highlighted the potential of the thermophoresis method to create hydrogel scaffolds with pre-programmed mechanical cues toward engineering complex microphysiological tissues. Technologically, this study further affirmed the capability of the thermophoretic fabrication platform to precisely manipulate hydrogel matrix mechanics at the micron-scale. The platform contributes a new addition to the stiffness gradient hydrogel toolkit available for mechanobiology research, especially in contexts where steep gradient transitions within narrow regions (<1000 μm) are needed. Taken together, this study can be considered a milestone because it demonstrated for the first time that thermophoresis could be harnessed as a functional bioengineering tool.

Through the various discussions with research groups actively developing gradient hydrogel systems, as well as other researchers in the broader mechanobiology community seeking to integrate them in their own studies, it became clear early on that the difficulties in fabricating stiffness gradients that work reproducibly and consistently remain a major technological bottleneck hindering widespread adoption of stiffness gradient hydrogels in general. This issue was also highlighted in a recent primer by Sunyer and Trepat[17]. In many cases, the major limitation lies in the unpredictable nature of conventional diffusion-based approaches and their high sensitivity toward external conditions. As such, we posit that the actively driven process of thermophoresis when coupled with microfluidic heating control strategies, could provide an inherently more robust and controllable fabrication route.

After having relocated our laboratory group from the University of Birmingham (UK) to the University of Sydney, extensive efforts in reproducing the experimental results from our foundational study confirmed that the thermophoretic fabrication technique is indeed transferable and repeatable. To further validate the precision of thermal patterning within the microsystem, I performed fluorescence thermometry across the sample microchannel region, confirming the generation of a continuous temperature gradient that decreases linearly from the hot channel to the cold channel (**Figure 5.9**). Additionally, **Figure 5.10** shows the AFM characterization results on two separate

gradient gel samples that I independently obtained by reproducing the conditions from **Figure 5.4d** (1.0 wt% Gellan gum; ~5.4 ºC mm^{-1} applied temperature gradient). The results demonstrated an overall good sample-to-sample consistency, which also closely matched the stiffness range initially reported during the main study period (**Figure 5.4d**).

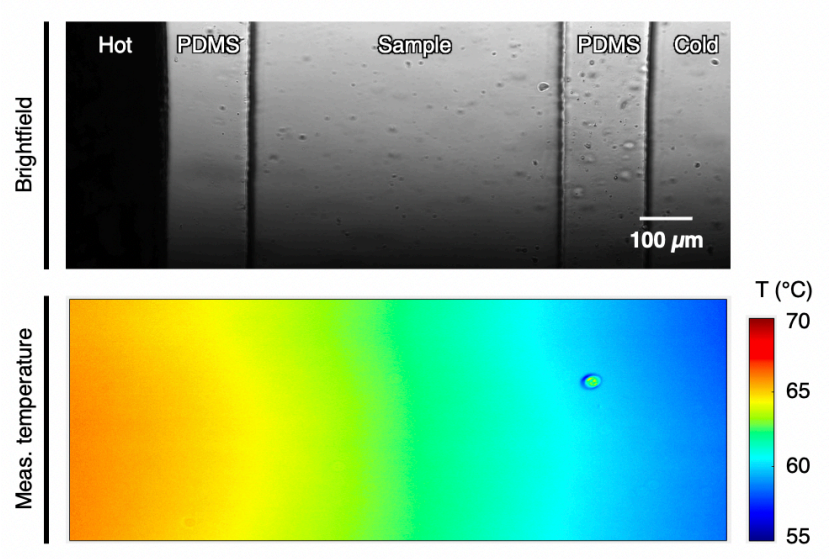

Figure 5.9: Zoom-in image of the microfluidic device around the sample channel (top), and example of the corresponding temperature distribution measured using the Rhodamine B fluorescence thermometry method described in Chapter 4 of this thesis (bottom).

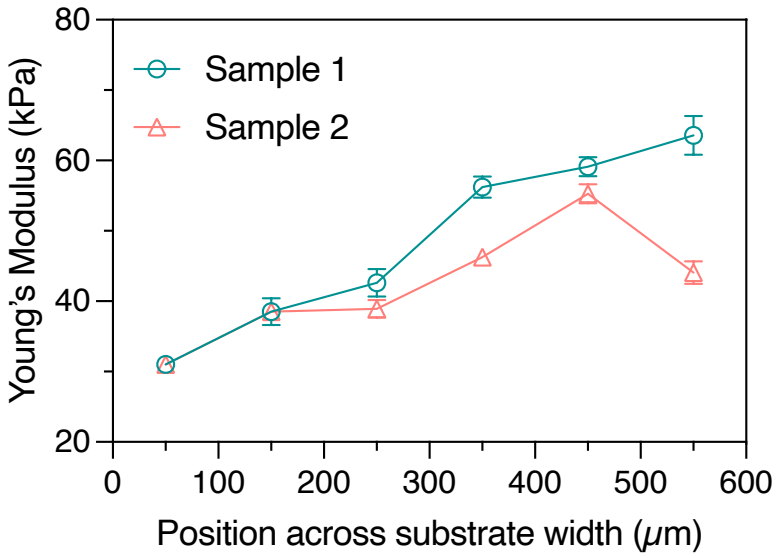

Figure 5.10: Independent repeat fabrication and AFM stiffness measurement of Gellan gum gradient hydrogels prepared at 1.0 wt% initial polymer concentration and 5.4 ºC mm^{-1} applied temperature gradient. Each point represents mean ± SEM of a force map acquired at the specified location.

As we moved the thermophoresis platform from a physics-centered stage to an application-oriented one, it soon became clear that the technological novelty alone was not a guarantee to achieve adoption. To many biologists unfamiliar with thermophoresis, this concept can often feel abstract or inaccessible. This observation was perhaps unsurprising, given how only until recently, the large proportion of thermophoresis publications are still focused on the fundamental physics principles and confined to niche technical journals. Yet, how the end-users interact with a new technology will be a critical factor of whether it can supplant or even complement existing methods. Before such novel thermophoresis-based biofabrication platform becomes a standard tool in mechanobiology labs, deliberate and thoughtful strategies must be in place to push forward the technology from its current state to a reliable, “plug-and-play” device.

One major complication of this platform iteration is associated with the need to confine the hydrogel precursor solution inside PDMS microchannels. In particular, the need to manually extrude hydrogels out of the microfluidic channel was technically very challenging and added significant time cost on top of the already relatively long thermophoresis process (**Figure 5.11**). This often resulted in tangled or even broken hydrogel samples, making such an extrusion approach not ideal for scaling to high-throughput fabrication typically required for more complex biological studies.

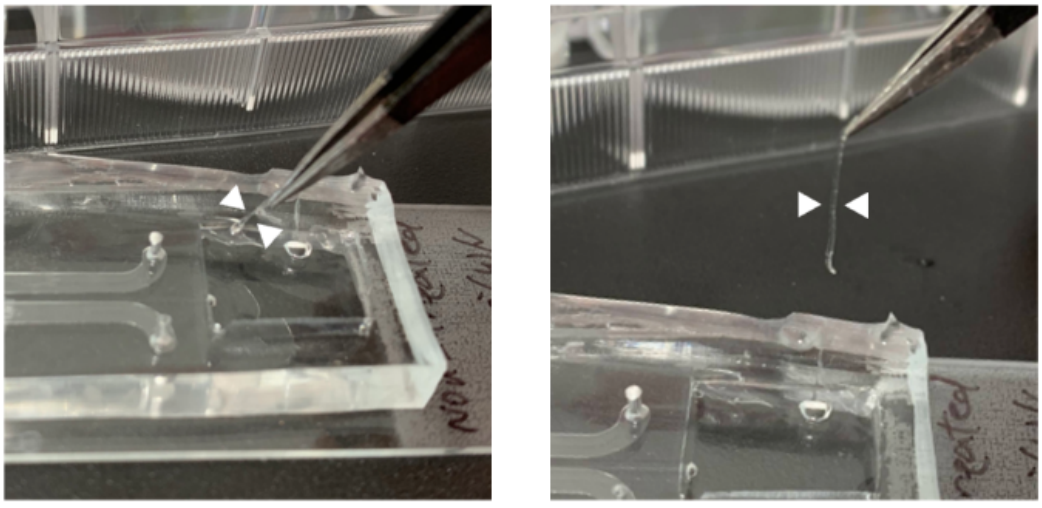

Figure 5.11: Digital images of the extrusion process of Gellan gum hydrogels, indicated between the white arrowheads. After crosslinking, the hydrogel was carefully extruded out of the microchannel into an adjacent water-filled reservoir. The hydrogel was then transferred onto a poly(ethyleneimine)-coated coverslip to enable attachment for downstream experiments.

Additionally, the microfluidic devices were initially designed with an explicit focus on short, linear stiffness gradients. Adjustments to the gradient material dimensions will also require new microfluidic master molds to be prepared, restricting rapid iterative material design and testing to achieve the desired biological outcomes. As a result, the operational complexity and limited flexibility of the current platform iteration have hindered its practicality in traditionally biology-focused laboratories.

From experience, arguably the most challenging aspect of the platform development lies in adapting the PDMS microdevice to accommodate the specific processing requirements of different hydrogel systems. Of note, the vapor permeability of PDMS meant that sample evaporation can occur during the thermophoretic gradient generation process. While this was found to be tolerable in the case of alginate[8], the much higher working temperatures (average 60 ºC) required for Gellan gum in this study may result in the formation of air plugs inside the microchannel, disrupting the thermophoresis process and damaging the hydrogel sample. As a mitigation solution, the PDMS devices were degassed for 20 min prior to the start of each experiment. On the other hand, when working with photopolymerized hydrogels, PDMS can be problematic as the high oxygen permeability of PDMS may cause incomplete or inhibited photopolymerization process[18]. Various strategies have been proposed to overcome this oxygen inhibition effect, such as benzophenone coating of PDMS[19] or creation of a glassy-skin layer by plasma treatment[20]. Although plausible (which I also attempted), these workarounds add to the platform's complexity and reduce its adaptability in the long term. This raises the question of whether such deployment challenges stem from the use of a non-ideal platform construction material. Indeed, this has so far limited the practical implementation of the thermophoresis method across a broad range of hydrogels, in spite of its initially touted appeal being a universally applicable process.

For a balanced discussion however, PDMS microfluidic system remains beneficial in enabling exceptionally stable and precise temperature control. In particular, the micron-scale channels for cooling and heating allow for highly responsive control of localized temperature gradients. Meanwhile, the low thermal conductivity of the bulk PDMS serves as an effective insulator against fluctuations in the external environment, contributing to the robustness of the thermophoretic gradient generation process.

Overall, an analysis of the early platform iteration suggests that the main obstacle that may hinder widespread adoption of the thermophoretic fabrication method lies less in the physical principle of thermophoresis, but rather in the implementation system. This led to an extensive reconsideration of the design choices that can be made in order to lower the barrier of entry for researchers in non-engineering disciplines. A simplified and more straightforward approach is believed to be the immediate necessary step to improve the user accessibility to this new fabrication method. Only then we can fully capitalize on the unique advantages of the thermophoresis phenomenon toward the development of an advanced biomaterials platform for future mechanobiology applications.

5.5 Conclusion

Collectively, the work in this chapter was primarily intended to demonstrate that thermophoretically fabricated stiffness gradient hydrogels could be applied to probe interesting questions in the domain of mechanobiology, with implications in controlling cell behavior by modulating their mechanical microenvironment. In doing so we established the precision and repeatability of the thermophoresis technique in controlling the micron-scale mechanical properties in hydrogels suitable as cell culture substrates, which is at least on par with the performance of other existing *in vitro* gradient hydrogel platforms.

As with many technologies built from first principles, the ingenuity of the underlying mechanism is only part of the equation, while its practical adoption hinges on how seamlessly the final device integrates into the experimental workflows of its target users. Early attempts in finding the “right” biological problems to solve have brought into sharp focus the strengths and limitations of the original platform implementation strategy. These lessons informed the subsequent reinvention of the thermophoretic method as a modular platform, with a focus on enhancing accessibility and simplifying the setup of gradient hydrogel experiments.

References

1. Kosmidis Papadimitriou, A. *et al.* Fabrication of gradient hydrogels using a thermophoretic approach in microfluidics. *Biofabrication* **16**, 025023 (2024).

2. Coutinho, D. F. *et al.* Modified Gellan Gum hydrogels with tunable physical and mechanical properties. *Biomaterials* **31**, 7494–7502 (2010).

3. Stevens, L. R., Gilmore, K. J., Wallace, G. G. & In het Panhuis, M. Tissue engineering with gellan gum. *Biomater Sci* **4**, 1276–1290 (2016).

4. Vieira, S. *et al.* Self-mineralizing Ca-enriched methacrylated gellan gum beads for bone tissue engineering. *Acta Biomater* **93**, 74–85 (2019).

5. Genin, G. M. *et al.* Functional grading of mineral and collagen in the attachment of tendon to bone. *Biophys J* **97**, 976–985 (2009).

6. Thomopoulos, S., Williams, G. R., Gimbel, J. A., Favata, M. & Soslowsky, L. J. Variation of biomechanical, structural, and compositional properties along the tendon to bone insertion site. *J Orthop Res* **21**, 413–419 (2003).

7. Caliari, S. R. & Harley, B. A. C. Structural and biochemical modification of a collagen scaffold to selectively enhance MSC tenogenic, chondrogenic, and osteogenic differentiation. *Adv Healthc Mater* **3**, 1086–1096 (2014).

8. Vigolo, D., Ramakrishna, S. N. & DeMello, A. J. Facile tuning of the mechanical properties of a biocompatible soft material. *Sci Rep* **9**, 7125 (2019).

9. Tang, J., Tung, M. A. & Zeng, Y. Gelling temperature of gellan solutions containing calcium ions. *J Food Sci* **62**, 276–280 (1997).

10. Engler, A. et al. Substrate Compliance versus Ligand Density in Cell on Gel Responses. *Biophys J* **86**, 617–628 (2004).

11. Doss, B. L. *et al.* Cell response to substrate rigidity is regulated by active and passive cytoskeletal stress. *Proc Natl Acad Sci* **117**, 12817–12825 (2020).

12. Khatiwala, C. B., Peyton, S. R. & Putnam, A. J. Intrinsic mechanical properties of the extracellular matrix affect the behavior of pre-osteoblastic MC3T3-E1 cells. *Am J Physiol Cell Physiol* **290**, 1640–1650 (2006).

13. Hartman, C. D., Isenberg, B. C., Chua, S. G. & Wong, J. Y. Vascular smooth muscle cell durotaxis depends on extracellular matrix composition. *Proc Natl Acad Sci* **113**, 11190–11195 (2016).

14. Wen, J. H. *et al.* Interplay of matrix stiffness and protein tethering in stem cell differentiation. *Nat Mater* **13**, 979–987 (2014).

15. Zhang, T. *et al.* Effect of matrix stiffness on osteoblast functionalization. *Cell Prolif* **50**, e12338 (2017).

16. Sun, M. *et al.* Extracellular matrix stiffness controls osteogenic differentiation of mesenchymal stem cells mediated by integrin α5. *Stem Cell Res Ther* **9**, 52 (2018).

17. Sunyer, R. & Trepat, X. Durotaxis. *Curr Biol* **30**, R383–R387 (2020).

18. Lipkowitz, G. *et al.* Injection continuous liquid interface production of 3D objects. *Sci Adv* **8**, 1349–1352 (2022).

19. Yuk, H., Zhang, T., Parada, G. A., Liu, X. & Zhao, X. Skin-inspired hydrogel-elastomer hybrids with robust interfaces and functional microstructures. *Nat Commun* **7**, 12028 (2016).

20. Nania, M., Matar, O. K. & Cabral, J. T. Frontal vitrification of PDMS using air plasma and consequences for surface wrinkling. *Soft Matter* **11**, 3067–3075 (2015).

Chapter 6

A modular platform to create simple-to-complex stiffness gradient profiles

The following chapter describes the development of a microfabricated platform that greatly simplifies the thermophoretic fabrication process and offers the flexibility to create more complex stiffness profiles beyond linear gradients. A crucial innovation in this modular workflow was the implementation of a fluorescence-based temperature characterization step to predict the final stiffness gradient shapes, enabling rapid material and process optimization cycles. Furthermore, this platform was designed specifically to be compatible with different hydrogel crosslinking modalities, demonstrated here using thermosensitive Gellan gum and photopolymerized GelMA. Extensive material stiffness characterization by AFM was performed to establish the precision and reproducibility of the modular platform. Finally, the effectiveness of this new platform to modulate the mechanical microenvironment of cells was verified through quantified stiffness-dependent fibroblast behavior across a range of linear, periodic, and anisotropic stiffness gradient hydrogels.

Chapter 5 has shown that thermophoresis, being an actively driven process, offers a promising alternative to conventional passive diffusion-based fabrication methods. Applying the technique to study a specific biological question seemed like a straightforward next step, but conversations with biologists highlighted a key challenge: for those unfamiliar with gradient hydrogels, it can often be difficult to know where to start – which fabrication method to use, how to tailor the gradient, or which parameters matter biologically. Existing methods (including earlier versions of our own thermophoresis platform) tend to offer limited flexibility, and their utility is often dependent on user expertise or tailored to narrow applications. In this chapter I sought to develop a modular platform to lower these barriers and support technology accessibility. By simplifying the implementation and enabling iterative material design, I hoped not only to advance thermophoresis-based fabrication method from a proof-of-concept into a robust research tool, but also to inspire new ways of using microengineered gradient hydrogels beyond what was initially intended.

Graphical abstract of chapter:

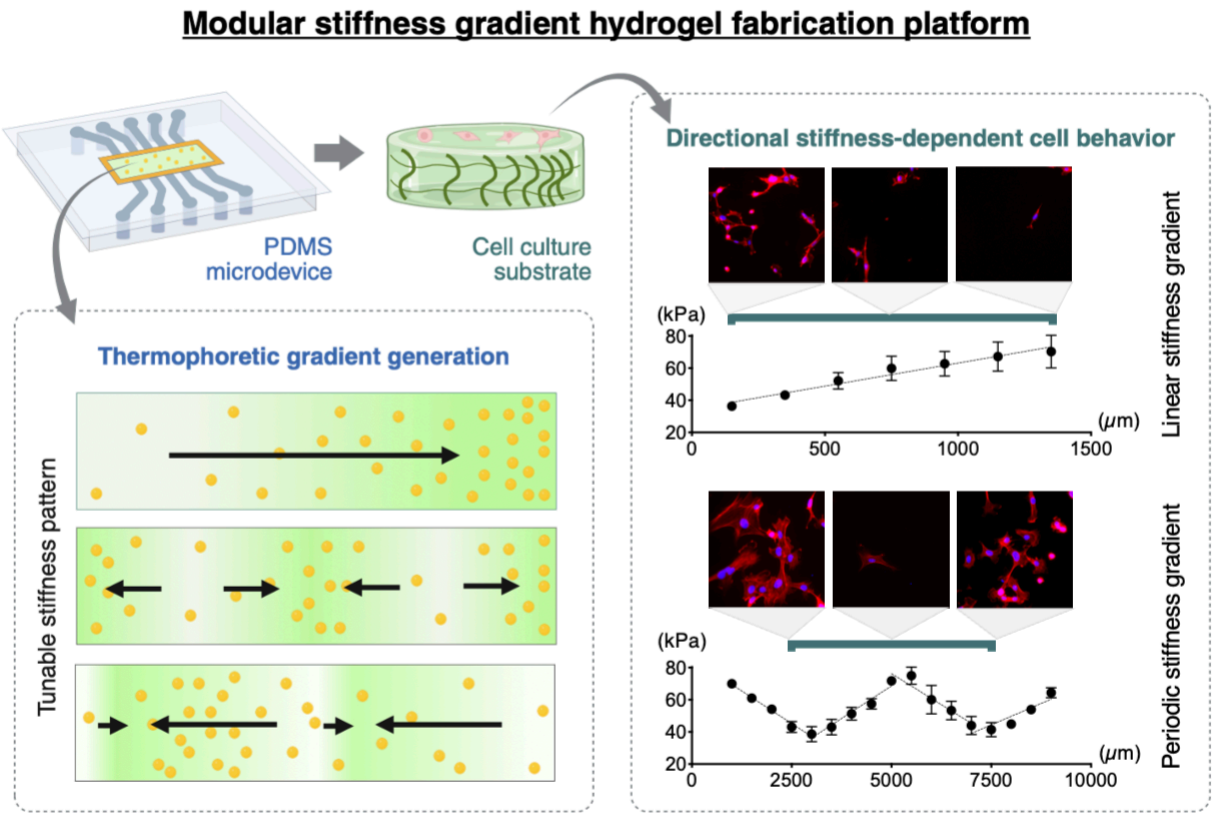

6.1 Introduction

Linear stiffness gradients created using polyacrylamide hydrogels have had successful applications for uncovering unique insights into the mechanisms of cell-ECM interplay[1,2]. The univariate elastic mechanics of polyacrylamide gels along with an accessible stiffness range from at least 0.1 kPa to 200 kPa were particularly useful to investigate the isolated effect of substrate elasticity on cell responses[3,4]. However, as the field continues to pursue a deeper understanding of how cells interpret matrix cues in more complex, *in vivo*-like microenvironments, it is anticipated that the applicability of stiffness gradient hydrogels should be enhanced by the ability to simultaneously modulate other mechanical, structural or biochemical cues within a single platform. Emerging concepts are, for example, consideration of viscoelastic properties[5,6], mimicking the mechanical anisotropy within specific tissue niches[7], incorporation of fibrous structures to facilitate long-range force transmission[8], and integration of stimuli-responsive functionality for dynamic cell regulation[9]. Continued research efforts in this area likely require experimentation with new hydrogel chemistries and so it will be useful to have a flexible platform that supports learning through iteration in pursuing advanced gradient hydrogel systems.

In this context, the present chapter was motivated by the unmet need of a universal biofabrication platform capable of interrogating the full physiological mechanical landscape while maintaining precise control of the gradient profile at single-cell length scale. By leveraging facile microfabrication strategies, the thermophoretic technique was developed into a next-generation platform that can be democratized for a wide range of hydrogels and stiffness gradient profiles.

As outlined in **Figure 6.1**, the modular platform introduced in this chapter was engineered with an emphasis on practical and scalable implementation by considering each step of the experimental workflow, from platform construction to process optimization and tunability for various biological applications.

Specifically, this approach leverages simple PDMS casting to rapidly produce a base microfluidic module that can be customized with varying heating configurations. This configuration defines the microscale temperature landscape within the system, which directly governs the resulting stiffness gradient profile in the hydrogel. Importantly, the

generated temperature profile can be experimentally mapped at high spatial resolution using the fluorescent-based method introduced in **Chapter 4**. This information provides a predictive framework for users to optimize the microfluidic module configuration and the fabrication process parameters, enabling precise control over the stiffness gradient characteristics. Overall, the flexibility, predictability, and rapid design-to-fabrication cycle of the modular gradient hydrogel platform offers a scalable solution to study cell-material interactions across a wide range of biologically relevant mechanical microenvironments, with promising future applications in biomaterials-based cell studies and tissue engineering.

It should be noted that the platform introduced in this thesis was developed with an initial focus on fabricating static 2D stiffness gradient hydrogels, but its modular design should enable future adaptation to 3D culture systems as experimental needs grow more complex.

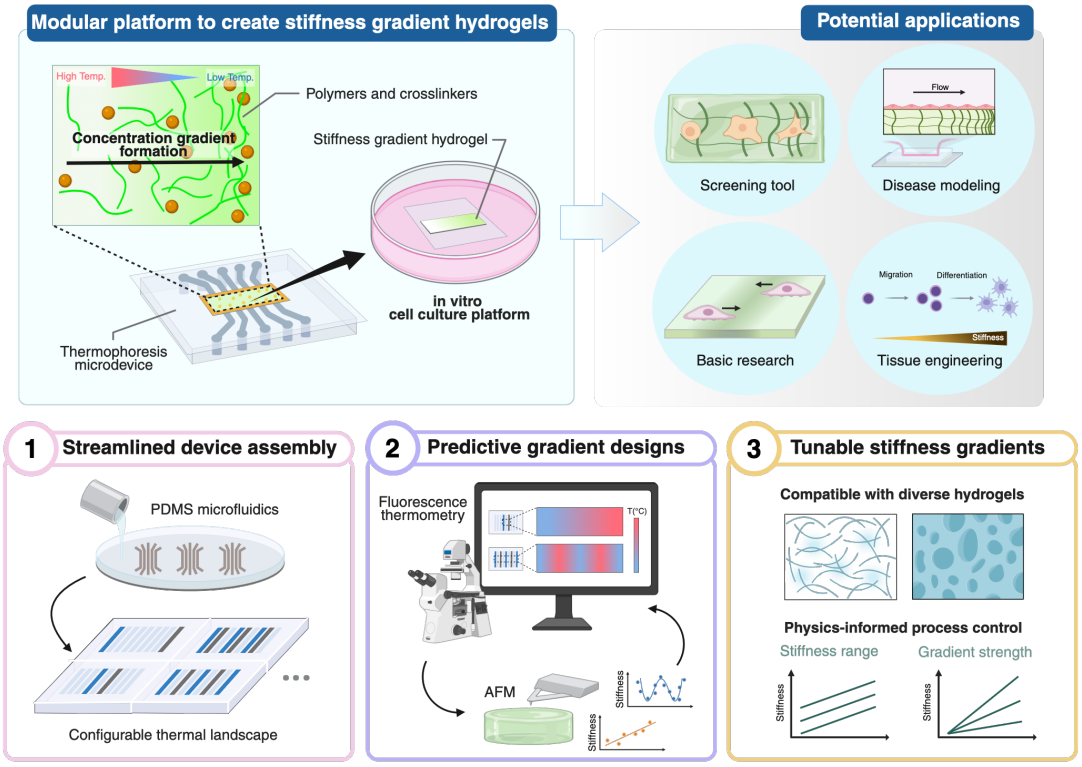

Figure 6.1: Conceptual illustration of a modular platform utilizing thermophoresis to fabricate stiffness gradient hydrogels for *in vitro* cell culture applications.

6.2 Experimental methods

This section contains additional methods that are specific to the experiments in this chapter, and should be read in conjunction with the general materials and methods presented in **Chapter 3**.

6.2.1 Microfluidic device design

The complete assembly of the modular platform is illustrated in **Figure 6.2**. A PDMS microfluidic device was plasma bonded to a No. 1 glass coverslip (24 × 50 mm, Trajan Scientific), on top of which a spacer was constructed to form the sample microchamber. The sample microchamber was made by cutting out a specified area on a 120 µm-thick spacer (2 layers of 60 µm-thick Kapton tape, Multicomp Pro), which was then manually aligned with the gradient region. During gradient gel fabrication, hydrogel solution was pipetted into the sample chamber, which was then covered using a chemically functionalized coverslip to facilitate hydrogel attachment and retrieval.

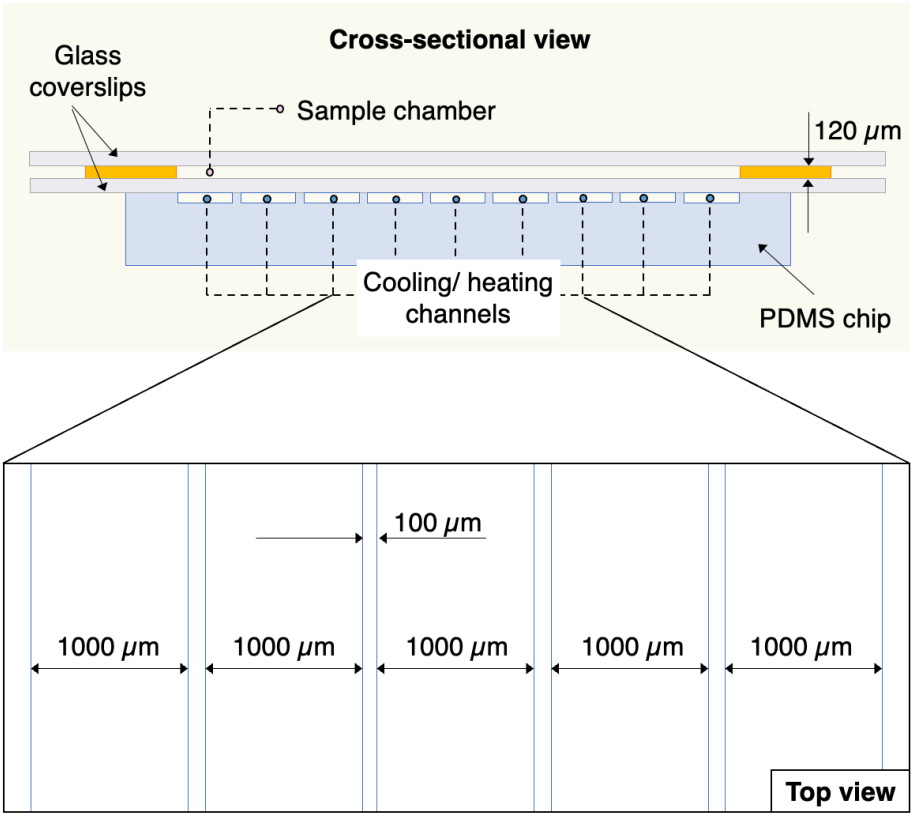

Figure 6.2: Schematic illustrating the complete assembly of the modular microfluidic platform.

6.2.2 Optimization of the microchannel array dimensions

Several variations of the microchannel array were tested to determine an optimal layout that balances the ease of fabrication, pattern customizability, and patterning resolution. As part of the optimization process, a range of channel widths from 100 μm to 2000 μm were explored. Although smaller (<400 μm) channels were initially considered to be desirable for achieving sharper gradients, they posed significant fabrication difficulties, especially in creating functional Joule heaters. Ultimately, a channel width of 1000 μm was selected, which also importantly defines the size of the narrowest linear stiffness gradient achievable. This aligns with the typical sizes of stiffness gradient hydrogels reported in literature, thus ensuring the relevance for probing cell-substrate interactions. To allow modular customization of the stiffness gradient size and shape, the final microchannel array design contains 9 parallel channels with cross-sectional dimensions of 1000 μm (width) × 100 μm (height), whereby adjacent microchannels are separated by a 100 μm-think PDMS wall running along the length of the channel (**Figure 6.2**). The 100 μm separation between adjacent channels was carefully optimized to be thick enough to prevent rapid heat transfer between channels which would otherwise flatten the intended temperature differences, at the same time, thin enough to allow a smooth temperature transition between channels rather than an abrupt thermal boundary. Furthermore, each of the channels was 1.8 cm long, designed specifically to ensure minimal variation in temperature gradient down the channel length; this was previously an issue with the longer microchannels in the previous design iteration, as discussed in Section 5.3.1.

6.2.3 Optimization of the sample microchamber design

Initially, multiple design iterations were made to construct the sample confinement system using PDMS (**Figure 6.3**; Approach 1). In this approach, the chemically functionalized coverslip was sandwiched between the base microdevice and another top PDMS layer. The sample coverslip was temporarily attached to the microdevice using thermal paste. For conventional studies in well plates, the top PDMS layer could be designed with a straight channel and placed directly onto the coverslip without plasma bonding. It was found that the prior chemical functionalization step (intended

for hydrogel attachment) was also advantageous in providing sufficient attachment strength between the PDMS and glass substrate to prevent leakage of the hydrogel solution, but allows the PDMS to be easily peeled off at the end of the fabrication process to expose a gradient hydrogel substrate for cell seeding. In another direction toward the concept of organ-on-a-chip, we briefly explored the feasibility of a “one-step” fabrication of stiffness gradient hydrogels in a PDMS chip with multicompartment design, which can be used directly for microfluidic cell culture without additional post-processing or device assembly steps. However, in both cases, there are major challenges that must first be addressed, notably sample evaporation through PDMS and accessibility for material characterization, which fall outside the scope of this thesis. Thus, it was decided not to further pursue the PDMS microchamber approach, in favor of the simpler spacer technique (**Figure 6.3**; Approach 2), as described in the previous sections.

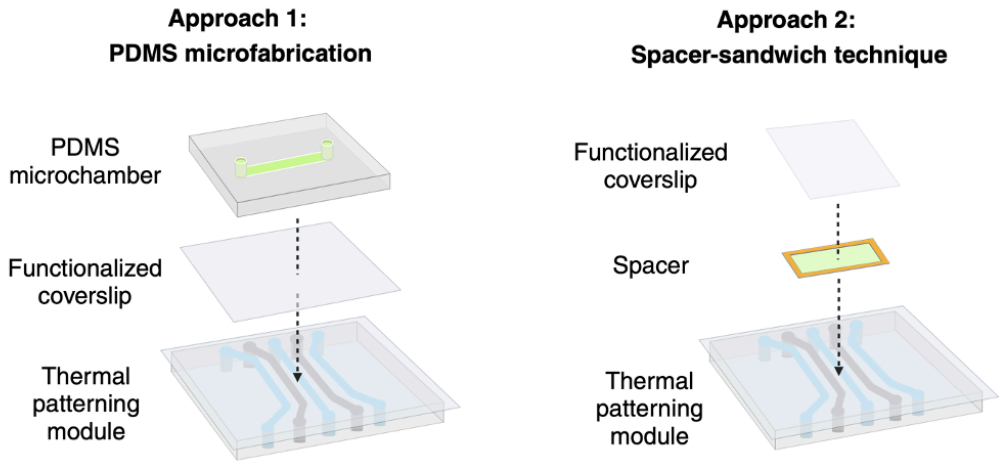

Figure 6.3: Two approaches of external sample confinement were explored, with Approach 2 being adopted in the final design. Green fill indicates the sample area.

6.2.4 Gradient hydrogel fabrication

The thermal microfluidic module was set up on a lab bench, with the coverslip side facing up to allow easy sample loading and retrieval (**Figure 3.4**). To maintain thermal stability during prolonged heating, the whole device (attached to a Peltier module) was placed on a heat sink (1.25 K W^{-1}, 75 mm × 100 mm × 40 mm, Fischer Electronik).

This setup was important to minimize heat accumulation and to ensure a consistent temperature profile throughout the gradient generation process.

In the general gradient hydrogel fabrication workflow, the thermal microfluidic device was first preheated at the desired water flow rate and Joule heater current for 5 min to establish a stable temperature gradient. In this work, the average system temperature was maintained above 60 ºC, which was critical to reduce the viscosity of the precursor solutions and prevent premature gelation. 20 µL precursor solution was pipetted into the sample microchamber and immediately covered with a pre-functionalized coverslip. Then, the temperature gradient was maintained for the specified duration to allow thermophoretic generation of a concentration gradient within the micro-confined volume of precursor solution. Subsequently, the resulting concentration gradient was “fixed” by reversing the polarity of the Peltier module, enabling rapid cooling of the whole system (~1 ºC s^{-1}). For Gellan gum, the system was kept at approximately 15 ºC for at least 1.5 min to ensure complete gelation. For GelMA, the system was further exposed to UV (365 nm, 0.22 W cm^{-2}) for 120 s to form covalently crosslinked hydrogels.

6.2.5 Cell culture and analysis

In all cases of uniform (control) and gradient GelMA hydrogels, 3T3-L1 fibroblast cells were fixed and stained at 24 h after seeding. For periodic gradient gels, an additional set of observations were performed after 72 h culture.

6.3 Overview of the modular platform

The modular platform features a two-part assembly that separates hydrogel confinement from the microfluidic structure.

The core component comprises a microfluidic device for controlling the local temperature conditions within the platform, which will be loosely referred to as the thermal patterning module. The base microfluidic module was fabricated via PDMS soft lithography and plasma sealed onto a glass coverslip (**Figure 6.4**, step i). The module was designed with an array of 9 microchannels, which can be selectively opened and employed for cooling (via syringe pump-driven water flow) or heating (via creation of embedded micro-Joule heater) (**Figure 6.4**, step ii). Thus, this modular design allows users to fabricate classical linear stiffness gradients that are most popularly used in studies to date, while also offering new possibilities to explore spatially more complex stiffness patterns, as demonstrated in this chapter through periodic and anisotropic gradients (**Figure 6.4**, step iii).

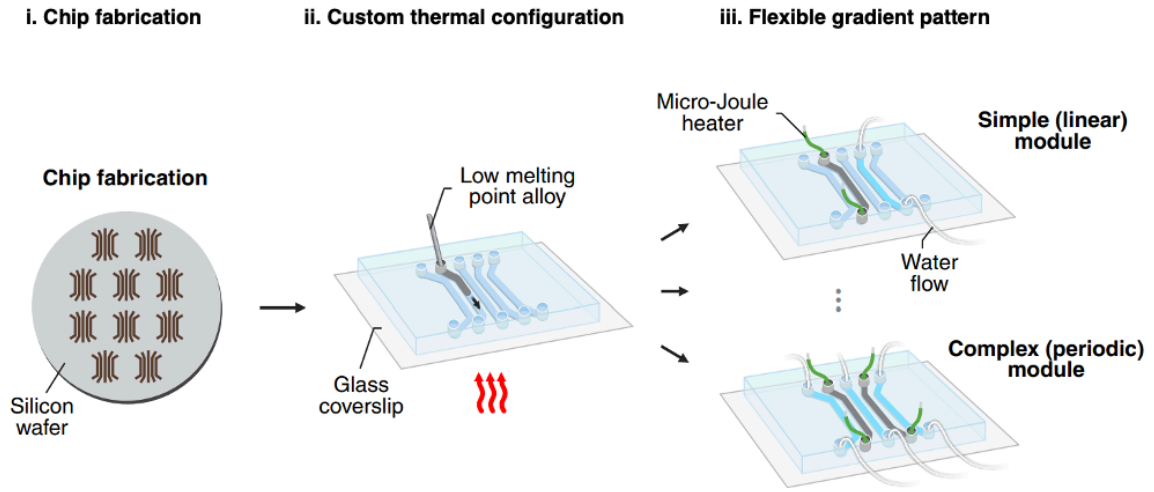

Figure 6.4: Schematic illustrating the modular construction of the thermophoresis microdevices.

The second component is an external hydrogel sample microchamber made by stacking cutouts of polymide (Kapton) adhesive tape which was then attached to the coverslip side of the thermal microfluidic module. In contrast to earlier designs whereby the gradient hydrogel would be fabricated inside the thermal microdevice[10,11], also utilized in **Chapter 5**, this new strategy overcomes key challenges such as

enabling easy hydrogel handling, reducing fabrication turnaround time, and facilitating reusability of the microdevices. In this respect, the modular thermophoretic fabrication platform approaches the simplicity of hydrogel mold casting methods[1], which should lower the barrier to entry for biologists.

Furthermore, the modularity of the microfluidic thermal patterning microdevice was designed to cover the requirements of different applications. This would enable researchers to study a wide range of stiffness gradients without the need to adopt several different fabrication methods[12], thereby streamlining experimental setup and enhancing accessibility to gradient hydrogel technology.

In the simplest case, linear gradient modules are built with a single pair of cooling and heating channels (**Figure 6.5a**). Given that the time required (t) for thermophoretic migration scales quadratically with the distance (d) to traverse (i.e., $t \propto d^2$), one could expect that the steepest stiffness gradients (spanning ~1000 μm) are created by utilizing adjacent pairs of channels in the microchannel array. Conversely, shallower gradients are created with increasing separation between the heating and cooling channels. Moreover, since it is possible to simultaneously control multiple cooling and heating channels, various shapes of complex stiffness gradients can be generated over a distance up to ~1 cm using the same platform (**Figure 6.5b**).

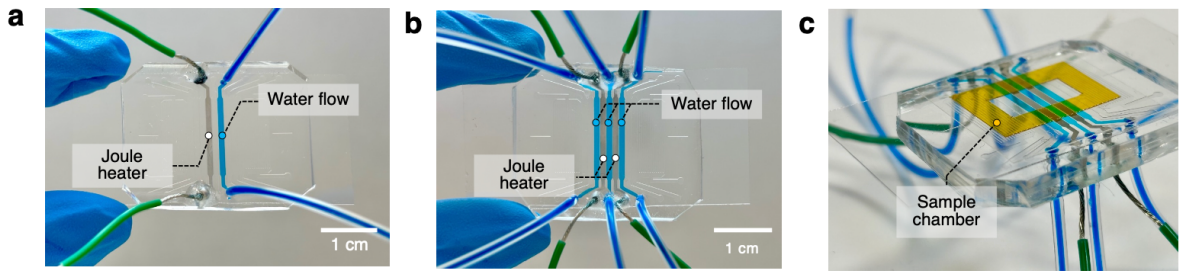

Figure 6.5: Images of the modular thermophoresis platform, including examples of (a) simple linear gradient module, (b) complex periodic module, and (c) complete platform assembly including a sample chamber.

Under essentially the same thermophoresis principles, solutes in the hydrogel precursor solution redistribute in the direction of the imposed temperature gradient, resulting in the generation of smooth and continuous stiffness gradients. Leveraging the fact that the resulting strength of precursor concentration gradient (and thus

stiffness gradient) is proportional to the magnitude of imposed temperature gradient, the modular platform not only offers customization in the gradient pattern and size, but also allows tunability in the stiffness range and gradient slope to suit the experimental requirements.

As the closest competing technology, microfluidic gradient generators can create highly controlled and well-defined microscale stiffness gradients[12,13], including spatially complex profiles[14]. However, these devices are typically single-use only and a unique microfluidic design is required for a specific gradient shape and size, which makes this method costly and time-consuming. These issues can be solved using the modular approach presented here, because the assembled thermal microdevices can be reused multiple times, requiring only replacement of the microchamber spacer between uses (**Figure 6.5c**).

6.4 The stiffness gradient hydrogel fabrication workflow

The step-by-step process for fabricating stiffness gradient hydrogels using the modular platform is summarized in **Figure 6.6** and further supplemented in Section 6.2.4.

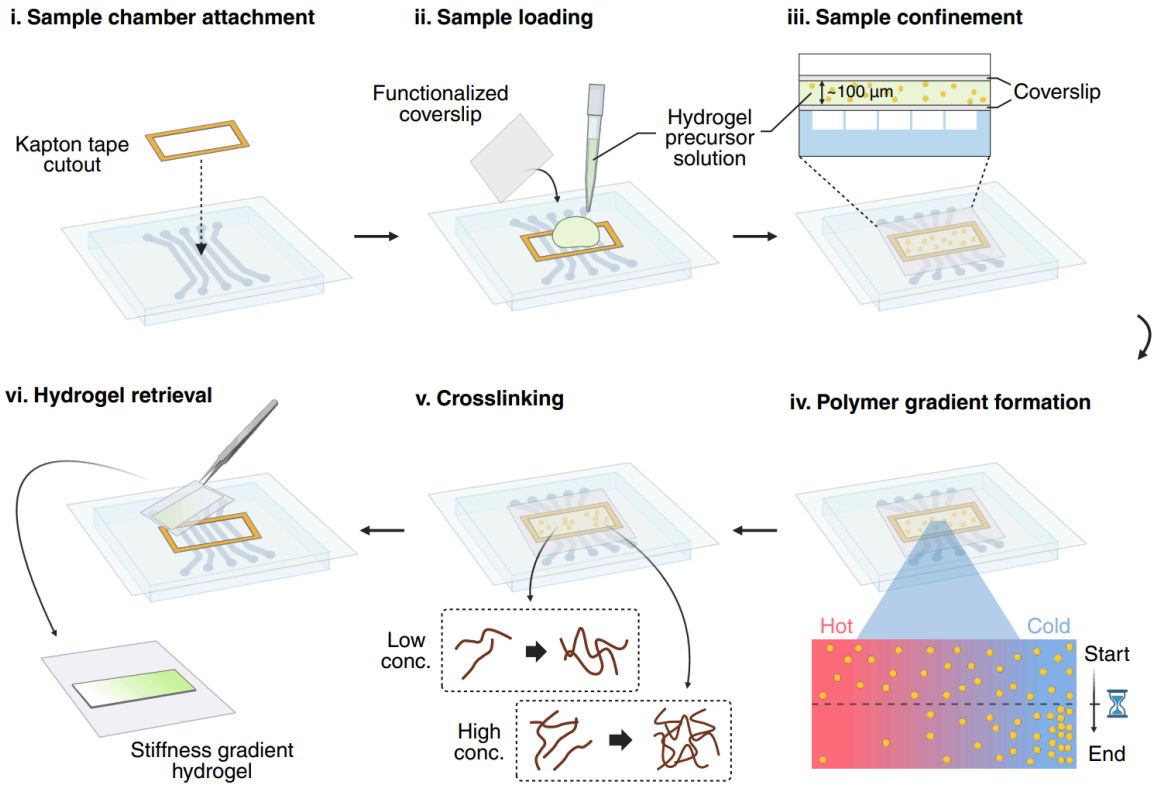

Figure 6.6: Schematic illustrating the stepwise fabrication of stiffness gradient hydrogels using the modular thermophoresis platform.

At the start of each fabrication round, the microdevice surface was wiped clean using ethanol followed by Milli-Q water to remove any contaminant (e.g., residual hydrogel from previous sample) and ensure conformal contact of the tape-based microchamber to the coverslip surface (step i). The platform was then primed at the specified thermal conditions, and the hydrogel precursor solution was pipetted to fill the microchamber (step ii). Immediately after, a chemically functionalized coverslip was placed on top of the microchamber, applying slight pressure to ensure a tight seal but taking care not to introduce air bubbles into the sample volume (step iii). Note that coverslip functionalization was carried out to enable hydrogel attachment to the coverslip upon crosslinking and is specific to the hydrogel chemistry (see details in Section 3.5.3).

Subsequently, the platform was maintained at the preset thermal conditions for 20-40 mins for thermophoresis to take effect, which allowed the formation of concentration gradients within the micro-confined precursor solution (step iv). For the hydrogel systems explored in this thesis, the precursor components redistributed toward colder regions of the system, and as such, the final stiffness gradient profile would be an inverted replica of the underlying temperature profile. After the specified duration, the external temperature field was removed, and the polymer solution was rapidly crosslinked (step v). During this step, regions of high polymer (and crosslinker) concentration effectively translate into higher local hydrogel stiffness, and vice versa. Finally, the coverslip was carefully peeled off the microdevice using a fine-point tweezer and flipped over to reveal the stiffness gradient hydrogel (step vi). At this stage, the gradient sample is ready for material characterization or cell seeding.

As with any biofabrication technique, the thermophoresis platform requires a moderate level of skills to achieve consistent stiffness gradients. Particularly, it can be challenging for new users to work at small scales using microfluidic devices. However, the choice of using an external microchamber design in this modular platform significantly lowered the requirement for fluid handling expertise, which has acted as a barrier to entry of the early designs (discussed in **Chapter 5**). In this case, the only fluidic operation per se is pumping water through straight microchannels, which can be achieved relatively easily using standard syringe pumps on an open lab bench, and does not require active user control during the thermophoresis fabrication process.

Importantly, the reproducibility of stiffness gradient hydrogels fabricated using this modular platform was found to depend mostly on the stability of the imposed temperature gradient throughout the thermophoresis process. Although continuous temperature monitoring is not necessary using the modular platform, it is recommended to check from time to time that water is flowing consistently out of the microdevice and the Joule heater current remains relatively stable, which are good indicators of stable thermal conditions within the platform.

With initial training and some practice, any user should be able to follow the steps in this protocol and obtain high-quality stiffness gradient hydrogels.

6.5 Establishment of stable thermal conditions and validation of thermophoresis effects

Given the importance of a well-defined and stable thermal pattern for effective implementation of thermophoresis, initial experiments to characterize the temperature control capabilities of the modular platform were focused on answering two key questions: (1) can different spatial arrangements of heating and cooling channels in the microfluidic module reliably generate distinct and controllable temperature gradient patterns? And if so, (2) can the temperature gradient established at the microfluidic interface propagate uniformly across the microchamber volume?

The initial characterization experiments were performed using a 5-channel microfluidic module designed to create periodic gradients, as this presented a more stringent test of temperature control and patterning fidelity (**Figure 6.7a**). Demonstrating the system's ability to generate and maintain such complex patterns would provide a strong basis for implementing simpler (e.g., linear) gradients with confidence.

To measure the temperature distribution using the fluorescence thermometry method (detailed in Chapter 4.2), a glass microcapillary filled with 0.1 mM Rhodamine B solution was attached to the microfluidic module in place of the microchamber. It is important to highlight that the microcapillary (depth ~100 μm) was selected specifically to have similar critical dimensions to the microchamber (depth ~120 μm). Thus, this experimental setup effectively captures the temperature profile inside the sample microchamber under fabrication-relevant conditions (**Figure 6.7b**).

Temperature characterization results confirmed the successful generation of a uniform periodic gradient across a wide temperature range (**Figure 6.7c**). The results also clearly demonstrated a tunable magnitude of temperature gradient from at least 4 ºC mm^{-1} to 20 ºC mm^{-1} while maintaining the gradient shape fidelity (**Figure 6.7d**). Notably, the local maxima and minima temperatures corresponded to the center of the heating and cooling channels, respectively. These findings suggest insignificant thermal diffusion (or "smearing") effects in the micro-confined solution, enabling precise thermal patterning.

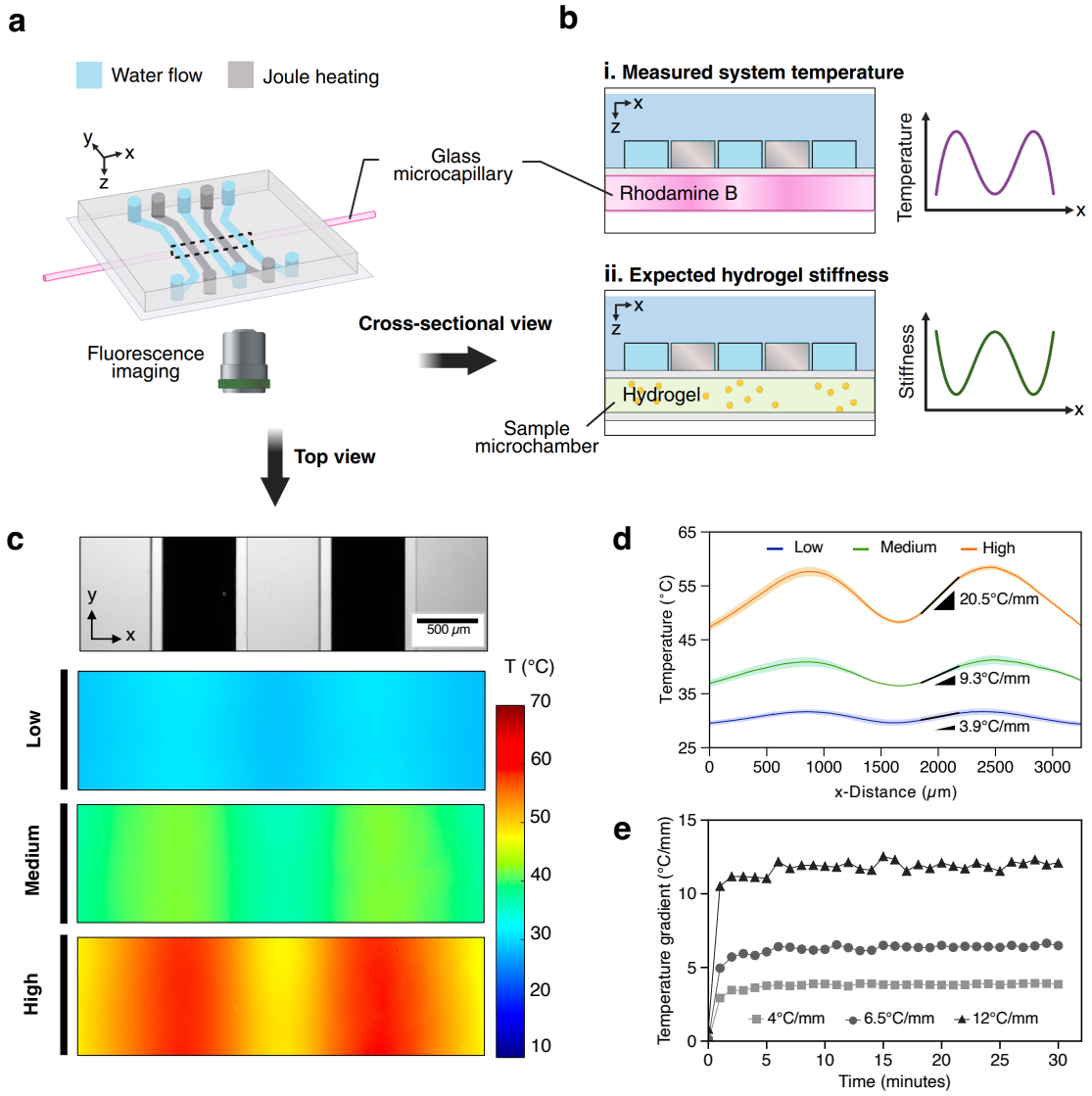

Figure 6.7: (a) Schematic of the experimental setup for fluorescence-based measurement the temperature distribution within the microfluidic system. (b) Graphical illustration of the system cross-section comparing the placement of (i) microcapillary for temperature characterization and (ii) microchamber for gradient hydrogel fabrication. (c) Optical micrograph showing the top view of a thermal patterning module configured with alternating water flow channel (bright lane) and micro-Joule heater (dark lane), (d) The corresponding temperature profile of (c) obtained by averaging in the channel direction (y-axis). Data reported as mean ± standard deviation of n=3 independent experiments. (e) The system temperature was controlled by varying the water flow rates and Joule heater current, demonstrating rapid and precise control over an extended duration.

Time-lapse analysis at various temperature gradient strengths further revealed that, upon initiating temperature control, the system rapidly (<2 min) approached the target temperature profile and remained stable for at least 30 mins, which is the typical thermophoresis process time for gradient hydrogel fabrication (**Figure 6.7e**).

Overall, these findings indicate that the proposed microfluidic thermal patterning strategy can be reliably used to impose distinguishable gradients as desired. Such precise temperature control of the platform enables “on-demand” and predictable progression of the thermophoresis process, which is essential to ensure highly reproducible stiffness gradients. It is worth noting that these system behaviors were also found to be consistent regardless of the thermal patterning configuration (**Figure 6.12, 6.14**), highlighting the versatility of the modular platform.

Next, thermophoresis experiments using fluorescent polystyrene nanoparticles (fluo-NP) were performed to verify the underlying mechanism for creating gradient materials using the modular platform (**Figure 6.8**). For these experiments, 0.3% fluo-NP suspension (100 nm, L1528, Sigma-Aldrich; prepared in water) was confined in a microchamber following the same experimental setup for gradient hydrogel fabrication.

Time-lapse imaging was performed to investigate the change in fluorescence intensity profile in the presence of a periodic temperature gradient. Across the range of temperature gradient strengths tested (4 ºC mm^{-1}, 6.5 ºC mm^{-1}, 12 ºC mm^{-1}), a progressive increase in fluorescence intensity around the cold regions and decreasing intensity around the hot regions was observed, indicating directed motion of fluo-NP in solution. Furthermore, a continuous distribution pattern of fluo-NPs was observed (**Figure 6.8**), which also correlated well with the imposed temperature profile (**Figure 6.7c**). These findings suggest the dominant effects of thermophoresis and negligible convective current within the platform (expected due to the micro-confinement), making it suitable for fabricating microscale stiffness gradient hydrogels.

Additionally, the results showed a more pronounced fluorescence intensity contrast (i.e. higher peak-to-through intensity difference) with increasing applied temperature strengths, further supporting the idea that thermophoresis can be harnessed to create spatially complex gradient hydrogels in a highly controlled fashion.

To our knowledge, this study is the first demonstration of utilizing thermophoresis to pattern spatially complex gradient materials within micro-confined geometries.

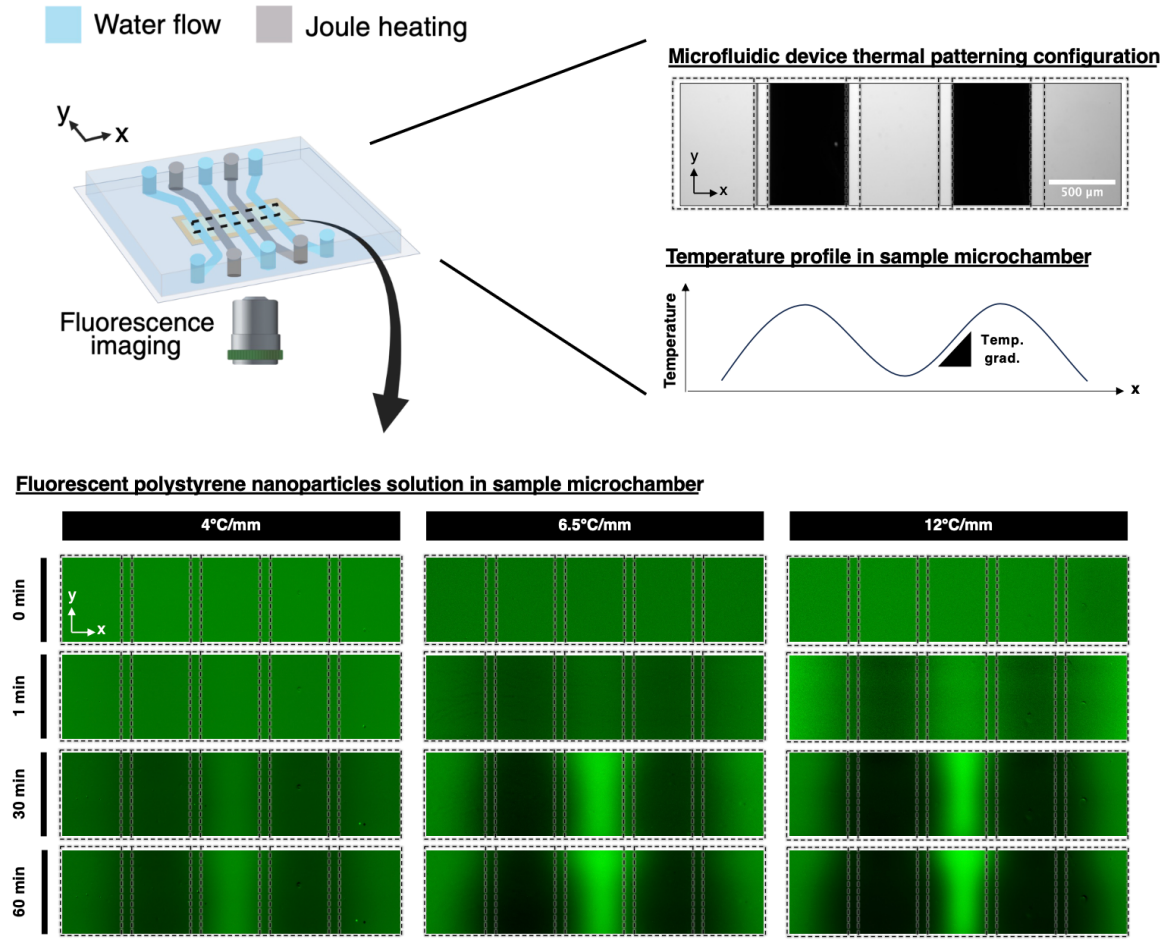

Figure 6.8: Time-lapse imaging showing thermophoresis in fluorescent polystyrene nanoparticle (fluo-NP) suspension in response to a periodic temperature gradient. The micrograph shows the top view of the microfluidic device, at the same position where the fluorescence images were captured. Note that the indicated temperature gradients represent the slope of a linear segment on the periodic gradient and correspond to the data in Figure 6.7e.

6.6 Optimization of process parameters

When planning a new biological study using gradient hydrogels, researchers typically start with a target stiffness profile, which subsequently requires exploration of potential design spaces to determine reliable processing parameters[4]. Existing workflows typically involve iterative trials of gradient gel fabrication and AFM characterization for process set up and optimization, which are time-consuming and labor intensive, often limiting practicality in traditionally “non-engineering” research environments.

In this context, a key advantage of this modular microfluidic system design is that the measured temperature profile precisely mirrors the resulting profile of the thermophoresis-driven concentration gradients and by extension, the stiffness pattern (**Figure 6.7b**). This feature offers the opportunity for users to qualitatively assess and compare the effects of different thermal module configurations or process parameters using the fluorescence thermometry tool. While it does not provide a quantitative prediction of the final stiffness magnitudes, this approach enables rapid screening of conditions likely to yield the desired gradient profile, significantly reducing the time for experimental trial-and-error.

To illustrate this approach, we take another example of a periodic gradient module as shown in **Figure 6.9**. Different shapes of symmetrical and asymmetrical periodic temperature profile were achieved by varying the water flowrate through the middle channel, keeping all other parameters constant (**Figure 6.9a**). The corresponding AFM measurement of fabricated GelMA gradient hydrogels revealed that the final stiffness profiles closely tracked the imposed thermal landscape fidelity (**Figure 6.9b**).

This brief result has two important implications. (1) The ability to generate high spatial resolution temperature maps enables rapid assessment of the expected hydrogel stiffness gradient fidelity. This can accelerate the initial process exploration phase, for example, to adjust the gradient pattern and size. (2) In the later optimization stages, the temperature maps can serve as an efficient screening tool for fine-tuning the process parameters to achieve the desired stiffness range and gradient strengths. By contrast, without these maps, optimization would be an arduous trial-and-error process: tuning the temperature inputs blindly, relying on sparse and imprecise thermocouple

readings[15], and then assessing the stiffness outcomes through AFM characterization alone.

The ability to visualize the full-field, high resolution temperature landscape within the platform facilitates quicker convergence toward the optimal fabrication process conditions. However, at this stage, it is fully acknowledged that the temperature maps do not directly inform the absolute stiffness values. Future work could further leverage the process input-output relationships to derive data-driven predictive models and design rules toward increasingly complex yet controlled gradient hydrogel systems[16].

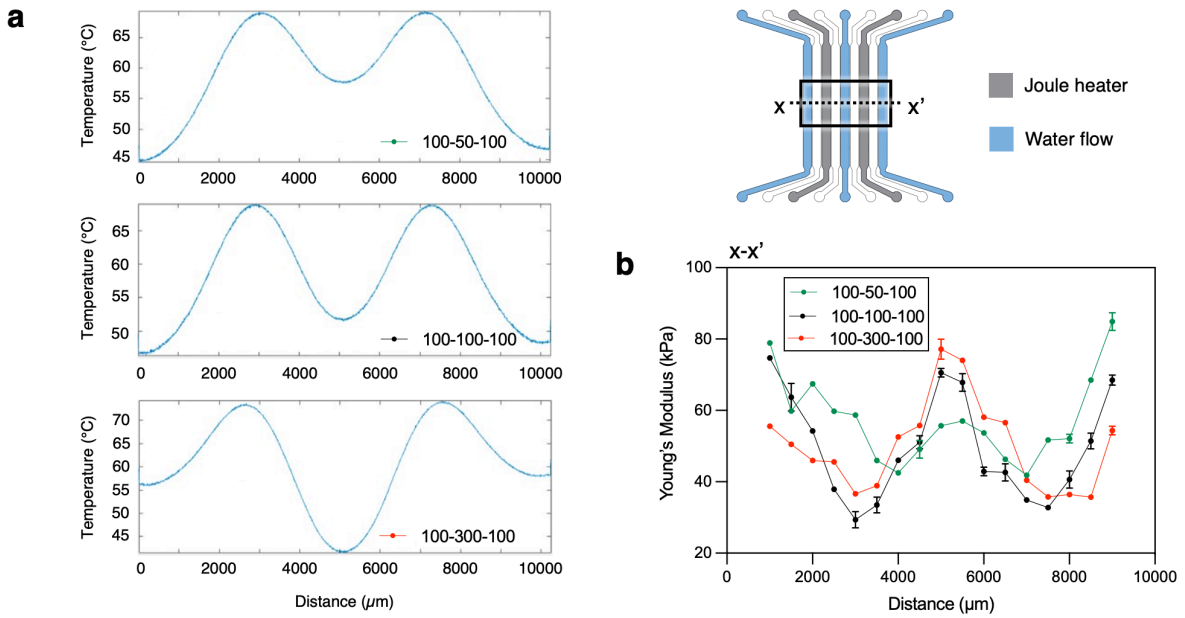

Figure 6.9: Fluorescence-based temperature mapping of a periodic pattern module, configured with alternating cold (blue) and hot (grey) channels. White channels represent closed, unused channels. Black bounding box indicates the sample microchamber area measuring 10000 μm × 5000 μm. (a) Temperature distribution across the module operated under different combinations of water flowrate. (b) Corresponding AFM-measured stiffness of gradient hydrogels fabricated using 10 wt% GelMA (n=1 sample). Figure legends indicate the water flowrate through the "left-middle-right" cooling channels, expressed in terms of μL min^{-1}. Each point represents mean ± SEM of a force map acquired at the x-location.

6.7 Compatibility with different hydrogel crosslinking modalities

Next, the versatility of the modular platform with different crosslinking modalities were demonstrated through Gellan gum and GelMA as a representative of thermally crosslinked and polymerized hydrogels, respectively. Gellan gum is a naturally occurring polysaccharide with attractive mechanical properties, making it a popular choice for osteochondral applications in tissue engineering (also discussed in **Chapter 5**)[17]. On the other hand, GelMA is a gelatin derivative that has been widely used for diverse biomedical applications due to the presence of desired cell-adhesion motifs, highly tunable biophysical properties, and versatility in terms of processing methods[18,19].

For these experiments, linear stiffness gradient hydrogels (1500 μm in width) were fabricated using three different temperature conditions, as summarized in **Table 6.1** and **Figure 6.12a**.

Table 6.1: Corresponding operational parameters used to generate the temperature gradient profiles presented in Figure 6.12. The indicated water flowrate and controlled current represent the value through individual cold and hot channels, respectively.

Gradient profile	Temperature gradient [°C mm^{-1}]	Water flowrate [μL min^{-1}]	Controlled current [A]	Process time [min]
(6.12a) Linear	7.5	50	0.6	30
(6.12b) Linear	11	60	0.7	30
(6.12c) Linear	15	100	0.9	30

AFM characterization was first performed to evaluate the precision and consistency of the thermophoretically fabricated stiffness gradient hydrogels using the modular platform. To demonstrate this, **Figure 6.10** shows a representative example of linear stiffness gradient GelMA hydrogels fabricated using 10 wt% initial polymer concentration and 15 °C mm^{-1} applied temperature gradient.

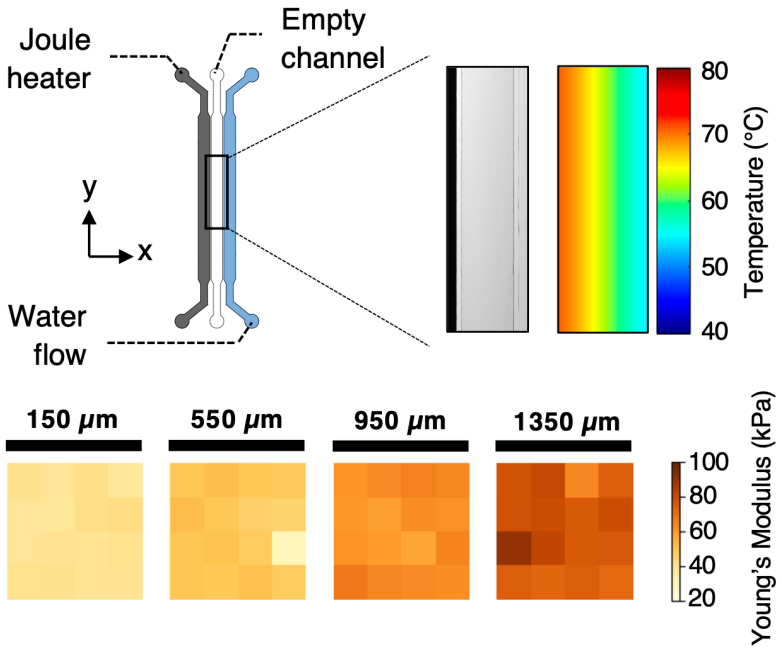

Figure 6.10: Representative experimental procedure for fabrication and characterization of stiffness gradient hydrogels, demonstrated using a linear gradient module. *Top:* The black bounding box indicates the magnified view of the sample microchamber area measuring 1500 μm × 5000 μm. The micrograph shows the top view of the region of the microfluidic module coinciding with the sample area. The heat map shows the corresponding temperature conditions imposed onto the sample solution during thermophoretic fabrication. *Bottom:* Stiffness of the resulting hydrogel was measured by taking AFM force maps at regular intervals in the x-direction. The numbers shown above each map indicate the x-distance from the sample edge corresponding to the hot side of the microfluidic module.

The results confirmed the successful generation of a linear stiffness gradient that closely matches the inverse profile of the temperature gradient. Notably, in order to identify the points for AFM indentation on the gradient gels, the location corresponding to the edges of the hot and cold channels were marked on the sample coverslip prior to hydrogel retrieval. This strategy allowed us to confirm that the stiffest spot on the gradient gel coincided with the center of the cold channel whereas the softest spot coincided with the center of the hot channel. These trends were found to be repeatable throughout the thesis, providing further affirmation of the platform's precision for patterning the microscale mechanical properties in hydrogels.

Importantly, AFM force maps (16-point grid, 20 μm × 20 μm area) acquired at each location exhibited highly uniform local stiffness. This attribute is valuable to facilitate investigations of how cells respond to spatially organized mechanical signals on the

micrometer to millimeter length scale, as opposed to variations at the subcellular level, which could have a confounding effect on cell-matrix mechanotransduction[20,21].

Furthermore, AFM measurements at various length axes demonstrated a uniform stiffness gradient across the whole gradient gel (**Figure 6.11**), consistent with the uniformity of the imposed temperature gradient (temperature heat map in **Figure 6.10**).

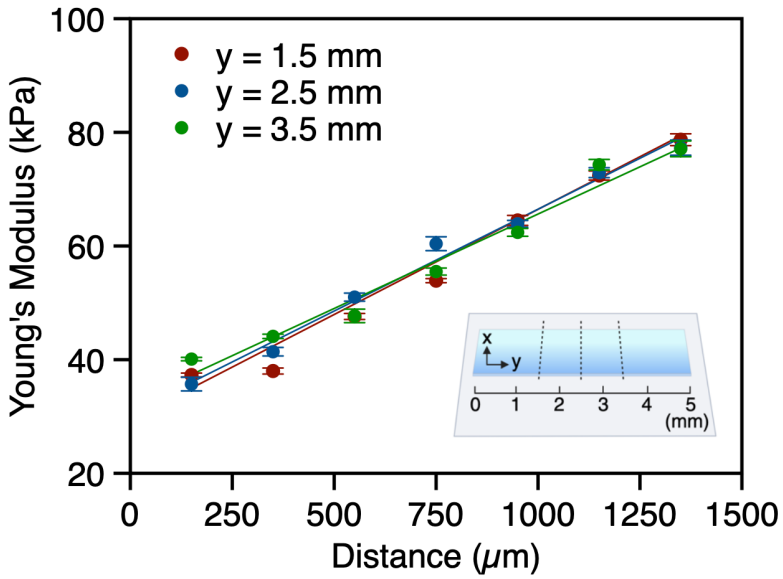

Figure 6.11: Stiffness line measurements performed at different y-positions on the same gradient gel confirmed consistent stiffness gradients throughout the sample. Each point represents mean ± SEM of a force map acquired at the x-location.

Taken together, these results strongly highlight the effectiveness of the proposed modular platform for manipulating polymers in microvolumes via thermophoresis effects, and limited dispersion of the established concentration gradient during the crosslinking process.

Following the thermophoretic (concentration) gradient generation process, rapid hydrogel crosslinking is the next crucial step to preserve this gradient and ensure reproducible stiffness gradients. Specifically, Gellan gum crosslinking was achieved by using the platform's integrated Peltier module to cool the platform below the gelation temperature (**Figure 6.12b**). On the other hand, GelMA was chemically crosslinked by exposing the entire platform to UV light (**Figure 6.12c**).

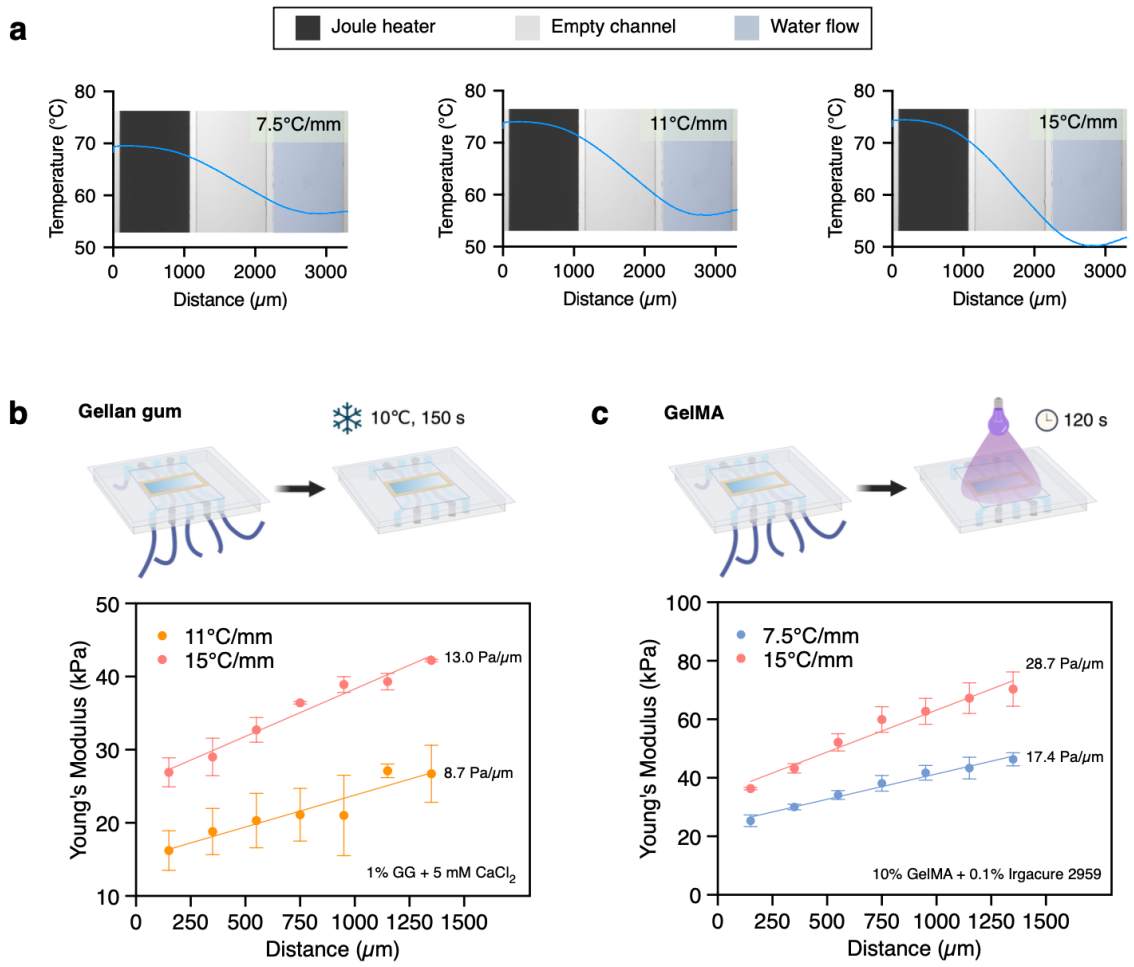

Figure 6.12: (a) Measured temperature profile superimposed onto the brightfield image of the microfluidic module configured for generating steep linear gradients. AFM stiffness measurement on (b) temperature-dependent crosslinked Gellan gum and (c) photopolymerized GelMA stiffness gradient hydrogels (n = 3 independent samples; mean ± SEM).

From the AFM measurements, it is clear that GelMA hydrogels yielded a steeper stiffness gradient compared to Gellan gum hydrogels at the same applied thermal conditions (**Figure 6.12b, 6.12c**). Furthermore, at 7.5 °C mm^{-1}, a measurable stiffness gradient was observed in GelMA but not Gellan gum hydrogels. In fact, it was noted that an applied temperature gradient >10 °C mm^{-1} was necessary to generate a discernible variation in stiffness across Gellan gum hydrogels. This can be explained since dispersed Gellan gum polymer chains are significantly larger than GelMA monomers, and thus, require a stronger temperature gradient to induce a sufficient thermophoretic force[22]. Nevertheless, the stiffness gradients in Gellan gum hydrogels exhibited a similar degree of spatial precision and fidelity in relation to the predefined thermal landscape, as initially demonstrated using GelMA hydrogels.

Overall, this section demonstrated that the same platform and fabrication workflow can be readily applied across different hydrogel crosslinking modalities. Compared to previous iterations, the switch to an external sample microchamber greatly improved performance for photopolymerizable hydrogels – arguably the most popular class of hydrogels used in cell culture studies nowadays. Specifically, the glass surfaces of the microchamber helped eliminate oxygen inhibition effects that may hinder photopolymerization in PDMS-based microdevices, while its "open" design allowed for more even and efficient UV exposure across the whole sample.

6.8 Customization of the gradient pattern

While the aforementioned results focused on short-range, steep linear stiffness gradients, the study of mechanobiological processes requires cellular analysis in gradients of different stiffness ranges, gradient slopes, and lateral dimensions of the gradient (on the order of micrometers to centimeters)[12,23]. As such, this section sets out to explore the range of gradient patterns that can be created using the modular platform.

In a preliminary set of experiments, the possibility of patterning periodic stiffness gradients was assessed as a continuation of the characterization study in Section 6.5. In addition to the previous positive results on GelMA (**Figure 6.9**), the process was also investigated using Gellan gum. However, in practice, Gellan gum is a much more challenging candidate for thermophoresis-based patterning due to its large molecular size and generally high viscosity[24]. Although the feasibility of forming linear stiffness gradients in Gellan gum hydrogels had been established (**Chapter 5**), at this point, it was uncertain whether more complex stiffness gradients at the micron-scale could be achieved. To test this concept, the same periodic module configuration depicted in **Figure 6.9** was used for thermophoretic fabrication with varying process time (**Table 6.2**).

Table 6.2: Corresponding operational parameters used to generate the temperature gradient profiles presented in Figure 6.13. The indicated water flowrate and controlled current represent the value through individual cold and hot channels, respectively.

Gradient profile	Temperature gradient [°C mm^{-1}]	Water flowrate [µL min^{-1}]	Controlled current [A]	Process time [min]
(6.13a) Periodic	12	100	1.0	20
(6.13b) Periodic	12	100	1.0	40

Figure 6.13 shows the AFM characterization data on the resulting hydrogels and highlights two important observations: first, the presence of well-defined periodic stiffness gradients with spatial profiles that closely mirrored the imposed thermal landscape; and second, that increasing the thermophoresis time resulted in steeper gradients without altering the average stiffness across the hydrogel. These trends are consistent with established thermophoretic behaviors, providing strong evidence that the complex stiffness gradient pattern in the Gellan gum hydrogels was not arbitrary but indeed a direct result of thermophoresis-driven polymer migration.

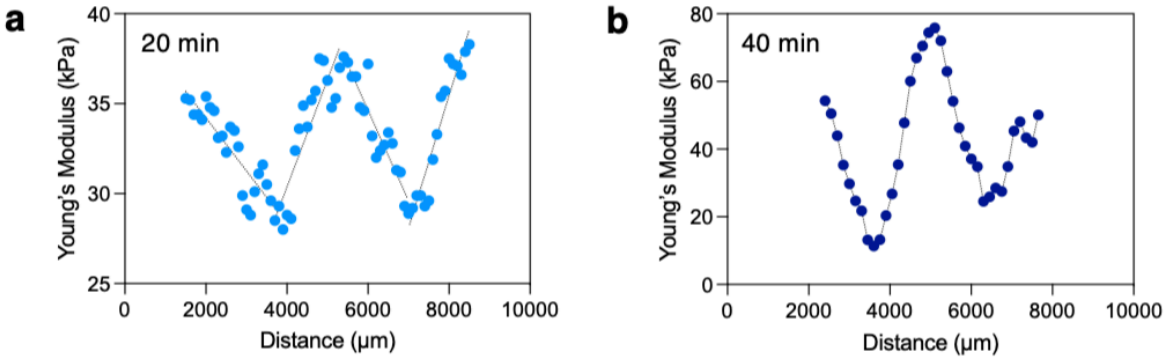

Figure 6.13: AFM stiffness measurement on periodic stiffness gradient Gellan gum hydrogels (1 wt% initial polymer concentration) fabricated with a thermophoresis process time of (a) 20 min and (b) 40 min. n=1 sample. Each point represents a single indentation.

Altogether, the results thus far demonstrated the potential of the modular platform to create spatially complex stiffness gradients across different hydrogel systems. Subsequent experiments in the chapter will focus on GelMA hydrogels, which were justified given their simple processing and broad tunability in stiffness range. On the other hand, there has been increasing interest in GelMA for gradient hydrogel cell

culture in recent years[25–28], making it a relevant benchmark. The goal was to demonstrate that the flexibility of this thermophoresis-based platform can complement existing fabrication methods while offering unique advantages in the gradient design and control.

The thermal patterning module configurations explored are schematically illustrated in **Figure 6.14**, and the corresponding process parameters are summarized in **Table 6.3**.

Table 6.3: Corresponding operational parameters used to generate the temperature gradient profiles presented in Figure 6.14. The indicated water flowrate and controlled current represent the value through individual cold and hot channels, respectively.

Gradient profile	Temperature gradient [°C mm^{-1}]	Water flowrate [µL min^{-1}]	Controlled current [A]	Process time [min]
(6.14a) Linear	5	200	0.9	30
(6.14b) Periodic	12	100	1.0	30
(6.14c) Sawtooth	10 (steep) / 6.5 (shallow)	100	1.0	30

Long-range, shallow linear gradients (< 5 Pa $µm^{-1}$) spanning ~10 mm in width were successfully generated by employing the end channels in the microfluidic module for temperature control (**Figure 6.14a, 6.14d, 6.14g, 6.14j**). In contrast to the steep, pathological-mimicking gradients (>10 Pa $µm^{-1}$) as shown in Section 6.7, these shallow gradients are useful to recreate certain tissue mechanical microenvironments, or in applications where durotactic behavior is undesired[1,29].

Beyond monotonic gradients, alternating heating-cooling channel configuration enabled periodic gradients (**Figure 6.14b, 6.14e, 6.14h, 6.14k**) as well as sawtooth gradients comprising a repeating period of steep positive slope and shallow negative slope (**Figure 6.14c, 6.14f, 6.14i, 6.14l**). Such continuously varying mechanical landscapes could facilitate a deeper understanding of cellular mechanosensitivity toward gradient strength and directionality, which is particularly valuable for migration-based studies[30–32]. By embedding multiple gradient cycles within a single substrate, these complex patterns could also support high(er) throughput screening of systematically varying mechanical conditions, or enhance statistical robustness through sampling of cells on recurring mechanical patterns[33]. For certain studies

investigating cell function and behavior in specific tissue contexts (e.g., fibrosis[34], striated muscle[35,36]), anisotropic mechanical gradients would provide a better representation of the spatial heterogeneity in native ECM, though this is currently a largely unexplored direction.

In all cases, the resulting stiffness profiles were in good agreement with empirical predictions based on the temperature characterization results. Moreover, this set of experiments demonstrated that tuneability in stiffness values can be achieved by adjusting the initial polymer concentration without compromising the resulting gradient shape fidelity (**Figure 6.14**; 5 wt% GelMA vs. 10 wt% GelMA).

Despite the clear biological relevance of spatially complex stiffness gradients *in vivo*, and considering the numerous advances in related bioprinting strategies[37], the availability of microfabricated complex gradient hydrogel systems has been far more limited. Although variations of the two-step polymerization method have been developed to pattern non-linear stiffness profiles[30,33,36], most studies are still largely skewed toward simpler linear gradients. This disparity likely stems from the inherent technical challenges in replicating the stiffness gradients observed *in vivo*. Current protocols involving diffusion-driven processes are often difficult to optimize, have limited spatial fidelity, and are subject to high inconsistencies, making them difficult to scale or adapt for nuanced biological applications (discussed in **Chapter 2**). In this respect, the modular thermophoresis platform was developed with the intention to enable rapid material design iteration and expand the library of stiffness gradient hydrogel systems. By enabling a more streamlined and efficient experimental workflow, the thermophoresis biofabrication approach could potentially enhance accessibility and applicability of complex gradient hydrogels for *in vitro* single-cell mechanobiology studies.

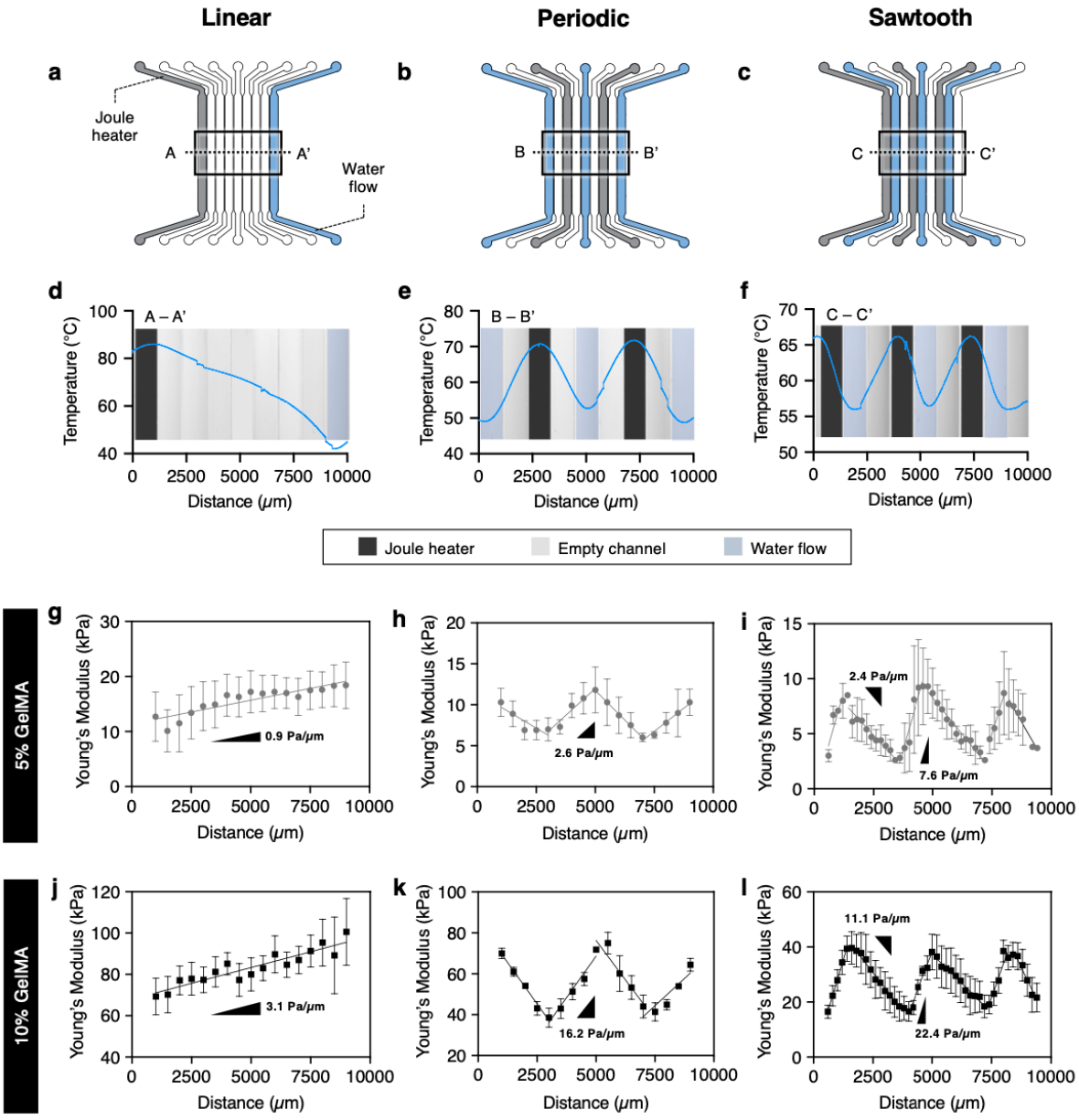

Figure 6.14: (a-c) Different gradient profiles can be achieved by altering the configuration of heating (Joule heater) and cooling (water flow) channels within the microfluidic module. Black bounding boxes indicate the sample microchamber area measuring 10000 μm × 5000 μm. Measured temperature profile superimposed onto the brightfield image of the microfluidic module configured for generating (d) shallow linear, (e) periodic, and (f) sawtooth gradients. Corresponding AFM measurements on stiffness gradients hydrogels fabricated using (g-i) 5 wt% GelMA and (j-l) 10 wt% GelMA (n = 3 independent samples; mean ± SEM).

6.9 Fibroblast cell behaviors on linear, periodic, and anisotropic stiffness gradient GelMA hydrogels

Having established that the modular thermophoresis platform can be used to fabricate simple linear and complex stiffness gradient hydrogels, 3T3-L1 fibroblasts were seeded on these gradient hydrogels to assess the potential of this gradient hydrogel platform for studying stiffness-dependent cellular responses.

For these experiments, 10 wt% GelMA system was selected as the base material to create three distinct stiffness profiles: a steep linear gradient (**Figure 6.15c**), a periodic gradient (**Figure 6.15e**), and a dual-slope gradient produced using a single period on the sawtooth pattern module (**Figure 6.15h**). The respective stiffness range and gradient strength are summarized in **Table 6.4**. Additionally, uniform stiffness GelMA hydrogel (~40 kPa) was included as a control sample. In all cases, the hydrogel samples were used directly as 2D cell culture substrates without additional ECM protein coating (**Figure 6.15a**). Cell nuclei and the actin cytoskeleton were stained for visualization, which were subsequently divided into multiple segments parallel to the direction of the gradient for quantitative cell analysis.

Table 6.4: Specifications of the stiffness gradient hydrogels for cell studies as presented in Figure 6.15.

Gradient profile	Stiffness range [kPa]	Gradient slope [Pa μm^{-1}]
(6.15c) Linear	~35-80	~28
(6.15e) Periodic	~40-80	~16 (linear part)
(6.15h) Dual-slope	~15-40	~22 (steep) / ~11 (shallow)

A stiffness-dependent cell distribution on the hydrogels was observed after 1 day of culture. As expected, cells on the uniform stiffness sample (control) did not exhibit a biased distribution in any direction (**Figure 6.15b**). On the other hand, the fibroblasts exhibited a graded cell distribution on the linear (**Figure 6.15c, 6.15d**) and periodic gradient gels (**Figure 6.15e, 6.15f**). Interestingly, a higher cell population was observed around the softer regions (~35-40 kPa), seemingly contrasting the conventional notion that fibroblasts exhibit positive durotaxis from “soft” to “stiff” regions on a substrate[13]. However, when cultured on the dual-gradient gels for 24 h,

cells exhibited a biased accumulation toward the stiffest point on the substrate, in this case was ~40 kPa (**Figure 6.15h, 6.15i**).

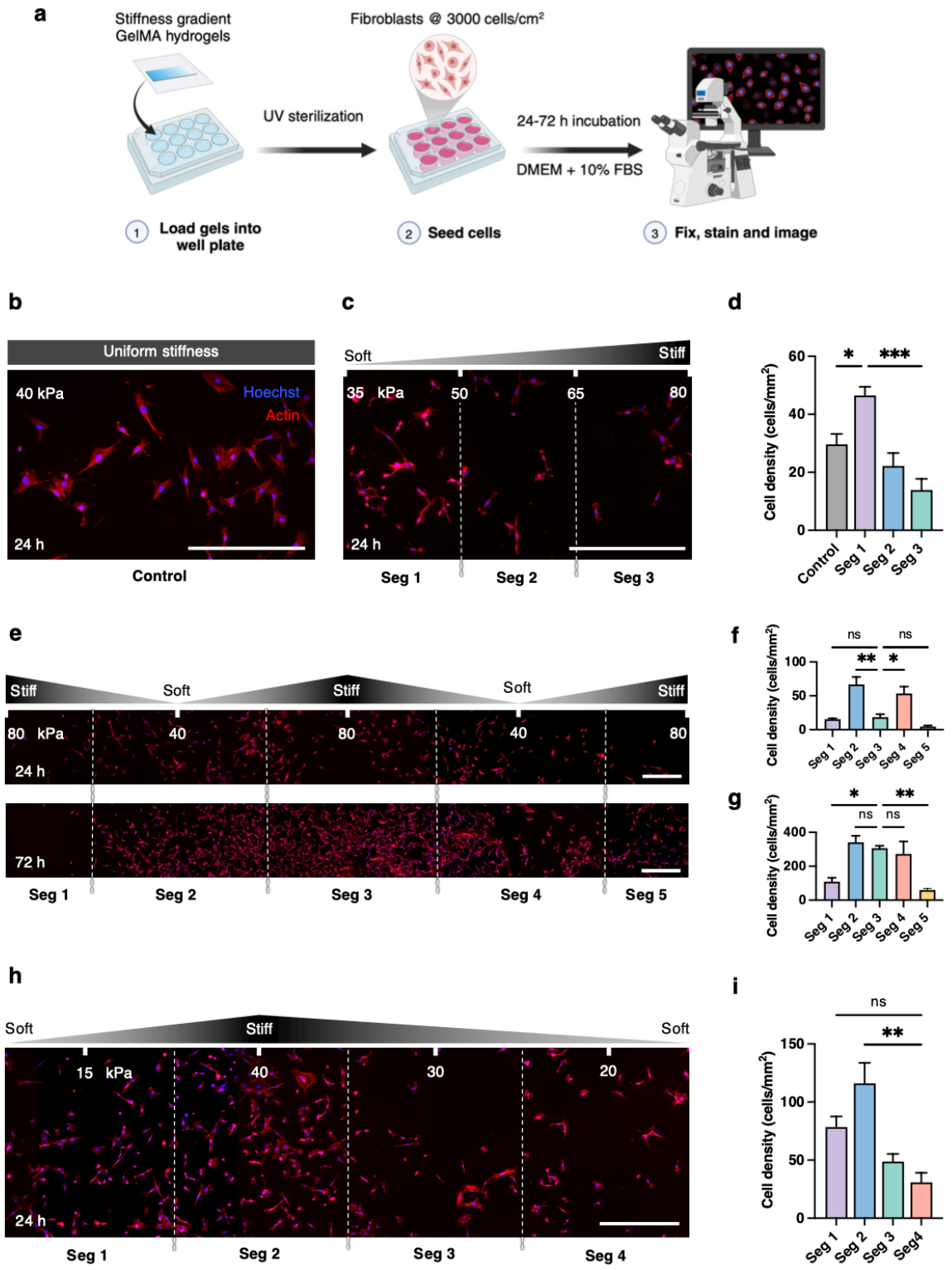

Figure 6.15: (a) Schematic of experimental procedure to examine 3T3-L1 fibroblast cell behavior on GelMA hydrogels with different stiffness gradient profiles. Representative images of fibroblasts on (b) uniform stiffness sample (control) and (c) linear stiffness gradient with a steep slope ~28 Pa μm^{-1} at 24 h. Quantification of cell distribution on the control and linear gradient gels are shown in (d). (e) Representative images of fibroblasts on symmetrical, periodic stiffness gradient with a slope of linear part ~16 Pa μm^{-1} at 24 h (top) and 72 h (bottom). Quantification of cell distribution on the periodic gradient gels at (f) 24 h and (g) 72 h. (h) Representative image of fibroblasts on anisotropic stiffness gradient comprising a steep positive slope (~22 Pa μm^{-1}) and a shallow negative slope (~11 Pa μm^{-1}). (i) Quantification of cell distribution on the dual-gradient gels at 24 h. Dashed lines indicate the boundary between segments along the imaged samples for cell analysis. Scale bars: 500 μm. Data reported as mean ± standard deviation of n = 3 independent samples.

An additional experiment was performed to examine fibroblast cell responses on periodic stiffness gradient gels over longer-term culture. After 3 days, there appeared to be a biased shift in cell distribution toward the center where the hydrogel stiffness peaks at ~80 kPa (**Figure 6.15e, 6.15g**). Further analysis revealed that the increased cell density on day 3 relative to day 1 was overall more pronounced at the stiffer regions (segments 1, 3 and 5) than the softer regions (segments 2 and 4) (**Figure 6.16**).

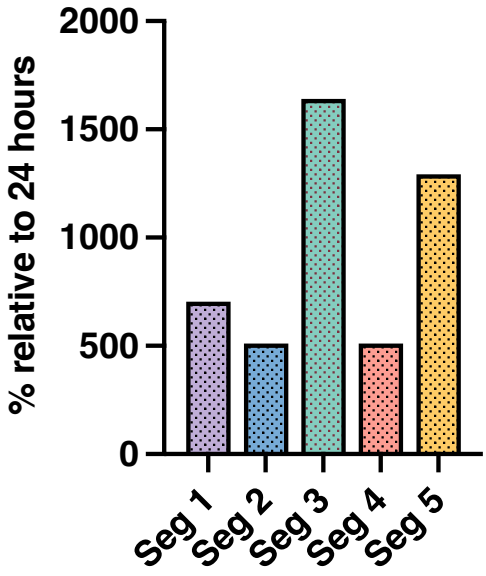

Figure 6.16: Relative increase in cell density at 72 h compared to 24 h on each segment of the periodic stiffness gradient hydrogels.

Taken together, these results suggest that the initial cell distribution was mainly influenced by a preferential attachment and proliferation around the 30-40 kPa stiffness range. However, as demonstrated with the periodic stiffness gradient gels, a gradient slope of >10 Pa μm^{-1} was sufficient to induce a net durotactic migration of fibroblasts from “soft” to “stiff” regions, thus resulting in a shift in cell distribution over time. Yet, the markedly higher overall cell density around the central (Seg 2-3-4; soft-stiff-soft) region of the substrate compared to the peripheral stiff regions (Seg 1 & 5) suggests that the presence of multiple stiffness transitions in the center might have localized the cell migration dynamics (**Figure 6.15g**). While the reason for the observation in this study is not entirely clear, it is hypothesized that the central stiff region (Seg 3) likely acted as a convergent point for migrating cells due to its position being adjacent to both of the soft regions (**Figure 6.15e**). On the other hand, the soft regions also exhibited significantly higher cell density than the peripheral stiff regions (**Figure 6.15g**). One possible explanation to this is that while cells directionally migrated toward stiffer regions on the substrate, higher proliferation rates around the soft regions might have persisted over the 3-day culture and contributed to increased local cell population. It should be noted that in all cases, the actual hydrogel area extended beyond the gradient region analyzed, which was achieved by using a sample microchamber wider than the specified gradient width. This ensured that the cells imaged were located well within the interior of the resulting hydrogel rather than near its physical boundaries, thus the observed cell behavior was unlikely to arise from edge effects. Nonetheless, given that fibroblasts are known to remodel their surrounding ECM in a gradient-dependent manner (recently reported by Zhao et al. using linear stiffness gradients[38]), future studies should look to investigate the ways in which matrix remodeling by fibroblasts progresses on more spatially complex stiffness gradients, and how this phenomenon affect the integrated stiffness-dependent cell responses.

In this section, the observed stiffness-dependent cell patterning across the gradient GelMA hydrogels was interpreted in terms of durotactic migration. Yet, it is fully acknowledged that the possibility of differential cell attachment and proliferation could not be completely ruled out based on this dataset alone. These effects were subsequently addressed in **Chapter 7**, where comparative analysis were performed under normal and serum-starved culture conditions to decouple the contributions of

proliferation and durotaxis. Additional observations were also taken at earlier time-points to assess the initial cell attachment behavior in different stiffness conditions. Taken together, the results from **Chapter 6** and **Chapter 7** support that the graded cell distribution reported here primarily reflects stiffness-mediated cell migration.

Nonetheless, the results in this section highlight that the absolute value of stiffness alone does not fully explain cell behavior. Instead, the pattern of stiffness change and the gradient slope can synergistically influence cell-material interactions in profound ways. In order to facilitate widespread use of complex stiffness gradients for practical biological applications, there are still a number of fundamental questions that we must first clarify – for example: how does the initial position of cells on the substrate influence their mechanosensitivity toward altering slopes of stiffness gradients[32,39]? Are there any localization or "mechanical trapping" effects on anisotropic gradients? Do cells retain memory of previously encountered stiffness conditions within asymmetric mechanical landscapes[40]? To unravel these complexities, a biomaterials platform such as that developed here can present various complex gradient profiles to provide more information on the cell-material interplay compared to solely testing on linear stiffness gradients, making it a promising platform to systematically study cell mechanotransduction on stiffness gradients.

6.10 Discussion

6.10.1 Generalizability with other hydrogel types

Through a series of work to date, we have demonstrated the versatility of the thermophoresis method using distinctly different classes of hydrogels – including ionic-crosslinked alginate[10], thermosensitive Gellan gum[11], and photocrosslinked GelMA (this thesis). Apart from varied crosslinking modality, this selection of hydrogels also showcased potential generalizability across different origin type (i.e. natural, synthetic), biochemical composition (i.e., carbohydrate-based, protein-based), and network structure (i.e., porous, fibrous). While it is acknowledged that these three hydrogel types so far do not fully represent the vast number of existing and emerging hydrogel chemistries in the field, it was not the focus of this thesis to test and optimize the developed modular platform with a comprehensive library of hydrogels. However,

based on the wealth of studies reporting thermophoresis of biopolymers and bionanoparticles in solution[41], it can be confidently concluded that the platform should also extend to other hydrogels provided that the following requisites are met:

1) The precursor components can be dispersed in solution prior to crosslinking.
2) The presence of temperature gradients in the solution will not prematurely trigger unwanted hydrogel crosslinking.
3) The precursor components have sufficiently low molecular weight to enable discernible thermophoretic movement within a reasonable timeframe.

From first principles, the platform's generalizability can be attributed to the fact that thermophoresis is a universal physical phenomenon that occurs in any aqueous system when subjected to a non-uniform temperature field (discussed in detail in Section 3.2). In this specific case, the platform works by leveraging thermophoresis effect to generate local variations in polymer (and crosslinker) concentration within the hydrogel precursor solution. It is important to note that hydrogel crosslinking is only initiated after the thermophoresis process is complete, meaning that the stiffness gradient generation mechanism is decoupled from the thermophoresis process.

From a practical standpoint, the generation of measurable stiffness gradients using the thermophoresis technique generally requires at least 20 min of applied temperature field exposure. Therefore, this method is most readily suited to hydrogel systems with on-demand crosslinking. These include a broad class of photo- and thermally crosslinkable hydrogels, where polymerization or gelation can be controlled externally through light exposure or temperature modulation. On the other hand, for rapidly gelling systems, such as click-based or ionic crosslinking of alginate with calcium ions, the gelation kinetics on the order of seconds to minutes may not permit sufficient time for solute redistribution. To address this issue, we previously demonstrated effective modulation of alginate crosslinking by using a system where calcium carbonate nanoparticles were dispersed in the precursor solution under mildly alkaline conditions, enabling thermophoresis to proceed as normally expected[10]. After the specified duration, an acidic oil phase was introduced (via diffusion through a membrane interfacing the sample microchannel) to lower the pH of the hydrogel solution, triggering the local dissolution of calcium carbonate nanoparticles to release

calcium ions and complete gelation after 2-5 min. Although similar strategies could be engineered for other fast-gelling systems, such adaptations would likely introduce additional formulation and design complexities, but their utility is limited to the specific use case.

Ultimately, the potential generalizability of this platform can open new avenues for researchers to explore diverse chemistries, offering precise control over stiffness gradients while simultaneously modulating other mechanical, structural, or biochemical cues. Nevertheless, the considerations outlined above should be judiciously considered to balance the desirable properties of the hydrogel with the practical requirements of the thermophoresis fabrication technique, ensuring that both material performance and gradient formation are optimized for the intended application.

6.10.2 Adaptability for 3D cell encapsulation applications

The platform utility was validated by examining fibroblast behaviors on GelMA hydrogels with varying stiffness gradient profiles. The findings highlight how the gradient pattern can be as important in influencing cell behaviors as other characteristics, including absolute stiffness and gradient strength. For a balanced discussion, however, it should be noted that the high temperatures (average 60 ℃) used in the current protocol would make it unsuitable to incorporate cellular components within the hydrogels during the thermophoretic fabrication process. In particular, the protocol was optimized with an initial focus on Gellan gum hydrogel, whereby an elevated temperature was necessary to prevent premature gelation (critical gelation temperature ~40 °C) and reduce sample viscosity to ensure effective and reproducible gradient generation[11]. This reflects the needs of the specific material rather than a limitation of the platform. To ensure consistency, the same process parameters were subsequently applied to fabricate stiffness gradient GelMA hydrogels.

However, it is important to note that the thermophoresis method is effective at any temperature. Although the concept of thermophoresis might intuitively suggest “heat treatment”, effective thermophoretic gradient generation does not require high absolute temperatures, but rather the presence of a well-defined temperature gradient. For example, in an early study from our group using the first iteration microfluidic

system[42], thermophoresis of amyloid fibril in suspensions was demonstrated across a broad range of average system temperatures from 12 °C to 60 °C. Therefore, we speculate that the developed modular platform could similarly be applied to other types of hydrogels (e.g., polyacrylamide, collagen) that do not require elevated processing temperatures and that remain liquid at physiological or sub-physiological temperatures. Continued efforts in this direction will further expand the utility of the thermophoresis platform for creating cell-laden gradient hydrogels to investigate unique mechanobiological behaviors in 3D contexts[43].

6.10.3 Biological contexts and applications

The design of this modular platform, especially with the use of GelMA, provides the flexibility to achieve stiffness ranges and gradient strengths relevant to various pathophysiological situations.

As previously reviewed in **Chapter 2**, the Young's modulus of different adult tissues can range from ~0.1 kPa to >100 kPa, as measured by AFM. In the context of mechanobiology, thermophoretically fabricated stiffness gradients with subtle yet precise changes (i.e., <5 kPa mm^{-1}; using 5 wt% GelMA system) will be useful to for screening stiffness-dependent cell morphology, contractile phenotype, and mechanomarker expression in a high-resolution manner. Notably, the established 1-20 kPa stiffness range suitably covers soft to moderately stiff tissues, such as the lungs and dermis layer. As a demonstration of this approach to enhance our understanding of fundamental cellular processes, Barber-Pérez et al. successfully employed a stiffness gradient spanning ~0.5-22 kPa to identify the stiffness threshold/responsiveness of fibrillar adhesion formation in fibroblasts, which has an important functional role in directing ECM remodeling[44]. In another study, Tan et al. fabricated linear stiffness gradient hydrogels with a range of ~2-30 kPa to recreate the measured stiffnesses of *ex vivo* airway smooth muscle tissue and used the platform to study how human airway smooth muscle cells mechanosense aberrant microenvironment during obstructive airway diseases, showcasing direct clinical relevance[29].

On the other hand, the steeper stiffness gradients (i.e., up to 30 kPa mm^{-1}; using 10 wt% GelMA system) are ideally suited to study durotaxis of single cells or cell clusters, in which case higher stiffness ranges are also often explored. For example, Isenberg et al. tested three gradient gels with stiffness ranges of 29.6-51.6 kPa, 0.93-41.7 kPa and 4.64-80.1 kPa, corresponding to a gradient slope of 10 kPa mm^{-1}, 20 kPa mm^{-1}, and 40 kPa mm^{-1} [ref. 45]. The study revealed that the vascular smooth muscle cell durotaxis depends on the substrate stiffness gradient strength, and multiple studies have since demonstrated similar systematic investigations using different cell types, such as mesenchymal stem cells[12] and carcinoma cells[2].

It should be noted that a more extreme gradient (>100 kPa mm^{-1}) may be required for some applications, particularly those related to modeling soft-hard tissue interfaces or injuries. To illustrate this point, Zhang et al. reported that the stiffness increases from ~60 kPa to ~25.9 MPa at healthy periodontal ligament-alveolar bone enthesis[33]. Meanwhile, the vascular walls in arteries are known to stiffen from 10-50 kPa to 100-300 kPa during aging, contributing to the onset and progression of many age-related cardiovascular diseases[46]. However, the range of stiffness variation achieved using the platform developed here was restricted by the maximum allowable polymer concentration of the starting solution, above which the hydrogel solution becomes too viscous resulting in impractically low thermophoresis kinetics. Thus, to enhance the biological relevance of our platform, it is necessary to further explore alternative hydrogel systems which is not only tunable across a wide stiffness range, but ideally also maintains a low viscosity at all concentration levels.

6.11 Conclusion

In this chapter, I introduced a new modular platform that would allow users to flexibly produce hydrogels with broad biologically relevant stiffness ranges and gradient patterns. The platform employs a combined microfluidic and thermophoresis approach that builds on our foundational work presented in Chapter 5, but offers unique advantages that focus on facilitating practical usability: simplified setup and operation, predictive optimization framework, direct compatibility with different hydrogel crosslinking modalities, and the ability to pattern complex gradients. The technological advancements introduced in this work represent a pivotal transition of the thermophoretic fabrication technique from a proof-of-concept toward a reliable and versatile research tool. In the broader context, the modular platform is considered a valuable addition to the current fabrication methods by expanding the library of microengineered stiffness gradient hydrogels, prompting new mechanobiology questions and applications.

References

1. Hadden, W. J. *et al.* Stem cell migration and mechanotransduction on linear stiffness gradient hydrogels. *Proc Natl Acad Sci* **114**, 5647–5652 (2017).

2. Pallarès, M. E. *et al.* Stiffness-dependent active wetting enables optimal collective cell durotaxis. *Nat Phys* **19**, 279–289 (2022).

3. Denisin, A. K. & Pruitt, B. L. Tuning the Range of Polyacrylamide Gel Stiffness for Mechanobiology Applications. *ACS Appl Mater Interfaces* **8**, 21893–21902 (2016).

4. Tse, J. R. & Engler, A. J. Preparation of Hydrogel Substrates with Tunable Mechanical Properties. *Curr Protoc Cell Biol* **47**, 10161 (2010).

5. Clark, A. G. *et al.* Self-generated gradients steer collective migration on viscoelastic collagen networks. *Nat Mater* **21**, 1200–1210 (2022).

6. Chaudhuri, O., Cooper-White, J., Janmey, P. A., Mooney, D. J. & Shenoy, V. B. Effects of extracellular matrix viscoelasticity on cellular behaviour. *Nature* **584**, 535–546 (2020).

7. Zhang, H., Lin, F., Huang, J. & Xiong, C. Anisotropic stiffness gradient-regulated mechanical guidance drives directional migration of cancer cells. *Acta Biomater* **106**, 181–192 (2020).

8. Davidson, M. D. *et al.* Programmable and contractile materials through cell encapsulation in fibrous hydrogel assemblies. *Sci Adv* **7**, eabi8157 (2021).

9. Tanaka, M., Nakahata, M., Linke, P. & Kaufmann, S. Stimuli-responsive hydrogels as a model of the dynamic cellular microenvironment. *Polym J* **52**, 861–870 (2020).

10. Vigolo, D., Ramakrishna, S. N. & DeMello, A. J. Facile tuning of the mechanical properties of a biocompatible soft material. *Sci Rep* **9**, 7125 (2019).

11. Kosmidis Papadimitriou, A. *et al.* Fabrication of gradient hydrogels using a thermophoretic approach in microfluidics. *Biofabrication* **16**, 025023 (2024).

12. Vincent, L. G., Choi, Y. S., Alonso-Latorre, B., Del Álamo, J. C. & Engler, A. J. Mesenchymal stem cell durotaxis depends on substrate stiffness gradient strength. *Biotechnol J* **8**, 472–484 (2013).

13. Zaari, N., Rajagopalan, P., Kim, S. K., Engler, A. J. & Wong, J. Y. Photopolymerization in microfluidic gradient generators: Microscale control of substrate compliance to manipulate cell response. *Adv Mater* **16**, 2133–2137 (2004).

14. Dertinger, S. K. W., Chiu, D. T., Noo Li Jeon & Whitesides, G. M. Generation of gradients having complex shapes using microfluidic networks. *Anal Chem* **73**, 1240–1246 (2001).

15. Lee, N. & Wiegand, S. Thermophoretic micron-scale devices: Practical approach and review. *Entropy* **22**, 950 (2020).

16. Verheyen, C. A., Uzel, S. G. M., Kurum, A., Roche, E. T. & Lewis, J. A. Integrated data-driven modeling and experimental optimization of granular hydrogel matrices. *Matter* **6**, 1015–1036 (2023).

17. Stevens, L. R., Gilmore, K. J., Wallace, G. G. & In het Panhuis, M. Tissue engineering with gellan gum. *Biomater Sci* **4**, 1276–1290 (2016).

18. Loessner, D. *et al.* Functionalization, preparation and use of cell-laden gelatin methacryloyl-based hydrogels as modular tissue culture platforms. *Nat Protoc* **11**, 727–746 (2016).

19. Yue, K. *et al.* Synthesis, properties, and biomedical applications of gelatin methacryloyl (GelMA) hydrogels. *Biomaterials* **73**, 254–271 (2015).

20. Sun, A. R., Hengst, R. M. & Young, J. L. All the small things: Nanoscale matrix alterations in aging tissues. *Curr Opin Cell Biol* **87**, 102322 (2024).

21. Yang, C. *et al.* Spatially patterned matrix elasticity directs stem cell fate. *Proc Natl Acad Sci* **113**, E4439-45 (2016).

22. Braibanti, M., Vigolo, D. & Piazza, R. Does thermophoretic mobility depend on particle size? *Phys Rev Lett* **100**, 108303 (2008).

23. Sunyer, R. & Trepat, X. Durotaxis. *Curr Biol* **30**, R383–R387 (2020).

24. Miyoshi, E., Takaya, T. & Nishinari, K. Rheological and thermal studies of gel-sol transition in gellan gum aqueous solutions. *Carbohydr Polym* **30**, 109–119 (1996).

25. Lavrentieva, A. *et al.* Fabrication of Stiffness Gradients of GelMA Hydrogels Using a 3D Printed Micromixer. *Macromol Biosci* **20**, 7 (2020).

26. Ko, H. *et al.* A simple layer-stacking technique to generate biomolecular and mechanical gradients in photocrosslinkable hydrogels. *Biofabrication* **11**, 025014 (2019).

27. Wu, Y. *et al.* The influence of the stiffness of GelMA substrate on the outgrowth of PC12 cells. *Biosci Rep* **39**, BSR20181748 (2019).

28. Kim, C. *et al.* Stem Cell Mechanosensation on Gelatin Methacryloyl (GelMA) Stiffness Gradient Hydrogels. *Ann Biomed Eng* **48**, 893–902 (2020).

29. Tan, Y. H. *et al.* Stiffness Mediated-Mechanosensation of Airway Smooth Muscle Cells on Linear Stiffness Gradient Hydrogels. *Adv Healthc Mater* **13**, 2304254 (2024).

30. Joaquin, D. *et al.* Cell migration and organization in three-dimensional in vitro culture driven by stiffness gradient. *Biotechnol Bioeng* **113**, 2496–2506 (2016).

31. Isomursu, A. *et al.* Directed cell migration towards softer environments. *Nat Mater* **21**, 1081-1090 (2022).

32. Hakeem, R. M. *et al.* A Photopolymerized Hydrogel System with Dual Stiffness Gradients Reveals Distinct Actomyosin-Based Mechano-Responses in Fibroblast Durotaxis. *ACS Nano* **17**, 197–211 (2023).

33. Zhang, H. *et al.* Cellular-Scale Matrix Stiffness Gradient at Soft-Hard Tissue Interfaces Regulates Immunophenotype of Mesenchymal Stem Cells. *Adv Funct Mater* **34**, 2309676 (2024).

34. Neelakantan, S. *et al.* Right ventricular stiffening and anisotropy alterations in pulmonary hypertension: Mechanisms and relations to function. *JAHA* **14**, 5 (2025).

35. Kah, D. *et al.* Contractility of striated muscle tissue increases with environmental stiffness according to a power-law relationship. *npj Biological Physics and Mechanics* **2**, 7 (2025).

36. Choi, Y. S. *et al.* The alignment and fusion assembly of adipose-derived stem cells on mechanically patterned matrices. *Biomaterials* **33**, 6943–6951 (2012).

37. Qazi, T. H. *et al.* Programming hydrogels to probe spatiotemporal cell biology. *Cell Stem Cell* **29**, 678–691 (2022).

38. Zhao, F. *et al.* Fibroblast alignment and matrix remodeling induced by a stiffness gradient in a skin-derived extracellular matrix hydrogel. *Acta Biomater* **182**, 67–80 (2024).

39. Moriyama, K. & Kidoaki, S. Cellular Durotaxis Revisited: Initial-Position-Dependent Determination of the Threshold Stiffness Gradient to Induce Durotaxis. *Langmuir* **35**, 7478–7486 (2019).

40. Yang, C., Tibbitt, M. W., Basta, L. & Anseth, K. S. Mechanical memory and dosing influence stem cell fate. *Nat Mater* **13**, 645–652 (2014).

41. Niether, D. & Wiegand, S. Thermophoresis of biological and biocompatible compounds in aqueous solution. *J Phys Condens Matter* **31**, 503003 (2019).

42. Vigolo, D. *et al.* Continuous Isotropic-Nematic Transition in Amyloid Fibril Suspensions Driven by Thermophoresis. *Sci Rep* **7**, 1211 (2017).

43. Saraswathibhatla, A., Indana, D. & Chaudhuri, O. Cell–extracellular matrix mechanotransduction in 3D. *Nat Rev Mol Cell Biol* **24**, 495–516 (2023).

44. Barber-Pérez, N. et al. Mechano-responsiveness of fibrillar adhesions on stiffness-gradient gels. J Cell Sci 133, jcs242909 (2020).

45. Hartman, C. D., Isenberg, B. C., Chua, S. G. & Wong, J. Y. Vascular smooth muscle cell durotaxis depends on extracellular matrix composition. Proc Natl Acad Sci 113, 11190–11195 (2016).

46. Lai, A. et al. Endothelial Response to the Combined Biomechanics of Vessel Stiffness and Shear Stress Is Regulated via Piezo1. ACS Appl Mater Interfaces 15, 59103–59116 (2023).

Chapter 7

Fluorescently labelled stiffness gradient hydrogels to probe cell-matrix interplay

In this chapter, a new strategy to fabricate stiffness gradient hydrogels using fluorescently labelled polymers is presented. Based on thermophoresis effects, the spatial fluorescence intensity across the resulting gradient gels directly reflects the local polymer concentration, thus providing a noninvasive yet quantifiable readout for stiffness characterization. Furthermore, linear stiffness gradients with comparable range and slope were fabricated using GelMA and Gellan gum, enabling direct comparisons of fibroblast stiffness responses across different hydrogel chemistries. Overall, the study highlights that under matching stiffness conditions, fibroblast cell mechanosensing is not only influenced by the surface ECM proteins, but also potentially by the underlying hydrogel chemistry.

Building on the approach of fluorescently labelled polymers in Chapter 4 and the modular platform in Chapter 6, this next exploratory study extended these experimental methods further to investigate cell-substrate interactions on thermophoretically fabricated stiffness gradient hydrogels. Specifically, I addressed whether the choice of hydrogel type or surface ECM protein coating would influence how cells respond to stiffness gradients. If this is true, the study would add to the growing notion in the field that “stiffness” alone is insufficient to explain cell-ECM mechanobiology, prompting further considerations to interpret cell mechanosensitivity to stiffness gradients in a broader, more holistic material context. In addition, by leveraging the interdependence between polymer concentration, fluorescence intensity, and hydrogel stiffness, I propose a fluorescence microscopy strategy for rapid validation and stiffness characterization of gradient hydrogels, potentially offering a more accessible alternative to specialized techniques such as atomic force microscopy for routine material assessment.

Graphical abstract of chapter:

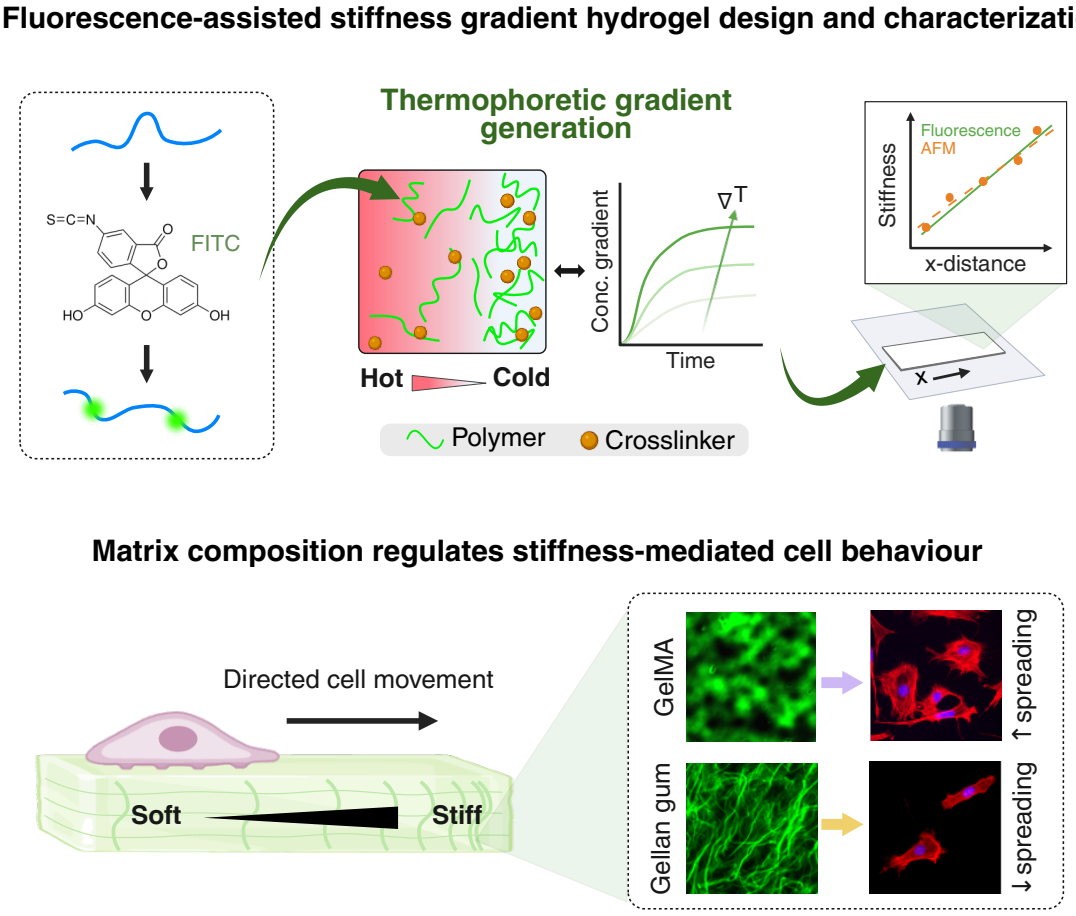

7.1 Introduction

Microengineered stiffness gradient hydrogels are valuable *in vitro* cell culture platforms for studying cell-ECM mechanobiology. Although the wide range of fabrication techniques developed in recent years has greatly improved the accessibility of stiffness gradient hydrogels to mimic distinct pathophysiological mechanical landscapes of native tissues, there are still critical challenges in the experimentation workflow that continue to limit their broad adoption in biological research.

These issues relate to the determination of the precise stiffness that cells encounter on the gradient materials. Typically, nanoindentation methods like atomic force microscopy (AFM) are needed to capture the local hydrogel stiffness on a similar scale at which cells probe their surrounding matrix through integrin-mediated interactions[1–7]. While AFM remains the mainstay technique for characterizing stiffness gradients, it presents numerous limitations. AFM measurements are cumbersome, low-throughput, and require specialized equipment and operator know-how that may not be readily available to every laboratory[8]. Furthermore, hydrogel stiffness characterization and biological assessment are generally performed on separate samples. Consequently, researchers rely on spatial position along the gradient gels as a reference to correlate substrate stiffness with cellular behaviors[6], leading to potential uncertainties in data interpretation. Additionally, undetected sample-to-sample variability in the stiffness gradient can compromise the reproducibility of biological experiments. Therefore, new solutions addressing these challenges are essential for enhancing the robustness of mechanobiological findings from gradient hydrogel studies and supporting the design of more predictive *in vitro* tissue models.

To that end, recent advances in the field have proposed the development of fluorescence-based strategies as an alternative to conventional AFM techniques for stiffness characterization. For example, a study demonstrated that the diffusion of fluorescein within a polyacrylamide precursor mix directly correlated with the resulting stiffness gradient, enabling fluorescence intensity to be used as an optical readout of local stiffness[9]. Although straightforward, this method can be extremely variable and is susceptible to photobleaching effects. In another approach, graded distribution of fluorescent microbeads within the hydrogel matrix was used to infer substrate stiffness from bead density[10,11]. Compared to freely diffusing fluorescein, the physically

immobilized microbeads provide a more stable, time-invariant proxy of the stiffness gradient. Importantly, however, these existing options do not provide a direct report of the hydrogel matrix architecture, potentially missing important information about their spatiotemporal changes on cellular mechano-responses. Nonetheless, these studies underscore the promise of fluorescence-based strategies for efficiently validating the stiffness gradient and *in situ* mapping of cell responses to the local substrate stiffness.

Here, we present a new strategy by which fluorescently labelled polymers enable direct visualization and quantification of stiffness gradient hydrogels in their native state. Specifically, fluorescein isothiocyanate (FITC) was chosen as the fluorescent probe due to its versatile conjugation chemistry, making it broadly applicable to both natural and synthetic hydrogel systems[12,13]. Using this approach, the fluorescence intensity accurately reflects the local polymer concentration, which also positively correlates with the hydrogel stiffness. The strategy uniquely offers a simultaneous means to assess the gradient gel morphology and uniformity.

Previously in **Chapter 4**, I demonstrated how these FITC-labelled polymers were valuable in enabling real-time monitoring of the thermophoretic gradient formation. This chapter focuses on establishing the feasibility of these FITC-labelled polymers in fabricating hydrogels for cell culture and the reliability of the resulting fluorescence signal for quantitative material characterization. As a continuation of the previous studies, I demonstrate the method based on the two hydrogel systems explored in this thesis: FITC-labelled GelMA (F-GM) and FITC-labelled Gellan gum (F-GG). In particular, two extremes of shallow and steep linear stiffness gradients were fabricated using F-GM, followed by the investigation of F-GM and F-GG gradient gels with matched stiffness range and slope despite their distinct chemistries.

This set of stiffness gradient hydrogel platforms enabled a direct comparative analysis of how stiffness range, gradient slope, and matrix composition collectively influence fibroblast cell-material interactions.

7.2 Experimental methods

This section contains additional methods that are specific to the experiments in this chapter, and should be read in conjunction with the general materials and methods presented in **Chapter 3**.

7.2.1 Microfluidic device design

This study utilizes the modular microfluidic system developed in **Chapter 6** for thermophoretic fabrication of stiffness gradient hydrogels. Specifically, a linear gradient configuration was employed by using two adjacent microchannels for water cooling and Joule heating. The sample microchamber was made by cutting out a specified area on a 120 μm-thick spacer (2 layers of 60 μm-thick Kapton tape, Multicomp Pro), which was then manually aligned with the gradient region. The imposed temperature ranges and gradient strengths were characterized using the rhodamine-B based fluorescence thermometry method, as described in **Chapter 4**.

7.2.2 AFM

AFM was used to characterize the Young's modulus of uniform stiffness hydrogels in Section 7.4, and to validate the stiffness gradient hydrogels in Section 7.6. Details of the AFM protocol can be found in Section 3.5.4.1.

7.2.3 Fluorescence-based stiffness mapping

By using fluorescently labeled polymers for hydrogel fabrication, it is possible to predict the Young's modulus of the stiffness gradient hydrogel based on the fluorescence signal measured using a confocal microscope. The core of the workflow consists of two main steps: 1) calibration curve generation and 2) intensity-stiffness correlation, as described below. All image processing and analysis procedures were performed using a customized MATLAB script.

Calibration curve generation

For each polymer system, calibration curves connecting the hydrogel concentration to the fluorescence intensity and AFM-measured stiffness were first generated. To do this, uniform F-GM and F-GG hydrogels were prepared at a series of concentrations. For each sample, 25 μm × 25 μm fluorescence images were taken at 5 random locations to calculate an averaged pixel intensity, followed by stiffness measurement by AFM. Separate concentration-intensity and concentration-stiffness plots were generated, then correlation equations were determined using simple linear regression. Note that in this study, the fluorescence intensity values were normalized by the intensity at 10 wt% for F-GM and 1 wt% for F-GG, chosen arbitrarily and defined as the reference concentration. This approach was implemented to account for variability in fluorescence readout between different imaging setups, meaning that the established calibration curve equations can be directly applied to subsequent experiments. It should also be noted that while the calibration curves in this study could be sufficiently described by a linear relationship, a different material system or concentration range might require a more complex fitting model; as such, it is recommended that users generate their own set of calibration curves according to the target design space.

Stiffness gradient hydrogel measurement

Stiffness analysis was performed by taking a single confocal plane image over the whole gradient region of the thermophoretically fabricated hydrogels. Each pixel intensity was normalized by a reference intensity value, defined as the absolute intensity at the reference polymer concentration (I_{ref}). Specifically, I_{ref} should be calculated for each sample image following the equation: $I_{ref} = \hat{I}_{img} / I_{N,ref}$, where $\hat{I}_{img}$ is the average intensity of the whole image, and $I_{N,ref}$ is the normalized intensity at the initial concentration (extracted from the concentration-intensity curve). This step works on the basis that $\hat{I}_{img}$ reflects the absolute intensity at the starting polymer concentration prior to thermophoretic gradient generation, due to mass conservation, as detailed in the previous section. Notably, this is a unique characteristic of the thermophoresis process, and which provides an internal reference point for calibration of each sample. After computing the normalized pixel intensity values, the distribution of the polymer concentration across the gradient region could be determined using the concentration-intensity correlation equation. Finally, the concentration values were

connected to the hydrogel stiffness using the concentration-stiffness correlation equation, yielding a heat map for each stiffness gradient.

The performance of this stiffness mapping method was evaluated in Section 7.7 and benchmarked against standard AFM measurements. Once validated, the fluorescence-based tool was deployed for characterizing the stiffness gradient samples used in cell culture experiments (Section 7.8, 7.9).

7.2.4 SEM

For each uniform sample or stiffness segment (“soft”, “Mid”, “Stiff”) along the gradient hydrogel, pore size distribution was evaluated from three randomly sampled areas with at least n = 80 and n = 230 pores for F-GM and F-GG samples, respectively.

7.2.5 Confocal imaging

Fluorescent images were taken using a Nikon Ti2 confocal microscope at 60x magnification. Hydrogels were usually imaged directly on the coverslips to which they were fabricated, with a drop of PBS added to prevent sample dehydration during experiments. For longer term storage, hydrogel samples were fixed in 4% PFA for 1 h, washed in Milli-Q water, and mounted onto a glass slide using Fluoromount-G. The mounted samples were stored at 4 °C and remained viable for at least 3 months.

7.2.6 Fibronectin coating and visualization

In Section 7.9, a study was performed to investigate the effect of fibronectin coating on cell responses to stiffness gradients. For these experiments, fabricated F-GG and F-GM gradient gels were functionalized using carbodiimide reactions. First, the hydrogel samples were washed (2 × 5 min) with 50 mM MES buffer at pH = 5.5 to prepare the surface for activation. The buffer was aspirated, then the hydrogels were

incubated with 100 mM EDC and 200 mM NHS in MES buffer at room temperature for 30 min. Following that, the gels were rinsed twice with PBS to remove unreacted functionalities and immediately incubated with 100 μg mL^{-1} fibronectin in PBS at 37 °C for 2 h. Finally, the fibronectin solution was removed, and the gels were washed (2 × 5 min) with PBS to remove non-specifically adsorbed fibronectin. The coated gel samples were kept immersed in PBS overnight at 4 °C before UV sterilization and cell seeding.

To characterize fibronectin distribution along stiffness gradients, the coated hydrogel samples were blocked for 1 h in 1 wt% BSA at room temperature, then incubated with a rabbit monoclonal anti-fibronectin antibody (ab26820, Abcam, 1:50 dilution) at room temperature for 1 h, followed by secondary goat anti-rabbit IgG antibody (Alexa Fluor 568, A11036, Invitrogen, 1:500 dilution) at room temperature for 30 min.

7.2.7 Cell culture and analysis

With the exception of the preliminary biological validation presented in Section 7.5 and the control group for the data reported in Figure 7.13, all other cell culture experiments in this chapter were performed under serum-starved conditions to suppress cell proliferation. To this end, 3T3-L1 fibroblast cells were prepared in fully supplemented DMEM media in T-25 flasks to 40-50% confluence. One day before the experiment, the cells were washed with warm DPBS and maintained in starvation media (DMEM containing high glucose and pyruvate supplemented with 1% FBS, 100 U mL^{-1} penicillin and 100 μg mL^{-1} streptomycin). The cells are harvested using TrypLE Express following standard procedure and immediately used for cell seeding within 12-15 h after incubation in starvation media. Cells were maintained in starvation media throughout the experiment. Cell attachment was measured 2 h after seeding, whereas cell migration was assessed after 24 h.

7.3 Development of FITC-labelled GelMA and Gellan gum

Besides giving a direct quantification of thermophoresis as shown in **Chapter 4**, the primary hypothesis in this study is that FITC-labelled stiffness gradient hydrogels can be used for simultaneous structural visualization and stiffness characterization via fluorescence visualization, while maintaining biocompatibility as cell culture substrates.

Toward that goal, a generalizable strategy was developed based on covalent attachment of FITC fluorophores directly onto the hydrogel polymer backbone. FITC was chosen due to its low cost, accessibility, and the established reactivity of its isothiocyanate group (–N=C=S) to form stable bonds with primary amines ($–NH_2$) or hydroxyl (–OH) groups, both of which are commonly found across both natural and synthetic polymers. Specifically, FITC conjugation occurred via amine residues in GelMA (**Figure 7.1a**) and hydroxyl groups in Gellan gum (**Figure 7.1b**). Unbound FITC molecules were removed through dialysis after the labelling procedure, which was important to ensure that the fluorescence signals originate specifically from the labelled polymers. In both cases of F-GM and F-GG, the final product was a yellow fibrous foam with a yield of ~85% and ~65% by weight, respectively (**Figure 7.3a, 7.3b**). Details of the FITC labelling procedure are found in Section 3.5.1.

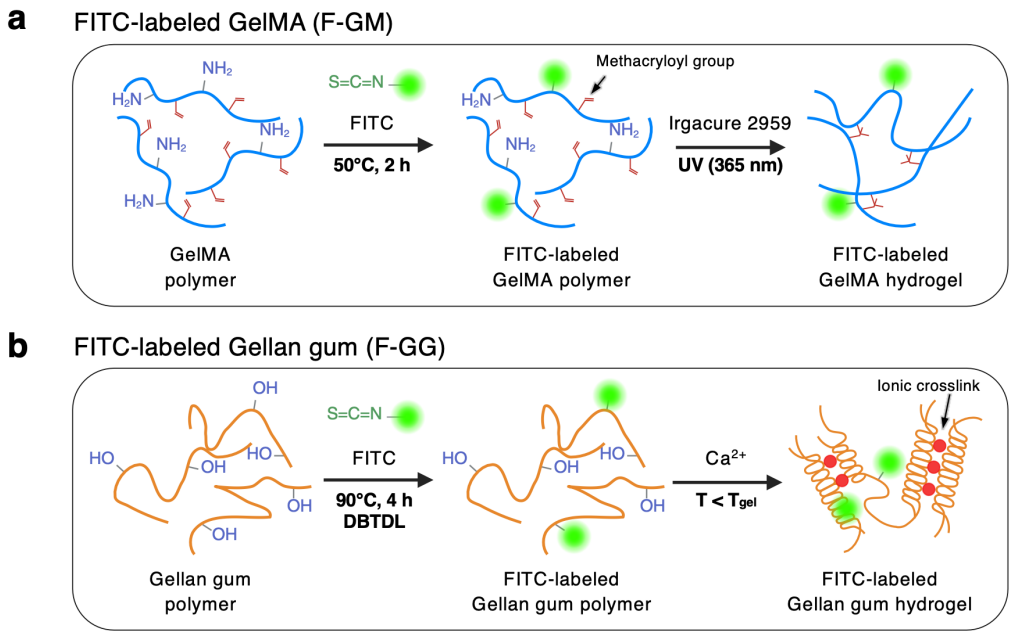

Figure 7.1: Graphical illustration of the synthesis and formation of FITC-labelled (a) GelMA and (b) Gellan gum hydrogels.

Importantly, the FITC labelling protocol was carefully optimized to ensure robust fluorescence signals without compromising the hydrogel crosslinking efficiency. Low labelling efficiencies were adopted to minimize potential disruptive effects from steric hinderance or excessive hydrophobic interactions. Quantitative assessment of the substituted FITC content was performed by measuring the fluorescence intensity of polymer solutions (~50 μg mL^{-1}; prepared in Milli-Q water) against a standard curve. The degree of substitution for F-GM was ~0.07 per lysine residue (**Figure 7.2a**). However, as the previous study did not report this value[13], a direct comparison is not possible at this stage. On the other hand, the degree of substitution for F-GG was ~0.007 per repeating tetrasaccharide unit (**Figure 7.2b**), which was within the typical range reported for FITC-labelled polysaccharides[12,14,15].

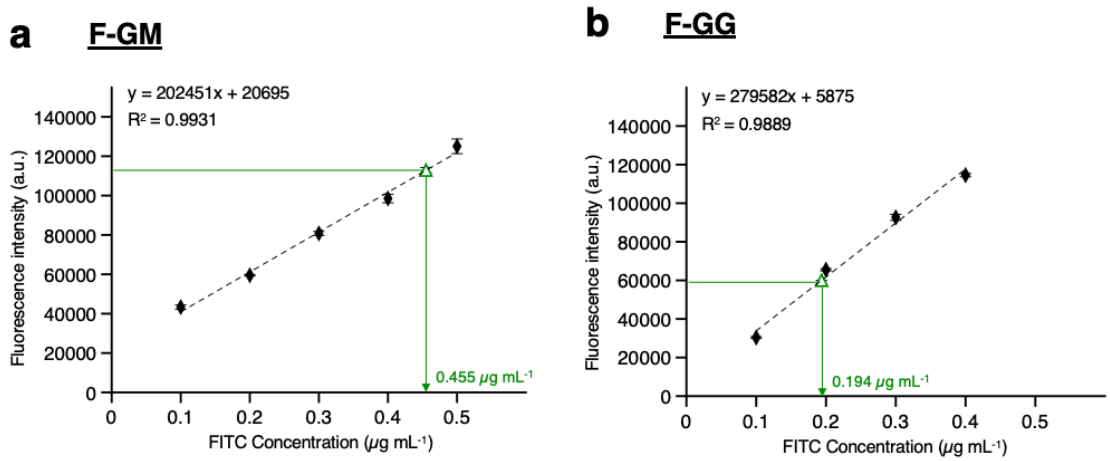

Figure 7.2: The degree of FITC substitution in the resulting (a) F-GM and (b) F-GG polymers was characterized using a microplate reader at an excitation wavelength of 483/14 nm and emission wavelength of 530/30 nm (n = 3 independent samples; mean ± SEM). Water was used as a blank control.

Figure 7.3c shows a uniform stiffness hydrogel fabricated using 10 wt% F-GM with 0.1 wt% Irgacure 2959 as photoinitiator, whereas **Figure 7.3d** shows a gel fabricated using 1 wt% F-GG with 5 mM $CaCl_2$ as ionic crosslinkers. It was observed that both F-GM and F-GG retained their crosslinking capacities under standard crosslinking procedures (**Figure 7.1**), yielding hydrogel constructs that were mechanically stable over at least 1 week in PBS. Additionally, the labelled hydrogels displayed stable fluorescence over the incubation period, as examined by comparing the fluorescence

intensity measured on day 1 and day 7 using fluorescence microscopy. Taken together, these findings support the use of the fluorescently labelled hydrogels for *in vitro* cell culture, while validating the potential of fluorescence signal from FITC-bound polymer as a stable, material-intrinsic readout.

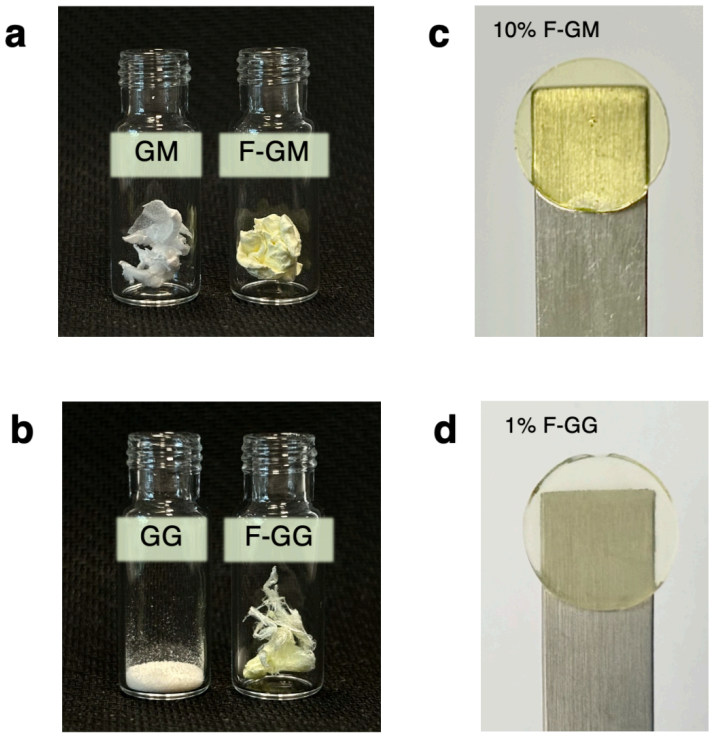

Figure 7.3: (a) Photograph of lyophilized GelMA before and after fluorescent labelling. (b) Photograph of Gellan gum powder as received commercially and the lyophilized form after fluorescent labelling. (c) Hydrogels were formed by standard photopolymerization for F-GM and (d) ionic crosslinking for F-GG.

7.4 Fluorescence microscopic visualization and characterization of hydrogels

To examine the relationship between polymer concentration, hydrogel stiffness and matrix structure, we first fabricated two sets of uniform hydrogels using different F-GM and F-GG concentrations, as summarized in **Figure 7.4**. Since our thermophoretic fabrication technique generates stiffness gradients through spatial variations in polymer concentration, these characterization experiments provide critical calibration parameters for subsequent gradient hydrogel design as well as the development of a fluorescence-based stiffness characterization tool. Importantly, the investigation of pore size alongside stiffness would facilitate a more comprehensive understanding of the material property landscape, enabling us to better contextualize the cellular responses on our gradient hydrogel systems.

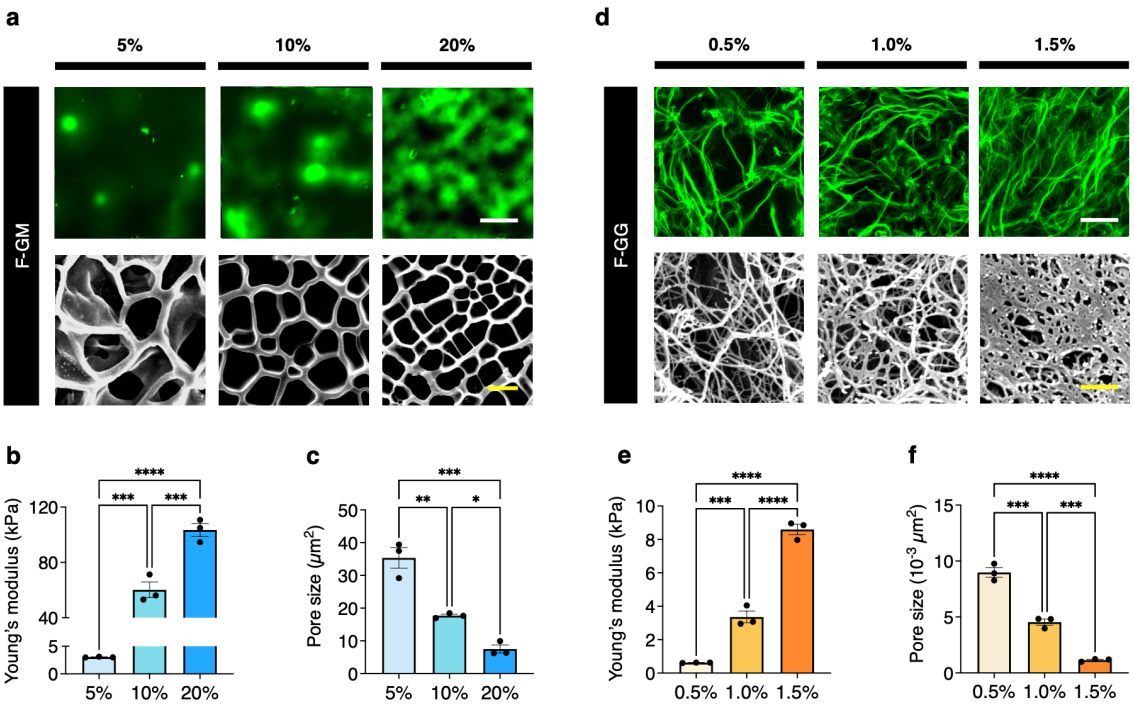

Figure 7.4: (a) Representative confocal (top) and SEM (bottom) images of F-GM hydrogels prepared at varied concentrations (5 wt%, 10 wt%, 20 wt%). Scale bar: 25 μm (confocal), 5 μm (SEM). The corresponding hydrogel Young's modulus and pore size are shown in (b) and (c), respectively (n = 3 independent samples; mean ± SEM). (d) Representative confocal (top) and SEM (bottom) images of F-GG hydrogels prepared at varied concentrations (0.5 wt%, 1.0 wt%, 1.5 wt%). Scale bar: 25 μm (confocal), 5 μm (SEM). The corresponding hydrogel Young's modulus and pore size are shown in (e) and (f), respectively (n = 3 independent samples; mean ± SEM). All pore size quantification was performed on SEM images.

To ensure consistency with subsequent gradient gels, the uniform stiffness hydrogels were fabricated on the thermophoresis platform but without application of thermal gradients. The thickness of hydrogel samples was kept constant at ~120 μm throughout the study.

Overall, an increase in polymer concentration resulted in a corresponding increase in substrate stiffness, as characterized by the AFM-based Young's modulus (**Figure 7.4b**, **7.4e**). Moreover, SEM analysis revealed that higher concentrations also led to a decrease in pore sizes (**Figure 7.4c**, **7.4f**), consistent with the denser polymer network formation (**Figure 7.4a**, **Figure 7.4d**).

Given the limitations of SEM techniques in providing a true representation of the hydrogel microarchitecture due to the need for prior sample dehydration[16], we initially hypothesized that fluorescent labelling of the polymers could offer a complementary method to observe the microarchitecture in a native, hydrated state for quantitative characterization. In this respect, confocal imaging of fluorescently labelled Gellan gum successfully revealed its fibrous polymer chains across different concentrations from 0.5 wt% to 1.5 wt% (**Figure 7.4d**; top row). Notably, confocal imaging clearly showed a sparser polymer network compared to that observed using SEM, suggesting considerable shrinkage and structural collapse during SEM sample preparation. Although preliminary, these results demonstrate the potential of fluorescence microscopic visualization techniques to more faithfully characterize the internal microstructure of hydrogels that govern much of their functional properties[17].

On the other hand, confocal imaging of fluorescently labelled GelMA revealed a more diffuse fluorescence signal, but generally resembled the porous structure observed using SEM (**Figure 7.4a**; top row). It is recognized that the spatial resolution using confocal microscopy was not sufficiently high for quantitative analysis of the pore sizes. However, as the polymer concentration was decreased from 20 wt% to 5 wt%, we observed a consistent increase in dark void regions, which was interpreted in terms of larger pore size. Here, it is also noted that our confocal images of F-GM hydrogels appeared to differ from the original study by Onofrillo et al.[13], which displayed a sheet-like morphology. However, from discussions with Dr Carmine Onofrillo (The University of Melbourne), it was concluded that this discrepancy most likely stemmed from differences in the sample preparation methods; in particular, their study was performed

on much thicker (2 mm) hydrogel constructs and the samples were cryo-sectioned prior to imaging. This contrasts with our approach, whereby the hydrogels were imaged immersed in liquid directly after fabrication. Therefore, while the microarchitecture of fluorescently labelled GelMA hydrogels was not optically resolved to render them useful for quantitative analysis at this stage, the qualitative differences in fluorescence patterns can still provide valuable insights into the native-state polymer distribution and gel uniformity.

Next, we assessed the correlation between fluorescence intensity and the AFM-defined Young's modulus. To do this, the concentration-stiffness data (F-GM: **Figure 7.4b**; F-GG: **Figure 7.4e**) were combined with the concentration-intensity data (F-GM: **Figure 4.8a**; F-GG: **Figure 4.9a**) for each specific material. Indeed, the analyses demonstrated that the substrate stiffness correlated positively to the fluorescence intensity in both cases of F-GM (**Figure 7.5a**) and F-GG (**Figure 7.5b**).

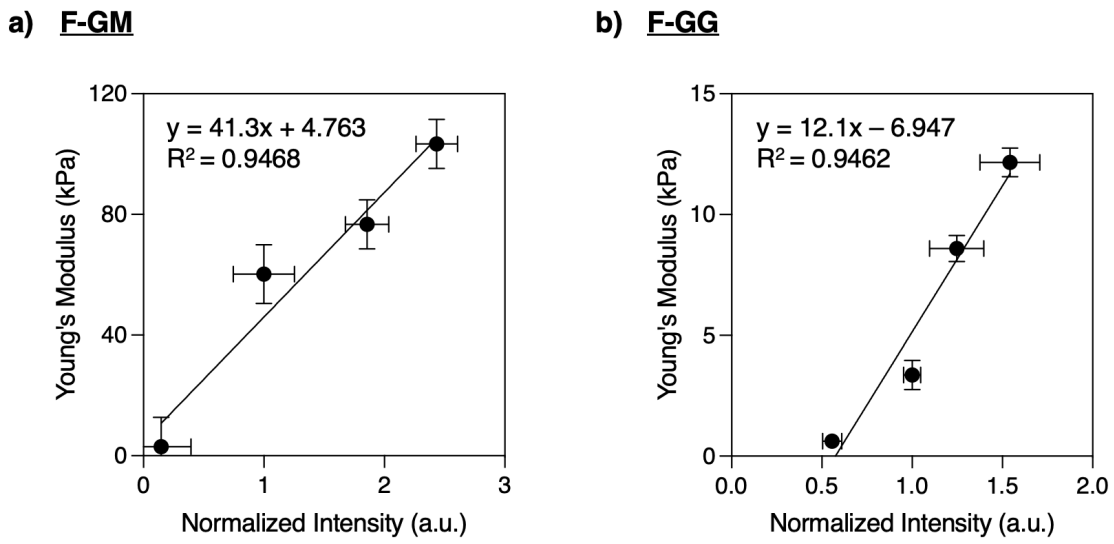

Figure 7.5: (a) Correlation curve of AFM-measured Young's modulus and fluorescence intensity of F-GM hydrogels with polymer concentrations ranging from 5 wt% to 20 wt%. The fluorescence intensity values were normalized to the intensity at 10 wt% polymer concentration. (b) Correlation curve of AFM-measured Young's modulus and fluorescence intensity of F-GG hydrogels with polymer concentrations ranging from 0.5 wt% to 2.0 wt%. The fluorescence intensity values were normalized to the intensity at 1 wt% polymer concentration. Data reported as mean ± standard deviation of n=3 independent experiments.

Once the correlation curve was generated from a set of uniform stiffness samples, it can be used to map the spatial stiffness changes of gradient hydrogels based on fluorescence images taken over the gradient region. In this study, the measured fluorescence intensity values were calibrated by the average intensity across the whole gel, which should correspond to the initial concentration of the polymer solution prepared. This leveraged the fact that thermophoresis simply leads to the redistribution of polymer chains within the confined sample volume (i.e., the total polymer content remains unchanged throughout the gradient gel fabrication process), thus providing an internal reference point for calibration and removing the need to separately characterize a uniform gel every time. However, it should be emphasized that this assumption is only valid provided that no evaporation occurs from the sample volume, highlighting the need to ensure a tight seal of the microchamber.

Finally, to evaluate the effect of FITC labelling on hydrogel properties, an additional analysis was performed by comparing the labelled and unmodified formulations of both GelMA and Gellan gum, keeping all other fabrication parameters constant. The results confirmed that the addition of FITC did not affect the mechanical and structural properties of GelMA (**Figure 7.6a**). In contrast, FITC-labelled Gellan gum exhibited drastically lower stiffness and larger pore size, which was also reflected by a lower crosslinking density as evident from the SEM images (**Figure 7.6b**). Changes in Gellan gum properties following FITC labelling were also reported in the reference study by Cho et al.[12]. However, their observations of altered pore size but not stiffness across unlabelled and labelled Gellan gum hydrogels (prepared at the same polymer concentration) raise some questions that warrant further scrutiny. The altered properties of F-GG hydrogels in this study were likely due to excessive FITC labelling, despite multiple optimization batches. Presumably, these effects were due to steric hindrance from the additional FITC molecules which introduce bulky aromatic moieties onto the polymer backbone, and thus, limit close packing of Gellan coils in the 3D network. Nevertheless, the resulting F-GG polymers still supported repeatable hydrogel formation that retained structural integrity as well as stable fluorescence signal under cell culture conditions. This also suggests that FITC conjugation did not directly interfere with hydrogen bonding (within or between Gellan helices) or ionic crosslinking (between carboxylate groups from neighboring helices) during the gelation process, which may otherwise prevent hydrogel formation altogether. Thus,

although the F-GG hydrogels were softer than the unlabelled counterpart, their material characteristics remained consistent between experiments, allowing us to proceed with the current protocol for subsequent experiments (noting that this could be further optimized if necessary for future applications).

Importantly, the results in this section further support the hypothesis that the fluorescently labelled hydrogel approach can provide a complementary, non-invasive means for hydrogel characterization.

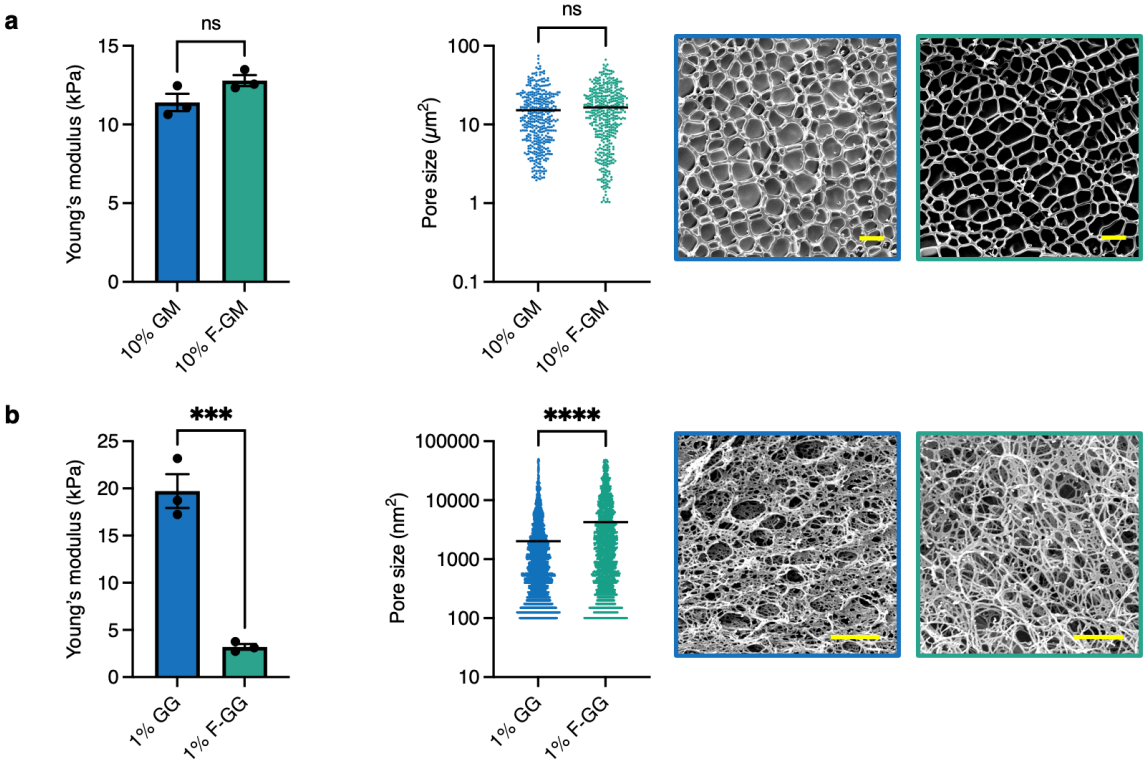

Figure 7.6: (a) AFM stiffness and SEM pore size characterization of 10 wt% GelMA hydrogels made using unmodified polymer (blue) or FITC-labelled polymer (green). Scale bars: 10 μm. (b) AFM stiffness and SEM pore size characterization of 1 wt% Gellan gum hydrogels made using unmodified polymer (blue) or FITC-labelled polymer (green). Scale bars: 1 μm. Young's modulus data are shown as mean ± SEM of n = 3 independent samples. Quantification of pore size is the mean of n = 3 independent samples, where each point depicts an individual pore analyzed. Note that the stiffness of GelMA samples is overall lower than that reported in Figure 7.4 due to a different UV exposure settings used in these preliminary experiments.

7.5 Preliminary biological validation

This section summarizes two key preliminary cell studies designed to establish the biocompatibility of the developed FITC-labelled hydrogels as cell culture substrates. Firstly, we used the F-GM system to assess possible cytotoxic effects from the FITC fluorophores. In the case of F-GG, the main challenge was related to the lack of cell binding sites. These bioactive cues are essential for enabling initial cell adhesion, spreading, and signaling, all of which are important to support proper cell function and behavior. As such, the focus was on identifying suitable protein coating strategies to allow for cell attachment.

7.5.1 F-GM: Effect of FITC labelling on cell growth

A series of uniform stiffness hydrogels were prepared using varying blend ratios of unmodified GelMA (GM) to FITC-labelled GelMA (F-GM). Subsequently, 3T3-L1 fibroblast cells and human umbilical vein endothelial cells (HUVECs) were seeded (~20000 cells cm^{-2}) on the substrates to assess their initial attachment and proliferation behaviors. As shown in **Figure 7.7**, all hydrogel formulations equally strongly supported cell attachment and spreading, indicating that the polymer-bound FITC fluorophores were stable and did not adversely affect the hydrogel biocompatibility. The fact that consistent results were observed across both cell types also suggests that FITC-labelling did not introduce cell-type specific effects, highlighting the potential broad utility of our fluorescently labelled hydrogel system for cell culture.

As a continuation of the cell study in **Chapter 6**, we selected the 3T3-L1 cell line for further experiments in this study, employing fully labelled hydrogel formulations to ensure maximum fluorescence signal for downstream analysis.

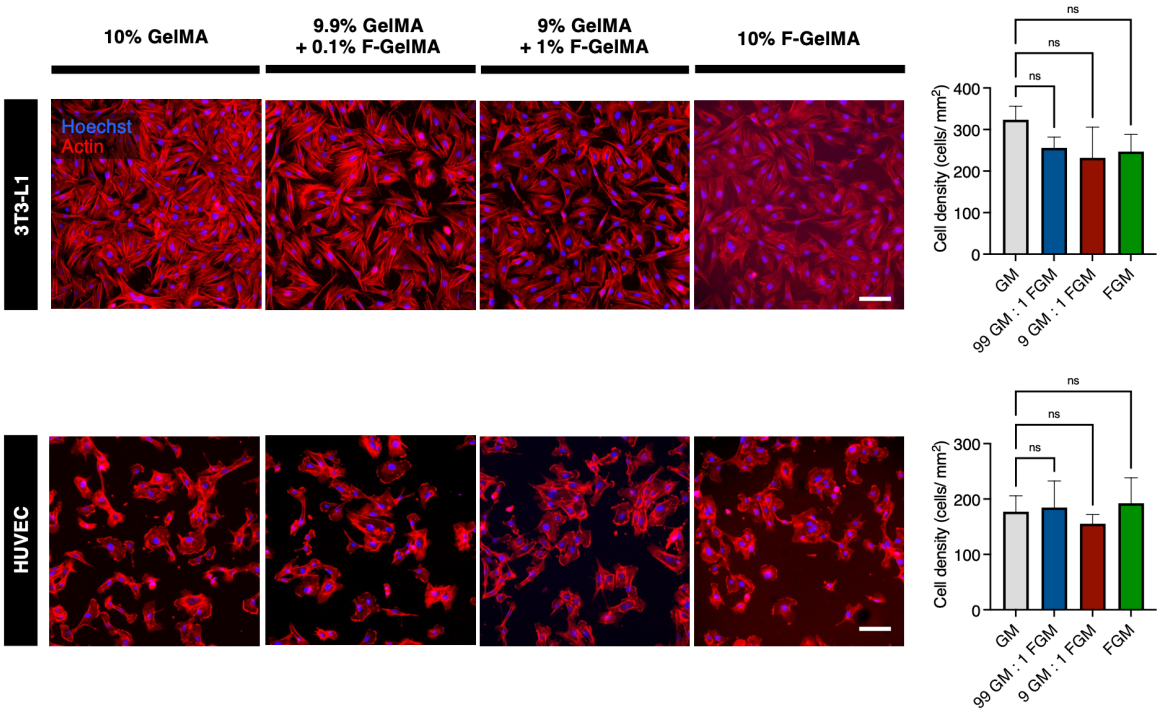

Figure 7.7: Representative fluorescence images and quantification of cell density of human umbilical vein endothelial cells (HUVECs) (top) and 3T3-L1 fibroblast cells (bottom) at 4 h after seeding on uniform stiffness GelMA hydrogels prepared using varying ratio of unlabelled polymer to FITC-labelled polymer. The total polymer concentration was kept constant at 10 wt% in all cases. Scale bars: 200 μm. The bars indicate mean ± SEM of n = 3 independent samples. The hydrogel matrix was not visualized in these images.

7.5.2 F-GG: Protein coating strategies for cell adhesion

In order to promote cell adhesion onto the Gellan gum hydrogels, two main strategies were explored: 1) non-specific protein adsorption, and 2) chemical conjugation of ECM proteins. Initially, we treated the fabricated F-GG hydrogels by incubating them in supplemented culture media or pure FBS solution prior to cell seeding[18,19]. While we previously found this approach adequate to induce adhesion and spreading of pre-osteoblast cells[5], this was not the case with fibroblast cells in this study, presumably due to the presence of FITC molecules which affected protein interactions and adsorption on the hydrogel surface. Instead of spreading, cells tended to aggregate into clusters over time, which were also easily washed away during media exchange (**Figure 7.8**; top row). This issue was subsequently overcome by covalent attachment of fibronectin, mediated via EDC/NHS chemistry[20] (see detailed protocol in Section

7.2.6). Overall, the F-GG hydrogels remained stable when subjected to the additional chemical processing steps and showed no considerable changes across the reaction pH range of 5-6. As shown in **Figure 7.8** (bottom row), the fibronectin-coated F-GG hydrogels were able to support cell attachment and subsequent spreading over 24 h, noting however that the cells displayed a rounder morphology compared to the GelMA-based substrates.

For further investigations, the concentration of fibronectin coating solution was increased from 50 µg mL^{-1} to 100 µg mL^{-1}, which was still within the typical range reported in literature and was found to better support healthy cell growth without undermining the gradient hydrogel properties.

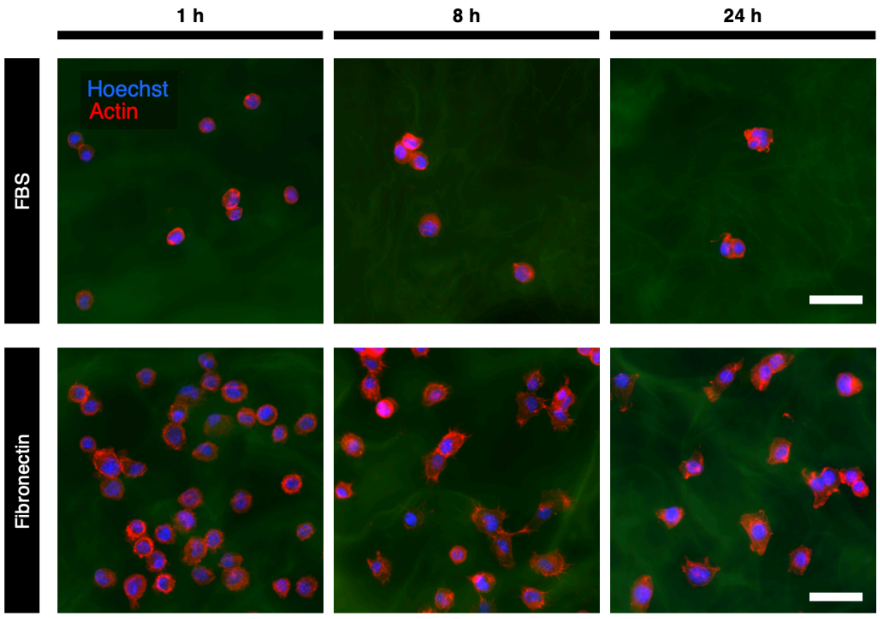

Figure 7.8: Representative fluorescent images of 3T3-L1 fibroblast cells over 24 h culture on uniform stiffness 1 wt% F-GG hydrogels pre-treated with FBS (top) and fibronectin (50 µg ml^{-1}) coating (bottom). Scale bars: 50 µm.

7.6 Thermophoretic fabrication of fluorescently labelled linear stiffness gradient hydrogels

Our previous observation of fibroblasts preferentially accumulating toward softer environments on a stiffness gradient (**Chapter 6**), in contrast to studies in the literature reporting durotaxis from soft to stiff substrates, prompted us to further investigate whether this behavior reflected cellular responses to the presence of a gradient stiffness or the absolute stiffness values themselves. Moreover, given the varied mechano-responses observed across studies employing different hydrogel systems, we hypothesized that the broader matrix properties beyond "stiffness" might effectively alter how cells interpret the underlying stiffness gradients. Taken together, this led us to systematically compare fibroblast behaviors across our two distinct gradient hydrogel platforms (GelMA and Gellan gum) with the aim of better understanding how ligand presentation might explain these divergent cellular mechano-responses and potentially reconcile the contradictory findings.

To do this, we employed the modular thermophoresis fabrication platform described in **Chapter 6** and produced linear stiffness gradients using fluorescently labelled GelMA and Gellan gum. The stepwise fabrication procedure is summarized in **Figure 7.9**.

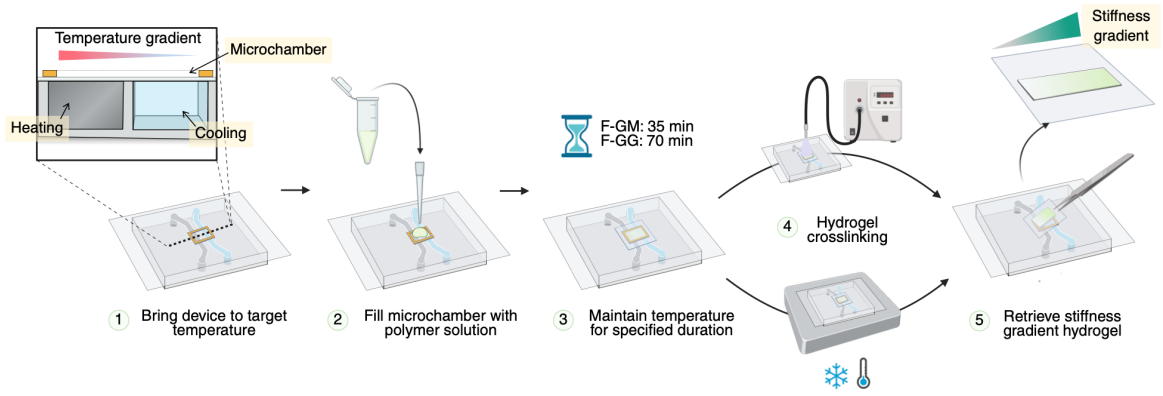

Figure 7.9: Illustration of the stepwise procedure for thermophoretic fabrication of linear stiffness gradient F-GM and F-GG hydrogels. 1, 2) The hydrogel precursor solution was added to an external microchamber mounted on a thermal microfluidic device. 3) The microchamber was sealed using a chemically functionalized coverslip and a uniform temperature gradient was applied for 35 min (F-GM) or 70 min (F-GG), allowing for thermophoresis-driven redistribution of precursors. 4) This created a concentration gradient in the solution that directly translated into a stiffness gradient upon crosslinking. 5) The finished stiffness gradient hydrogel was removed from the microchamber which completes the fabrication process.

As further illustrated in **Figure 7.10**, a thermal microfluidic module configured with a pair of heating and cooling channels side-by-side was used to pattern linear gradients over d~1000 µm. The operational parameters were informed based on the thermophoresis characterization experiments described in Section 4.3 and were kept consistent throughout the study (**Table 7.1**).

Stiffness gradients with different slope profiles were produced in F-GM hydrogels using 5 wt% (softer, narrow gradient) or 10 wt% (stiffer, wide-range gradient) initial polymer concentration. Meanwhile, gradient F-GG hydrogels were produced using 1 wt% initial polymer concentration, which was intended to match the softer range gradient of the F-GM samples.

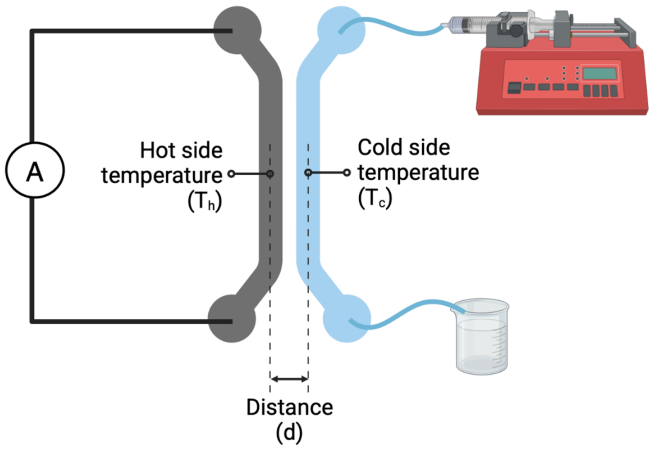

Figure 7.10: Schematic of the thermal microfluidic system comprising a pair of Joule heating and water-cooling channels used to create a controlled linear temperature gradient across the microsystem. The Joule heater was operated using a power supply unit with controlled DC current, whereas the water flow rate was set using a syringe pump.

Table 7.1: Summary of operational parameters used for gradient hydrogel fabrication. With reference to Figure 7.10, the temperature range was defined as (T_h-T_c) while the corresponding temperature gradient was evaluated by [(T_h-T_c) / d].

Hydrogel type	Water Flowrate [uL min^{-1}]	Controlled current [A]	Temperature gradient [°C mm^{-1}]	Temperature range [°C]	Process time [min]
F-GM	100	1.0	9	~55-65	35
F-GG	90	1.1	15	~55-75	70

7.7 Fluorescence-assisted stiffness gradient characterization

Figure 7.11 shows a summary of the stiffness profile and pore size distribution of the resulting gradient hydrogels. Using the thermophoretic technique, we consistently observed a gradient of fluorescence intensity which also coincided with the linear region of the applied temperature gradient (**Figure 7.11a**, **7.11b**, **7.11c**). Additionally, SEM analyses revealed that brighter regions of the gels corresponded to a smaller pore size (**Figure 7.11g**, **7.11h**, **7.11i**). Together, the findings support the hypothesis that the measured fluorescence signal reflects the local polymer concentration, and thus, can be used as an indicator of substrate stiffness.

In the thermophoretically fabricated gradient gels, the measured fluorescence intensity gradient means a gradient in polymer concentration; since concentration is directly linked to the hydrogel stiffness, the fluorescence gradient also indicates the presence of a stiffness gradient.

To examine the accuracy and precision of the fluorescence-based stiffness characterization method, we first performed fluorescence imaging of a gradient gel sample and estimated the stiffness using the established calibration curve, then performed AFM indentation measurements on the same sample for direct comparison (**Figure 7.11d**, **7.11e**, **7.11f**) A summary of the results is provided in **Table 7.2**.

Table 7.2: Summary table comparing the stiffness gradient properties obtained using the fluorescence-based method and AFM. Data presented as mean ± SEM of n=3 independent samples.

Gradient hydrogel	Stiffness range [kPa]		Gradient slope [kPa mm^{-1}]	
	Fluorescence	AFM	Fluorescence	AFM
10% F-GM	Low: 44 ± 7 High: 106 ± 3	Low: 42 ± 5 High: 137 ± 20	~87	~108
5% F-GM	Low: 7 ± 1 High: 18 ± 1	Low: 6 ± 1 High: 15 ± 2	~14	~10
1% F-GG	Low: 3 ± 1 High: 12 ± 1	Low: 4 ± 1 High: 11 ± 2	~9	~8

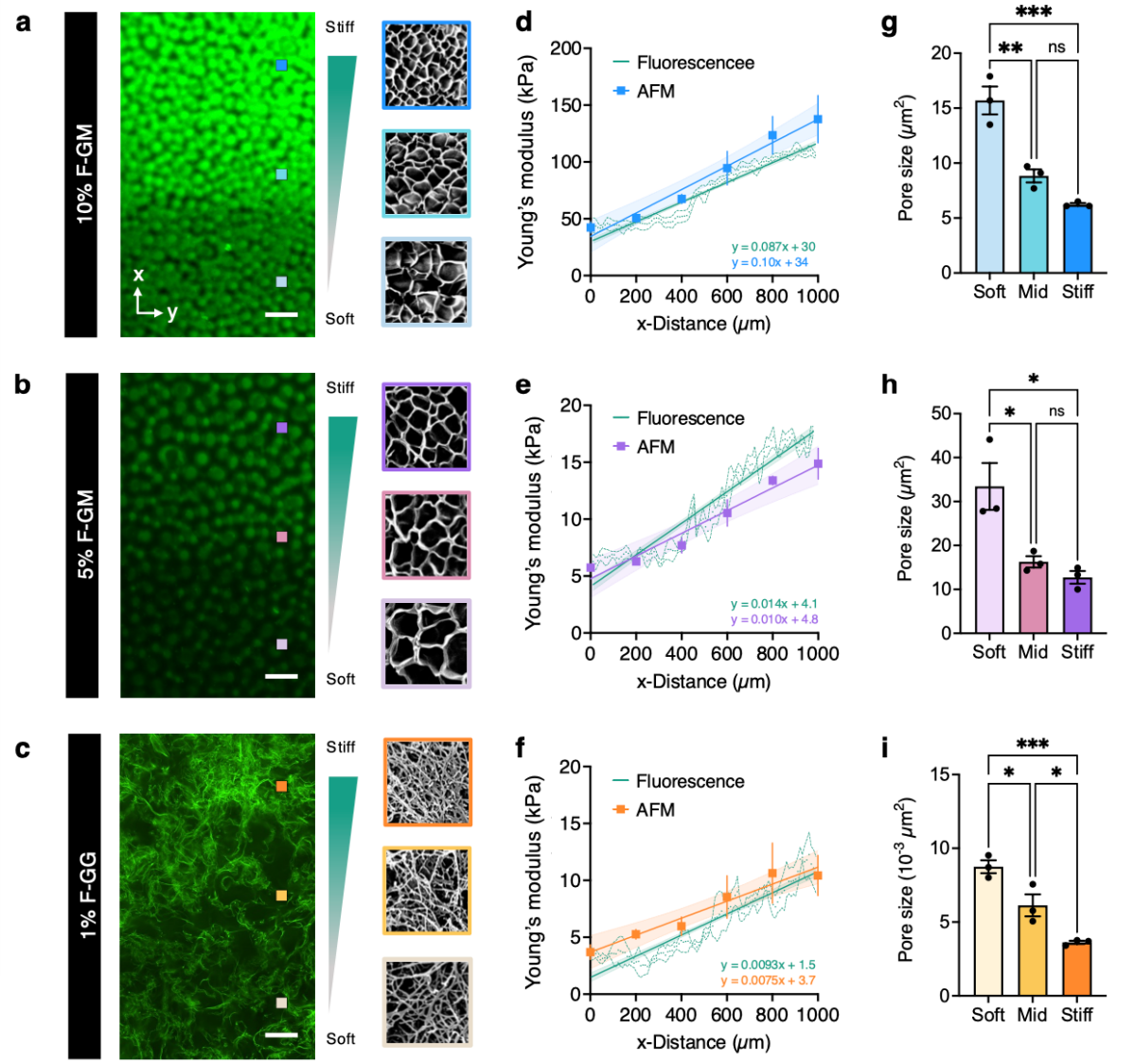

Figure 7.11: Representative fluorescent images of gradient gels fabricated using (a) 10 wt% F-GM, (b) 5 wt% F-GM, and (c) 1 wt% F-GG polymer systems. Scale bars: 100 μm. Colored squares indicate the approximate locations where SEM images were acquired, corresponding to stiff (top), moderately stiff (middle), and soft (bottom) regions of the gradient gels. Each SEM micrograph is 25 × 25 μm for F-GM samples and 2 × 2 μm for F-GG samples. The change in Young's modulus of the gradient gels was measured by AFM nanoindentation and fluorescence mapping, yielding (d) steep gradient F-GM, (e) shallow gradient F-GM, and (f) shallow gradient F-GG hydrogels (n = 3 independent samples; mean ± SEM). Solid lines are simple linear regression plots with 95% confidence intervals shaded accordingly. Corresponding quantification of the pore size showed an inverse correlation with stiffness for (g) steep gradient F-GM, (h) shallow gradient F-GM, and (i) shallow gradient F-GG hydrogels (n = 3 independent samples; mean ± SEM).

Overall, the fluorescence imaging technique showed a stiffness range and slope comparable to the gold standard AFM technique. Yet, the latter required a much longer time for sample measurement and data analysis (approximately 30 min vs. 60 min per sample). It is worth highlighting that while the fluorescence technique was demonstrated here using confocal microscopy, we found that the intensity-stiffness correlation would still hold based on images acquired using standard wide-field fluorescence microscopy (**Figure 7.12**). Notably, widefield fluorescence microscopy offers an even faster and simpler assessment. However, precautions must be considered for reduced spatial stiffness accuracy due to non-uniform hydrogel thickness or out-of-focus light.

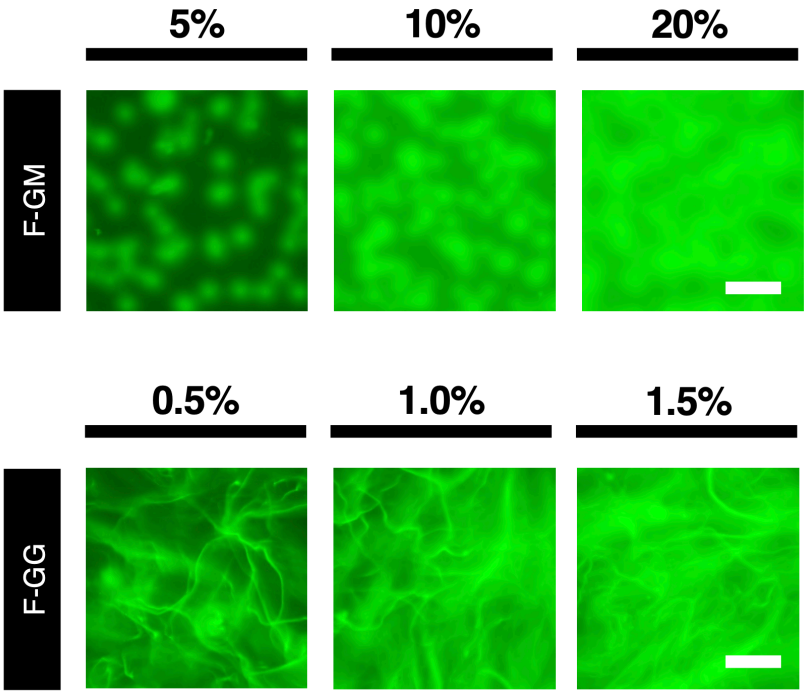

Figure 7.12: Representative fluorescent images of uniform stiffness F-GM (top) and F-GG (bottom) hydrogels fabricated using different polymer concentrations. Images captured using a standard widefield fluorescence microscope. Scale bars: 50 μm.

A key benefit of the fluorescently labelled gradient hydrogels is that they enable rapid validation of the resulting stiffness gradient quality. For example, when fabricating multiple samples for replicate experiments, users can visually inspect the gradient gels under a fluorescence microscope to identify aberrant gradient formation, in which case the gels should be excluded from cell studies. Furthermore, conventional AFM indentation techniques can potentially damage the delicate hydrogels. Fluorescently

labelled gels avoid such risk by enabling non-invasive characterization, thus preserving the same samples for subsequent cell culture. More importantly, the fluorescence signal provides an *in situ* means to spatially correlate the local hydrogel properties with the observed cellular responses. In future studies, this feature can be very valuable for assessing cell-substrate interactions at multiple time points on the same substrate, where the hydrogel properties may change due to cellular matrix remodeling or hydrogel degradation.

In all, the proposed fluorescence-based approach has great potential to enhance the reliability of gradient hydrogels for studying complex cell-substrate interactions in mechanobiology research, as they can be generalized across different stiffness patterns and hydrogel types.

7.8 Fibroblasts migrate toward an optimal stiffness range

To determine the role of stiffness range and gradient slope on fibroblast proliferation and migration, cells were cultured on linear stiffness gradient F-GM hydrogels with two distinct gradient profiles, including a shallow gradient spanning lower stiffness values (~7-18 kPa, ~14 kPa mm^{-1}) and a steeper gradient across higher stiffness range (~44-106 kPa; ~87 kPa mm^{-1}). The fabricated F-GM hydrogels were used directly for cell culture without additional ECM coating.

In this chapter, cell analyses were performed by dividing the immunofluorescence images of the gradient hydrogel samples into three equally sized segments, representing “soft”, “mid”, and “stiff” zones along the gradient of stiffness. Cell density results were discussed in terms of relative values normalized to the density on the corresponding “soft” zone of each gel. For reference, the raw cell density data is also supplemented in the corresponding results section.

After 24 h in standard culture conditions, cells clearly showed a biased distribution toward the stiffer regions on the shallow gradient (**Figure 7.13**; 5% F-GM, normal media). However, on the steeper gradient, higher cell densities were observed toward the softer regions of the substrate (**Figure 7.13**; 10% F-GM, normal media).

To examine whether the cell distribution patterns resulted from directed migration or differential stiffness-induced proliferation, a parallel set of experiments was performed using fibroblast cells that were serum-starved for 12-15 h prior to cell seeding. This strategy is commonly reported in literature to suppress cell division[21,22]. After 24 h of culture, overall, the cell densities were lower across all gradient gels, but the same trend in cell distribution was observed (**Figure 7.13**; starvation media).

In all, the results suggest that the biased cell distributions are indicative of directed migration in response to stiffness gradients. With a focus on understanding cellular migration behaviors, subsequent studies were performed under cell starvation conditions.

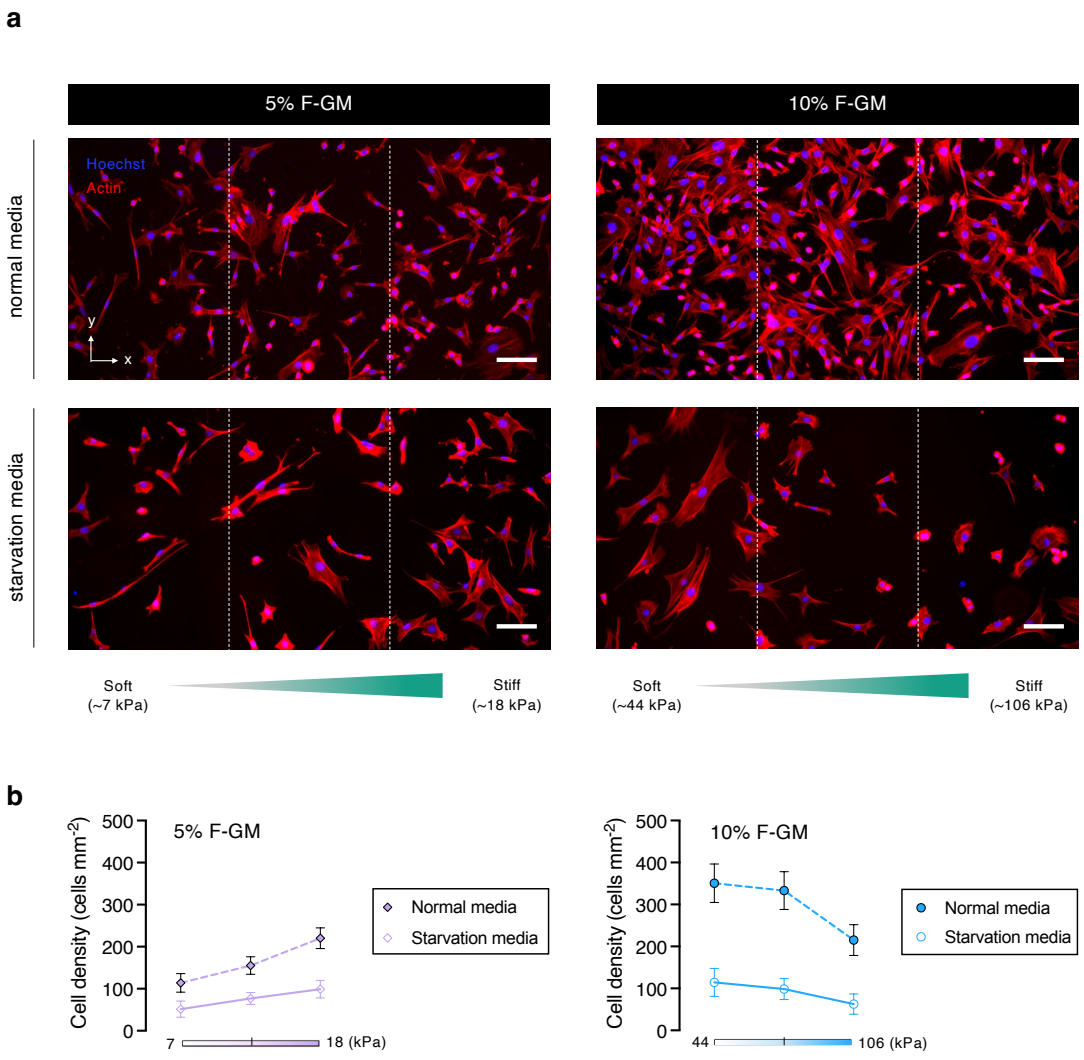

Figure 7.13: (a) Representative fluorescent images of fibroblasts cultured on shallow (5 wt%) and steep (10 wt%) linear stiffness gradient F-GM hydrogels, using normal (top) or starvation (bottom)

media. Scale bars: 100 μm. (b) Corresponding quantification of cell density along the stiffness gradients at 24h. Data shown as mean ± SEM of n = 4 independent experiments. The hydrogel matrix was not visualized in these images.

Next, to characterize the initial cell attachment on stiffness gradients and the influence on cell behavior over time, we performed further experiments to assess fibroblast cell behavior at 2 h and 24 h (**Figure 7.14a**). The results at 2 h showed that the cell density was not significantly different across both 5% F-GM and 10% F-GM stiffness gradients, indicating that our gradient hydrogels did not induce biased cell attachment (**Figure 7.14b**; top, **Figure 7.15**; 2h data).

Previously in **Chapter 6**, we reported that fibroblast cells cultured on linear stiffness gradient GelMA hydrogels with a range of ~35 kPa to ~80 kPa exhibited preferential accumulation toward the softer end of the substrate after 24 h. Here, our analysis further confirmed that fibroblast cells tend to migrate toward an optimal mechanical niche. By employing two separate gradient systems covering a broad stiffness range from ~7 kPa to ~106 kPa, we demonstrated that cells directionally accumulated toward regions of intermediate substrate stiffness (~20-40 kPa), regardless of whether cells were exposed to softer or stiffer environments on the same substrate (**Figure 7.14b**; bottom, **Figure 7.15**; 24 h data). Importantly, the consistent increase in cell population toward a preferred stiffness range despite over five-fold difference in the slope of both gradient systems suggests that absolute stiffness had a greater influence on the fibroblast mechano-responses to stiffness gradients *in vitro*.

Quantitative analysis of cell area (**Figure 7.14c**, **Figure 7.14e**) and aspect ratio (**Figure 7.14d**, **Figure 7.14f**) further revealed altered fibroblast morphology in response to stiffness gradients. Generally, cells exhibited increased spreading toward the 20-40 kPa stiffness region, though the aspect ratio remained mostly consistent across the stiffness range.

The presence of an optimal stiffness for cell migration has also recently been reported in other cell types, following the molecular-clutch model which describes directed migration toward an intermediate stiffness region where cell-generated tractions are maximal[11,23]. The fact that traction force generation directly affects cell spreading also

explains the biphasic response observed[24]. The optimal stiffness range for migration is known to be cell-specific. To our knowledge, this is the first demonstration of applying gradient hydrogels to probe positive and negative durotactic responses in 3T3-L1 fibroblast cells.

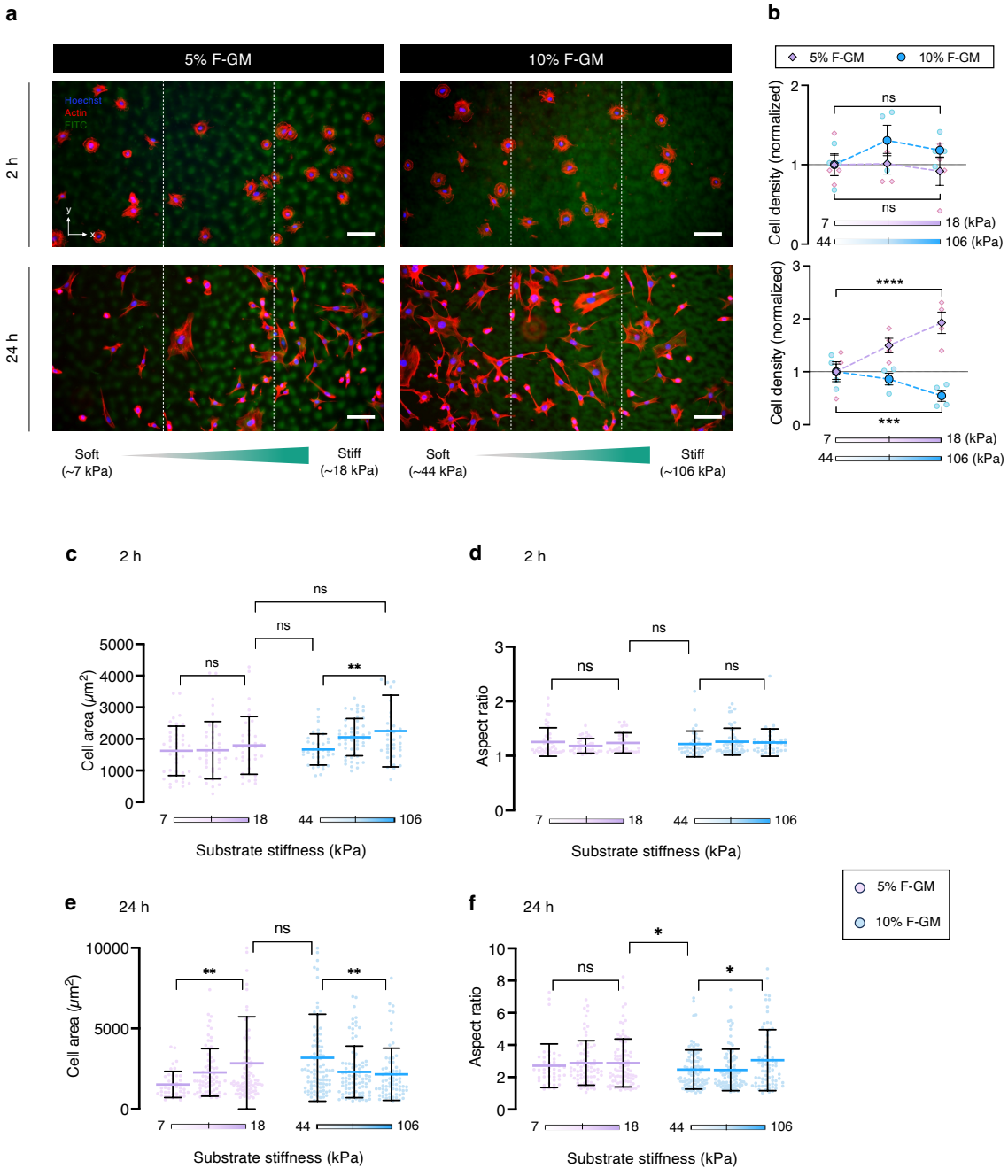

Figure 7.14: (a) Representative fluorescent images of fibroblasts cultured on shallow (5 wt%) and steep (10 wt%) linear stiffness gradient F-GM hydrogels, observed at 2 h (top) and 24 h (bottom) after seeding. Scale bars: 100 μm. (b) Quantification of cell density along the stiffness gradients at 2 h (top) and 24 h (bottom). Data shown as mean ± SEM of n = 4 independent experiments. Data at each

analyzed stiffness region were normalized to the mean cell density at the softest region of the corresponding gel. (c) Quantification of cell area and (d) aspect ratio of fibroblasts along the stiffness gradients at 2 h. Data shown as mean ± standard deviation of n = 4 independent experiments. (e) Quantification of cell area and (f) aspect ratio of fibroblasts along the stiffness gradients at 24 h. Data shown as mean ± standard deviation of n = 4 independent experiments.

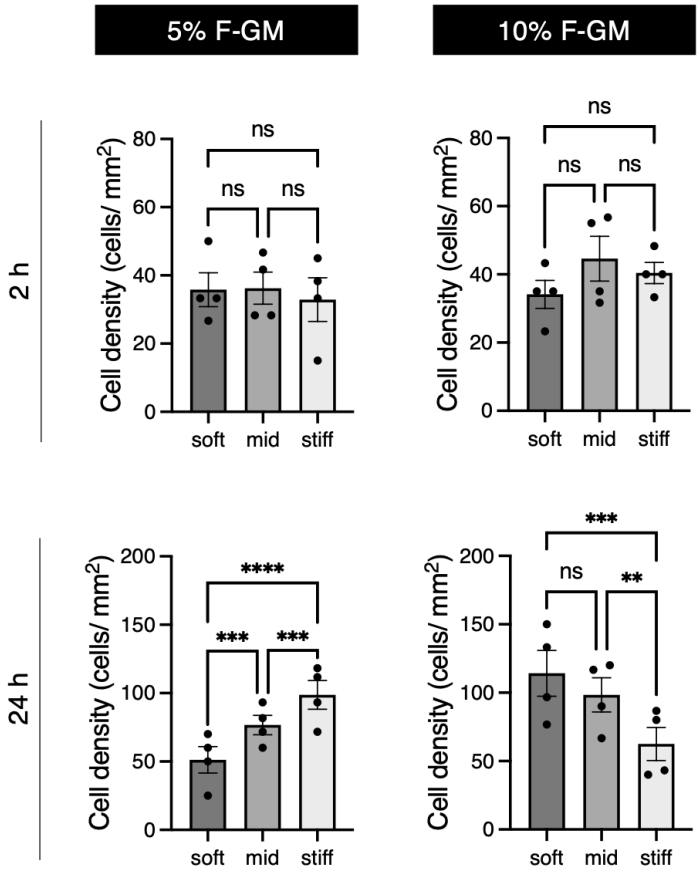

Figure 7.15: Cell density quantified by mean nuclei per analyzed region (“soft”, “mid”, “stiff”) along the stiffness gradient gels reported in Figure 7.14. Data shown as mean ± SEM of n = 4 independent experiments.

7.9 Fibroblast interpretation of stiffness gradients is dependent on the matrix composition

To further demonstrate the potential of our platform for independently modulating hydrogel matrix composition from the stiffness gradient profile, we investigated whether the choice of hydrogel type impacts the behavior of fibroblasts in response to stiffness gradients (**Figure 7.17a**).

To that end, linear stiffness gradients with similar range (~5-15 kPa) and slope (~10 kPa mm^{-1}) were fabricated using F-GM and F-GG hydrogels. Although GelMA contains intrinsic RGD cell binding motifs that support cell attachment, we also coated F-GM hydrogels with fibronectin, similarly to F-GG hydrogels. This standardization ensured that fibronectin was the primary ECM protein encountered by fibroblasts across both material systems, enabling us to investigate the direct impact of hydrogel chemistry on fibroblast stiffness responses without the potential confounding effects of ECM protein coating[25,26]. Additionally, to test the impact of fibronectin coating on F-GM hydrogels, we repeated the experiment using the steep linear stiffness gradient F-GM hydrogels (~44-106 kPa; ~87 kPa mm^{-1}).

To rule out a possible effect of stiffness-dependent fibronectin binding on the F-GG and F-GM gradient hydrogels, the resulting fibronectin-coated gels were immunostained and the measured fluorescence intensities were correlated to the local stiffness conditions (**Figure 7.16**; see Section 7.2.6 for detailed procedure). Briefly, fluorescent images of the gel samples were divided into three equally sized segments along the known direction of the stiffness gradient, consistent with the different stiffness zones (“soft”, “mid”, and “stiff”) for cell analyses. The amount of fibronectin coated on the hydrogel surface was measured as the sum of pixel intensity, and changes in intensity with increasing stiffness were compared relative to the “soft” zone within each sample. The relative total fluorescence in each stiffness zone for all F-GG and F-GM gradient hydrogels showed no significant differences, confirming spatially uniform fibronectin coating. Characterization of negative control samples (without fibronectin coating) was also performed to ensure that the observed fluorescence was due to specific protein binding rather than hydrogel autofluorescence or non-specific staining (**Figure 7.16**). The results showed minimal fluorescence signal in all cases

(<0.09 relative total fluorescence intensity), validating that any difference in cellular responses observed in the following experiments was not a consequence of differential levels in fibronectin density.

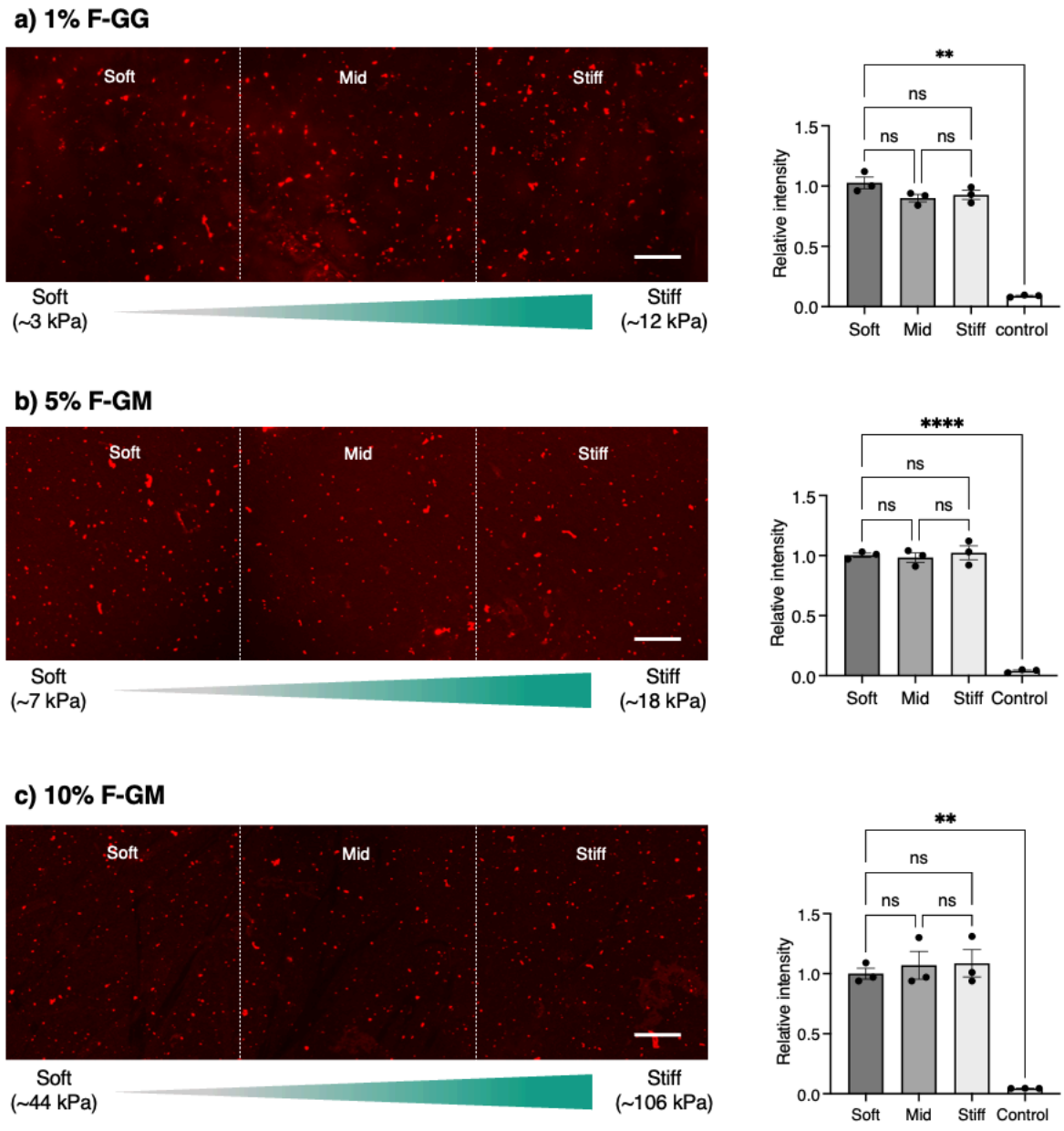

Figure 7.16: Representative fluorescent images and quantification of fibronectin attachment on the surface of linear stiffness gradient hydrogels fabricated using (a) 1 wt% F-GG, (b) 5 wt% F-GM, and (c) 10 wt% F-GM polymer systems (n = 3 independent samples; mean ± SEM). Data were normalized by dividing the sum of fluorescence intensity at each stiffness region ("soft", "mid", or "stiff") by the total fluorescence at the corresponding "soft" region. Scale bars: 100 μm. Negative control samples were prepared using uniform stiffness hydrogels (1 wt% F-GG, 5 wt% F-GM, 10 wt% F-GM) without fibronectin coating.

Our analysis revealed evenly distributed initial cell attachment across the F-GG gradient gel, while fibronectin coating modestly promoted attachment from soft to stiff regions on the F-GM gradient gels, albeit non-significantly for the shallow gradient (**Figure 7.17b**; 2 h). Moreover, after 24 h culture, a graded distribution in cell density toward stiffer substrate regions was observed across all gradient gel systems (**Figure 7.17b**; 24 h). However, it was noted that the extent of accumulation differed between the shallow gradient F-GG and F-GM hydrogels. Interestingly, the combined results for the F-GM gels with fibronectin coating revealed that instead of a biphasic response, cells displayed a continuously increasing cell population across the ~7-106 kPa stiffness range, though the differences were much more modest beyond ~40 kPa (**Figure 7.17a**; 24 h images of 5% F-GM + FN vs. 10% F-GM + FN, **Figure 7.18**).

Furthermore, in the presence of fibronectin surface coating, cells exhibited a significant increase in projected cell area on F-GM hydrogels compared to F-GG hydrogels (**Figure 7.17d**, **Figure 7.17f**). However, there appeared to be no discernible differences in cell spreading (**Figure 7.17d**, **Figure 7.17f**) and aspect ratio (**Figure 7.17e**, **Figure 7.17g**) across the stiffness range investigated for each hydrogel type. Previous studies have highlighted the importance of cytoskeletal remodeling in governing substrate stiffness mechanosensing, which is also dependent on the ECM composition[10,27,28]. During the initial attachment stage, cells on F-GG and uncoated F-GM generally exhibited an orthoradial pattern of actin filaments in the cell cortex, characteristic of immature adhesion (**Figure 7.17c**; top). In contrast, cells on fibronectin-coated F-GM appeared more well-spread with directionally aligned stress fibers, implying behavior on “stiff-like” substrates. At 24 h, cells seeded on unmodified F-GM adopted a spindle-like shape, contrasting to cells on fibronectin-coated F-GM, which had a rounder morphology (i.e. lower aspect ratio) and displayed higher levels of stress fiber formation (**Figure 7.17c**; bottom). On the other hand, cells on F-GG substrates exhibited a distinctive cobblestone shape.

Overall, these findings confirmed the influence of biochemical cues on fibroblast attachment, migration, and morphology. Presumably, the mechanosensing pathways governing fibroblast cell stiffness-responses are strongly influenced by the ECM protein composition, but can be modulated by the underlying hydrogel chemistry. More importantly, this study showcased the utility of our gradient hydrogel platform to flexibly

tune the stiffness profile and change different hydrogel types for systematic cell investigations.

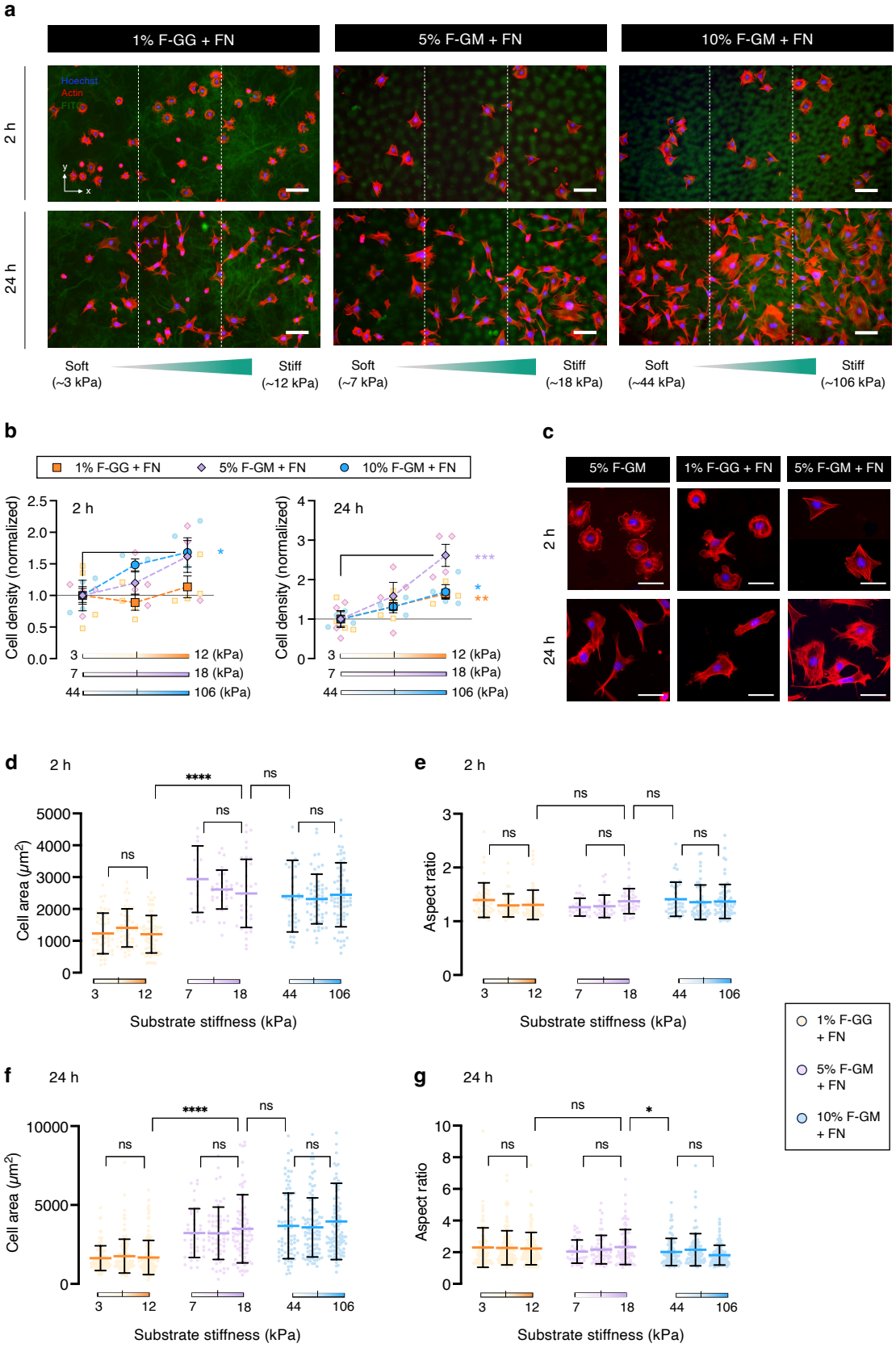

Figure 7.17: (a) Representative fluorescent images of fibroblasts cultured on varying linear stiffness gradient F-GG and F-GM hydrogels with fibronectin coating, observed at 2 h (top) and 24 h (bottom) after seeding. Scale bars: 100 μm. (b) Quantification of cell density along the stiffness gradients at 2 h (left) and 24 h (right). Data shown as mean ± SEM of n = 4 independent experiments. Data at each analyzed stiffness region were normalized to the mean cell density at the softest region of the corresponding gel. (c) Representative zoom-in fluorescent images of cell morphology on varying linear stiffness gradient F-GG and F-GM hydrogels, observed at 2 h (top) and 24 h (bottom). For consistency, cells were selected from the "stiff" zone on each gradient system. Scale bars: 50 μm. (d) Quantification of cell area and (e) aspect ratio of fibroblasts along the stiffness gradients at 2 h. Data shown as mean ± standard deviation of n = 4 independent experiments. (f) Quantification of cell area and (g) aspect ratio of fibroblasts along the stiffness gradients at 24 h. Data shown as mean ± standard deviation of n = 4 independent experiments.

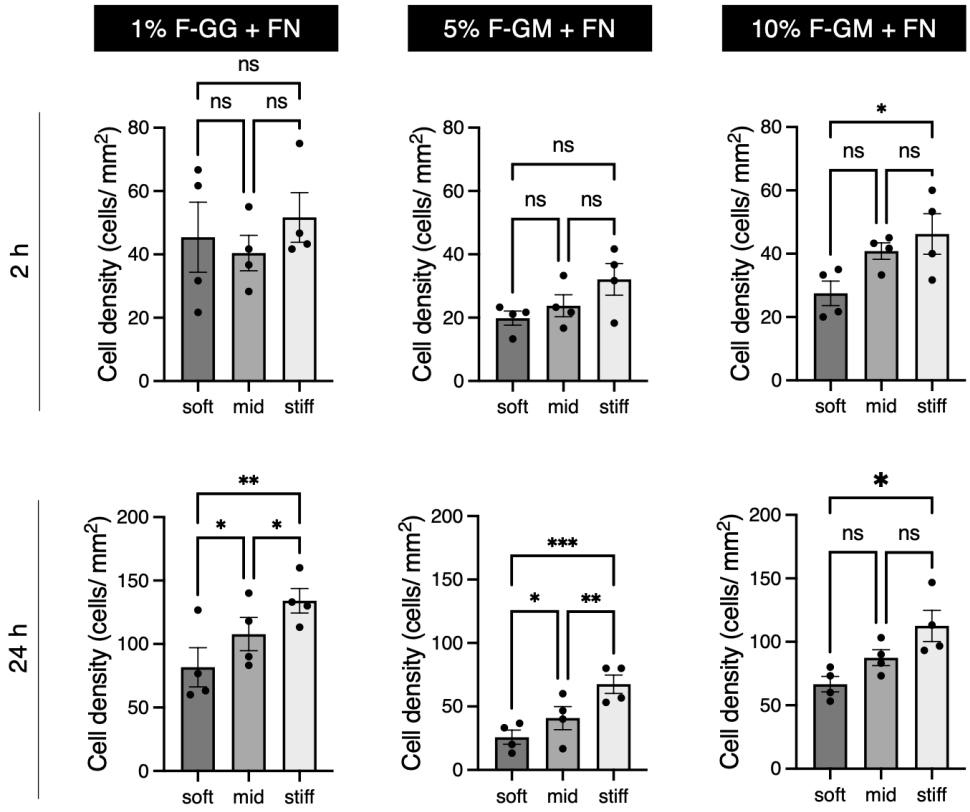

Figure 7.18: Cell density quantified by mean nuclei per analyzed region ("soft", "mid", "stiff") along the stiffness gradient gels reported in Figure 7.17. Data shown as mean ± SEM of n = 4 independent experiments.

7.10 Discussion

The fluorescently labelled gradient hydrogels developed in this work represent a new class of *in vitro* stiffness gradient systems for studying the complex cell-material interplay. While substrate stiffness has been classically known to be a major regulator of cell behavior, mounting evidence highlights the critical role of ECM protein compositions in modulating cellular stiffness-responses[26,29]. The majority of the studies on 2D stiffness gradients have been performed using biologically inert polyacrylamide hydrogels functionalized with the ECM proteins, such as fibronectin, laminin, and collagen[1,7,9,11,25]. Recently, the influence of substrate material on the differential cellular mechano-sensitivity toward substrate bulk stiffness and ECM protein has also been reported, demonstrated using polyacrylamide and PDMS[30]. These responses are likely driven by the way cells interact with the material interfaces possessing unique viscoelastic properties[31,32], wettability[19,33], roughness[34] etc.. However, comparative studies on different substrate materials are difficult due to constraints in current fabrication strategies, especially in the context of micro-engineered stiffness gradients.

To address this issue, we previously developed a modular platform based on thermophoresis that can streamline the fabrication of stiffness gradient hydrogels using different hydrogel types (**Chapter 6**). In this study, we used the platform to fabricate fluorescently labelled GelMA and Gellan gum hydrogels with linear stiffness gradients. Compared to traditional 2D gradient hydrogel systems, our approach offers unique features: 1) visualization of the native hydrogel microarchitecture, 2) material-intrinsic fluorescence readout for noninvasive stiffness characterization, 3) rapid gradient quality validation for cell studies, and 4) the ability for *in situ* correlation of hydrogel properties with cellular responses.

Using the fluorescence-based system, we demonstrated a biphasic stiffness-mediated responses of 3T3-L1 fibroblast cells on linear stiffness gradient GelMA hydrogels without additional ECM protein coating. Cells exhibited preferential spreading and migration toward an “optimal” stiffness range, which offers a possible reconciliation of this apparently contradictory finding[35] by suggesting that fibroblast durotaxis is not solely driven by the presence of a stiffness gradient but is also dependent on the absolute stiffness values.

A particularly interesting finding from this study is the synergistic effects of hydrogel type and ECM protein coating on fibroblast mechano-sensitivity to stiffness gradients. Under a similar stiffness range and gradient slope, cells displayed significant differences in migration and morphological behavior when cultured on Gellan gum, GelMA, and fibronectin-coated GelMA hydrogels. Notably, we observed distinct cytoskeletal organization patterns across these systems, suggesting that the matrix composition might alter cells' interpretation of substrate "stiffness". Further investigations are required to understand the exact mechanism(s) by which different combinations of substrate material and ECM protein type modulate cell mechano-responses, as well as to establish the generalizability of this coupling effect across different cell types. To that end, future studies could incorporate live-cell tracking to quantify single-cell migration dynamics on the stiffness gradients (e.g., speed, directional persistence, durotactic index) as well as temporal changes in morphology or protrusive activity[11]. Moreover, traction force microscopy could be a valuable tool to provide a direct measurement of cell-generated forces on the underlying substrate and how these forces may vary across different stiffness regimes[22]. By correlating the magnitude and distribution of cellular traction force with the morphological behavior, it is possible to disentangle the effects of stiffness gradients and matrix composition. To further assess stiffness-mediated mechanotransduction, inhibition studies could also be designed to provide additional insights into the role of cytoskeletal contractility or specific signaling pathways. For instance, treatment with blebbistatin is often used to inhibit cell mechanosensing by impacting actin-myosin activity, which is fundamental for contractility and cytoskeletal regulation processes[25]. Nevertheless, the present study highlights the development of advanced biomaterial features that make 2D microengineered stiffness gradients an enabling *in vitro* platform to address many of these questions.

The concept of fluorescently labelled hydrogels offers a potential generic strategy for rapid, noninvasive characterization of biophysical gradients, allowing for precise correlation of the local material properties with cellular responses. Considering the increasing advances and accessibility of fluorescence microscopy techniques, we envision that this work could inspire new approaches to study cell-substrate interactions. For example, future efforts could explore real-time visualization of the dynamic cell-substrate remodeling process which may cause alterations to the

substrate stiffness. Beyond fundamental research, these insights would enable a more comprehensive understanding of the material structure-function relationships toward the goal of designer biomaterials for tissue engineering and regenerative applications.

7.11 Conclusion

This chapter describes the combined utility of the thermophoretic technique and fluorescently labelled polymers to fabricate stiffness gradient hydrogels. By demonstrating that it is possible to successfully predict from fluorescence signal alone the stiffness at any location of the hydrogel, this work opens new avenues for investigations into critical questions and debates on the complex cell-substrate interplay, such as revisiting the role of “stiffness” as primary regulator of cell mechano-responses, the influence of matrix chemical composition, and the importance of stiffness range vs. gradient slope. More generally, by offering a simple means for visual validation of the gradient gels, this fluorescence-based approach should enhance the accessibility and reliability of *in vitro* gradient hydrogels in mechanobiology cell studies.

References

1. Hadden, W. J. *et al.* Stem cell migration and mechanotransduction on linear stiffness gradient hydrogels. *Proc Natl Acad Sci* **114**, 5647–5652 (2017).

2. Tse, J. R. & Engler, A. J. Preparation of Hydrogel Substrates with Tunable Mechanical Properties. *Curr Protoc Cell Biol* **47**, 10161 (2010).

3. Zhao, F. *et al.* Fibroblast alignment and matrix remodeling induced by a stiffness gradient in a skin-derived extracellular matrix hydrogel. *Acta Biomater* **182**, 67–80 (2024).

4. Hakeem, R. M. *et al.* A Photopolymerized Hydrogel System with Dual Stiffness Gradients Reveals Distinct Actomyosin-Based Mechano-Responses in Fibroblast Durotaxis. *ACS Nano* **17**, 197–211 (2023).

5. Kosmidis Papadimitriou, A. *et al.* Fabrication of gradient hydrogels using a thermophoretic approach in microfluidics. *Biofabrication* **16**, 025023 (2024).

6. Lee, D. *et al.* Fabrication of Hydrogels with a Stiffness Gradient Using Limited Mixing in the Hele-Shaw Geometry. *Exp Mech* **59**, 1249–1259 (2019).

7. Hetmanski, J. H. R. *et al.* Membrane Tension Orchestrates Rear Retraction in Matrix-Directed Cell Migration. *Dev Cell* **51**, 460–475 (2019).

8. Norman, M. D. A., Ferreira, S. A., Jowett, G. M., Bozec, L. & Gentleman, E. Measuring the elastic modulus of soft culture surfaces and three-dimensional hydrogels using atomic force microscopy. *Nat Protoc* **16**, 2418–2449 (2021).

9. Koser, D. E. *et al.* Mechanosensing is critical for axon growth in the developing brain. *Nat Neurosci* **19**, 1592–1598 (2016).

10. Barber-Pérez, N. *et al.* Mechano-responsiveness of fibrillar adhesions on stiffness-gradient gels. *J Cell Sci* **133**, jcs242909 (2020).

11. Isomursu, A. *et al.* Directed cell migration towards softer environments. *Nat Mater* **21**, 1021–1090 (2022).

12. Cho, H. H. *et al.* Development of fluorescein isothiocyanate conjugated gellan gum for application of bioimaging for biomedical application. *Int J Biol Macromol* **164**, 2804–2812 (2020).

13. Onofrillo, C. *et al.* FLASH: Fluorescently LAbelled Sensitive Hydrogel to monitor bioscaffolds degradation during neocartilage generation. *Biomaterials* **264**, 120383 (2021).

14. Horinaka, J. I., Kani, K., Honda, H., Uesaka, Y. & Kawamura, T. Local chain mobility of gellan in aqueous systems studied by fluorescence depolarization. *Macromol Biosci* **4**, 714–720 (2004).

15. Merck. FITC-labelled polysaccharides. https://www.sigmaaldrich.com/AU/en/technical-documents/technical-article/cell-culture-and-cell-culture-analysis/imaging-analysis-and-live-cell-imaging/fluorescently-labeled-dextrane?srsltid=AfmBOooPvoEHWhDaSdZEo2UK4BMHsCRsF6pjEZwUfCjWqvsRsuEsFSjx#ref (2025).

16. Aigoin, J. *et al.* Comparative Analysis of Electron Microscopy Techniques for Hydrogel Microarchitecture Characterization: SEM, Cryo-SEM, ESEM, and TEM. *ACS Omega* **10**, 14687-14698 (2025).

17. Zhong, J., Zhao, T. & Liu, M. Fluorescence microscopic visualization of functionalized hydrogels. *NPG Asia Mater* **14**, 38 (2022).

18. Gandavarapu, N. R., Mariner, P. D., Schwartz, M. P. & Anseth, K. S. Extracellular matrix protein adsorption to phosphate-functionalized gels from serum promotes osteogenic differentiation of human mesenchymal stem cells. *Acta Biomater* **9**, 4525–4534 (2013).

19. Da Silva, L. P. *et al.* Engineering cell-adhesive gellan gum spongy-like hydrogels for regenerative medicine purposes. *Acta Biomater* **10**, 4787–4797 (2014).

20. Ajam, A., Huang, Y., Islam, M. S., Kilian, K. A. & Kruzic, J. J. Mechanical and biological behavior of double network hydrogels reinforced with alginate versus gellan gum. *J Mech Behav Biomed Mater* **157**, 106642 (2024).

21. Jonkman, J. E. N. *et al.* Cell Adhesion & Migration An introduction to the wound healing assay using livecell microscopy An introduction to the wound healing assay using livecell microscopy. *Cell Adh Migr* **8**, 440–451 (2014).

22. Pallarès, M. E. *et al.* Stiffness-dependent active wetting enables optimal collective cell durotaxis. *Nat Phys* **19**, 279–289 (2022).

23. Bangasser, B. L. *et al.* Shifting the optimal stiffness for cell migration. *Nat Commun* **8**, 15313 (2017).

24. Lerche, M. *et al.* Integrin Binding Dynamics Modulate Ligand-Specific Mechanosensing in Mammary Gland Fibroblasts. *iScience* **23**, 100907 (2020).

25. Tan, Y. H. *et al.* Stiffness Mediated-Mechanosensation of Airway Smooth Muscle Cells on Linear Stiffness Gradient Hydrogels. *Adv Healthc Mater* **13**, 2304254 (2024).

26. Li, L. *et al.* A Protein-Adsorbent Hydrogel with Tunable Stiffness for Tissue Culture Demonstrates Matrix-Dependent Stiffness Responses. *Adv Funct Mater* **34**, 2309567 (2024).

27. Gupta, M. *et al.* Adaptive rheology and ordering of cell cytoskeleton govern matrix rigidity sensing. *Nat Commun* **6**, 7525 (2015).

28. Rickel, A. P., Sanyour, H. J., Leyda, N. A. & Hong, Z. Extracellular Matrix Proteins and Substrate Stiffness Synergistically Regulate Vascular Smooth Muscle Cell Migration and Cortical Cytoskeleton Organization. *ACS Appl Bio Mater* **3**, 2360–2369 (2020).

29. Conway, J. R. W. *et al.* Defined extracellular matrix compositions support stiffness-insensitive cell spreading and adhesion signaling. *Proc Natl Acad Sci* **120**, 2017 (2023).

30. Li, J., Han, D. & Zhao, Y. P. Kinetic behaviour of the cells touching substrate: The interfacial stiffness guides cell spreading. *Sci Rep* **4**, 3910 (2014).

31. Chaudhuri, O., Cooper-White, J., Janmey, P. A., Mooney, D. J. & Shenoy, V. B. Effects of extracellular matrix viscoelasticity on cellular behaviour. *Nature* **584**, 535–546 (2020).

32. Chaudhuri, O. *et al.* Hydrogels with tunable stress relaxation regulate stem cell fate and activity. *Nat Mater* **15**, 326–334 (2016).

33. Song, W. & Mano, J. F. Interactions between cells or proteins and surfaces exhibiting extreme wettabilities. *Soft Matter* **9**, 2985–2999 (2013).

34. Hou, Y. *et al.* Surface Roughness and Substrate Stiffness Synergize to Drive Cellular Mechanoresponse. *Nano Lett* **20**, 748–757 (2020).

35. Zaari, N., Rajagopalan, P., Kim, S. K., Engler, A. J. & Wong, J. Y. Photopolymerization in microfluidic gradient generators: Microscale control of substrate compliance to manipulate cell response. *Adv Mater* **16**, 2133–2137 (2004).

Chapter 8

Conclusion and outlook

In this final chapter, I summarize the main achievements in this thesis and lessons learnt from developing a biological tool from an engineering perspective. I also offer a brief perspective on the future impact of microengineered gradient hydrogels in the broader context of biomedical research.

8.1 Summary of achievements

Miroengineered stiffness gradient hydrogels provide a useful *in vitro* experimentation platform in modern mechanobiology. This thesis serves to contribute to the field by developing and applying a new gradient gel fabrication method based on thermophoresis effects for probing cell-substrate interactions. Recently, thermophoresis (i.e., the induced motion of solutes along a temperature gradient) was proposed as a fundamentally new gradient patterning technique that allows for active user control and works universally across different hydrogel types (discussed in **Chapter 1** and **Chapter 3**). The practical feasibility of the technique was demonstrated and refined over the course of this thesis, presenting a potential solution to the longstanding “reproducibility” problem associated with existing fabrication methods. This challenge relates to the difficulty in generating precise and consistent stiffness gradients for robust biological interpretation and statistical analysis. By solving this technological bottleneck, the thermophoretic technique could further expand the applicability of stiffness gradient hydrogels for advanced cell studies.

Toward that goal, this thesis presents a winding journey through first principles thermophoresis investigations, microfabrication strategies, and biomaterials engineering – all within the context of biologically relevant stiffness gradients.

8.1.1 Foundational platform development and proof-of-concept

At its core, the proposed technique utilizes microfluidic devices to pattern microscale temperature landscapes and leverages thermophoresis effect to precisely guide the distribution of hydrogel precursor molecules (or “building blocks”) into the desired gradient pattern. The concentration gradient is fixed through a subsequent hydrogel crosslinking step, yielding a final stiffness gradient.

One of the first achievements in this thesis was the development of a foundational framework for implementing thermophoresis as a biofabrication strategy (**Chapter 4**). Importantly, this development was enabled by the strategic integration of two key experimental methodologies:

- A fluorescence thermometry protocol designed specifically for high-resolution spatial mapping of the temperature distribution within the microfluidic system;
- A standardized approach for fluorescent labelling of the polymers to enable direct visualization under a fluorescence microscope.

With that, the unique thermophoretic behavior of different polymer systems could be measured and characterized under fabrication-relevant conditions. These experiments revealed critical insights into the link between the input process conditions and the final material outcomes, which were leveraged to guide the selection of reliable process parameters for gradient gel fabrication. From a practical standpoint, the set of general design guidelines was an essential first step in making the thermophoretic technique more approachable by providing a clear roadmap for optimizing the process to the desired substrate stiffness, gradient geometry, or hydrogel type.

The first iteration of the thermophoretic fabrication platform was designed as a fully enclosed microfluidic system. Using this platform, Gellan gum hydrogels with steep stiffness gradients ranging from 20 kPa to 90 kPa over 600 μm were created, and their potential utility for interrogating stiffness-dependent cell behavior was demonstrated through directed migration and increased mineralization tendency of osteoblast precursor cells toward stiffer regions on the gradient (**Chapter 5**). The study represented a pivotal project milestone as the first biological proof-of-concept of the effectiveness of the thermophoretic technique in modulating the mechanical microenvironment of cells. More importantly, this work provided valuable early lessons on the development of biological tools, highlighting that successful translation of physics principles into practical applications requires designing for usability requirements at each stage of the development cycle.

8.1.2 Modular platform for improved flexibility and accessibility

The main achievement of this thesis was the development of a next-generation, modular platform that transformed the thermophoresis technique from a proof-of-concept demonstration into a practically useful research tool (**Chapter 6**). The modular platform features a two-part design comprising a microfluidic layer (for thermal

patterning) interfaced with an external microchamber (for hydrogel confinement). Compared to the first iteration platform, the modular platform offers unique advantages:

- Simplified platform setup and operation (reduced fluidic handling requirements);
- Straightforward sample loading and retrieval (open-top microchamber design);
- The capability to pattern linear and spatially more complex gradients;
- Flexible gradient span of up to ~1 cm (defined by microchamber size);
- Streamlined workflow for various hydrogel crosslinking modalities.

The modular platform was applied to create a range of stiffness gradients (e.g., steep linear, shallow linear, periodic, anisotropic) using thermosensitive Gellan gum and photocrosslinked GelMA hydrogels, which illustrates the versatility of the thermophoretic technique. Extensive AFM stiffness characterization performed in this study complements the previous studies[1,2], firmly establishing the thermophoretic technique as a reliable gradient hydrogel fabrication method.

A major goal in the field of stiffness gradient hydrogels is to recreate the broad physiological and pathological mechanical landscape. In this respect, the modular platform can enable researchers to rapidly test different stiffness gradient designs (i.e., stiffness range, gradient slope, gradient shape) within a single platform. This unified approach would greatly simplify experimental workflows by removing the need for multiple specialized fabrication techniques[3], and further contribute to expanding the library of accessible gradient gel systems to ask new questions in mechanobiology. Future iterations of the platform can also be designed with more channels in the microfluidic channel array, further enhancing the capacity for high-throughput fabrication (e.g., multiple linear gradient gels can be fabricated in parallel on a single setup).

8.1.3 Fluorescence-based characterization of stiffness gradients

In addition to enabling experimental characterization of thermophoretic behavior, I showed how when FITC-labelled polymers were used to fabricate stiffness gradient hydrogels, the resulting fluorescence signal could act as a direct indicator of the local hydrogel stiffness (**Chapter 7**). This was possible because of the mechanism by which

thermophoresis creates stiffness gradients in hydrogels through spatial variation in polymer concentration. The fluorescence-based characterization was intended as a simpler alternative to conventionally used AFM, which is not practically feasible for routine characterization of each sample used in cell experiments.

Notably, the FITC-labelled stiffness gradient hydrogels can allow for simultaneous structural visualization and stiffness characterization through widely accessible fluorescence imaging, while maintaining biocompatibility for cell culture. Key features of the technique include:

- Visualization of structural features within the hydrogel in its native state;
- Rapid validation of successful gradient formation and assessment of the gradient uniformity;
- Noninvasive, sample-wide estimation of AFM-based Young's modulus;
- The ability for *in situ* correlation of local stiffness with cellular responses.

The estimated stiffness values obtained using the fluorescence-based method was shown to be in good agreement with the actual AFM-measured Young's modulus, indicating the reliability of the fluorescence technique. This approach is generalizable and should be applicable to a variety of hydrogel systems beyond GelMA and Gellan gum demonstrated in this thesis, which opens up exciting opportunities for direct visualization of the dynamic cell-substrate interactions or monitoring changes in the hydrogel stiffness over time.

8.1.4 Insights into the complex interplay of matrix stiffness and composition

Having established the capabilities of the thermophoretic technique to create biologically relevant stiffness gradients, I sought to apply the technique to answer questions about the complex cell-material interplay. A particularly novel finding from this thesis is the effect of matrix composition on cell mechano-responses to stiffness gradients (**Chapter 7**). To that end, the modular fabrication platform and the fluorescently labelled hydrogel systems were uniquely combined to systematically vary the stiffness range (~5-15 kPa vs. ~44-106 kPa), gradient slope (~10 kPa mm^{-1} vs. ~90 kPa mm^{-1}), hydrogel type (GelMA vs. Gellan gum), ECM protein coating

(fibronectin vs. no coating). Such comparative studies were previously difficult to perform due to limitations using conventional fabrication techniques, which further highlights the versatility of the thermophoretic approach.

Of note, 3T3-L1 fibroblasts cultured on these gradient gels revealed that:

- Fibroblast cells migrated toward an “optimal” intermediary stiffness range on uncoated GelMA gradients but displayed consistent migration from soft-to-stiff regions on fibronectin-coated GelMA gradients;
- Under similar stiffness conditions, fibroblasts displayed significant differences in migration and morphological behavior when cultured on Gellan gum vs. GelMA substrates.

Interestingly, distinct cytoskeletal organization patterns observed across the different material systems suggests that both the ECM protein composition and the choice of underlying substrate could jointly modulate cell mechanosensing.

While the majority of 2D stiffness gradient hydrogel studies have traditionally relied on polyacrylamide gels functionalized with different ECM proteins[4], this study highlights the potential value of extending investigations to a broader range of cell culture substrates. These efforts could facilitate a more nuanced material-centric perspective in mechanobiology, one where “stiffness” is not singly analyzed as the predominant regulator of cell behavior, but as part of richer mechano-chemical landscape that cells actively interpret.

8.2 Perspectives

In the beginning of my thesis, I asked the question of how to increase the adoption of stiffness gradient hydrogel technology in mainstream biological research, and what makes one method better than the other. On the one hand, majority of the gradient hydrogel platforms to date originated from biology groups to solve unmet needs in their own niche research questions, but their broad applications are limited. On the other hand, the breadth and depth of impact guided by a more engineering-oriented approach may be highly valuable for the field, but there is often a disconnect between development and deployment.

In my opinion, the development of biological tools to enable future advances in research and applications is increasingly at the crossing of these two disciplines. Many specific future research directions have been discussed in the results chapters and so I will not list them here again. Instead, drawing on lessons gained from completing this thesis, here I offer a general perspective on how we (engineers) can contribute to driving forward gradient hydrogel technology for biological applications.

8.2.1 Technological novelty vs. biological utility

To begin with, I reiterate the notion I put forward in **Chapter 5** that the way end-users interact with a new technology will be a critical factor of whether it will be adopted. One needs to articulate and understand the essence of “right balance” between technical advances and practical relevance, as this relates to the core design philosophy.

In engineering, there can be a tendency to impose new technological features that promise improved performance where it might not necessary be needed or wanted. However, the biological research context should be reconsidered carefully. For example, the most primitive stiffness gradient fabrication method based on diffusion at the interface of two adjacent drops containing different precursor compositions, first described by Lo et al. in 2000[ref.5], is still employed in high profile biological studies today[6,7]. Presumably, the simplicity of the technique was deemed more important to scale for more complex and higher throughput studies, despite known variability issues. For screening applications or systematic studies, however, high patterning precision

and reproducibility are required to ensure robust results, in which case, more sophisticated techniques would be employed.

I would argue that there is no straightforward playbook to guarantee successful technology adoption. However, engineers can make deliberate design choices to lower the barrier of entry for biologists, especially relating to infrastructure and specialized knowledge requirements. This highlights the need for continued dialogue between engineers and biologists during platform development. The goal should be to create solutions that build on biologically validated approaches, while adding functionalities that enable new avenues of biological inquiry.

8.2.2 Fostering multidisciplinary collaborations

A good strategy to foster productive collaborations across engineering and biology domains during the development process can significantly enhance technology transfer to non-engineering users. Especially in today's rapidly evolving research landscape, it is no longer sufficient to assume that technological promise or novelty will automatically attract attention and inspire routine adoption. Researchers from the engineering/physics community should proactively engage collaborators from biology/clinical laboratories, and vice versa. In reality, this can often be a difficult challenge due to the "language barrier" that exists between different disciplines. On the other hand, this approach can sometimes feel counterintuitive to the traditional academic mindset that emphasizes scientific exploration and persistence when problems arise, which might lead to oversight in developing application trends and opportunities. For evidence, I draw parallel observations to the field of micro/nanofluidics; despite significant advances in our understanding of the fluid physics, their practical applications remain disproportionally limited due to the persistent separation between laboratories pursuing basic research and those focused on translational developments[8]. Fortunately, researchers have increasingly recognized the benefits of direct interaction and feedback from the end-user at each stage of the development process. In the case of this thesis, it was through conversations at mechanobiology conferences that I learnt about the largely unmet

needs to probe beyond the effect of “stiffness” and precisely determine the local stiffness along the gradient that inspired much of the work in **Chapter 7**.

New applications and ideas can often be generated from biology collaborators that engineers, non-experts in cell biology or clinical research, would have never considered.

8.2.3 Promising upcoming applications

The future impact of microengineered stiffness gradient hydrogels is closely tied to rapid advancements in *in vitro* disease modeling and personalized medicine.

For instance, integrating hydrogel-based ECM in organ-on-a-chip models has been increasingly explored to improve their physiological relevance for disease modeling[9–11]. Currently, these systems mainly rely on uniform substrates to mimic a single tissue region. However, considering the heterogeneity of tissues *in vivo*, spatially controlled stiffness gradient hydrogels could further enable organ-on-a-chip systems for modeling complex tissue interfaces and studying their dynamic processes, such as at the boundaries of fibrotic tissues[12].

Recently, organoids have gained enormous traction as a simplified version of organ systems *in vitro* for studying tissue development, disease modeling, and drug testing[13]. Multiple studies have highlighted the potential of combining organoids with hydrogels to investigate how material cues (e.g., stiffness, viscoelasticity) affect organoid behavior in specific pathophysiological contexts, though they have only been explored using discrete hydrogels[14,15]. One can envision that stiffness gradient hydrogels could be applied as a screening tool to study organoid mechano-responses in a dose-dependent manner, potentially facilitating deeper insights compared to testing a few independent values. In another interesting potential application, localized stiffness patterns could be leveraged to guide deterministic organoid formation, as recently demonstrated by Lutolf’s group through spatially controlled crypt formation[16].

One possibility for the limited utility of stiffness gradient hydrogels to date is related to their spatial continuum, making them unsuitable for analysis using traditional

molecular assays such as qPCR and Western blot. With advances in microfabrication methods as well as spatially resolved functional and genomic assays, this could open new research territories for deep biological understanding of the causal effect of microenvironmental gradients on cell/ tissue phenotype[17]. Leveraging the intrinsic nature of stiffness gradients for high-throughput mechanical screening, the pool of generated data could be combined with artificial intelligence (AI) to develop a virtual cell model[18]. In the immediate term, AI models have already been employed to allow predictive development of complex material systems such as granular hydrogels[19], and should similarly benefit the advancement of biophysical gradient hydrogel systems.

8.3 Concluding remarks

My deep conviction is that stiffness gradient hydrogels hold great promise for mechanobiology research and its related translational applications. The ability to present spatially organized biophysical cues at the microscale opens many unique opportunities to probe cell biology *in vitro*, bridging the knowledge gap between simplistic well-plate/ bulk hydrogel studies and sophisticated *in vivo* animal models. Even if the current platforms are still fairly basic and faced with numerous practical challenges that must first be resolved, linear stiffness gradient hydrogels have already been successfully applied to uncover previously unappreciated insights into how cells sense and respond to biophysical cues in their microenvironments. Toward increasing technology accessibility and applicability, this thesis contributes to new fabrication capabilities and material characterization strategies. The design framework and experimental methodologies developed in this thesis would inspire further exploration of gradient hydrogel technology and facilitate the transition to next-generation cell studies.

We, as a field, are still in a period of discovery where researchers (both from within and outside the realms of mechanobiology) will determine how to better deploy microengineered stiffness gradient hydrogels for cell-based applications. In the fullness of time, when we find the “right problem” to solve where such gradient materials introduce truly enabling functionality compared to standard bulk hydrogels, then the chances of contributing to technology with real practical impact are substantially higher.

References

1. Vigolo, D., Ramakrishna, S. N. & DeMello, A. J. Facile tuning of the mechanical properties of a biocompatible soft material. *Sci Rep* **9**, 7125 (2019).

2. Kosmidis Papadimitriou, A. *et al.* Fabrication of gradient hydrogels using a thermophoretic approach in microfluidics. *Biofabrication* **16**, 025023 (2024).

3. Vincent, L. G., Choi, Y. S., Alonso-Latorre, B., Del Álamo, J. C. & Engler, A. J. Mesenchymal stem cell durotaxis depends on substrate stiffness gradient strength. *Biotechnol J* **8**, 472–484 (2013).

4. Tse, J. R. & Engler, A. J. Preparation of Hydrogel Substrates with Tunable Mechanical Properties. *Curr Protoc Cell Biol* **47**, 10161 (2010).

5. Lo, C. M., Wang, H. B., Dembo, M. & Wang, Y. L. Cell movement is guided by the rigidity of the substrate. *Biophys J* **79**, 144–152 (2000).

6. Isomursu, A. *et al.* Directed cell migration towards softer environments. *Nat Mater* **21**, 1081-1090 (2022).

7. Barber-Pérez, N. *et al.* Mechano-responsiveness of fibrillar adhesions on stiffness-gradient gels. *J Cell Sci* **133**, jcs242909 (2020).

8. Chong, S. W., Shen, Y., Palomba, S. & Vigolo, D. Nanofluidic Lab-On-A-Chip Systems for Biosensing in Healthcare. *Small* **10**, 2407478 (2024).

9. Kutluk, H., Bastounis, E. E. & Constantinou, I. Integration of Extracellular Matrices into Organ-on-Chip Systems. *Adv Healthc Mater* **12**, 2203256 (2023).

10. Jiang, F. *et al.* Intravasation-On- μ Device (INVADE): Engineering Dynamic Vascular Interfaces to Study Cancer Cell Intravasation. *Adv Mater* **37**, 2501466 (2025).

11. Baksamawi, H. A., Alexiadis, A., Vigolo, D. & Brill, A. Platelet accumulation in an endothelium-coated elastic vein valve model of deep vein thrombosis is mediated by GPIbα—VWF interaction. *Front Cardiovasc Med* **10**, 11167884 (2023).

12. Haack, A. J. *et al.* Suspended Tissue Open Microfluidic Patterning (STOMP). *Adv Sci* **12**, 2501148 (2025).

13. Hofer, M. & Lutolf, M. P. Engineering organoids. *Nat Rev Mater* **6**, 402–420 (2021).

14. Pahapale, G. J. *et al.* Directing Multicellular Organization by Varying the Aspect Ratio of Soft Hydrogel Microwells. *Adv Sci* **9**, 2104649 (2022).

15. Chrisnandy, A., Blondel, D., Rezakhani, S., Broguiere, N. & Lutolf, M. P. Synthetic dynamic hydrogels promote degradation-independent in vitro organogenesis. *Nat Mater* **21**, 479–487 (2022).

16. Gjorevski, N. *et al.* Tissue geometry drives deterministic organoid patterning. *Science* **375**, eaaw9021 (2022).

17. Auxillos, J. *et al.* Spatially resolved analysis of microenvironmental gradient impact on cancer cell phenotypes. *Sci Adv* **10**, eadn3448 (2024).

18. Bunne, C. *et al.* How to Build the Virtual Cell with Artificial Intelligence: Priorities and Opportunities. *Cell* **187**, 7045–7063 (2024).

19. Verheyen, C. A., Uzel, S. G. M., Kurum, A., Roche, E. T. & Lewis, J. A. Integrated data-driven modeling and experimental optimization of granular hydrogel matrices. *Matter* **6**, 1015–1036 (2023).

Publications

Publications arising from this thesis:

*Fabrication of gradient hydrogels using a thermophoretic approach in microfluidics.**
A. Kosmidis Papadimitriou, **S.W. Chong**, Y. Shen, O.S. Lee, T.P.J. Knowles, L.M. Grover, D. Vigolo.
Biofabrication, **2024**, 16 (2): 025023.
* Special issue: Biofabrication for Mechanobiology.

*A modular microfluidic system to generate gradient hydrogels with simple-to-complex stiffness profiles for mechanobiology.**
S.W. Chong, J. Sardharwalla, G.S.P. Masonsong, J. Cosgrove, A. Katselas, I.J. Gresham, M.M.M. Bilek, Y. Shen, C. Neto, D. Vigolo.
Advanced Materials Technologies, **2025**, e01457.
* Hot topic: Microfluidics

Fluorescently labeled gradient hydrogels reveal matrix-dependent cell responses to substrate stiffness.
S.W. Chong, L. Liu, D. Kempe, Y. Zhang, K. Kalantar-Zadeh, M.M.M. Bilek, L.A. Ju, M. Biro, D. Vigolo.
Submitted.
Available on bioRxiv: https://doi.org/10.1101/2025.09.23.677581

Microengineered gradient hydrogels for mechanobiology.
S.W. Chong, D. Vigolo.
In preparation.

Publications arising from other research activities:

Nanofluidic lab-on-a-chip systems for biosensing in healthcare.
S.W. Chong, Y. Shen, S. Palomba, D. Vigolo.
Small, **2025**, 21 (1): 2407478.

Application of microfluidic technologies in veterinary science with a view toward development of animal-on-a-chip models.
Q. Yin*, Z. Yang*, **S.W. Chong***, J. Li, X. Liu, D. Vigolo, J.J. Li, P.A. Sheehy, K.T. Yong.
VIEW, **2025**, 6 (1): 20240073.
* Equal-first author

Neuromorphic imaging cytometry on human blood cells", Neuromorphic Computing and Engineering.
Z. Zhang, H. Yang, J. Lin, **S.W. Chong**, J.K. Eshraghian, K.T. Yong, D. Vigolo, H.M. McGuire, O. Kavehei.
Neuromorphic Computing and Engineering, **2025**, 5 (2): 024001.

Synthesis of anisotropic gold microparticles via L-Glutathione-mediated pathways in droplet microfluidics.
Z. Yang, Q. Yin, M. He, **S.W. Chong**, Z. Xu, X. Liu, C. Vega-Sanchez, A. Jaiswal, D. Vigolo, K.T. Yong.
Particle & Particle Systems Characterization, **2024**, 41 (10): 2400056.

Presentations

National and international level:

*A modular approach to create stiffness gradient hydrogels **(poster)**.**
5th International Symposium on Mechanobiology (ISMB), Nov. 2024, Tainan, Taiwan.
* **AusMB travel award**.

*Integrating microfluidics and gradient hydrogels towards advanced in vitro models for mechanobiology studies **(poster)**.*
12th World Biomaterials Congress (WBC), May. 2024, Daegu, South Korea.

*Creating gradient hydrogels with complex stiffness profiles **(oral presentation)**.**
Australian Society for Mechanobiology (AusMB) annual meeting, Nov. 2023, Melbourne, Australia.
* **Best student talk** and **AusMB travel award**.

*Microfluidic technique to create gradient hydrogels for cell biology studies **(poster)**.*
28th Australasian Society of Biomaterials and Tissue Engineering (ASBTE), Apr. 2023, Christchurch, New Zealand.

School and University level:

*Microengineered gradient hydrogels for cell biology **(oral presentation)**.*
USYD Biomedical Research Showcase, Apr. 2025, Sydney, Australia.

*From microfluidics to nanofluidics **(guest lecture)**.*
BMET5963: Microfluidics in Healthcare, Oct. 2024, University of Sydney.

*Gradient hydrogels to probe cell mechanobiology **(oral presentation)**.*
USYD Pub Talks, Mar. 2024, Sydney, Australia.

*Creating gradient hydrogels in microfluidics to probe cell biology **(guest lecture)**.*
BMET1960: Biomedical Engineering 1A, May. 2023, University of Sydney.

*Programming hydrogels to probe cell biology: thermophoretic approach to create gradient substrates **(poster)**.*
Sydney Nano Institute Microfluidics/Nanofluidics Workshop, Oct. 2022, Sydney, Australia.

*Creating gradient substrates in microfluidics **(oral presentation)**.**
Biomedical Engineering HDR Student Symposium, Sep. 2022, Sydney, Australia.
* Symposium organizer; funded through **HDR Student Life Grant** (AUD 2000)